UNIVERSITY
OF TRENTO - Italy
Department of Materials Engineering
and Industrial Technologies

Doctoral School in Materials Science and Engineering – XXIV cycle

Porous calcium phosphate granules for biomedical applications

Marzio Piccinini

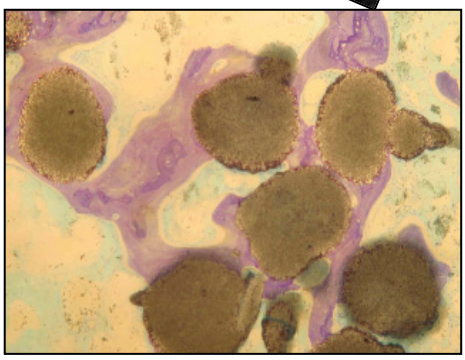

Tutor

Prof. Vincenzo Maria Sglavo

April 2012

To my family

PUBLICATIONS

M. Piccinini, V.M. Sglavo, P. Robotti, **"Granuli porosi in idrossiapatite per applicazioni biomediche"** , *Proceedings of 10° AIMAT*, (2010);

F. Bucciotti, **M.Piccinini**, V.M. Sglavo; **"Metodo per la realizzazione di un biomateriale a base di calcio fosfato sotto forma di granuli e/loro aggregati e biomateriale ottenuto con lo stesso"**, *Italian patent application*, (2011);

V.M Sglavo, **M. Piccinini**, A. Madinelli, F. Bucciotti; **"Hydroxyapatite scaffolds for bone tissue engineering with controlled porosity and mechanical strength"**; *Proceedings of 35th of ICACC*, (2011), 95-98;

M. Piccinini, V.M. Sglavo, F. Bucciotti; **"Synthetic porous calcium phosphate granules for bone substitutes"**; *Clinical Oral Implant Research*, Abstracts EAO 2011, September 2011;22; 9: 1098;

F. Bucciotti, **M. Piccinini**, V.M. Sglavo; **"Method for the realization of a biomaterial comprising calcium phosphate shaped as granules and/or their agglomerates and biomaterial obtained with this method"**; *International patent application*, (2012);

M. Piccinini, A. Rebaudi, V.M. Sglavo, F. Bucciotti, P. Robotti; **"A new HA/TTCP material for bone augmentation: an in vivo histologic pilot study in primates sinus grafting"**, *Implant Dentistry*, 2012, *submitted*.

CONGRESSES

10th Congress of Italian Association of Material Engeneering (AIMAT) 2010, Capo Vaticano (Italy), **"Granuli porosi in idrossiapatite per applicazioni biomediche"**; *Oral presentation*

35th International Conference and Exposition on Advanced Ceramics and Composites (ICACC) 2011, **"Hydroxyapatite scaffolds for bone tissue engineering with controlled porosity and mechanical strength";** *Oral presentation*

Congress of Italian Society of Biomaterials (SIB) 2011, Bari (Italy), **"Calcium phosphate granules with controlled size, composition and microporosity";** *Oral presentation*

13rd International Congress of Ceramic, Cells and Tissue (CCT) 2011, Faenza (Italy); **"Porous hydroxyapatite scaffolds for bone tissue substitutes by modified sponge replica method";** *Poster*

12th Conference of the European Ceramic Society (ECerS) 2011, Stockholm (Sweden); **"Hydroxyapatite porous scaffolds for bone tissue engineering";** *Poster*

8th Congress of Italian Interuniversitary Consorce of Science and Material Technology (AIMAT) 2011, Catania (Italy), **"CaP-Granules with controlled size, micro-porosity and composition";** *Poster*

Congresses

24th European Conference on Biomaterials (ESB) 2011, Dublin (Ireland), **"Porous calcium phosphate granules with controlled size, micro-porosity and composition";** *Poster*

20th Anniversary Meeting of the European Association for Osseointegration (EAO) 2011; Athens (Greece); **"Synthetic porous calcium phosphate granules for bone substitutes";** *Poster*

Summer School on Biomaterials and Regenerative Medicine 2011, Trento (Italy), **"Microporous CaP granules with controlled size and composition for bone void fillers applications";** *Oral presentation*

GLOSSARY

A.A.	acetic acid
Alg	sodium alginate
αTCP	alpha-tricalcium phosphate
βTCP	beta-tricalcium phosphate
CDHA	calcium deficient hydroxyapatite
CaP	calcium phosphate
Chi	chitosan
HA	hydroxyapatite
MES	2-(N-morpholino) ethanesulfonic acid
Ksp	solubility product parameter
SBF	simulated body fluid
TRIS	hydroxymethyl aminomethane
TTCP	tetra-calcium phosphate
TTP	sodium tripoly-phosphate

INDEX

INDEX

INDEX

ABSTRACT

The repair or replacement of damaged or diseased hard tissue is a biomedical field that has been the subject of more and more interest in many areas of research and especially in the development of new biomaterials. The rise in the average age of the world population, increasing osteoporosis treatments and the spread of cancer and genetic bone diseases, has brought about the need to find solutions for patient care. To achieve this target/objective, biomaterials must simulate the body environment as much as possible and favour tissue repair by integrating them into the host site.

Calcium phosphates are used as medical implants because they have a chemical composition similar to the mineral of human bones, i.e. apatite. For this reason they are biocompatible and they can interact in a bioactive way with bone tissue.

In the present work a specific form of bone graft, in the form of calcium phosphate granules, has been developed by using the droplet extrusion technique. The granules were characterized chemically and physically, with specific attention to in vivo and in vitro analyses. The proposed method has allowed us to obtain spherical granules in very narrow micrometric size distribution (300-1200 μm) without the use of solvents or oils thus avoiding time consuming washing processes. Granules were produced with several controlled mineralogical compositions including: pure Hydroxyapatite (HA) and β-Tricalcium Phosphate (βTCP), mixtures of HA/βTCP and

ABSTRACT

Hydroxyapatite/Tetracalcium phosphate (HA/TTCP), and compositions doped with zinc (for antibacterial purposes) and strontium (for anti-osteoporosis purposes). Of several interesting features, the produced granules show high interconnected microporosity (0.1-10 μm) and surface roughness, properties necessary for osteoconductivity.

The solubility behavior of granules was studied and demonstrated that the morphology and microporosity are more important in dissolution processes than chemical or mineralogical composition. Products were tested in simulated body fluid (SBF), and among the different compositions, HA/TTCP has been found to be bioactive during in vitro studies. In fact an intense precipitation of a carbonated layer of apatite was observed, associated with the high dissolution of a TTCP phase. All pure granules were demonstrated to not be cytotoxic. Bone implantations in different animal models (rabbits and primates) showed good performance of granules in the repairing of bone. The granules stimulated the bone growth without any inflammatory reactions. In particular, HA/TTCP granules exhibited excellent biomechanical properties by increasing the stability of neo-formed bone. These preliminary investigations were sufficient to show that the developed granules can be used for bone repair or replacement. However, more studies, especially for doped products, such as in vitro cells experiments, have to be performed to assure the biocompatibility and the effective stimulation of bone growth.

This work was performed in collaboration with Eurocoating S.p.A. (Trento, Italy), a company expert in biomedical coatings for prostheses and implants, and it is a part of "CaP project" co-sponsored by Provincia Autonoma di Trento (Italy).

1 INTRODUCTION

Medical research has always been an active field for the study and production of new materials with different functions and purposes. Biomedical applications are one of the most active research areas in materials science. During the last few decades, both an aging population and the proliferation of high-risk sports have led to an increase of bone-related diseases, skeletal defects, tumor resection, skeletal abnormalities and bone fractures originating from trauma. All of these must be treated through tissue replacement therapies. The most common treatments for skeletal defects are artificial replacements for hips, knees and teeth, periodontal disease, maxillofacial reconstruction, augmentation and stabilization of the jawbone, spinal fusion and bone fillers after tumor surgeries and fractures.

In order to be accepted by the living body, all implantated devices must be prepared using a special class of materials denoted biomedical materials or biomaterials. Included in this class are biometals, biopolymers, bioceramics and biocomposites. All have the role is to replace or regenerate human tissue.

A great variety of biomaterials are described in literature for bone bioengineering purposes. For these cases, the material must present:

- biocompatibility, i.e. the lack of a cytotoxic reaction or any other detrimental effects;
- adaptableness to the damaged area;

• osteoconductivity, characterized by good adhesion, proliferation and maturation of osteoprogenitor cells;
• ability to act as a barrier to surrounding tissues;
• time of resorption compatible with the requirements for bone formation, without interfering with the substitution of the material by neoformed bone;
• biocompatibility, non-immunogenicity and atoxicity;
• radioluscence, allowing the radiographic distinction of graft from newly formed bone;
• easy manufacture and sterilization (by autoclave, gamma rays, ethylene oxide);
• easy handling during surgery, avoiding complex pre-operatory procedures which increase the risk of infection;
• acceptable microarchitecture, including interconnections and porosity (200-900 μm), allowing the penetration of osteocompetent and endothelial cells and the vascularization of the neoformed tissue.

1.1 Bone: tissue and remodelling

Bone represents a specialized connective tissue. It is a complex composite of a biopolymer and a biomineral. It originates from the esenchyme like other connective tissues, and is composed of cells, fibers and a complex, mineralized matrix, which distinguishes organic and inorganic matters.

INTRODUCTION

The peculiarity of the bone tissue is that it is calcified. The inorganic portion (65% of the intercellular substance) consists mainly of calcium and phosphate salts, in the form of calcium - hydroxyapatite, $Ca_{10}(PO_4)_6(OH)_2$, and, in smaller quantities, of calcium carbonate and other minerals. Within the extracellular matrix, highly ordered organic fibers are dispersed, consisting of 90% collagen and the remaining part of various proteins.

The structure accounts for numerous remarkable properties such as hardness and mechanical resistance. The composition and the distribution of proteic components of the matrix are responsible for elasticity and resistance to fracture. The bone tissue, in addition, represents the main deposit of calcium ions for the metabolic needs of the whole organism: the deposition of calcium in bone and its mobilization, finely controlled by endocrine mechanisms, contribute to the regulation of the ion levels in the plasma.

From a macroscopic point of view, there are two types of bone: spongy (or trabecular) and compact. The spongy bone is suitable to withstand compression stresses and, for this reason, is present mainly in the short and flat bones, and in the epiphysis of long bones. Its structure is characterized by the presence of spongiform multi-oriented trabeculae and intersecting in a three-dimensional network.

The compact bone is named because of the rigidity that characterizes and makes it resistant to compression, tension and torsion. It is located in the diaphysis of long bones and covers the spongy tissue of short and flat bones. Its main unit, the osteon, consists of concentric lamellae formed by the ordinate deposition of collagen fibers around the Haversian channels, which contains the blood vessels.

Despite the apparent immobility and the effective stiffness, the bone tissue is extremely dynamic during its life stages and is constantly subject to cycles of resorption and deposition. These cycles are targeted to meet the metabolic requirements and functional accretion or to adjust the skeletal structure as it issubjected to mechanical stresses.

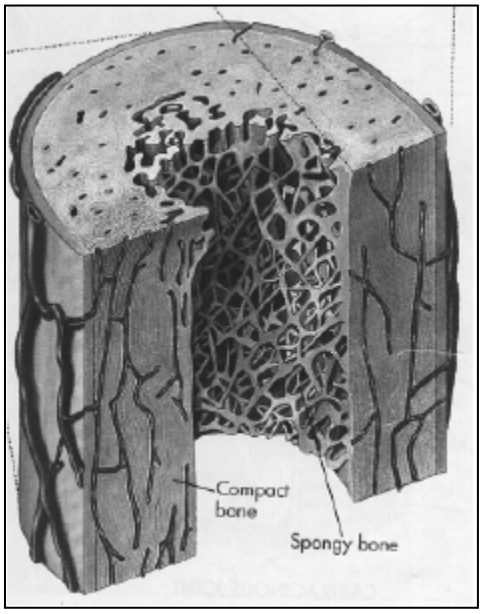

Fig. 1.1 Cross-section of human bone [1].

This set of processes, for the removal and formation of new tissue, is called bone remodeling. They occur through a close functional correlation between the bone cells and many factors coordinating the activities for regulating and maintaining skeletal homeostasis.

Bone tissue usually presents a remarkable capacity for repairing and regenerating tissue, which is very similar to the original bone. This is in

contrast to other tissues that present the formation of fibrous connective tissue during repair (*i.e.* muscle and tendons).

1.2 Bone graft substitutes

Many biomaterials have been studied for the repair of bone defects or the restoration of bone tissue functionality. During the last two decades, extensive research on ceramic materials, like calcium phosphates, have shown that these materials are suitable as bone substitutes due to their biocompatible, bioactive, biodegradable, and ostoconductive characteristics, and, when implanted in vivo, they are non toxic and do not induce any antigenic response.

There are four characteristics that an ideal bone graft material should exhibit:

- osteointegration, the ability to chemically bond to the surface of bone without an intervening layer of fibrous tissue;
- osteoconduction, the ability to support the growth of bone over its surface and to orient the formation of new bone through its support matrix, acting as a scaffold that can be simultaneously absorbed and substituted by bone tissue;
- osteoinduction, the ability to induce differentiation of pluripotential stem cells from surrounding tissue to an osteoblastic phenotype, a mechanism is directly related to the activity of bone morphogenetic proteins (BMPs). The formation of new tissue during the bone remodeling process is observed by using platelet-rich plasma, growth factors and demineralized lypholized bone [2];

- osteogenesis, the formation of new bone by osteoblastic cells present within the graft material.

The most commonly used bone grafting materials include autografts, allografts, xenografts and synthetic composites.

1.2.1 Autograft , allograft and xenograft

Currently, autografts, bones obtained from another anatomic site in the same subject, are the standard for bone repair because they possess all four cited characteristics. Disadvantages are the cost and trauma to the patient, limited availability, increased operative time, ossibility of donor site morbidity associated to blood loss, wound complications, local sensory loss and chronic pain.

Allografts are bones taken from another subject, such as processed cadaver bones. Advantages of allograft include availability and the avoidance of morbidity associated with harvesting an autogenous graft. Allografts are of particular importance when there are large bone defects, which require structural support, or when inadequate autogenous graft volume is available.

Complications associated with allograft include fracture, non-union and infection. Allograft union is difficult to assess and discrepancies have been found between clinical, radiological and histological union. Bacterial infection is more common with increased size of graft and may be seen in more than 10% of massive allografts. Viral transmission (hepatitis B, C, HIV) is also a potential risk that has been historically and serologically screened for. Despite the exceedingly low risk, transmission of HIV 1 from seronegative cadaveric

donors has occurred. Autografts and allografts, while having the important advantage of being osteogenic or osteoinductive (i.e., inducing bone formation), suffer from several disadvantages [3].

Xenografts are a valid alternative to both autografts and allografts. They are obtained from different species than the recipient. The most common grafts are collected from bovine bone, but literature has also described porcine or caprine materials. Their use presents similar advantages of allogeneic grafts, with predictable results when surgical standards are followed. On the other hand, there are also disadvantages including; 1) the risk of interspecific transmission of infectious diseases, 2) host immune response and 3) lower acceptance by patients and professionals due to cultural and religious aspects of using animal material [4].

Therefore, there is a critical need for the development of bone substitute materials that match the properties of bone without the drawbacks of autografts or allografts, while being available at any time, in any amount and at a lower cost. For this reason there has been a great need to develop synthetic alternative biomaterials for bone replacement, repair, and growth.

1.2.2 Synthetic bone graft

The dilemma of graft choice is left to the orthopaedic surgeon and the bone defect present. It is sensible to assume that not all bone graft substitutes will perform the same way. The variety of the available scaffolds in industry and their combinations

(composite grafts), represent not only the different clinical needs and scenarios encountered, but the diversity of the expected clinical outcomes as well. The surgeon must choose the appropriate substitute graft and surgical techniques based on the type of bone defect to be grafted and the mechanical and biological requirements of the area. He must also weigh the essential properties needed (osteogenetic, osteoinductive, and osteoconductive) and what are actually available or missing in a particular type of graft.

The validation of any bone-graft substitute in one clinical site may not necessarily predict its performance in another location. The choice of the appropriate bone substitute product should be based on several parameters, bearing in mind that the standard remains harvesting autologous cortical and cancellous bone from the iliac crest. All other forms of bone grafting have disadvantages compared to autografts and, as such, their use is sub-optimal. Technological evolution, along with better understanding of bone-healing biology, has led to the development of several bone graft substitutes made of synthetic materials that are available to orthopaedic and dental surgeons.

Current commercial substitute materials to replace or repair teeth and bones include: metals, biopolymers (collagen), synthetic ceramics (aluminium oxide, calcium phosphates, calcium sulfates, calcium carbonate, bioactive glasses, glass ionomers), and composites, which are obtained by mixing several distinct materials. Products differ mainly by their grade of re-absorpiton and mechanical properties (Table 1.1).

Biomaterials	Composition	Features	Form	Mechanical properties	Resorption	Product name	New bone in total defect	New bone and allogeneic materials in total defect
Glass ionomer	Calcium aluminium fluorosilicate glass powder + polycarboxylic acid	Direct bone union. Porous. Requires dry field	Powder	Compressive strength and modulus of elasticity comparable to cortical bone	Non-reabsorbable: therefore is not replaced by bone	—	—	—
β-tricalcium phosphate	Calcium phosphate	Direct bone union. Porous or solid	Blocks Granules	Brittle Porous form structurally similar to cancellous bone	Dissolution 6-18 months; therefore faster than the replacement by bone	—	—	—
Calcium phosphate cements	Calcium phosphate	Porous Non-ceramic	Paste	Good compressive strength Weak in distraction	Years	—	—	—
Aluminium oxide	Alumina	Ceramics Non osteoinegrante	Blocks Granules	Stronger than hydroxyapatite	Non-reabsorbable	—	—	—
Calcium sulphate	Calcium sulphate	Dry environment before and after to use	Powder	Bad mechanical properties	In 5-7 weeks	—	—	—
Bovine xenograft	Mineral osseous matrix (hydroxyapatite), deproteinized bovine bone	Porous (75-80%) It can contain organic residues	Granules	Compressive strength of 35 Mpa: > than cancellous bone < than compact bone	It is resorbed slowly	Bio-Oss™	47,4 ±7,1	80,1 ± 5,1**
Bioactive glass	Sodium oxide, calcium oxide, phosphorus pentoxide, silicon dioxide	Bond directly to bone Hard and solid (not porous)	Blocks Granules Rods	Stronger than hydroxyapatite	Non reabsorbable o reabsorbable depending on the proportion of its components Biogran: reabsorbable	Biogran™	30,6 ±9,7	33,1 ± 8
Synthetic hydroxyapatite	Calcium phosphate	Porous or solid Ceramic and non-ceramic Orthoss™: solid	Blocks Granules Orthoss™: granules	Good compressive strength Brittle. Modulus of elasticity higher than bone	Ceramic form: 1-2% per year Non- ceramic form: ¾ higher Orthoss™: non- reabsorbable	Orthoss™ HA-500	45,3 ±6,2	67, 7 ± 7**
Cornalline hydroxyapatite	Calcium phosphate	Porous The structure of calcium carbonate turns into phosphate	Blocks Granules Interpore™ 500: blocks	Structurally similar to the cancellous bone, fragile	Practically irreabsorbable, it allows the regeneration inside	Interpore™ 200	38,5 ±9,3	67,1 ±8,1**
Calcium carbonate and calcium phosphate	Calcium carbonate covered by calcium phosphate	Internal core of carbonate surrounded by a cap of phosphate	Blocks	Structurally similar to the cancellous bone	Calcium carbonate is quikly reabsorbable, calcium phosphate is slower	Pro-Osteon™ 500	34,7 ±8	39,8 ±6,7
Composite polymer	Polymethylmethacrylate Polyhydroxyethylmethacrylate Calcium hydroxide carbonate	Constructed in concentric cups	Granules	Porous and resistant matrix	Non- reabsorbable	Bioplant™ HTR	37,1 ± 8	69,4 ± 7,1**
Control group	—	—	—	—	—	—	42,2 ± 6,4	42,2 ± 6,4

Table 1.1 Bone graft: different grade of resorption and mechanical properties [5].

Moreover, metals and alumina cannot be considered bioactive because they do not exchange ions between implant and bone and are not biodegraded in the physiological environment, remaining in the implantation site permanently. Biopolymers are collagens that contribute to mineral deposition, vascular ingrowth and growth factor binding, providing a favourable environment for bone regeneration. Nevertheless, they may carry potential immunogenicity and provide minimal structural support. For this reason collagen is associated with other bone substitutes such as hydroxyapatite. Bioactive glasses possess both osteointegrative and osteoconducitve properties. In fact, a mechanically strong bond between bioactive glass and bone forms as a result of a silica-rich gel layer, which grows on the surface of the bioactive glass when exposed to physiologic aqueous solutions. Within this gel Ca^{2+} and PO_4^{2-} ions combine to form crystals of hydroxyapatite (HA) similar to that of bone, allowing for a strong chemical bond. They have good mechanical strength and resist drilling and shaping, but they can fracture during surgery process and they are difficult to fix to the skeleton. Table 1.2 shows some available bone grafts and their main properties.

Materials also react in a different way with host tissue (Table 1.3). Inert materials, like alumina or zirconia, are covered in carfibrous membrane around the implant. Bioactive material form an interfacial bond like calcium phosphate that is is resorbable and degrades with time.

The most used biomaterial in recent decades, for bone grafts, is a bioceramic based on calcium phosphate. Its chemical composition is similar to the carbonate apatite nanocrystals already present in the bone and has other properties such as bioactivity, biodegradability and osteoconductivity. This

has justified their wide scale use in the preparation of biomaterials for hard tissue substitution and repair.

Type	Graft	Osteoconduction	Osteoinduction	Osteogenesis	Advantages
Bone	Autograft	3	2	2	"Gold standard"
	Allograft	3	1	0	Availability in many forms
Biomaterials	DBM	1	2	0	Supplies osteoinductive BMPs, bone graft extender
	Collagen	2	0	0	Good as delivery vehicle system
Ceramics	TCP, hydroxyapatite	1	0	0	Biocompatible
	Calcium phosphate cement (CPC)	1	0	0	Some initial structural support
Composite grafts	β-TCP/BMA composite	3	2	2	Ample supply
	BMP/synthetic composite	–	3	–	Potentially limitless supply

Score: 0 (none) to 3 (excellent). DBM: demineralised bone matrix, TCP: tricalcium phosphate, BMA: bone marrow aspirate, BMP: bone morphogenetic protein.

Table 1.2 Different bone substitute materials [6].

Classification	Tissue response	Implant/ tissue bond	Examples
Toxic	Tissue dies	None	Lead oxide, arsenic oxide
Near inert	Formation of a non-adherent fibrous membrane around implant	None	Alumina, zirconia, carbon
Bioactive	Formation of an interfacial bond with the implant	Chemical	Hydroxyapatite, bioactive glasses, and glass–ceramics
Resorbable	Tissue replaces implant as it degrades	Chemical	Tricalcium phosphate, calcium sulfate, bioactive glasses, calcium-phosphate bone cements

Table 1.3 Classification of tissue response of different synthetic bone graft [7].

1.3 Bioceramics: calcium phosphates

Bioceramics can have structural functions as joint or tissue replacements, be used as coatings to improve the biocompatibility of metal implants, as well as function as resorbable lattices, providing temporary structures and frameworks that are dissolved and/or replaced as the body rebuilds the damaged tissues. Bioceramics are needed to alleviate pain and restore functions to diseased or damaged calcified tissues (bones and teeth) of the body. Their surface reactivity contributes to bone bonding ability and enhancing effect on bone tissue formation. During implantation, various interactions occur at the material/tissue interfaces that lead to time-dependent changes in the surface characteristics of the implanted bioceramics and the surrounding tissues. In the past many implantations failed due to infections and, furthermore, the infections tended to be exacerbated in the presence of implants, since they provided a region inaccessible to the body's immunologically competent cells. Due to this lack of knowledge about the toxicity of the selected materials, application of calcium phosphates appears to be adequate because of their similarity with the mineral phases of bones and teeth. In fact, CaP materials are not toxic and do not causes cell death in the surrounding tissues. Calcium phosphates are already present in our body in different biologic systems as pathologic calcifications or diseased states (Table 1.4).

calcium phosphates	occurrence
amorphous calcium phosphates, ACP	soft-tissue calcifications
dicalcium phosphate dihydrate, DCPD	dental calculus, dental caries
octacalcium phosphate, OCP	dental calculus, urinary stone
Mg-substituted tricalcium phosphate, β-TCMP	dental calculus, soft tissue calcifications
carbonate hydroxyapatite, CHA	dental calculus, urinary stone, mineral phases of enamel, dentin, cementum, bone, fish enameloids
carbonate fluorapatite, CFA	fish enameloids
calcium pyrophosphate dihydrate, CPPD	joints

Table 1.4 Calcium phosphate in biologic systems [8]**.**

In this work, the attention was focused on a specific class of bioceramics; in particular on bioactive materials such as calcium phosphates (CaP). Calcium phosphates are considered bioactive stimulants for bone tissue formation and therefore directly bond with bone, thus forming uniquely strong biomaterial-bone interfaces. As bioactive materials, they dissolve slightly but allow formation of direct chemical bonds to bones. They are also bioresorbable materials that dissolve over time (regardless of the mechanism leading to the material removal) and allow a newly formed tissue to grow. Consequently, the functions of CaP materials are to participate in dynamic processes of formation and re-absorption occurring in bone tissues.

CaP biomaterials mainly have the following characteristics:

- composition similar to bone mineral;
- ability to form bone apatite like material on their surfaces;

- solubility and capability to release Ca and orthophosphates ions that promote cellular functions and expression resulting in new bone formation;
- resorbability that make them able to participate in dynamic process of formation and re-absortption occurring in bone tissue;
- ability to provide the appropriate scaffold or template for bone formation.

They can not be considered osteoinductive, they do not form bone ex novo, for example by forming bone in non-osseous sites. This important property of the bone is due to the morphogenetic proteins (BMPs) and osteogenic proteins (collagen, osteonectin) present in extracellular matrix, but not in inorganic materials. These properties are common to all CaP bioresorbable materials, but can be enhanced by means of the proper design of physico-chemical properties such as:

- micro and macroporosity in order to enhance body fluids and cells invasion
- 3D structure to support cells adhesion and to stimulate cells differentiation
- dissolution/resorption rate in order to participate and stimulate bone remodeling process
- chemical composition, crystal phases and molecular structures for bone bonding formation.

A defect of CaP materials is that they possess low fracture strength and they are not suitable for load bearing areas. Depositing CaP coatings on dental and orthopaedics it is possible to combine the bioactivity of CaP and the strength

of the metal. [8] The mechanical properties are strictly linked to the structure. The strength decreases almost exponentially with porosity increasing and also the pore geometry influence the mechanical resistance of porous bioceramics. It is difficult to reach in the the same time, the compressive strength and porous structure of natural bone. Table 1.5 shows typical compressive strength values of natural bone and calcium phosphates [1][9].

At present synthetic calcium phosphates are used in different applications such as dental implants, percutaneous devices and use in periodontal treatment, healing of bone defects, fracture treatment, total joint replacement (bone augmentation), orthopaedics, cranio-maxillofacial reconstruction, otolaryngology, ophthalmology and spinal surgery [131]. Calcium phosphates can be divided into different compounds depending on the chemical composition associated to molar Ca/P ratio and solubility. In general, as lower the ratio Ca/P is as more acidic and soluble the calcium phosphate becomes in water (Table 1.6)

Material	Compressive strength [MPa]
Trabecular Bone	150
Sponge bone	1.9
Hydroxyapatite (HA) dense	350-450
Hydroxyapatite (HA) porous (40%)	60-120
Hydroxyapatite (HA) porous (80%)	0.5-5
Tricalcium phosphate (TCP) dense	120
Tricalcium phosphate (TCP) porous (50%)	13
Tetracalcium phosphate (TTCP) dense	120-200

Table 1.5 Mechanical properties of bone and calcium phosphate materials [2][8].

Compound	Formula	Ca/P ratio	Solubility at 25°C
Monocalcium phosphate monohydrate (MCPM)	$Ca(H_2PO_4)_2 \cdot H_2O$	0.5	1.14
Monocalcium phosphate anyhydrous (MCPA)	$Ca(H_2PO_4)_2$	0.5	1.14
Dicalcium phosphate dihydrate (DCPD)	$CaHPO_4 \cdot 2H_2O$	1.0	6.59
Dicalcium phosphate anhydrous (DCP)	$CaHPO_4$	1.0	6.90
Octacalcium phosphate (OCP)	$Ca_8H_2(PO_4)_6{*}5\ H_2O$	1.33	96.6
α-tricalcium phosphate (α-TCP)	$\alpha\text{-}Ca_3(PO_4)_2$	1.5	25.5
β-tricalcium phosphate (β-TCP)	$\beta\text{-}Ca_3(PO_4)_2$	1.5	2.5
Hydroxyapatite (HA)	$Ca_{10}(PO_4)_6(OH)_2$	1.67	116.8
Tetracalcium phosphate (TTCP	$Ca_4(PO_4)_2$	2.0	38-44

Table 1.6 Existing calcium phosphates and major properties [10].

Hydroxyapatite (HA, $Ca_{10}(PO_4)_6(OH)_2$) is the most stable and least soluble of all calcium orthophosphates (Table 1.6). Pure HA crystallizes in the monoclinic space group $P2_1/b$. However, at temperatures above 250 °C, there is a monoclinic to hexagonal phase transition in HA. (space group $P6_3/m$).

The lattice parameters as reported by Kay et al. are a=59.432 Å, c= 56.881A Å. The crystal structure of HAP (Fig. 1.2) can be described as a hexagonal stack of isolated PO_4^{3-} tetrahedrons creating two kinds of tunnels parallel to the c-axis. The first kind of tunnel is filled with Ca^{2+} (1) ions which form CaO_9-polyhedra, whereas the second one, which is lined by oxygen and other Ca ions, is occupied by OH^- anions. The Ca^{2+} (2) ions at z=1/4 and z=3/4 form triangles. Each of the three ions at the corners of the triangle is bonded to the central OH^- anion in the tunnel, which is displaced below or above the triangle plane. The diameter of such tunnels (3 Å in HA) gives apatites ion exchanger

properties but only at high temperatures, and it can also act as a host to small molecules. [11]

Some impurities, like partial substitution of hydroxide by fluoride or chloride ions, stabilize the hexagonal structure of HA at ambient temperature. For this reason, the very rare single crystals of natural HA always exhibit a hexagonal space group.

HA can be produced in three different methods:

(i) Titration of $Ca(OH)_2$ with H_3PO_4;

(ii) Dropwise addition of HPO_4^{2-} solution to Ca^{2+} solution, pH > 9;

(iii) Hydrolysis from other phosphates.

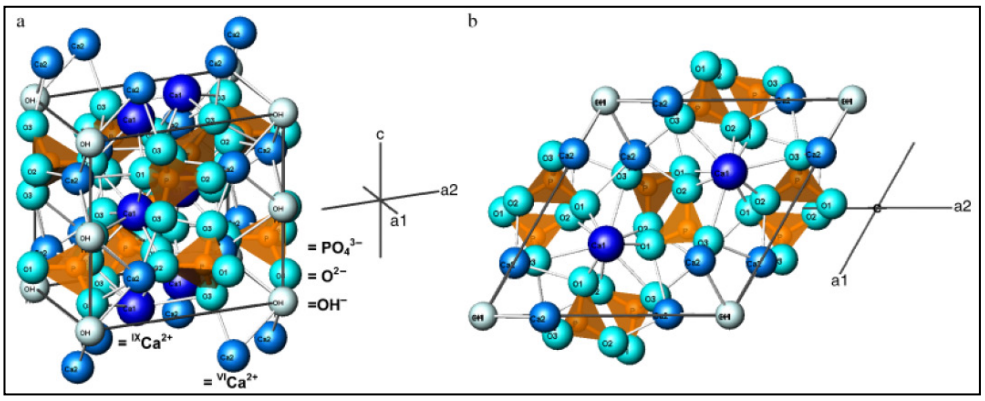

Fig. 1.2 (a) Crystal structure of hydroxyapatite after Wilson et al. projected perpendicular to c-axis. (b) Crystal structure of hydroxyapatite after Wilson et al. projected on (001). [11]

β-tricalcium phosphate (β-TCP, β-$Ca_3(PO_4)_2$) is the ™true calcium phosphate" of the stoichiometric composition $Ca_3(PO_4)_2$. Tricalcium phosphate $Ca_3(PO_4)_2$ was found to crystallize in three polymorphic modifications: β-TCP below

1180°C, α-TCP between 1180°C and 1430°C, and α'-TCP above 1430°C. As reported by Dickens and colleagues, the β-TCP crystallizes in the rhombohedral space group R*3c* with unit-cell parameters a=10.439 Å and c=37.375 Å, the unit cell contains 21 formula units of $Ca_3(PO_4)_2$.The structure (Fig. 1.3) can be described as disrupted layers of PO_4 tetrahedrons and the Ca ions lie in the centers of these layers [11].

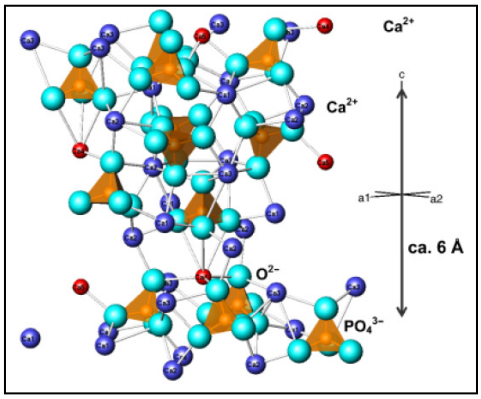

Fig. 1.3 Crystal structure of b-tricalcium phosphate after Dickens et al. projected perpendicular to c-axis [11].

It cannot be precipitated from solution, but may only be prepared by calcination, e.g. of CDHA (Eq.1), at temperatures above 800 °C

$$Ca_9(HPO_4)(PO_4)_5OH \rightarrow Ca_3(PO_4)_2 + 2H_2O \qquad (1)$$

At temperatures above 1125 °C, it transforms into the high temperature phase β-TCP. β–TCP synthesis is performed in solid state reaction [12]. Being the stable phase at room temperature, β-TCP is less soluble in water than α–TCP. Pure β-TCP never occurs in biological calcifications.

Tetracalcium phosphate (TTCP, $Ca_4(PO_4)O$) is the only calcium phosphate phase with a Ca/P ratio greater than stoichiometric hydroxyapatite (HA), and it is formed in the ($CaO-P_2O_5$) system at temperatures >1300 °C. The compound is metastable, therefore the synthesis of phase-pure TTCP requires either rapid quenching or the absence of moisture to prevent decomposition into HA and lime in the temperature range 1000–1200 °C. TTCP cannot be precipitated from aqueous solutions, owing to the oxygen atom in its formula, precipitates formed in basic aqueous solutions with a Ca/P ratio of 2 will incorporate hydroxyl ions and therefore always consist of carbonate and/or hydroxyl ion-containing apatitic phases. Hence, common methods for the synthesis of TTCP are limited to solid-state reactions at high temperatures. These methods are usually based on mixtures of calcium carbonate ($CaCO_3$) and dicalcium phosphate anhydrate ($CaHPO_4$) with a Ca/P ratio of 2, which are then heated to 1450–1500 °C for 6-12 h in a stream of dry nitrogen. The reaction is given by the Eq.2.

$$2CaHPO_4+2CaCO_3 \rightarrow Ca_4(PO_4)O+2CO_2+H_2O \qquad (2)$$

After heating, the mixtures must be rapidly quenched to room temperature in order to avoid the formation of undesired secondary phases such as HA, calcium oxide (CaO), $CaCO_3$ and β-TCP [13].

TTCP crystallizes in monoclinic, space group P_21. The unit cell contains cell 4 of $Ca_4(PO_4)O$. The lattice parameters as reported by Dickens at al. are a=7.023 Å, b=11.986 Å, c=9.473 Å.

TTCP is the most alkalinic calcium phosphate and its solubility in water is higher than HA. TTCP is not very stable in aqueous solutions; it slowly hydrolyses to HA and calcium hydroxide. Consequently, TTCP is never found in biological calcifications. In medicine, TTCP is widely used for the preparation of various self-settingcalcium phosphate cements [14].

It has been known since the mid 1980s that the existing monophasic calcium phosphates listed might form biphasic, triphasic and multiphasic (polyphasic) combinations, in which the individual components frequently cannot be separated from each other. Obviously, the individual phases in such formulations are homogeneously and intimately "mixed" at the submicron (<1 μm) level and, therefore, are strongly integrated with each other. The presence of each individual phase is easily observed by XRD, which clearly indicates that they remain unchanged.

Different combination of **biphasic calcium phosphates** (BCP) were studied in last decades and have found different applications. Two example of BCP are **HA/βTCP** and **HA/TTCP**.

The first preclinical application of **HA/βTCP** was reported by Nery et al. in 1975 using a calcium phosphate they described as "tricalcium phosphate" but was analyzed using X-ray diffraction as a mixture of HA and β-TCP and, consequently, such a mixture was described as a biphasic calcium phosphate, BCP. Compared with the XRD pattern of human ilia, the porous bioceramic HA/TCP has the phase structure similar to that of natural human bone, which consists of HA containing partial TCP.[15]

The production of BCP was first introduced by LeGeros in 1986 [16]. The efficacy of BCP was based on the preferential dissolution of the β-TCP compared to HA, allowing the manipulation of bioactivity or biodegradation by manipulating the HA/β-TCP ratio.

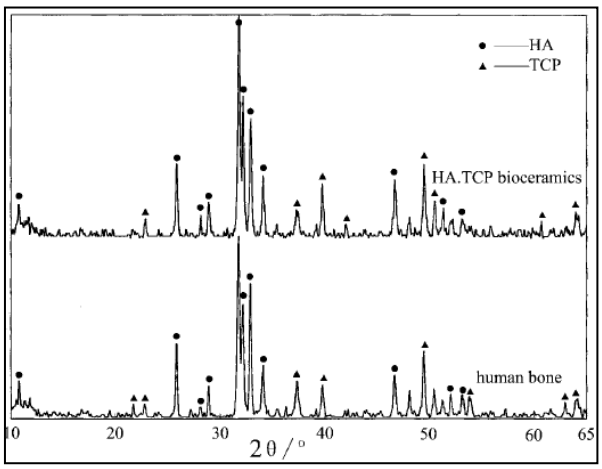

Fig. 1.4 XRD of human bone compared to HA/TCP bioceramic [15].

BCP is obtained when a synthetic or natural calcium deficient hydroxyapatite (CDHA) is sintered at temperature above 700°C. The extent of calcium deficiency depends on the method of preparation, the reaction pH and the temperature in the preparation of the non-sintered apatite. The calcium deficiency determines the HA/βTCP ratio in BCP. [16]. Another method for produce HA/βTCP material is simplest mixing of HA and βTCP where TCP is in contact with HA during sintering, the TCP is converted into Ca-deficient HA by the diffusion of Ca originating from HA [17]. BCP was also obtained by hydrolysis of commercial dicalcium phosphate dihydrate and subsequent

sintering of the formed calcium-deficient apatite (CDA) [18]. Although the rate of biodegradation depended on the method of preparation, the rate of new bone formation was not significantly different for BCP ceramics. Thus, the BCP with the HA/β-TCP ratio of 20/80 was the most effective in eliciting a greater bone formation; however, the BCP with the ratio of 80/20 showed the best result in repairing surgically created periodontal defects [19]. The most used ratio for BCP in commercial products is 60/40 as example MBCP Tricos™ [20] or Bonesave®.

Concentrated studies on their development and applications were made by Daculsi et al .Thus, through the combination of a balanced rate between a more stable phase (HA) and a more soluble one (β-TCP), it was possible to formulate a BCP with a controlled dissolution rate and different mechanical properties [5].

The presence of porosity and a bioactive surface facilitate cell attachment, proliferation, and differentiation and, consequently, provide a more biocompatible, osteoconductive, and in some cases, osteoinductive ceramics, which can favor increased bone formation.

HA/TTCP biphasic materials have been developed in different forms, but they have not the success than HA/β-TCP product because their production process is more complicated. There are some examples in CaP coatings where a synthesis of biphasic coatings made of HA and bioresorbable TTCP by pulse laser deposition trough systematic control of the phase composition in the coatings with varying deposition parameters. They have been compared with traditional HA coatings, where TTCP is considered foreign phase. XRD analysis

of HA/TTCP coatings reveals that all of the TTCP phase in the biphasic coatings dissolves quickly within 12 h in a simulated body fluid solution, while the HA phase in the coatings remains essentially unaltered for periods in excess of one month. This may represent a route for triggering optimized biological response shortly after implant insertion, followed by a period of strong bone growth on a still robust non-resorbable coating or other bone substitutes. A recent review of 2012 about biphasic, triphasic and multiphasic calcium phosphates emphasize the use of HA/β-TCP and not cite any work about HA/TTCP [21]. For these reasons this chemical combination can be considered still new and unknown completely in bone repair application.

1.3.1 General properties of calcium phosphates

Bioceramic are materials with well-established **biocompatibility** [22] and they have been widely tested for clinical applications. In vitro test has shown that calcium phosphates are able to support human osteoblastic cells adhesion and proliferation [23].

Osteoblastic cells cultured for days in direct contact with porous microspheres of HA and HA/TCP attached and spread through the available surface, exhibiting adequate osteoblast morphology [24][25][26]. Moreover there are studies that demonstrate the capability of HA and βTCP to support cells culture [27][28][29]:not only they are no cytotoxic but they are also able to offer favorable surfaces for osteogenic tissue formation.

Also cultures of fibroblast like cells in direct contact with HA, HA/TCP, and βTCP demonstrate no acute cytotoxic reaction and attest adhesive and proliferative properties of these materials [30][31][32].

The cytotoxicity studies can differ in:

- type of cells utilized (osteoblasts, fibroblasts, bone marrow derived cells);
- time of exposure (from 24 h to weeks);
- parameters of evaluation (morphology, proliferation, cellular activity, proteins production, etc.);
- evaluation techniques (MTT test, cytotoxicity assay, differentiation markers quantification, optic microscope, SLM, CLSM, fluorescence microscope observations, etc.).

Nevertheless, it is important to prove the absence of potential cytotoxicity in the product: among all the biological evaluation for the biomaterials, cytotoxicity is the most important for CaP because it is related to chemical composition, morphology and manufacturing process.

Osteoconductivity: it is the ability of the material to serve as a scaffold or template to guide formation of the newly forming bone along their surfaces. An interaction between a general implant and surrounding tissues is a dynamic process. Water, dissolved ions, biomolecules and cells surround the implant surface during initial few seconds after the implantation. It has been accepted that no foreign material placed within a living body is completely compatible.

The reactions occurring at the biomaterial/tissue interfaces lead to time-dependent changes in the surface characteristics of both the implanted biomaterials and the surrounding tissues.

In vivo experiments are necessary to evaluate the bioactivity and the osteoconductivity of biomaterials in a real physiological environment. It is necessary to understand the *in vivo* host response in the development of new biomaterials.

No particular inflammatory reactions or local toxicity were observed in many years using calcium phosphate based biomaterials. The biological response to implanted calcium phosphate follows a similar cascade in fracture healing includes: a hematoma formation, hematoma formation, neovascularization, osteoclastic resorption and a new bone formation.

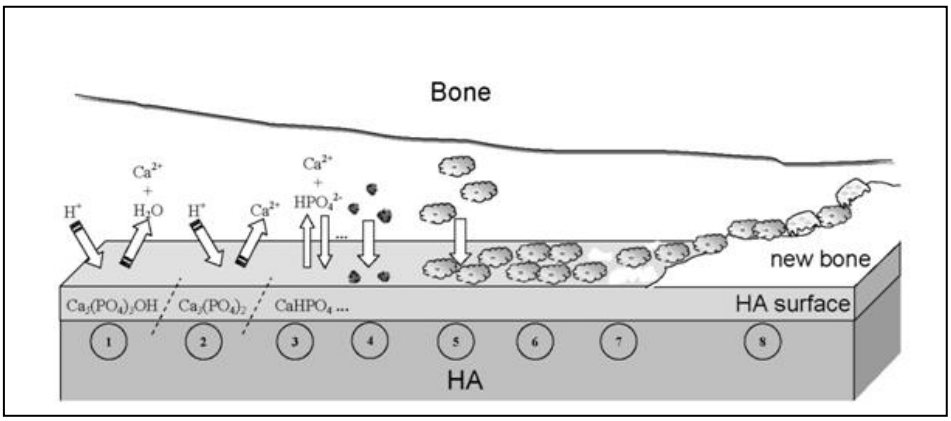

Fig. 1.5 Schematic diagram of the bonding mechanism for HA [10].

The bonding mechanism of calcium phosphate to living tissue involves a sequence of eight different steps as shown in Fig. 1.5 for an HA graft and they are:

- beginning of the implant procedure, where a solubilization of the HA surface starts;
- continuation of the solubilization of the HA surface;
- the equilibrium between the physiological solutions and the modified surface of HA has been achieved (changes in the surface composition of HA does not mean that a new phase of DCPA or DCPD forms on the surface);
- adsorption of proteins and/or other bioorganic compounds;
- cell adhesion;
- cell proliferation;
- beginning of a new bone formation;
- new formed bone .

Between the bone graft and bone an intermediate a thick layer of fibrous tissue has never been detected. CaP granules in different form display the ability to directly bond to bone [33][34][35].

Test *in vivo* are useful also for understanding how the morphological and mechanical properties of the same material influence the performance of bone graft. Biomaterials for bone substitutes can be tested in different shape: cylinder, cube, disc, rod, paste or block. Implant size should be taken in consideration when discussing animal model dependent differences in osteoconductive potential of biomaterials. In vivo test has to simulate much as possible the final application, even if a real application is confirmed by only clinical used. For example specific properties of the granule bone substitute can be tested as the pore dimension [36][37], granulometry [38],[39], micro- or macro-porosity [40] and the combination with other materials [41].

In vivo studies included differ in animal models, implantation site, latest explantation times; despite these differences many studies attest the biocompatibility and the bioactivity of CaP materials and they prove the osteoconductive properties and the osteointegration potential of CaP class.

Distinct animal models have been proposed to understand the CaP granules performance and they differ by the dimension and by metabolism of the animal chosen: rat [20], rabbit [42], sheep[43], dog [44] or more models in the same study [45]. Comparison of different materials implanted in distinct group of animal has to take in account the individual genetic and some characteristics as sex, age, weight and strain.

Bones used for the test are usually long bone as femur [46] or tibiae [47] to use drilling distinct sites in the same animal. Considering the ethical aspects related to in vivo tests and since CaP granules are commonly known implant materials, a particular attention has been used in the design of the study in order to use the fewer animals as possible.

Explantation time is chosen on expected resorption time of the biomaterial in vivo. The time is an important factor because for evaluating the performance and adverse reaction and depends also by the animal model. The methabolism of the rat cannot be comparable with that of sheep; the bone formation and implant resorption has to be different.

For *in vivo* experiments evaluation the more extensive method used is the histological analysis that permits to understand the quality and quantity of newly formed bone and also the mechanism of osteconduction. Presence of inflammatory signs, such as monocytes, mono- and multi- nucleated-macrophages, lymphocytes or fibrous tissue could indicate if and how the

immune system contributes to the mechanism of bone formation by biomaterials. Histological analyses are in 2D and depends on the position at which a section is made; for this reason an additional analysis using a X-ray microcomputed tomography (μCT) can help to quantify the volume of both ceramic material and mineralized bone as in other studies [35][41].

Dissolution is a physical chemistry process, which is controlled by some factors, such as solubility of the implant matrix, surface area to volume ratio, local acidity, fluid convection and temperature. In general, dissolution rates of calcium phosphates are inversely proportional to the Ca/P ratio, phase purity and crystalline size, as well as it is directly related to the porosity and surface area, CaP degrade in calcium and phosphorus.

The solubility of CaP materials is an important parameter to evaluate the degradability at 37°C at different pH because it has a role in the osteoconductivity [48].

Calcium phosphate are biocompatible and bioresorbable and the products of the degradation reaction change the inflammatory response, which influences the tissues regeneration progress [49].

Degradation of CaP occur by either physicochemical dissolution or cellular activity (so called, bioresorption), as well as by a combination of both processes [10].

Resorption is an important characteristic for biomaterials; it has a large influence on bone-bonding properties. Resorption characteristics must be considered from two viewpoints:

1. solution-mediated dissolution processes

2. cell-mediated (phagocytic and/or resorbable) processes, which are particularly important for bone-replacing materials.

It is biological process mediated by cells, mainly, osteoclasts and, in a lesser extent, macrophages. Osteoclasts attach firmly to the implant and dissolve calcium phosphates by secreting an enzyme carbonic anhydrase or any other acid, leading to a local pH drop to ~ 4–5. Furthermore, small particles of calcium orthophosphate can also be phagocytosed by osteoclasts, i.e. they are incorporated into cytoplasm and thereafter dissolved by acid attack and/or enzymatic processes. In any case, biodegradation of calcium phosphates is a combination of various non-equilibrium processes, occurring simultaneously and/or in competition with each other.

Depending on characteristics by many factors: specific surface area [50][30] the ionic substitution and crystallinity [51],chemical composition [52], size, microstructure, pore content and distribution [53], the tissue response and the resorption could be different. In addition to above mentioned factors also clinical factors like defect size and localization, the general health situation, and age of the patient play a role

For example comparing inert biomaterial as alumina with bioactive bioceramics as HA and Bioglass at same grain size, the tissue bone response in femur rabbit is totally different [38]. There was no contact between trabecular bone for alumina; new bone bound directly to the HA granules and faster bone ingrowth around Bioglass granules and much denser (Fig. 1.6).

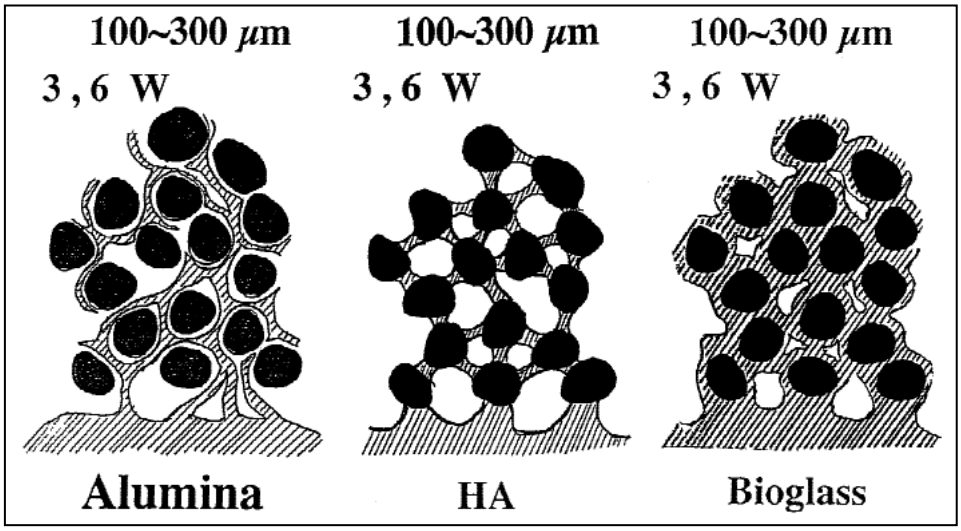

Fig. 1.6 Representation of tissue response of different materials [38].

In the case of βTCP, αTCP granules were taken in the trabecular bone and the size diminished with time, but the shape was retained. For TTCP (or TeCP), new trabecular bone was formed around granules that became smaller with time as new formed bone. The original shape is not maintained and granules became indistinguishable from the surrounding bone (Fig. 1.7) Also granules 10 μm were tested; in the case of HA the particle size must > 10 μm for bone augmentation; βTCP and αTCP stimulated new bone formation but the bone ingrowth was seen only at the periphery of the total mass; TTCP powders were being gradually incorporated in the trabecular bone surrounding the mass and were replaced by new bone. This work demonstrated how the properties of the material can influence the resorption mechanism and the subsequent bone ingrowth.

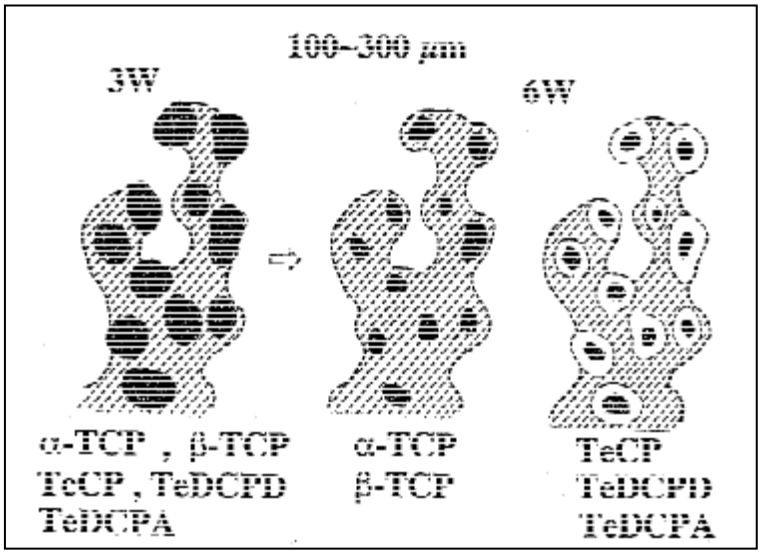

Fig. 1.7 Representation of tissue response of different materials [38].

Bioactivity: Bioactive material interacts with surrounding bone generally resulting in formation of a chemical bond to this tissue (bone bonding) and is "one which has been designed to induce specific biological activity". The bioactivity phenomenon is determined by both chemical factors, such as crystal phases and molecular structures of a biomaterial, and physical factors, such as surface roughness and porosity. The bioactivity test *in vitro* is useful for the first evaluation of the material capacity in apatite forming when a particular product is immersed in simulated body fluid (SBF) and was proposed for the first time by Kokubo in 1991. [54] This test was chosen for a brief evaluation of CaP products capacity to produce a Ca-P precipitate layer on the surface. From different study the bioactivity method is not best way for evaluating the ability of apatite formation in sintered ceramic as HA or βTCP

[55] This method is useful prior to doing in vivo bone bioactivity experiments and can significantly reduce the number of animals needed for in vivo evaluation. Moreover in vitro immersion study can simplify the complicated interaction of many factors in vivo to study single factor's contribution to bone-like apatite formation on calcium phosphate ceramics and so as to explore the mechanism of osteoinduction. Other methods to see the effect of ceramics on osteogenic differentiation using cell experiments are certainly more accurate. A large part of the scientific community has accepted the paradigm that in vitro cell testing can be used to test the in vitro bioactivity of bioceramics. This method has been widely used in testing the bioactivity of bioceramics.

Crystallization of apatite happens because the SBF solution is supersaturated; in fact the system is metastable and will become thermodynamically stable by forming apatite crystals. The induction or nucleation time depends on the rate at forming crystal nuclei large enough to be thermodynamically stable and hence large enough to grow. Bioactive is a material that accelerates heterogeneous apatite crystallization in a solution supersaturated towards HA. This can be achieved by several strategies:

- providing apatite nuclei that remove the need to nucleate apatite crystals,
- providing a surface with a low interfacial energy with apatite,
- changing the local supersaturation towards apatite precipitation.

Another way to modify locally the saturation and solution composition is to use a material soluble in SBF that can release large quantities of calcium and/or phosphate ions.

Different materials developed in this study have been already tested in vitro by immersion in SBF solutions. Calcium phosphate ceramics can be characterized by the time to new phase formation in vitro; the minimum time for measurable precipitate formation was found to increase in the order: not-well-crystallized HA < well-crystallized HA < alpha-TCP, TTCP<beta-TCP. For example HA granules show the capability to promote the precipitation of new calcium phases after soaking for 7 days into SBF solutions. Besides the major species HA and TCP, minor phosphate phases such as OCP, CaO, $Ca_2P_2O_7$, and $CaHPO_4$ strongly contribute to the dissolution behavior of the granule and to the precipitation of the new calcium phosphates [56]. HA/βTCP smooth dense ceramics surface immersed in static SBF do not show any detectable apatite layer on the surface instead of product with rough surface where local concentration of Ca and P is higher and precipitation is faster [57]; it has been demonstrated that the surface is important on SBF test. Other bioactivity test conducted in the SBF for 1 week showed that flake-like tiny carbonate apatite crystals on HA/βTCP granules (confirmed by FT-IR) were observed to form evenly on the two bicalcium phosphates but not on the pure HA [58]. Another test on biphasic calcium phosphate (60%HA and 40% β-TCP) was performed and after two weeks in SBF immersion needlelike crystals of apatite were present on the surface [59]. Sintered β-TCP ceramics exhibit a poor ability of inducing apatite formation in comparison with other calcium phosphates as HA, HA/β-TCP or αTCP [60], even if it has also been widely considered to be bioactive.

1.4 Doped calcium phosphates

Biological apatites differ from stoichiometric HA in several respects, including non-stoichiometry, small crystal dimensions and low degree of structural order. Biological apatites are indeed carbonated apatites, and they contain significant amounts of further foreign ions, either incorporated in the apatite crystal lattice or just adsorbed on the crystal surface. The mineral phases of bone, enamel and dentin exhibit slightly different ionic composition (Table 1.7). Nucleation and growth of CaP in biological systems occur in an environment rich in ions, which can affect both the kinetics and the thermodynamics of crystallization, and then the relative stability of calcium phosphates [61]. In particular two types of ions have been taken in consideration: zinc and strontium in different studies.

	Enamel	Dentine	Bone
Ca (wt.%)[a]	37.6	40.3	36.6
P (wt.%)[a]	18.3	18.6	17.1
CO_2 (wt.%)[a]	3.0	4.8	4.8
Na (wt.%)[a]	0.70	0.1	1.0
K (wt.%)[a]	0.05	0.07	0.07
Mg (wt.%)[a]	0.2	1.1	0.6
Sr (wt.%)[a]	0.03	0.04	0.05
Cl (wt.%)[a]	0.4	0.27	0.1
F (wt.%)[a]	0.01	0.07	0.1
Zn (ppm)[b]	263	173	39[c]
Ba (ppm)[b]	125	129	
Fe (ppm)[b]	118	93	
Al (ppm)[b]	86	69	
Ag (ppm)[b]	0.6	2	
Cr (ppm)[b]	1	2	0.33[d]
Co (ppm)[b]	0.1	1	<0.025[d]
Sb (ppm)[b]	1	0.7	
Mn (ppm)[b]	0.6	0.6	0.17[d]
Au (ppm)[b]	0.1	0.07	
Br (ppm)[b]	34	114	
Si (ppm)			500[e]
Ca/P[a]	1.59	1.67	1.65

Table 1.7 Comparative of human enamel, dentine and bone [62]

Zinc is known to be an essential trace element for life. Zinc (Zn) is present in small amounts in the enamel of human teeth and bone. It is probably the most important element in medicine because of its role in as many as 200 enzymes. Elevated concentrations in areas of damaged tissues or inflammatory lesions could enhance the ATP-mediated response [63]. Zinc has multiple important functions in biological systems. It is a trace metal required for the activity of a large number of metalloenzymes, including those involved in nucleic acid and protein synthesis, cellular replication, immune function, and antioxidant systems.

Zinc is a constituent of various enzymes and proteins such as alkaline phosphatase, lactate dehydrogenase and carbonic anhydrase, steroid hormone receptors, and transcription factors [64].

Likewise, it is an important mineral in the normal growth and development of the skeletal system and its deficiency is associated with a decrease in bone density. Zinc content normally ranges between 0.012 and 0.025 wt.% in human bone. Zinc plays an important role in proliferative effects on osteoblastic cells apart from inhibiting osteoclastic resorption. HA doped with 5% mol of Zn dissolves more rapidly than pure HA or HA doped with low concentrations of Zn. Moreover, this concentration of Zn leads to the formation of a Ca-P layer which contains Mg [65].

Zn ion is one of the most effective of the simple metal ions in inhibiting HA crystal growth [66]. Nonetheless, it can be quantitatively incorporated into HA lattice by direct synthesis under mild conditions [67] and the substituting limit of Zn was estimated at about 15 mol% in Zn-substituted Ca hydroxyapatite [68].

The substitution for Ca ions occurs up to about 20 at.%, whereas the apatite structure does not sustain higher Zn incorporation. The decrease in the lattice parameters observed up to 10 at.% substitution is consistent with the smaller ionic radius of Zn^{2+}(0.75 Å) with respect to Ca^{2+} (0.99 Å).

A correct evaluation of cell parameters at relatively high Zn content is hindered by the progressive broadening of the XRD peaks due to the reduction of crystal sizes and/or the increase of crystal strain with increasing Zn concentration [66]. Chemical analysis indicates that both Ca/P and (Ca + Zn)/P ratios decrease on increasing Zn content and, as a consequence, stoichiometry is no longer maintained.

The loss in crystallinity is confirmed by scanning electron microscopy observations: apatite crystals display regular shapes, whereas the Zn-substituted apatite crystals are irregular and form agglomerates that grow in size with increasing Zn content. Zn exhibits an evident inhibitory role on the synthesis of HA through a reduction in crystallite size and a decrease in thermal stability [66].

The presence of Zn^{+2} at very low concentration incorporated into bioceramics has proven to have a significant effect on increasing the growth of bone cells. HA doped with 5 % at of Zn dissolves more rapidly than pure HA or HA doped with low concentrations of Zn. Moreover, this concentration of Zn leads to the formation of a Ca-P layer which contains Mg. This layer is created in a biological environment and represents bioactive properties of the bioceramic [69].

Zn-containing apatite has also been obtained after hydrolysis of Zn-containing α-TCP powders [70]. The starting material was obtained as a single phase

above 1300°C. The higher the heating temperature, the more Zn is incorporated into α-TCP, with a maximum Zn content of 1.26 wt%, obtained at 1450°C. Soaking of Zn-containing α-TCP powders for 12 h in water resulted in α-TCP conversion with almost complete transfer of Zn from α-TCP to the apatite structure.

In another study, TCP phases were formed in the ZnHAP ceramics when the zinc content rose to more than 0.13 wt%. A monophasic ZnHAP ceramic was obtained only when HAP with a zinc content of less than 0.13 wt-% was sintered from 1050 to 1150°C. The amount of TCP phases increased with increasing zinc content in ZnHAP. Zinc was incorporated in the HAP crystal lattice when the zinc content was less than 0.15 wt%. The presence of TCP phases was necessary for the release of zinc from ZnHAP ceramics to modulate cell proliferation and a zinc content exceeding the solid solution limit was required. The solid solution limit was estimated as 0.13 wt%, which is about 10 times higher than that in adult humans, but is much lower than that in β-ZnTCP (6.17 wt-%) and α-ZnTCP (more than 1.2 wt%). Without the TCP phases, ZnHAP ceramics did not influence MC3T3-E1 cell proliferation in vitro. The zinc concentration in a-MEM+10%FBS after the cytocompatibility test of the ZnHAP ceramics containing less than 0.13 wt-% Zn was almost the same as that before the test. ZnHAP ceramics containing more than 0.20 wt-% Zn influenced the proliferation of MC3T3-E1 cells. The relative cell growth rate on ZnHAP ceramics maximised at a zinc content of 0.34 wt-%. At a zinc content of more than 1.28 wt%, the ZnHAP ceramics showed cytotoxicity with a significant decrease in cell density. The ZnHAP ceramics containing 2.57 wt% Zn released zinc through the dissolution of zinc oxide in the culture

medium, resulting in the elevation of the zinc concentration to cytotoxic levels. [71]

Other limits of Zn content were found in other works. For example, in form of Zinc oxide, an amount of 1.5 wt% increases cell spreading and growth on the TCP surfaces and 3.5 wt% ZnO in TCP sample showed low cell density, poor cell adhesion and some cell death [72]. In the preparation of Zn-doped β-tricalcium phosphate bioceramics the Live/Dead counts were peaked for the 2900 ppm Zn-β-TCP samples, whereas the ALP (alkaline phosphatase) activity was found to be the highest (Fig. 1.8)[73].

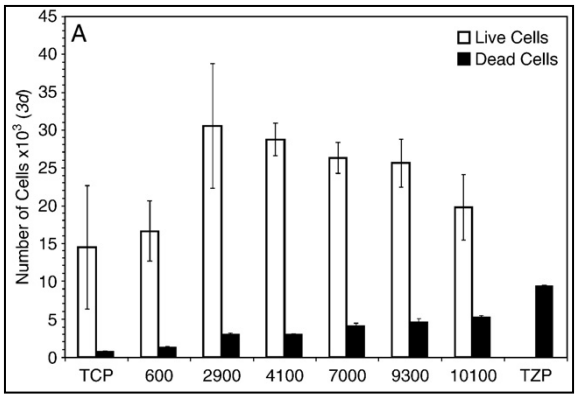

Fig. 1.8 Live/Dead cell in contact Zn-β-TCP samples with different content of Zn [ppm] [73].

MTT assay regarding cell proliferation of pure TCP, and with 0.25% ZnO and 0,25% ZnO-1% MgO dopants. The optical density is a representative of number of living cells on the substrate. It can be seen that both doped samples had significantly higher number of living cells compared with pure TCP, a good sign for cell proliferation [1].

Zn inhibits osteoclast differentiation and promotes osteoblast activity and thus promotes bone formation. Also ZnTCP/HAP with a zinc content of 1.2 wt% significantly increased osteoblastic MC3T3-E1 cell proliferation and alkaline phosphatase activity of rat stromal cells in vitro. ZnTCP/HAP with a zinc content of 0.316 wt.% increased bone formation by 51% in 4 weeks after implantation in rabbit compared to the control without zinc [74].

The effects of ZnO on the biological role of the cement in the present study have also become an important topic in the research field of bone formation recently. In the study, ZnO in the cement powder can react with water or acid inducing Zn release, which may help facilitate more rapid new bone formation and thus accelerate bone defect repair. The bone neoformation around the implant was prominent, and at 12 weeks after surgery the gap between the implant and host bone was almost completely filled with new bone [75].

The antimicrobial activity of zinc ions must be underline and follows three main mechanisms. First, metal ions bind to proteins deactivate them. Second, metal ions can interact with microbial membrane, which causes structural change and permeability. Finally, metal ions interact with microbial nucleic acids, preventing microbial replication [76].

Strontium: it is present in the mineral phase of bone, especially at the regions of high metabolic turnover [77], and its beneficial effect in the treatment of osteoporosis is well known and its administration as Sr ranelate has recently been shown to reduce the incidence of fracture in osteoporotic patients [78]. Sr ranelate decreases bone resorption by inhibition of osteoclast-resorbing activity and osteoclastic differentiation, and it promotes bone formation by

enhancing pre-osteoblastic cell replication and osteoblastic differentiation. The oral strontium salts have recently been used as a drug associated with treating osteoporosis. Local delivery of strontium with HA in cement has been shown to induce new bone formation and effective in reducing fracture risk in osteoporosis.

Sr (ionic radius 1.20 Å) can replace Ca (ionic radius 0.99 Å) in the structure of HA over the whole range of composition, causing a linear expansion of the lattice constants. A detailed structural and morphological investigation carried out on HAs precipitated from aqueous solutions at different Sr concentrations demonstrated that relatively low Sr replacement of Ca induces a decrease in the coherent length of the perfect crystalline domains and disturbs the shape of the crystals, whereas the crystallinity, as well as the mean dimensions of the crystals, significantly increase at relatively high Sr content [79].

Destabilization of crystal structure by the larger Sr atom has been invoked to justify the significant increase in solubility with Sr content verified by solid titration of Sr-substituted HA [80]. The increased solubility is further confirmed by the greater release of Ca in Hanks' balanced synthetic fluid from Sr-substituted HA than from HA granules [81]. Moreover, the extent of precipitation from simulated body fluid (SBF) and from a CaP supersaturated solution has been reported to decrease on increasing Sr content in solution [82]. The incorporation of low-dose strontium introduces more lattice distortions into the structure of hydroxyapatite and thus increases its solubility. The dissolution of Sr-HA results in the release Ca^{2+}, which increases the ionic activity product of the apatite in surrounding fluid, and thus readily induces apatite precipitation [83].

In vitro tests on as-prepared materials have been performed only on Sr-substituted HAs [84]. The results of the investigation carried out that Sr substitution for Ca into hydroxyapatite up to about 7 atom % has a beneficial effect on bone cells. Sr concentrations in the range of 3–7 atom % significantly stimulate osteoblast activity and differentiation, as shown by the increased production of ALP, CICP (I C-terminal collagen propeptide), and OC (osteocalcin) with respect to both pure HA and the sample at smaller Sr content.

Sr was added to the culture medium at concentrations of 0, 0.5, 1.0, 2.0, 5.0, 20, and 100 μg/mL Compared to the control group (0 μg/mL Sr), a significantly reduced nodule formation in the presence of an intact mineralization was found for the lowest 0.5 and 1 μg/mL Sr doses, suggesting an impaired in vitro osteoblast differentiation. Both nodule formation and mineralization were normal for the 2 and 5 μg/mL doses. For the highest Sr doses (20 and 100 μg/mL) a reduced mineralization was observed in the presence of an intact nodule formation indicating an inhibitory effect on the hydroxyapatite formation [85].

In a recent in vitro experiment using primary osteoblasts isolated from fetal rat calvaria, it was also observed a complex multiphasic effect of strontium. Indeed, at low doses (1.0 μg/ml Sr in the culture medium) a reduced nodule formation was noticed in the presence of an intact mineralization; at intermediate concentrations (5μg/ml) no effect was seen; at high concentrations (20‑100 μg/ml) an intact nodule formation was accompanied by a reduced mineralization. These results suggest an effect of the element at

the level of cell function/differentiation at low doses and a physicochemical interference with the hydroxyapatite formation at high doses [86].

1.5 Calcium phosphate bone grafts

Calcium phosphates are proposed in many forms and compositions to satisfy as much as possible all application of dentistry and orthopedics area where necessaries are the bone repair or replacement. Bulk materials are available in dense or porous form and in spite of the important mechanical limitation; calcium phosphates are made in various physical forms: powders, particles, granules, dense blocks, porous scaffolds, self-setting formulations, implant coating and composite component of different origin (natural, biologic or synthetic). Bone grafts are also proposed as non-hardening pastes (=putty), a combination of CaP powders or granules with a glue, typically a highly viscous hydrogel. Table 1.8 shows main forms of CaP bone graft developed and used in medicine.

Form	Defect form	Mechanical stability	Resorption / bone formation	Handling
Granules (0.1 – 5 mm in diameter)	Open	Negligible	Throughout the defect	Fair (granule migration during and after surgery)
Macroporous blocks	Open and defined shape	Fair provided there is press-fitting into the defect	Throughout the defect	Very good (problems might arise to fit the block within the defect)
Cement paste	Closed	Fair	Peripheral	Fair to good (the paste might set too fast or might be poorly injectable)
Putty	Open or closed	Negligible	Peripheral or throughout the defect depending on the composition	Very good for pastes that have to be mixed in the operating room to excellent for ready-mixed pastes (the paste might be poorly-injectable)

Table 1.8 Forms of CaP materials used as bone graft [10].

The bone graft shape is also customized like wedges for tibial opening osteotomy or cones for spine and knee.

CaP granules are used for open defect, where is not necessary a mechanical stability, in fact they are proposed for no-load bearing applications. Bone graft resorption has to follow by the bone formation throughout the defect. Commercial granules are available in the range 0.1-5 mm.

CaP scaffold or macroporous blocks have a more defined shape than granules and they possess big macroporosity (typical range 50-500 μm) that has a big role in osteconductivity mechanisms. It is impossible to achieve the same macroporosity in granules form, because the granules size is equivalent to macropres size. Scaffolds have to be fixed into the open defect that is bigger than in the granules case and for the correct adaption to the implantation site they must to be drilled and cut for screw insertion.

Another problem relating to these bone substitutes include the inability to shape them in situ in the operating theatre, so that they must be used in the

form of granules or blocks with the possible associated problems of lack of mechanical integrity due to their migration away from the implant site. In contrast, calcium phosphate cements (CPCs) can self-set in the bone cavity without machining. The CPC powder can be mixed with an aqueous liquid to form a paste that can be placed in the bone cavity to form hydroxyapatite. Due to its excellent osteoconductivity and bone replacement capability, CPC is highly promising for clinical applications. However, the drawbacks of CPC, including the lack of macroporosity for bone ingrowth, low strength and poor injectability have limited its clinical use [87].

Putties do not need to support load, in fact mechanical properties might be negligible. Moreover their injectability is not comparable with cements, because they can be used only for open defect. The must has to be the easy handling in surgical procedure, putties has to be ready to use in few steps.

1.6 Calcium phosphate granules

The attention of some groups of researchers has focused on porous calcium phosphate ceramic granules which are used widely as filler or packing materials.

The different forms of granular calcium phosphate include irregular multifaceted granules and round smooth granules, with solid or porous structures. However, the behavior of granules in the body depends on their morphology and microstructure.

1.6.1 Applications

Different authors intended to propose a method for preparing granulates with different dimensions and varying pore size distribution, made from hydroxyapatite (HA) and designed for a wide range of medical applications, such as products for osteosynthesis, fillers, cosmetic restoring, drug dispensers, restoring of bone parts and liquid drainers [88]. The particulate form of ceramic materials finds various in medical applications. Dense and porous HA of different sizes have been used for the reconstruction of various bone and dental defects such as cystic defects, periodontal pockets, surgical bone defects and resorption of alveolar ridge. Other biomedical applications could be as fillers, delivery of antibiotics and macromolecules or contraceptives, and as a matrix for haemoperfusion or high performance liquid chromatography (HPLC) and as delivery of macromolecular drugs, human serum albumin protein [89].

BCP ceramic microspheres can also used as drug delivery carriers, for example for doxycycline release thanks to interconnected microporosity [90].

Examples of the use of CaP as bone filler and for bone augmentation in dental, maxillofacial and orthopedics field are reported in Table 1.9 with its specific applications.

Biomedical field	Specific application
Dental	Filling of cysts [91]
	Reconstruction of alveolar defects [91]
	Sinus floor elevation [91][92][93][94][95][96]
	Alveolar ridge augmentation [91]
	Periodontal defects [91]
	Implant bed preparation [91]
Orthopedic	Hip re-endoprosthesis [97]
	Reconstructive surgery of the jaws [98] [99]
	Total hip replacement [100]
	Treatment of cancellous impaction fractures [101][102]
	Scoliosis surgery [103]
	Spinal surgery [104]

Table 1.9 List of specific applications of granules.

1.6.2 Properties

Granulometry/Size: pharmaceutical granules typically assume sizes between 0.2 and 4.0 mm, and in orthopedic surgery granules between 1 and 2 mm, whereas in periodontal surgery granule sizes of 0.25–1 mm are preferred. Particles with smaller diameter are fully resorbed and cannot act as a substrate for upregulation of mesenchymal cells. Granules under 50 μm in size implanted in bone were phagocytosed by macrophages which then were activated so that bone resorption was stimulated [105]. The proposed range of

size has to kept large because smaller particles tend to obstruct the spaces among the larger particles, thus reducing vascularization [106].

Morphology: although easy to prepare, particles, obtained by crushing of porous blocks, pose some acute problems because their irregular shape. Particles of irregular shape packed poorly in columns and created large voids that robbed the systems of their efficiency and sharp edges of the particles fractured easily, clogging the systems [107]. Spherical granules have greater flexibility in filling irregular geometry and can be packed closer than irregular one [108].

Porosity: the important feature in the physical structure of a synthetic ceramic is its porosity. Pore size, volume of porosity and interconnections between the pores are three crucial parameters. Pore structure is of great importance for osteoconduction. The level of porosity, pore size distribution and degree of pore interconnectivity significantly influence the extent of bone ingrowth [37]. Pore size must exceed 100 μm to allow new bone ingrowth [109]. For obtaining a a bimodal pore-size distribution, composite granules made of hydroxyapatite (HA) and a biopolymer can be and then calcined (Fig. 1.9). Calcination, by which the biopolymer material is burnt out, caused the buildup of narrow pores (intrapores) in the granules, and the stacked arrangement of granules provided conditions for the occurrence of intergranular communicating pores (interpores)[110].

Aggregates: agglomeration of granules can be an alternative for controlling the intergranular pores dimension that does not depend by the surgical procedure, but it built up during the production process. Some studies presented this type of product, αTCP spherical agglomerated adding a

colloidal silica by spray pyrolysis technique and conversion of αTCP into HA in SBF were obtained. The presence of the silica, however, gets dirty the CaP material [111]. Calcium phosphate agglomerates were also made by spray-pyrolysis in combination freeze-drying technique [112]. In both cases the aggregates size was around 1-10 μm, too small as bone filler applications.

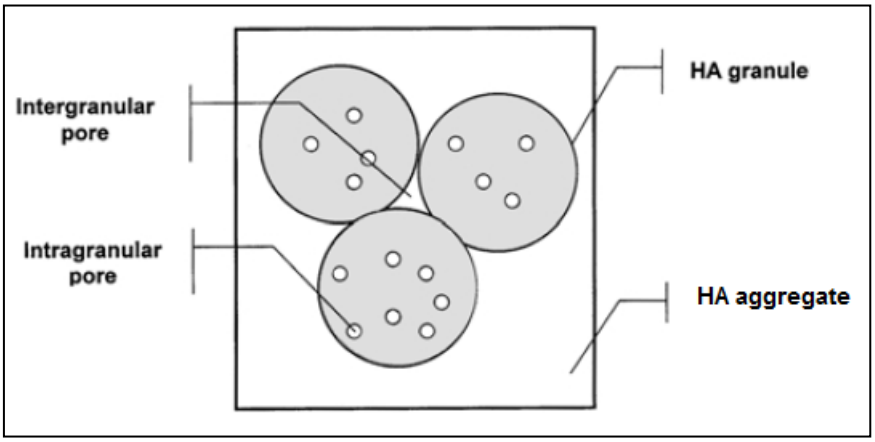

Fig. 1.9 Bimodal pore distribution: intergranular pore and intragranular pore. Adapted from [50].

Aggregates could have 3 level of porosity: the granules microporosity, the macroporosity that are formed between the granules sintered together to form the aggregates and the macroporosity that are formed between the aggregates while there are stacked together inside a bone cavity. Granules instead present only the first two porosity level.

Microporosity: bone structure is oriented according to physiological needs with interlinked tunnels, of non-uniform shape and width, whose boundaries are the trabeculae. The granulate model for bone simulation should also have microchannels (which in dentine and bone show identical extension of 1-2

μm), which play an active role in cellular attraction processes on the surfaces [88].

Bioceramic microporosity (pore size < 10 μm), which is defined by its capacity to be impregnated by biological fluids, results from the sintering process, while the pore dimensions mainly depend on the material composition, thermal cycle and sintering time.

Microporosity is an important parameter to achieve bioresorption an high osteogenic property; osteconduction may be associated to the microporosity [113]. The micropores in the macropore surface enlarged greatly the surface area for protein adsorption, more proteins could be absorbed on the surface; the larger surface area could also facilitate ion exchanges and bone-like apatite surface formation by dissolution and re-precipitation process [113]. Microporous granules favor the body fluid and blood circulation, which supply nutrients and mineral ions for the bone regeneration [114].The interconnected micropores could also provide a suitable microenvironment for cell differentiation and bone matrix deposition [113]. The microporosity provides both a greater surface area for protein adsorption and increased ionic solubility. For example, embedded osteocytes distributed throughout microporous rods might form a mechanosensory network, which would not be possible in scaffolds without microporosity. Hydroxyapatite ceramic granules with micropores on their surface can induce bone formation under skin of dogs, but no bone formation was induced by hydroxyapatite ceramic granule without micropores [113]. Differences in porogens influence the macroporosity, while differences in sintering temperatures and conditions affect the percentage of microporosity. Usually, the higher is the sintering

temperature, the lower both the microporosity content and the specific surface area of bioceramics.

Macroporosity: the presence of macrostructural features, such as macropores, channels or void between particles has been shown to be a prerequisite for osteoinduction by synthetic biomaterials [48]. The macroporosity is not an intrinsic property of CaP granules, but represent the void space between granules. However a vigorous packing (finger-packing increase density) is likely to increase resorption times of the bone void filler with βTCP granules [102]. An excessive packaging limits the porous structure, the bone graft integration and the nutrients supply. Some models are proposed to calculate the macroporosity between spherical granules. The intergranular porosity is closely associated with the manner in which spherical granules are packed. Monodisperse granules can be loosely packed in a raw specimen containing 30 – 40 vol. % of intergranular pores. This kind of packing roughly corresponds to a coordination number 7 (Eq.3).

$$N = 11.6\ (1 - Po) \qquad (3)$$

where Po is the volume fraction of open pores. This value is close to the coordination packing number of atoms in a body-centered cubic lattice. The least-area cross-section through pore space for packed monodisperse spherical granules may be conceived of as corresponding to the (100) plane of a body-centered cubic structure.

For monodisperse granules of size 500 μm thus patterned, the least-area cross-section through pore space is roughly 100-200 μm, which conforms with

the require requirement of a minimum pore size of 100– 135 mm needed for osteointegration [110].

1.6.3 Production methods

Granulation, as it is understood and commonly used in the pharmaceutical industry, is the process in which powder particles are made to adhere (with the help of a binder that locks the powders together as granules and prevents disintegration) to form larger entities called granules.

Therefore, it would not have been unusual to inspire from the granulation processes and procedures of pharmaceutical industry to produce CaP granules for skeletal repair and biomedical applications.

Pharmaceutical industry typically uses planetary mixers, fluidized-bed granulators, spheronizers, rotors, extruders and pelletizers in forming granules from wet masses containing the desired ingredients. However, sieving (or screening), in pharmaceutical granulation technology, is only regarded as a secondary tool of transforming the as-formed granules into monosized granules.

Drip casting method was used by Liu to produce HA granules starting from slurry of polyvinyl-butyral added to CaP powder. A plaster mould was prepared with design cavities in a semispherical geometry where the slurry is cast by dripping through a pipette device. After drying and sintering, spherical granules were obtained [114]. HA granules can be fabricated based by liquids immiscibility effect using the HA/gelatin suspension and oil as liquids [115]. Hydrothermal method was introduced by Ioku at al., for preparation of HA

granules from a mixture of α-TCP powder and gelatin that after drying and sintering steps are to exposed to high water pressure vapor where the transformation of α-TCP into hardener HA happens [116].

Spherical microspheres were obtained starting from a suspension of 2.5 % of chitosan, paraffin and HA. The dispersion was stirred in stainless steel half–moon paddle. The crosslinking of chitosan in the emulsion with glutaraldeheyde resulted in HA filled chitosan microspheres that were treated at high temperature to burn out the binder and obtain microstructured HA particles were produced [107]. This method was used also by Paul and Sharma for HA granules for protein delivery [89], but it is difficult to control the crosslinking density of structure as in biopolymers.

The HA/biopolymer granules were prepared using the effect of immiscible fluids. A suspension of hydroxyapatite in an aqueous solution of biopolymer was dispersed in a water-immiscible fluid using a blade agitator rotated at a speed of 200 to 500 rpm. Granules of nearly perfect spherical shape were formed under the action of surface tension forces. The granule size can be varied depending on the suspension concentration, dispersion fluid temperature, and agitator speed. The granules were filtered on a Büchner funnel, washed, and dried [110].

BCP (HA and βTCP) microspheres as drug release carrier are made with this method An appropriate suspension of gelatin and fine BCP powder was dispersed in light paraffin oil in an analytical flask by stirring with a glass paddle stirrer. The precipitated microspheres were washed in acetone followed by ethanol and dried in air. The gelatin bound beads were heated for an hour at 550 °C to burn off the gelatin and sintered at 950 °C in air to

strengthen the microspheres. The microspheres were then thoroughly washed in distilled water to remove any unburned gelatin and dried in an oven [90].

More interconnected HA/TCP granules were produced by crushing porous block produced by sponge method [117]. Different shape and size (2-18 mm) can be reproduced very easily but the presence of edge and the high content of porosity decrease the mechanical properties and the handling during the surgical procedure.

Non-stoichiometric HA granules were proposed by Zyman and were produced by spinning a paste (HA and polystyrene) between two parallel plane disc, which have one axe, but rotated in opposite directions. This technique is useful for producing big granules, until up of 6 mm [97]

Kawai et al. used the spray granulation process to produce only microsized CaP granules, which were too small to be handled by the orthopedic or periodontal surgeon [118].

Tas proposed for the first time a method to produce HA granules without any sintering process or high temperature calcinations to develop their handling strength. He mixed together cement powder and NaCl and passing through an aqueous solution of $NaHPO_4$ he produced dried granules. The granules of carbonated and Ca-deficient Ap-CaP stoichiometry were formed and in situ hardened at the ambient temperature by the cement setting reaction. After leaching out the NaCl porogen in water, CaP porous spheres were obtained [119].

1.7 Droplet extrusion

All methods presented for producing CaP granules are valid and have been achieved all targets about morphology, composition and microporosity using different techniques, but one method proposed first for drug delivery microcapsules and modified for CaP granules by the Portuguese research group of INEB was considered suitable for this study and was developed and applied on all products. The method is called “Droplet extrusion”.

This method is based on the gelification mechanism that involves natural polysaccharide. The need was to find a system to produce natural hydrogel for use as potential carriers in controlled drug delivery. Hydrogels are three dimensional, hydrophilic networks capable of imbibing large amount of water or biological fluids, mimics biological tissue. Microencapsulation has become a common technique in the production of controlled release dosage forms. The polymeric gel beads are prepared by using number of natural, biodegradable polymers. Much research efforts have been concentrated on the development of hydrogel beads using natural polymers as they are derived from natural sources, do not require organic solvents (toxic), easily available and qualified for a number of chemical modifications. Polyelectrolyte polymers are utilized in the preparation of hydrogel matrix beads, the most used are alginate and chitosan, but also gellam gum and carboxymethyl cellulose have been applied.

Alginate: it is a non-toxic, biodegradable, naturally occurring polysaccharide obtained from marine brown algae, certain species of bacteria. Sodium alginate is a sodium salt of alginic acid a natural polysaccharide and a linear

polymer composed of 1,4-linked β-D-Mannuronic acid (M) and α-D-gluronic acid (G) residues in varying proportions and arrangements. The homopolymer regions composed of M-blocks and G-blocks are interspersed with M-G heteropolymeric regions known as "egg box junction" (Fig. 1.10) [120].

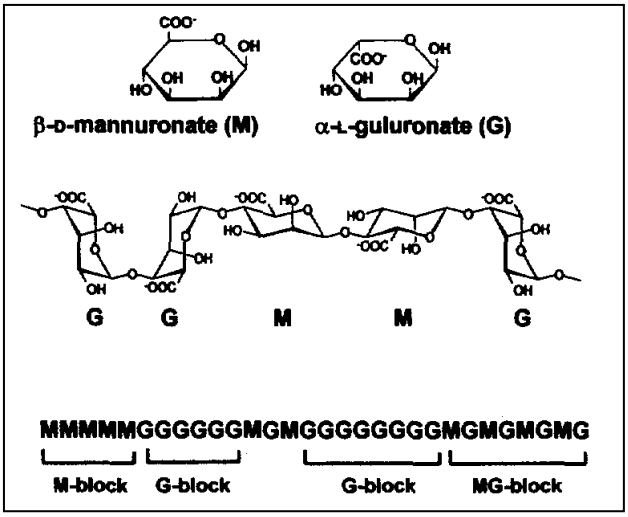

Fig. 1.10 Alginate structure [121].

Chitosan: it is a deacetylated derivative of chitin. Actually, the hetero-polymer is constituted of glucosamine and acetyl-glucosamine units (Fig. 1.11). Their relative proportion fixes the degree of acetylation (DA) that controls many properties of the polymer: its acid–base properties and its solubility [122]. The protonation of amine groups causes the polymer to dissolve in acidic solutions. Another consequence of amine group protonation is a decrease in the sorption of metal cations in acidic solutions due to the competition of protons and metal cations for interaction with amine groups. Another

important characteristic of chitosan is the molecular weight influencing the polymer's solubility and viscosity in solution.

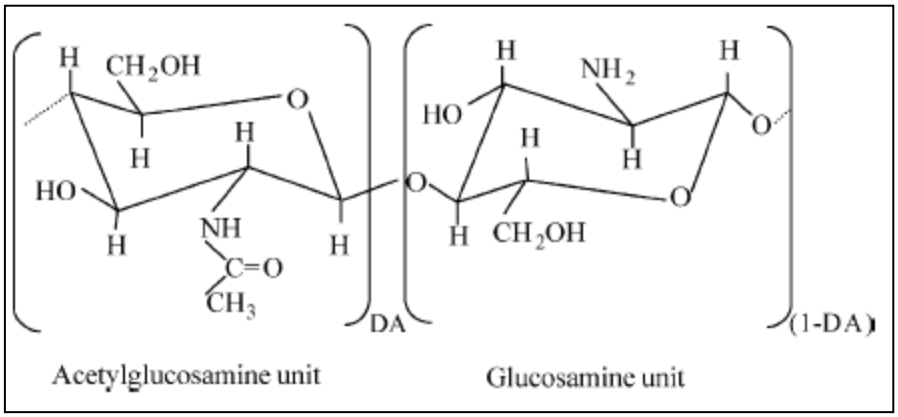

Fig. 1.11 Chitosan structure [122].

Ionotropic gelation: sodium alginate is soluble in water and form a reticulated structure which can be cross-linked with divalent or polyvalent cations to form insoluble meshwork. Calcium and zinc cations have been reported for cross-linking of acid groups of alginate. Alginate appeared to be highly promising owing to its non-toxic, biodegradable and biocompatible nature. Divalent ions (Ca^{2+}, Ba^{2+}, Cu^{2+}, Sr^{2+}, Zn^{2+}) are chelated by carboxyl groups of guluronic acid (GG) and ion-alginate gel is instantaneously formed (Fig. 1.12).

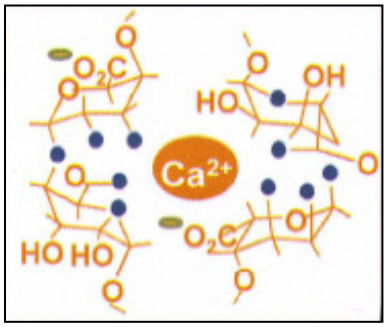

Fig. 1.12 Ionotropic gelation mechanism between acid guluronic chains and Ca^{2+}.

The ionotropic gelation occurs at room temperature and pH 7. The gel density depends by ions concentration in crosslinking solution and by hardening time. An ionotropic gel can be also produced in a process of physical cross-linking between a polycationic (in this case a polyelectrolyte) and a polyanionic (in this case a multi-charged ion) component [123]. The ionotropic complexation is a mild method and does not require organic solvents or toxic cross-linking reagents. It is imperative to maintain a pH value lower than 5 in order to have a chitosan fully protonated, on the contrary pH of 3 is the minimum value for the TPP to possess three charges (Fig. 1.13). Therefore, the complexation between chitosan and TPP and the resultant crosslinking density is pH dependent, since their charge density depend on pH values [124]; for an acceptable and stable complexation the values must range between 3 and 5.5.

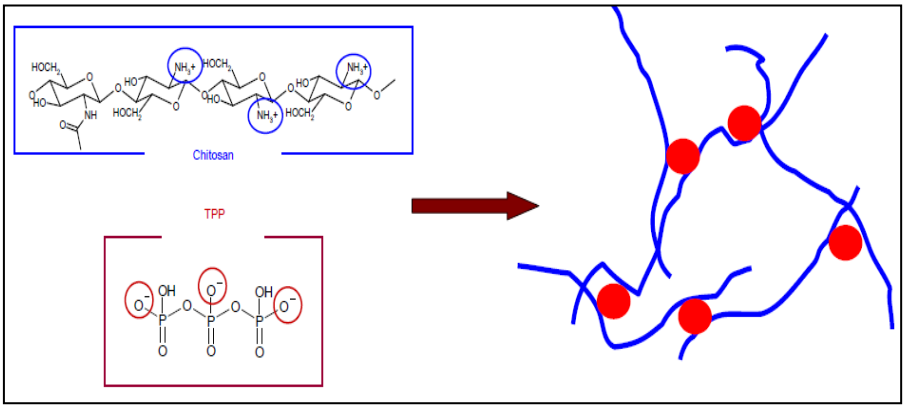

Fig. 1.13 Ionotropic complexation between the free charged ammines and the three negative charges of the TPP [125].

Polyelectrolyte complexation: chitosan-polyanions complexes have been widely investigated for applications like drug and protein delivery, cell transplantation, enzyme immobilization. Among these, complexes, chitosan-alginate complex may be the most important drug delivery hydrogel system.

The strong electrostatic interaction of amine groups of chitosan with the carboxyl groups of alginate lead to the formation of chitosan-alginate complex (Fig. 1.14). The chitosan-alginate gel beads with a chitosan core and a chitosan-alginate skin are prepared by dropping a solution of alginate into chitosan solution. Due to the protonation of amino group on chitosan and the ionization of carboxylic acid group on alginate, the stability of chitosan influenced by the environmental parameters such as pH and ionic strength. It was found that the macromolecular chitosan rapidly bind onto the surface of alginate droplet, but were limited to diffuse into the inner core. In order to increase the stability of chitosan-alginate complex, chitosan solution,

consisting of calcium chloride was used for the gelation of alginate. The presence of calcium ions in the chitosan solution during the incubation had a great effect on the ability of a gel bead to bind chitosan. As the concentration of calcium chloride increases, the rate and extent of chitosan binding process also proportionally increases [120].

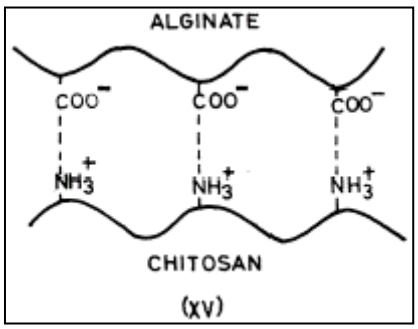

Fig. 1.14 Polyelectrolyte complexation between alginate and chitosan [126].

Different technologies were proposed for automate the beads production and for up-scale to an industrial application. All available methods are showed in Fig. 1.15 and they are: coaxial air flow, electrostatic, vibration and jet-cutter by simple cutting mode or soft landing mode.

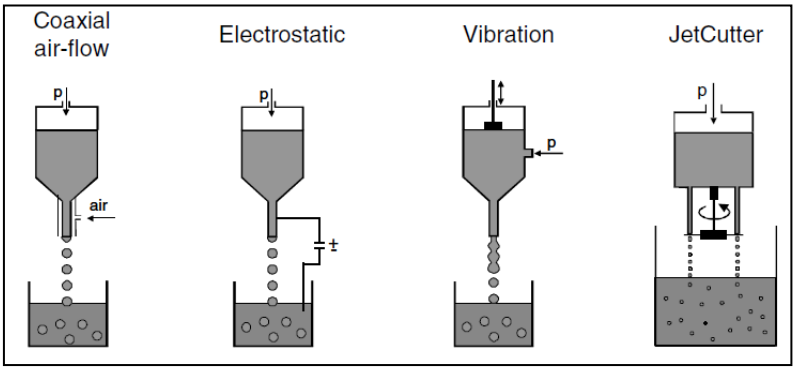

Fig. 1.15 Schemes of different technologies used in production beads [127].

1.7.1 Droplet extrusion adapted to CaP granules

The first publications about droplet extrusion method applied for production of calcium phosphate microspheres are presented by Ribeiro at al. in 2003. They were about a novel route to for the preparation of injectable ceramic porous microspheres for bone tissue engineering using the droplet extrusion method. HA powder was mixed with sodium alginate solution (3% w/v) at a ratio of 0.2 w/w and well homogenised. The paste was extruded drop-wise into a 0.1M $CaCl_2$ crosslinking solution, where spherical-shaped particles instantaneously formed and were allowed to harden for 30 min. The size of the microspheres was controlled by regulating the extrusion flow rate using a syringe pump and by applying a coaxial air stream (Encapsulation Unit Var J1, Nisco). At completion of the gelling period, microspheres were recovered and rinsed in water in order to remove the excess $CaCl_2$. Finally, they were dried overnight in a vacuum-oven at 30ºC, and then sintered at 1100ºC for 1h, with a uniform heating rate of 5ºC/min from room temperature. Ribeiro at al. [128]

introduced the droplet extrusion method for the production of CaP/alginate microspheres also as enzyme delivery matrices. He underlined the differences between this method and compared techniques for producing ceramic-polymer microspheres [108]. This process presents the advantage of being simple, it is performed at room temperature and in the absence of organic solvent, which makes it suitable for enzyme drug carrier. The spherical particles can be easily obtained without the need of fastidious washing processes and present a very narrow size distribution even without subsequent sieving procedures. They combine alginate with hydroxyapatite powder in different concentration of polymer and different ratio ceramic/polymer.

Ganja at al. [129] showed an interesting route to promote localized bone regeneration, especially with the incorporation of cells or cell-targeted molecules. Chitosan-HAp microspheres were prepared and characterized in terms of size, morphology, water sorption and structure an interesting route to promote localized bone regeneration, especially with the incorporation of cells or cell-targeted molecules. Chitosan-HAp porous microspheres were successfully prepared using tripolyphosphate (TPP) as coagulating agent. 1% (w/v) chitosan solutions in 1% (v/v) CH_3COOH were prepared. Composites were obtained by adding HAp powder (1 to 30% w/v) under stirring, until homogenization. After degassing under reduced pressure, beads were formed by dropping the mixture through a syringe into a 5% (w/v) sodium tripolyphosphate (TPP) solution. The size was controlled by applying a coaxial air stream. The microspheres were cured during 30 min, washed with water, frozen at -70ºC and lyophilized. The size increased and the water sorption

decreased with increasing HAp contents. The ceramic particles were well embedded and homogeneously distributed within the polymer matrix. A homogeneous distribution of the HAp particles within the polymeric matrix was observed, and the ceramic was well embedded in the chitosan matrix. Cross-sections of microspheres revealed considerable interconnectivity, as opposed to their surface.

Subsequent studies performed by Barrias at al. demonstrated that alginate/hydroxyapatite microspheres are able to support human osteoblastic cells adhesion and proliferation [23] and moreover a biological evaluation of calcium alginate microspheres as a vehicle for the localized delivery of a therapeutic enzyme and brought good results [130].

Alginate/HA microgranules for drug delivery were also produced by Krilova at al. in 2002 by using a modified technique with a rotator [131]. The concentration of HA was too low to considered the material only formed by calcium phosphate.

Ribeiro and its group in 2006 proposed the droplet extrusion method for producing microspheres for bone regeneration field [132]. The production technique was the same of previous work, but the target was different. Calcium titanium phosphate and hydroxyapatite were mixed with sodium alginate to produce spherical particles with uniform size that would lead to a regular inter-particle porosity, thus contributing to easier migration of bone cells. The sphericity and regular size would improve the injctability and the flowing properties, necessary in surgical procedure. Moreover Microspheres with different porosities may be produced by this method, by varying the granulometry of the ceramic powders. It was also found that the ratio between

the ceramic phases and the polymer solution is a critical parameter in the composition of the sintered microspheres and must be carefully selected.

Fu at al. [133] introduced a modified method to produce porous CaP bead for releasing an antibiotic was developed, based on an alginate gel form with calcium ions and polyethylene powder as pore agent. From the experimental results, regardless of the raw materials being HAp, TCP or biphase, when they were sintered at 1250 °C by the alginate interacting Ca ions mechanism on addition of a pore-forming polyethylene (PE) powder, the $Ca_9(HPO_4)(PO_4)_5OH$ phase (CDHA) was formed only. Porous beads of various calcium phosphates with different sizes (0.9–1.1 mm) and pore size groups (60–120 μm and lower than 10 μm) appeared.

Mateus at al. [134] compared different nano-hydroxyapatite microspheres for medical application produced by droplet extrusion method. HA and HA/βTCP microspheres were obtained from mixing of two distinct nanosize HA with sodium alginate and drop the bioceramic suspension in 0.1 M of $CaCl_2$. Microspheres had different micropores size (0.53 and 0.82 μm) due to the distinct raw powder dimension (Fig. 1.16)

The surface roughness is an important parameter in the basic biologic responses improving cell attachment and proliferation; in this study, HA microspheres presented slight higher cell viability than HA/βTCP, whereas HA/βTCP microspheres presented higher roughness than HA. This fact could be related to the composition (HA but HA/β-TCP) revealing that this, the chemical composition, would have higher influence than the roughness on the cellular response. Moreover cells built bridges between adiacent microspheres, forming cell clusters in both type of materials.

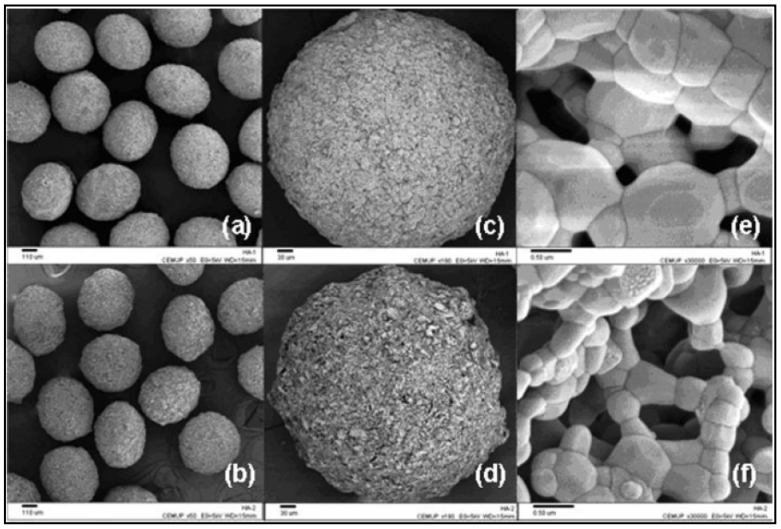

Fig. 1.16 SEM micrographs of HA and HA/βTCP microspheres [134].

Moreover, by adding calcium phosphate powder to alginate beads alloed to improve the cell adhesion, as demonstrated by Barrias at al. [135]. For the lower ceramic-to-polymer ratios (formulations 10/3, 20/3 and 40/3) only dispersed round cells and/or multicellular aggregates could be observed on the microspheres surface.

2 AIM OF THE WORK

The main goal of the present research work was the production of calcium phosphate granules as bone fillers for no-load-bearing biomedical applications. More specifically, to identify a processing procedure that could be easily transferred to a real production line. Conditions in terms of raw materials, forming techniques and thermal treatments have been analyzed and optimized trying to simplify each step as much as possible. In addition, in order to obtain different dissolution or resorption behavior and tailored bone growth stimulation after in vivo implantation, one further goal was to develop processing conditions for realizing granules with different chemical and mineralogical compositions.

3 MATERIALS & METHODS

In this chapter all the materials used in the present work and the experimental procedures are described in details. The main part of the chapter regards the production process i.e. the droplet extrusion method. This method allows the production of spherical drops starting from a bioceramic suspension containing natural polysaccharides that allows the instantaneous gelification in a crosslinking solution. Gelification mechanisms, as from previous studies, were applied to produce bioceramic spheres by droplet extrusion. Drops of different compositions were obtained that always maintained a round morphology and microporous structure. Chemical and physical characterization techniques are described in details. Developed products were tested in vitro for evaluating: the solubility and the degradability in specific solutions at different pH; the bioactivity of the bioceramic surface in simulated body fluid (SBF); and the cytotoxicity of the material in contact with cells. In vivo test were performed as well, to study the biocompatibility and the bone regeneration activity in animals such as rabbits or primates.

3.1 Raw Materials

Calcium phosphate powders: these were the main ingredients for realizing bone substitutes. They were used in different Ca/P ratios for obtaining different mineralogical compositions. In this study three different calcium phosphate powders were employed:

- Hydroxyapatite (HA);
- Calcium deficient Hydroxyapatite (CDHA);
- Beta-tricalcium phosphate (βTCP).

HA powder was supplied by Eurocoating SpA (Pergine Valsugana, Trento, Italy). Commercial CDHA powder was supplied in two different average sizes, 2.5 μm and 5 μm. Two different commercial βTCP powders were used. β-TCP_1 powder contains more than 98% pure crystalline βTCP and β-TCP_2 consists of pure βTCP.

Polysaccharides: two types of polysaccharide were used in this work: sodium alginate and chitosan. Alginates used in this study were supplied by Sigma Aldrich and are shown in Table 3.1.

Sodium Alginate	Alga	Viscosity [cPs]	Acid Mannuronic (MM)/ Acid Guluronic (GG)	%GG blocks
A	Brown alga	31.40	1.56	16
B	Macrocystis pyrifera	250	1.56	16
C	Laminaria hyperborea	-	0.8	57

Table 3.1 Sodium alginate types.

Chitosan was also supplied by Sigma Aldrich. It is a low molecular weight product with specific viscosity of about 20-300 cPs in 1% of acetic acid where the deacetylation grade is more than 75%.

Salts: they were used for the crosslinking solution and were supplied by Sigma Aldrich. For pure granules two types of salt were used:

- calcium chloride dihydrate ($CaCl_2*2H_2O$);
- sodium tripolyphosphate (TPP).

For doped granules two different metal salts, soluble in water, were used:

- zinc acetate ($Zn(CH_3COO)_2$);
- strontium chloride esahydrate ($SrCl_2*6H_2O$).

3.2 Equipment and process layout

Each step of the layout was important to reach this work's target. For all types of granules, the general layout process was fit to different chemical compositions and granulometries. Different steps were necessary to produce spherical and microporous granules with specific chemical composition. They are:

- Production of bioceramic suspension;
- Droplet extrusion with an automatic encapsulator;
- Hardening in crosslinker solution;
- Washing ;
- Microwave drying;
- Sintering;

- Sieving.

Fig. 3.1 shows the complete layout of the production process used for all types of products, pure and doped.

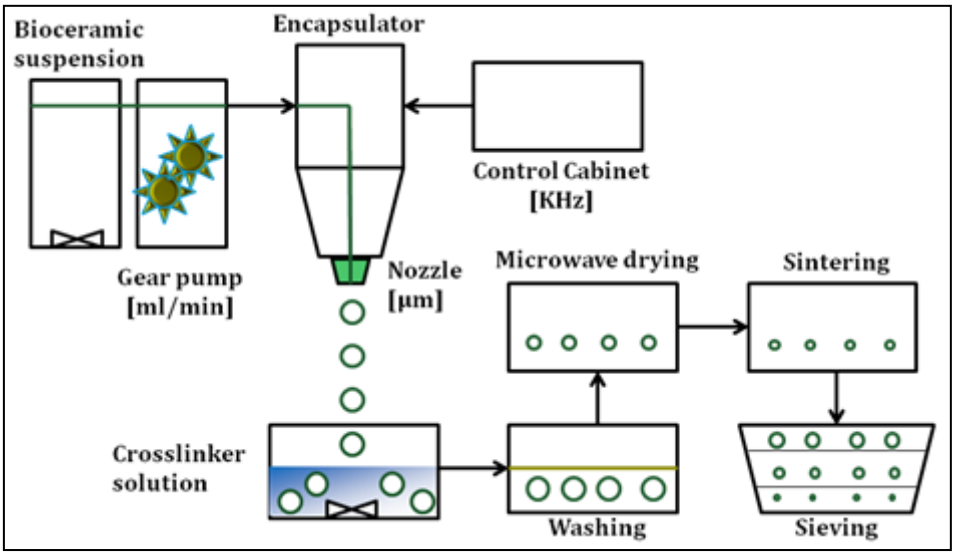

Fig. 3.1 The layout of the production process.

Mechanical and magnetic mixers: a mechanical mixer was necessary to prepare the polysaccharide solutions and bioceramic suspension. Magnetic mixers were sufficient for crosslinker solution preparation because the viscosity was not too high.

Automatic encapsulator: an automatic encaspulator, VarD Professional (Nisco Engineering, Switzerland), was used to produce the wet granules. The unit (Fig. 3.2) has a single vibrating nozzle (frequency and amplitude can be adjusted digitally). A gear pump produced a steady pulsation free flow

through the vibrating nozzle. The generated drops can be observed by means of an LED-stroboscopic light as a stationary chain of drops. The unit is composed of:

A. Feeding system with gear pump, Reglo Z Digital (Ismatech)

B. Vibration unit

C. Control cabinet

D. Stroboscobic light

Fig. 3.2 Automatic encapsulator unit.

Gear pump: this system was necessary to pump the ceramic suspension continuously within a tube connected to a vibrated nozzle. The pump flux could be regulated in range between 0.1 to 84 ml/min.

Vibration unit: it was necessary to cut the laminar flow to a precise frequency and make spherical drops.

LED-Stroboscopic light: it was automatically synchronized with the adjusted vibration frequency. This special equipment (Fig. 3.3) was important for checking the best parameters for obtaining spherical drops and then round granules. Moreover, the light facilitated the monitoring of the process.

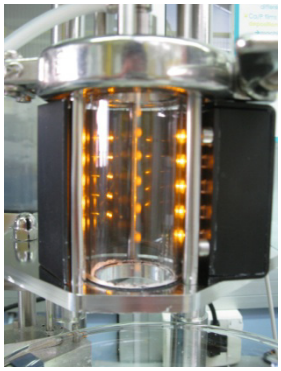

Fig. 3.3 LED-stroboscopic light and falling drops of ceramic suspension.

Nozzles: they were available to produce granules with very narrow size distribution with an average size related to the nozzle choice. The size nozzles used here were: 400, 500, 600, 800, 1000, 1200, 1400 µm.

Industrial microwave drier: SAM 255 (CEM) was used for faster drying rather than a conventional drying method like an electric oven.

Furnace: all thermal treatments at high temperature were performed in a LH120-14 (Nabertherm) furnace in static air; samples were always placed in alumina crucibles.

Mechanical sieve: An IG/1 Special (Giuliani) sieve was used to determine the granules size distribution. Moreover, the sieving step was effective at eliminating the fine and raw part of granules that was formed during the whole process. Sieves were available in the range 300-5000 µm.

3.3 Suspension and solution preparation

The preparation of the **polysaccharide solutions** was the first stage of the process. At the beginning, the polysaccharide was dissolved in deionized water with a mechanical mixer. Two distinct polysaccharide solutions were used during this study: aqueous alginate solution and chitosan acetic acid aqueous solution. Chitosan in acidic medium became a polyelectrolyte because of the protonation of the $-NH_2$ groups (Eq.4)

$$\text{Chit-NH}_2 + H_3O^+ \leftrightarrow \text{Chit-NH}_3^+ + H_2O \qquad (4)$$

Acetic acid is commonly used to solubilise chitosan at a concentration of 0.1 M or 1% [136]. In this work the amount of acetic acid was kept constant at 1% and it was enough to dissolve chitosan loads up to 2% (20 g/l). Polysaccharide solutions were continuously stirred at room temperature until complete homogeneity was reached. They were immediately used or stored in refrigerator at 4°C to avoid the biopolymer degradation in water. Typical characteristics of the polysaccharide solutions used here are shown in Table 3.2.

Polysaccharide solution	Concentrations		Solvent	pH
Alginate	1-2%	10-20 g/l	Deionized water	6-7
Chitosan	1-2 %	10-20 g/l	Deionized water + 1% Acetic acid	4-4.5

Table 3.2 Polysaccharide solutions.

Calcium phosphate powder was added to the polysaccharide solution in concentrations ranging between 60 g/l to 90 g/l. Polysaccharide solutions and

CaP powders were mixed by a mechanical mixer. A concentration of 60 g/l was used. This concentration gave the correct viscosity for droplet extrusion. Moreover, the powder concentration has an influence on the shrinkage of the granules as reported in a previous work [137]. When comparing 40 g/l and 50 g/l samples, the lower the powder load, the higher the linear shrinkage. For this reason the powder amount was kept to 60 g/l to decrease the linear shrinkage. This had an influence on the microporosity of the granules. The bioceramic suspension was agitated for 2-3 hours to reach the best homogeneity. Before the droplet extrusion process the suspension was filtered with a 40 micron mesh sieve to eliminate any coarse powder grains. Table 3.3 illustrates the powder concentrations used here.

Bioceramic powder	Polysaccharide solution	Powder concentrations	pH
HA, CDHA calcined	Alginate	60-90 g/l	6-7
βTCP	Chitosan	60-90 g/l	4-5

Table 3.3 Bioceramics suspension concentrations.

Crosslinker or hardening solution is necessary for the instantaneous gelification of the ceramic drops because it provides the ionic charge necessary for the gel reticulation. Different solutions were prepared using the method. For crosslinker solutions, $CaCl_2$, $ZnCH_3COOH_2$, $SrCl_2$ or TPP salts were simply dissolved in deionized water. Two different solutions were used in the production of pure granules, containing $CaCl_2$ or TPP, as reported in Table 3.4.

Crosslinker solution	Molarity or concentration range	pH
$CaCl_2$	0.05-0.1M	7
TPP	30-50 g/l	7.5-8.5

Table 3.4 Concentration ranges of crosslinking solutions used for pure granules production.

For solutions containing chitosan, the biopolymer was dissolved in 1% acetic acid solution in amounts of 0.1-0.3 g/l. The concentration of chitosan was kept low because the crosslinker solution must not be too viscous to allow the drop to move through the solution. Table 3.5 shows the concentration ranges of chitosan crosslinker solutions used during the development of pure chemical compositions.

Crosslinker solution	Concentrations	Acetic Acid	pH
Chitosan in Acetic Acid	0.1-0.3 g/l	0.5%=5ml/l 1%=10ml/l	3-4

Table 3.5 Concentration ranges for chitosan crosslinking solution.

Two types of solutions were used in the production of doped granules, containing $SrCl_2$, or $ZnCH_3COOH_2$, as reported in Table 3.6.

Crosslinker solution	Molarity [M]	pH
$ZnCH_3COOH_2$	0.01-0.1	7-8
$SrCl_2$	0.01-0.1	7-8

Table 3.6 Molarity ranges of crosslinker solutions used in the droplet extrusion method for doped granules.

Moreover, combined crosslinker solutions were produced to analyze the effect on the gelification process and on chemical compositions mainly for doped products. Table 3.7 shows the different combinations used.

Crosslinker solution	Molarity [M]
$CaCl_2$ + $ZnCH_3COOH_2$	0.05-0.1
$SrCl_2$ + $ZnCH_3COOH_2$	0.01-0.1
$CaCl_2$ + $SrCl_2$	0.01-0.1

Table 3.7 Combination ranges of crosslinker solutions used in the droplet extrusion method for doped granules.

3.4 Gelification mechanisms

As described in the introduction, the gelification mechanism used in CaP granules production with droplet extrusion method is the **ionotropic gelation** with $CaCl_2$. The combination of Na-alginate with Ca^{2+} allows instantaneous gelation of the wet granules. The introduction of CaP powder into the polysaccharide solution allowed obtaining hard, wet spheres that

could be manipulated during the entirety process. Typically, the conventional gelation process starts from the drop surface and proceeds towards the interior of the granules. When a ceramic powder was added to alginate solution, the ionotrpic gelation was accelerated because the structure composed by an organic matrix interrupted by powder allowed easily the Ca^{2+} ions penetration inside the sphere and the chemical interaction with the internal alginate. Moreover, by using CaP powder, the availability of Ca^{2+} ions was increased due to the dissolution of the ceramic in the polysaccharide solution during the mixing.

Ionotropic gelation both chitosan and sodium trypolyphosphate (TTP) solution were used in granules production according to Granja *et al* [129]. [138]. In the present study, this method was modified by using βTCP powder and a thermal treatment at the end to obtain a microporous structure left after burning away the gel TTP-chitosan. At the pH of TPP solution, both OH^- and tripolyphosphoric ions in TPP solution diffuse within the chitosan droplet during the curing period to react with NH_3^+ functional groups. The beads were formed by coacervation together with slight ionic crosslinking.

The conventional **polyelectrolyte complexation** mechanism between alginate and chitosan was modified to obtain CaP granules (Fig. 3.4). Many studies were carried out on alginate-chitosan production, but the method was never applied to make CaP granules. The combination of alginate and chitosan leads to ionic interaction between the carboxylate moieties on alginate and the protonated amines on chitosan to form a polyelectrolyte complex were used to make beads. These beads, at low concentrations of Chitosan (0.1-0.3 g/l), do not have the necessary consistency to be managed during remainder

of the process. It was found that the macromolecular chitosan rapidly binds onto the surface of alginate droplet, but has limited diffusion into the inner core [139]. In fact, CaP particles have a double effect because they interrupt the homogenous gel membrane in the external part of the beads and allow the chitosan solution to penetrate towards the interior of the drop thus favouring the internal gelation.

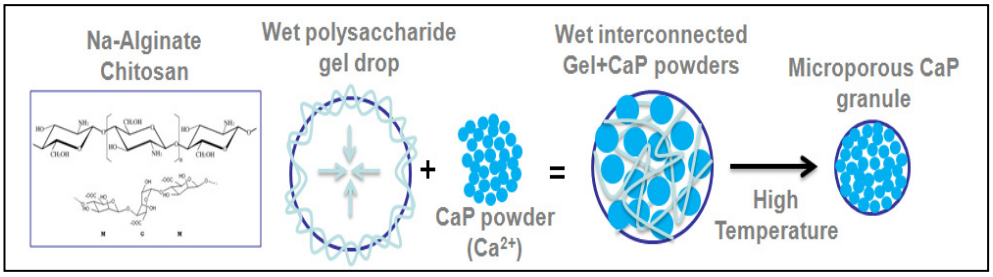

Fig. 3.4 Gelification mechanism of alginate-chitosan and CaP powder.

The conventional **ionotropic gelation** was modified by using different divalent ions, instead of calcium, to produce alginate beads with CaP powders (Fig. 3.5). The substitution of calcium ions with zinc or strontium ions results in a difference in gelification mechanism because these ions have different ionic radius. Zn ion is smaller than Ca and does not interact in the same way with the GG chain of alginate. The guluronic/mannuronic ratio has to be higher to allow carboxyl group to chelate small Zn ions. In the case of Sr, the gelification picrocess is very similar to Ca because the ion radii are very similar and ionotropic gelation is preferred. Another modification of conventional method was the application of a combined hardening solution, where two different ions were present. In this study three combinations were considered: Ca+Zn, Ca+Sr, Zn+Sr. By working with a low total molarity, in a

range of 0.001-0.03, the combined molarity was calculated as sum of each molarity, by considering negligible the reciprocal influence on the total value.

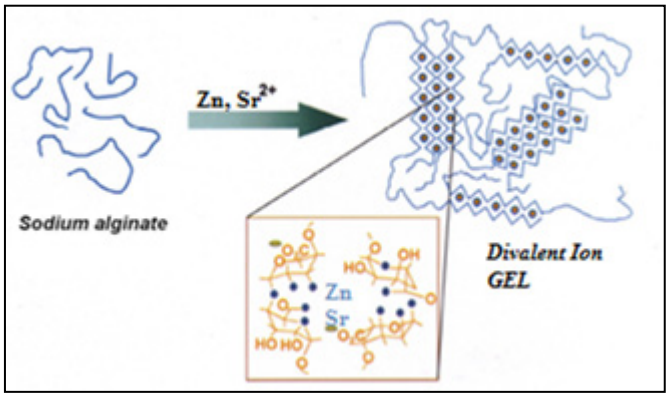

Fig. 3.5 Ionotropic gelation mechanism used for doped granules.

Monophasic or biphasic crosslinker solutions were used to change the final composition combining different stabilization mechanism. Different combination of polysaccharide and crosslinkers were used to try to obtain various pure or doped chemical compositions (Table 3.8).

Polysaccharide	Crosslinker solution	Gelification mechanism	Pure granules	Doped granules
Alginate	$CaCl_2$	IG	X	
Alginate	Chitosan	PC	X	
Chitosan	TPP	IG	X	
Alginate	$ZnCH_3COOH_2$	IG		X
Alginate	$SrCl_2$	IG		X
Alginate	$CaCl_2 + ZnCH_3COOH_2$	IG		X
Alginate	$CaCl_2 + SrCl_2$	IG		X
Alginate	$SrCl_2 + ZnCH_3COOH_2$	IG		X

Table 3.8 Gelification mechanism used for pure and doped granules: IG = ionotropic gelation and PC = polyionic complexation.

The molarity of crosslinker solutions were linked to the possibility to gelify spherical drops and to the amount of the doped ion that was found in the sintered granules.

3.5 Process parameters

Before the optimizations of the final composition, many experiments were carried out to correctly select the ingredients to reach the desired properties. In Table 3.9 it is summarized how different parameters influence properties such as morphology and mineralogical composition of CaP granules. Parameters underlined in Table 3.9 have been investigared carefully during this work. Some processing parameters were kept fixed according to a previous study [137]. The powder concentration was maintained at 60g/l for all tests. Moreover, after preliminary experiments, the drop height (the distance between the nozzle and the free surface of crosslinking solution) was fixed at 25 cm. Hardening solution time was fixed between 30 and 45 min depending on the wet granules size as in a previous work [132] [140].

Granules Property	**Materials**	**Processing parameters**	**Thermal treatments**
Chemical composition	**Bioceramic powder type** **Alginate type and concentration** **Crosslinker type and concentration**		**Sintering temperature**
Shape	Bioceramic powder concentration **Alginate type and concentrations** **Crosslinker type concentration**	Drop height **Pump flux** **Vibration frequency** Hardening solution time	

Size		Drop Height **Nozzle** **Pump Flux** **Vibration frequency** Hardening solution time	**Sintering temperature**
Surface roughness and interconnected microporosity	**Powder morphology** **Alginte type and concentration** **Crosslinker type concentration**		**Sintering temperature**
Aggregation	**Alginate and crosslinker type** and concentration		**Drying method** **Sintering temperature**
Doping effect	**Crosslinker type and concentration**		

Table 3.9 Influence of parameters on granules properties.

Fig. 3.6 represents a schematic resume of the relation between process parameters and beads properties.

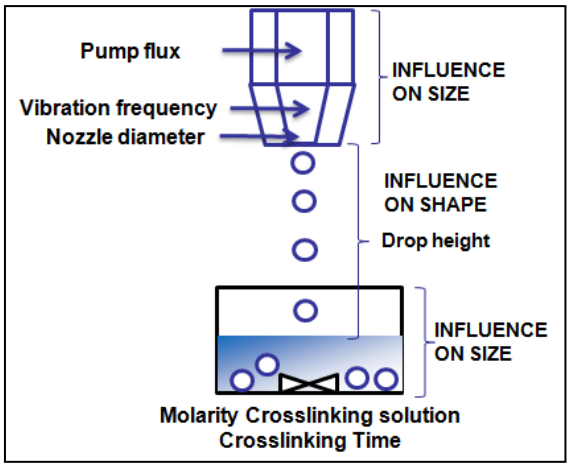

Fig. 3.6 Processing parameters that can influence the shape and the size of wet granules.

3.6 CaP aggregates

Agglomeration mechanism of granules was suitable for all chemical composition, but mechanical consistency depends on the ingredients involved in the gelification process that allows for obtaining spherical microspheres. Aggregates were formed during the drying process by using a special plate with semispherical cavities (Fig. 3.7). A method to make aggregates was optimized starting from a random agglomeration to a controlled process by using wet granules from the 800 μm nozzle for producing bone grafts that were more regular and with enough mechanical strength to be handled.

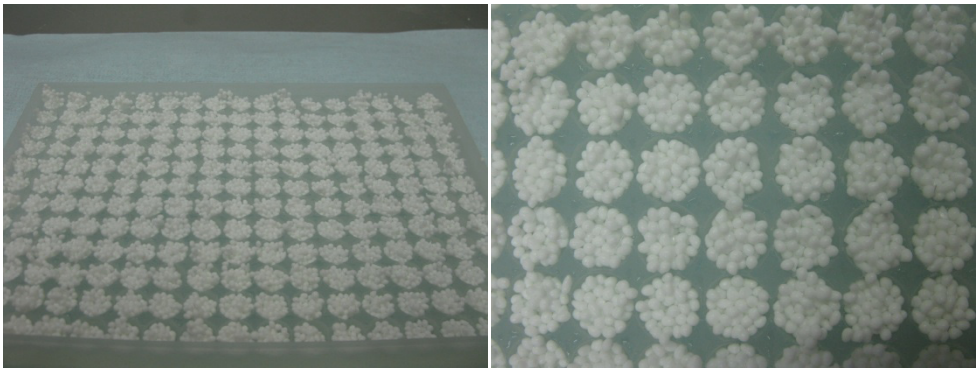

Fig. 3.7 Example of aggregates production from wet granules.

In the aggregate production the action of acetic acid contained in crosslinker suspension for HA and HA/βTCP families and bioceramic suspension for βTCP was used [141].

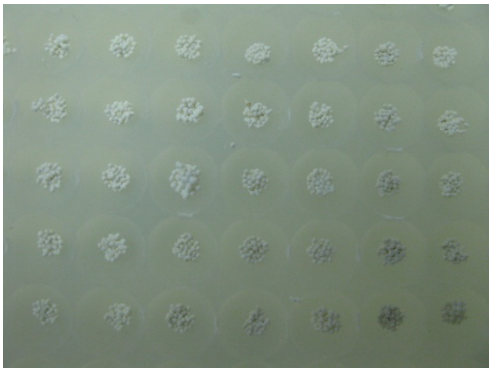

Fig. 3.8 Dried granules in silicon plates with semicavities used for aggregates production.

3.7 Chemical-physical characterization methods

3.7.1 Thermo-gravimetric (TG) and differential thermal analysis (DTA)

Thermo-gravimetric analyses were useful to calculate the weight loss during thermal treatment at high temperature. The differential thermal analysis allowed pointing out endothermic and exothermic reactions that occur during the sintering process. TG/DTA (STA409 Netzsch GmbH, Bayern, Germany) measurements were carried out in flowing air on pure, dry granules.

3.7.2 X-ray diffraction (XRD)

X-ray diffraction (XRD) characterization of granules was carried out using the XRD patterns recorded with a Rigaku Dmax III diffractometer. It uses Ni filtered Cu Ka radiation over the 2θ range of 20-60° at scan rate of 2°/min with a sampling interval of 0.010° at 15 mA and 30 kV.

The quantitative analysis was performed by Maud (Material Analysis Using Diffraction), software developed by Prof. Lutterotti of University of Trento. It is a general diffraction/reflectivity analysis program mainly based on the Rietveld method. Phases were downloaded from CIF database, CrystalloFigurey Open Database (COD) (http://www.crystalloFigurey.net/). For quantitative analyses the following reference phases were used:

- icds 151414 for HA,
- icds 97500 for βTCP,
- icds 1000044 CaO,
- icds 9011144 TTCP
- icds 923 for αTCP
- icds 1001556 $Ca_2P_2O_7$
- Calcite , $CaCO_3$ Maud Default Structures
- Zincite , ZnO Maud Default Structures

3.7.3 Fourier transformation infrared spectrometry (FT-IR)

Chemical characterization was performed by using FTIR spectroscopy. For this purpose, granules were reduced to powder and analyzed as KBr pellets by using a Thermo Nicolet Avatar 330 spectrometer. The wavelength range is 400-4000 cm^{-1} and the test was performed in transmittance.

3.7.4 Inductively coupled plasma optical emission spectrometry (ICP-OES)

Chemical analyses of bone substitute samples were performed by ICP-OES (Spectro Ciros). The sampls for the ICP-OES analyses were obtained by dissolving 10 mg portions of powder samples from machined bone graft in 3.27 ml of 65% concentrated HNO_3 solution (Carlo Erba). The solution was heated to favour the solubility and cooled with distilled water until a volume 100 ml was reached.

3.7.5 Heavy metals analysis

According to the requirements of ISO 13779-3 and ASTM 1185-03 for Hydroxyapatite surgical implants and ASTM F 1088 for Beta-Tricalcium Phosphate surgical implants, heavy metals detection analysis was carried out by using inductively coupled plasma/mass spectroscopy (ICP/MS).

3.7.6 Optical microscopy (OM, SEM)

Granules and aggregates morphology was analyzed by optical microscope (Stemi 2000_C, Zeiss) and by scanning electron microscopy (SEM) (JEOL-JSM-5500). In this second case, the samples were first coated with a thin layer of gold-palladium by sputtering (Polaron SC7620). Then, they were analyzed using an accelerating voltage between 10 to 20 kV.

3.7.7 Specific surface area analysis by nitrogen adsorption method and porosimetry

The analysis of specific surface area was performed with ASAP 2010 (Micrometrics) machine and N_2 gas adsorption.

Hg porosimetry was used to measure porosity, pore size distribution and other properties such as bulk and apparent densities. For the determination of macropores Hg porosimetry (Pascal 140, CE Instruments, Milano, Italy) was used. For calculating the micropores high pressure porosimetry (Porosimeter 2000, CE Instruments, Milano, Italy) was employed.

3.8 *In vitro* experiments

3.8.1 Solubility test

The work followed an experimental protocol written on the basis of the norm ASTM F1926/F1926M-10 “Standard test method for evaluation of the

environmental stability of calcium phosphate granules, fabricated forms, and coatings".

Granules of HA, βTCP, HA/βTCP (60%/40%) and HA/TTCP (60%/40%) with a fixed granulometry, 300 - 600 µm, were used for the test. A control reference was chosen for evaluated the solubility behavior in determined solutions of these products. The standard reference was pure HA powder of National Institution of Standard and Technolgy (NIST).

Two different buffer solutions were prepared: MES pH 5.5 and TRIS pH 7.3. All the reagents were of analytical grade and were purchased from Sigma Aldrich and used without any further purification.

MES pH 5.5 solution was prepared by using 195.2 g MES, 4.67 mg, NaCl, 8.88 mg $CaCl_2$, 10.61 mg K_3PO_4, 1g NaN_3; the substances were dissolved in 800 ml of water (HPLC grade) in a 2 l flask, sonicated for 5 min and then brought to volume. The solution was then transferred to a jacketed reactor, heated to 37°C and adjusted to pH 5.5 with NaOH 0.1 N. The buffer was then preserved in a glass bottle. TRIS pH 7.3 was prepared by using 157.6 g TRIS, 4.67 mg NaCl, 8.88 mg $CaCl_2$, 10.61 mg K_3PO_4, 1g NaN_3; the substances were dissolved in 800 ml of water (HPLC grade) in 2 l flask, sonicated for 5 min and then brought to volume. The solution was then transferred to a jacketed reactor, heated to 37°C and adjusted to pH 7.3 with NaOH 0.1N. The buffer was then preserved in a glass bottle.

The analysis was carried out in a jacketed glass reactor of 200 ml of buffer solution, tightly closed and kept at 37 ± 0.5°C by a chiller with internal temperature control. A flow of nitrogen was developed within the reactor through two holes. The stirring rate was maintained at 100 ± 20 rpm by

using magnetic stirrers and PTFE stirring rods (30x6 mm^2). The sample was maintained in solution by means of a sample holder consisting of a cylinder with a mesh of 100 μm. A further hole with a hermetic cap was used for the input of the pH-meter, thermometer and a pipette for sampling. Nine glass reactors could work simultaneously. The solubility apparatus is showed in Fig. 3.9.

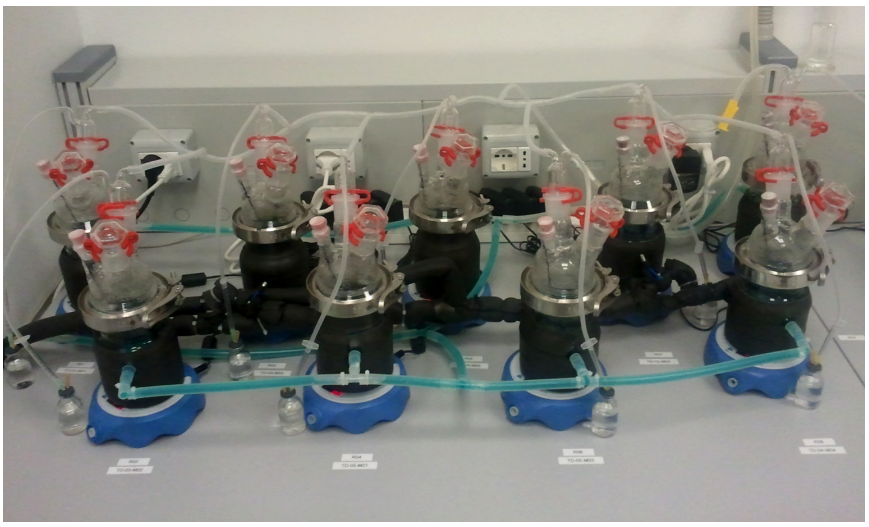

Fig. 3.9 Solubility test apparatus.

The procedure was the same for all type of analyses i.e. Ksp evaluation, kinetic dissolution and dissolution behavior. The sample, 200 mg of granules, was accurately weighed and inserted into the sample holder, a highly porous plastic cylinder that easily allowed the passage of the solution but maintained the granules inside to avoid any contact with the magnetic stirrer that could damage the granules and accelerate their dissolution. The sample holder was

inserted into the reactor that contains 200 mL of buffered solution and the magnetic stirrer. At the beginning of the test the sample holder had to be housed within the reactor but suspended so it did not touch the solution. A nitrogen flow was used for at least 2 h in order to saturate the environment and allow solution to reach 37°C. When equilibrium was obtained, the experiment was started by lowering the sample holder into the solution. At previously fixed intervals, depending on the analysis, a volume of 300 µL was taken from the solution. Each sample was placed in a glass vials with a screw cap sealed and properly labeled, and stored until FT-IR analysis was performed in order to evaluate calcium and phosphate concentration.

Temperature and variation of pH were also monitored during the duration of the test. At previously fixed intervals the measurements of pH and temperature were made by immersing the pH-meter and thermometer through the neck of the reactor. The pH-meter was calibrated daily by using standard buffer solutions.

The Ksp evaluation and dissolution rate differed in the duration, sampling intervals and buffer solution used.

The dissolution behavior consisted of plotting the data, concentration values of Ca and P versus time, collected for the calculation of Ksp and concentration product (using TRIS buffer solution pH 7.3), to build the curve that shows the dissolution trends during the 70 days of analysis. The solubility analyses used to investigate the dissolution rate were conducted both in TRIS buffer solution, pH 7.3, and in MES buffer solution, pH 5.5. The dissolution rate analysis gives information about the initial rate of solubilisation of the

material and is related to the solubility product (Ksp) but also the exposed surface area of the material, so it could also be called kinetic dissolution.

The analysis of the **dissolution rate** was performed for 48 h; 32 sampling of 300 µL were made for each analysis, at the following intervals:

- beginning of the analysis;
- every 15 minutes during the first 2 h;
- every hour from the 2nd to the 5th h;
- every hour from the 19th to the 29th h;
- every hour from the 43rd to the 47th h;
- every 15 minutes from 47th at 48th h;

Each sample was placed in a glass vial with screw cap sealed and properly labeled and stored until analysis. At the end of the 48 h, the samples were analyzed with FT-IR analysis to determine the concentrations of calcium and phosphorus. Analysis of each family of granules was repeated 3 times in both buffered solution.

The solubility analysis in order to calculate the **solubility parameter Ksp and the comparative concentration product** value was performed in TRIS buffer solution at pH 7.3. At the same hour each day a volume of 300 µl was taken from the solution through the neck with a special cap. Each sample was placed in a glass vial with screw cap sealed, properly labeled and stored until FT-IR analysis to determine the concentrations of calcium and phosphorus. The duration of the analysis is determined by the time required to reach equilibrium, meaning that the solubility limit of the specific calcium phosphate

is reached. The estimated necessary time to reach the equilibrium is equal to 10 weeks. The analysis of each family of granules was repeated 3 times.

Ksp was calculated by using data from [Ca] and [P] once equilibrium was attained, when no longer significant change in concentration of the solution is registered, so this analysis could be also called thermodynamic dissolution. Ksp for HA and βTCP were calculated using the Eq.5 and Eq.6.

$$Ksp_{(HA)} = [Ca^{2+}]^{10}[PO_4^{3-}]^6 \quad (5)$$

$$Ksp_{(\beta TCP)} = [Ca^{2+}]^{3}[PO_4^{3-}]^2 \quad (6)$$

Eq. 5 and Eq. 6 are specific for monophasic HA and βTCP compounds and are not useful to calculate Ksp value for biphasic compounds because the Ksp can only refer to one product; nevertheless, in order to only compare both HA (HA granules and HA NIST) and other different material (HA/βTCP (60%/40%) and HA/TTCP (60%/40%)) the product of concentrations $[Ca^{2+}]^{10}[PO_4^{3-}]^6$ can be calculated.

Data collected for the calculation of the Ksp (using TRIS buffer solution pH 7.3) were used to build up the curve that shows the **dissolution behavior** during the 70 days of analysis, by plotting the concentration values of Ca and P versus time.

The determination of the **concentration of calcium** in solution was performed by using FT-IR analysis; in order to avoid errors in the calcium quantification due to other interfering signals the kit Calcium-Colorimetric Method Arsenazo III (Futura System, L.) was used. A fixed quantity of 5 µl of samples, blank and standard solution A (prepared with 50 µl of standard calcium solution 10mg/dl + 75 µl of distilled water) were distributed in a 96

wells plate, 200 µl of Arsenazo III reagent was added in each well as reported in Table 3.10. The plate is left incubated for 5 minutes at RT.

	Blank	Samples	Std A
Distilled water	5 µL		
Sample		5 µL	
Standard			5 µL
Reagent	200 µL	200 µL	200 µL

Table 3.10 Fixed quantities for standards solutions, blank and samples

The absorbance of each well was measured with a FT-IR spectrophotometer Varian Cary 50 equipped with a microplate reader at 620 nm; the calcium concentration was calculated by using the formula (Eq. 7) based on the Arsenazo kit instruction.

$$[Ca](mg/L) = \frac{Sample\ absorbance}{Calibrator\ absorbance}\ x\ 40 \qquad (7)$$

The determination of the **concentration of phosphorus** in solution was performed by using FT-IR analysis; in order to avoid error in the phosphorus quantification due to other interfering signals the kit Malachite Green Phosphate Detection Kit (R&D System, L.1253271) was used. Six standard solutions with different concentration, 50/25/12.5/6.25/3.12/1.56 µl, were prepared to build up the calibration curve as instructed by the Malachite detection kit. A fixed quantity of the six standard phosphate solutions, blank and samples were put in 96 well plates as reported in Table 3.11.

	Quantity	Concentration
Std 1	50 µL	50 µM
Std 2	50 µL	25 µM
Std 3	50 µL	12.5 µM
Std 4	50 µL	6.25 µM
Std 5	50 µL	3.12 µM
Std 6	50 µL	1.56 µM
Blank	50 µL of H2O	-
Sample	5 µL of sample + 45 µL of H2O	-

Table 3.11 Fixed quantities for standards solutions, blank and samples.

In each well 10 µL of Machalite Green Reagent A were added and the plate was left incubated for 10 min at room temperature; then, 10 µL of Machalite Green Reagent B were added in each well and the plate was left incubated for 20 minutes at RT. The absorbance of each well was measured with a FT-IR spectrophotometer Varian Cary 50 equipped with a microplate reader at 620 nm. The calibration curve was built up by plotting the concentration of standards (µM) versus the absorbance measured (A_{620}) according to the Eq. 8 indicated in the Malachite kit.

$$y\,(A_{620}) = m\,x\,(\mu M) + q \qquad (8)$$

The concentration of phosphorus in the sample was calculated with Eq.9.

$$Sample\ Concentration\ (\mu M) = \frac{A_{620} - q}{m}\ \text{x}\ 10 \qquad (9)$$

3.8.2 Degradation test

The evaluation of degradation products of calcium phosphate granules was performed following the standard ISO 10993-14 "Identification and quantification of degradation products from ceramic" for biological evaluation of medical devices. The standard presents two different analyses that differ in the pH of the solution, where the granules are immersed, to identify and quantify the degradation products of ceramics materials. Because CaP granules would be primarily used in dental application, the acidic solution, pH 3, was chosen over the neutral solution, pH 7, because it better simulate the pH that can be found within the oral cavity. However, the use of a low pH solution does not modify the degradation process and only increases the rates of the degradation in order to reduce the time of the analysis [142]; therefore, it would be representative also for the other indicated sites. The test was performed on all the 4 different composition of calcium phosphate granules, HA, HA/β-TCP, HA/TTCP and β-TCP, by using a fixed granulometry 300-600 μm suggested by the standard. Cerasorb granules (Curasan, granulometry 150-500 μm), made of β-TCP, and Calcitite 4060 granules (Calcitek, granulometry 250-420 μm), made of HA, are used as a commercial reference for β-TCP and HA granules in the analysis. The acid solution was prepared dissolving 21 g of citric acid monohydrate in 500 ml of water in a 1 l volumetric flask. Then 200 ml of 1M sodium hydroxyde solution should be added and then diluted using water to the mark. To obtain the buffered citric acid solution, 40.4 ml of the prepared solution is added to 59.6 ml of 0.1M

hydrochloridric acid. The acid solution did not contain significant concentration of Ca and P (Table 3.12) or other impurities (Table 3.13).

Element [ppm]	Acid solution standard
Ca	0.043
P	0.017

Table 3.12 Solid concentrations of Ca and P in ppm in acid solution.

Element [ppm]	Acid solution standard
Mg	0.004
Na	0.00
K	0.37
Mn	0.001
Ba	0.0004

Table 3.13 Solid concentrations of impurities in ppm in acid solution.

Each sample, 1 g of granules, was accurately weighed and then placed in a plastic container with 20 ml of acidic solution (extreme solution). The sealed plastic containers were left for 5 days at 37°C agitated using a longitudinal movement. The granules were then filtered, rinsed three times with distilled water and dried at 37°C until they reached a constant mass and then weighted again to determine the amount of dissolved material. Each filtered solution was characterized using ICP analysis to determine the Ca/P content and other possible impurities. The CaP granules were accurately weighed by using an analytical scale and have been characterized using XRD and SEM analysis

before and after the degradation test. Commercial products were characterized by using the same method and condition used for CaP granules.

3.8.3 Bioactivity test

Pure and doped granules (500-600 μm) were used in bioactivity studies. A reference commercial βTCP Cerasorb granules (500-1000 micron) was chosen to compare the bioactivity with the products developed here.

The preparation procedure for SBF solution is explained in details in a Kokubo's study [54]. The dissolution of reagents had to be added follow the order from the 1st to the 10th at 36°C±1.5°C and the solution had to maintain the transparency thus avoiding the deposit on the surface of the bottle. The following powder reagent grade chemicals were stored in a desiccator. Ion-exchanged and distilled water was used for the preparation of SBF:

- sodium chloride (NaCl),
- sodium hydrogen carbonate ($NaHCO_3$),
- potassium chloride (KCl),
- di-potassium hydrogen phosphate trihydrate ($K_2HPO_4*3H_2O$),
- magnesium chloride hexahydrate ($MgCl_2*6H2O$),
- calcium chloride ($CaCl_2$),
- sodium sulfate (Na_2SO_4),
- Tris-hydroxymethyl aminomethane: $((HOCH_2)_3CNH_2)$
- 1M (mol/l) Hydrochloric Acid, 1M-HCl,
- pH standard solution, (pH 4, 7 and 9).

The volume of SBF that was used for testing was calculated with Eq.10.

$$V_s=S_a/10 \qquad (10)$$

where V_s was the volume of SBF (ml) and S_a was the apparent surface area of specimen (mm^2).

Pure and doped granules (500-600 μm) were immersed in 6.4 ml SBF solution at 37°C in plastic bottles and attached at the bottom with 64 mm^2 of conductive adhesive to permit the consequent observation of the exposed surface by SEM. In two different extraction times, 7 and 28 days, CaP products were taken out of the solution and observed by SEM.

3.8.4 Cytotoxicity test

Pure granules (HA, HA/β-TCP, HA/TTCP, β-TCP) and doped granules (Zn-β-TCP, Zn-HA/β-TCP, Sr-HA/β-TCP, SrZn- HA/β-TCP) in the size range of 300-600 μm were used in citototoxicty test. The specific granulometry (300-600 μm) was chosen as the worst case also for cytotoxicity test because smaller size range can cause greater and faster cytotoxic reaction [39] [143] due to higher dissolution rate caused by higher specific surface area [7] and a higher possibility of leachable and degradation products that could lead to cytotoxicity. All products were sterilized by gamma rays before the test in specific polyethylene (PE) packaging.

In vitro direct contact and extract studies with various cell types (BalbC 3T3) evaluated the cytotoxic potential. Tests were carried out by Eurofins Biolab

under GLP conditions. The experimental design included a 12 wells plate containing confluent cell monolayer, subdivided in following groups:

- 3 Blank
- 3 Test sample : 30mg has been deposed on filter paper placed in the middle of each well
- 3 Negative control: filter paper placed in the middle of each well
- 3 Positive control : 30 mm^2 of latex placed in the middle of each well

2 ml of cell suspension were placed from a confluent culture to a plate having 22 mm diameter wells. The plate was incubated at 37°C in a 5% CO_2 atmosphere, this allowing cell sedimentation and the constitution of a confluent monolayer. Subsequently the medium was replaced and the test sample was added through direct deposition. The plate was incubated in a thermostat at 37°C in CO_2 for 24 hours. After qualitative evaluation each well was then treated with 2 ml of neutral red medium for 3 hours, then washed with PBS and treated with 2 ml of desorb solution, and then plate was put in a stirring for 10 minutes to homogenize the solution. The optic density was then calculated after 540 nm spectrophotometric reading. After 24 hours the plate was observed by an inverted microscope and biological reactions (cell degeneration and malformations) were qualitative evaluated with a scale ranging from 0 to 4, according to ISO 10993-5 (Table 3.14).

GRADE	REACTIVITY	DESCRIPTION OF REACTIVITY ZONE
0	None	No detectable zone around or under specimen
1	Slight	Some malformed or degenerated cells under specimen
2	Mild	Zone limited to area under specimen
3	Moderate	Zone extending specimen size up to 1,0 cm
4	Severe	Zone extending farther than 1,0 cm beyond specimen

Table 3.14 Example of qualitative evaluation of ISO 10993-5.

The achievement of a numerical grade greater than 2 is considered as a cytotoxic effect. Optical density was measured at 540 nm by Gen5 software (Biotek). The percentage of cell viability was calculated with Eq. 11.

$$\%\ \text{of cell viability} = \frac{OD_{\text{test product}} - OD_{\text{blank}}}{OD_{\text{negative control}} - OD_{\text{blank}}} \cdot 100 \qquad (11)$$

A cellular vitality reduction more than 30% was considered a cytotoxic effect.

3.9 *In vivo* experiments

3.9.1 Implantation test

The aim of the study was to perform a biological test on the CaP porous granules and in particular to evaluate local toxicity and inflammatory effect after implantation. Another target was to compare different chemical

composition and distinct morphology of granules in the same conditions of implantation. Moreover, the degradation rate of CaP granules could be evaluated on basis of three different explantation times and with respect to one commercial control currently used in clinical applications.

The bone implantation study was planned and designed in agreement with ISO 10993-6 and was implemented in a certified laboratory (Biolab Spa, Vimodrone, Milan, Italy).

The test was performed on four types of biomaterials: HA; βTCP; HA/ βTCP; HA/TTCP. The granules size range chosen was 300-600 μm and this was justified by previous studies where it was explained that an initial inflammatory reaction due to small particles can enhance osteoconductive properties of granules [144]. Materials were sterilized by Gamma-rays in specific packaging before implantation. Commercial βTCP granules , Cerasorb (Curasan), 150-500 μm size were chosen as representative control material because βTCP in vivo is known to resorb faster than HA, HA/β-TCP and HA/TTCP and was therefore a suitable reference for the evaluation of local tolerance and biodegradation/resorption behavior. In addition, both products had similar granulometry, spherical morphology and microporosity. CaP aggregates were not implanted for economical reasons and for using as few animals as possible.

The rabbit animal model and the implantation site were selected in agreement with ISO 10993-6 standard and on the basis of bone metabolism of the animal, since animal models with faster turnover help to emphasize and anticipate potential adverse reactions. HA, HA/β-TCP, HA/TTCP, β-TCP granules are intended to be applied in both orthopedic and oral/maxillofacial bone sites

and are not intended as bone supporting device. The rabbit femur bone type is considered representative for these clinic indications because it is a standardized model for the evaluation of non-supportive bone devices and because the fast metabolism will provide early results. Twelve New Zealand White Rabbit weighting about 2 kg each were divided into three groups composed by 4 albino male rabbits. Each group represented three explantation times.

Explantation times (aiming review between 6, 26 and 52 weeks after implantation) were selected. After 6 weeks the trauma due to surgical intervention is eased and the initial bone integration should become clear. At 26 weeks full bone integration should be observed combined with replacement of the implant material by new bone. The total duration of the test (52 weeks) was scheduled in order to investigate and exclude the possibility that advanced degradation of product can cause release of potentially toxic components or particles that can cause inflammatory reaction. The 52 weeks observation period is regarded sufficient for the long term local tissue evaluation. Depending on the local tissue and degradation results of the intermediate observation periods the final observation periods can be adjusted during the course of the study.

To investigate the biological safety and the absence of any local toxicity of bioresorbable materials ISO 10993-6 recommends inserting the implant in the mid-shaft cortical bone of tibia or femur. Therefore, in this study granules and control sample were implanted in the mid shaft of the two femurs of each animal: the right femur of each animal was treated in three different sites with the test sample, the left femur will be treated with control sample. The femur

was reached from the lateral side of the thigh with a longitudinal incision. Skin and subcutaneous tissues was incised to reach the point of union between the femoral biceps muscle and the tensor muscle that was detached. After the detachment the vastus lateral muscle and femoral biceps was divaricated with the purpose to expose the femur. To prepare the implant sites an osteotribe (Ø 1mm) was used at low speed, then, with a 2mm Ø tip to executed a series of three holes using low drilling speed and intermittent drilling using profuse irrigation with physiological saline solution and suction, because overheating could result in local tissue necrosis. A series of 3-hole bone/femur at 6 mm deep were prepared. Each hole was filled with the test sample or control sample: as the μCT analyses on the explanted femur demonstrate, test samples and control samples were put in contact both with the cortical bone and with bone marrow in the medullary canal.

At the end of each explantation time, all treated sites were removed and observed macroscopically to determine any injuries to the subcutaneous tissue. After each explantation femurs of all animals was put in formalin 10%.

Histological analysis was conducted at GLP Test Site Accelera Srl (GLP Certification N.000/061/2009 released by the Italian Ministry of Health). The histological analyses on the retrieved samples were designed as indicated in the ISO 10993-6 “Test for local effect after implantation”. The following analyses were performed: macroscopic evaluation of the implantation sites and qualitative evaluation of the images acquired by optical microscope on histological samples (decalcified and non decalcified) in order to asses absence of necrosis, absence of inflammatory reaction, absence of bone resorption, absence of fibrotic tissue around the implant, absence of local

toxicity of the degradation products, osteointegration of products and bone formation around implants.

Table 3.15, Table 3.16 and Table 3.17 represent how the histological evaluation system was carried out referred to cell/response, the global response for neovascularisation, fibrosis and fatty infiltrate and bone tissue changes.

Cell type/response	Score				
	0	1	2	3	4
Polymorphonucelar cells	0	Rare, 1-5/phf [a]	5-10/phf	Heavy infiltrate	Packed
Lymphocytes	0	Rare, 1-5/phf	5-10/phf	Heavy infiltrate	Packed
Plasma cells	0	Rare, 1-5/phf	5-10/phf	Heavy infiltrate	Packed
Macrophages	0	Rare, 1-5/phf	5-10/phf	Heavy infiltrate	Packed
Giant cells	0	Rare, 1-2/phf	3-5/phf	Heavy infiltrate	Sheets
Necrosis	0	Minimal	Mild	Moderate	Severe

[a] phf = per high powered (400x) field

Table 3.15 Example of a histological evaluation system – cell/type response – Table E.1 of ISO 10993-6.

Reaction	Score				
	0	1	2	3	4
Neovascularisation	0	Minimal capillary proliferation, focal, 1-3 buds	Groups of 4-7 capillaries with supporting fibroblastic structures	Broad band of capillaries with supporting structures	Extensive band of capillaries with supporting fibroblastic structures
Fibrosis	0	Narrow band	Moderately thick band	Thick band	Extensive band
Fatty infiltrate	0	Minimal amount of fat associated with fibrosis	Several layers of fat and fibrosis	Elongated and broad accumulation of fat cells about the implant site	Extensive fat completely surrounding the implant

Table 3.16 Example of a histological evaluation system – Response - Table E.2 of ISO 10993-6.

Bone tissue changes	Score				
	0	1	2	3	4
New Bone Formation	Not present	Minimal	Slight	Moderate	Marked
Bone Resorption	Not present	Minimal	Slight	Moderate	Marked

Table 3.17 Example of a histological evaluation system – Bone tissue changes.

In addition to the analyses that are recommended in ISO 10993-6, micro-computed tomography (µCT) analyses on the retrieved samples were also performed in order to qualitatively investigate the bone ingrowth potential, osteointegration level and degradation rate of products. The µCT analysis is a powerful technology that allows investigating the quality of the new bone formation by means of the measurement of the histomorphometric parameters of the trabecular structure of the bone tissue around implants. Because µCT analysis was performed in addition to histology, only one samples for each materials were scanned. The samples were scanned by micro-computed tomography (µCT 100, Scanco Medical AG, Bruttisellen, Switzerland). The contour of the original shaft of the femora was manually contoured along the long bone. This contour was later used to separate the callus bone from the original bone shaft. A semi-automatic segmentation procedure was used to separate callus bone, old shaft bone and biomaterial from background (Fig. 3.10 A) and B)). For the analysis, three cylindrical masks were created and manually placed at the location of the defects (Fig. 3.10 C)). Masks were called Top-Mask, Mid-Mask and Bot-Mask, where Top-Mask refers to the most proximal defect and Bot-Mask to the most distal defect. In the cases where only two defects were present, the masks were called Top-Mask and Bot-Mask and in the case where only one defect was present the mask was called Top-Mask. The masks were aligned on the

outside of the shaft and placed using a visual best guess. Fig. 3.11 shows a three-dimensional rendering of the different phases and the placement of the masks. The sample shown is βTCP.

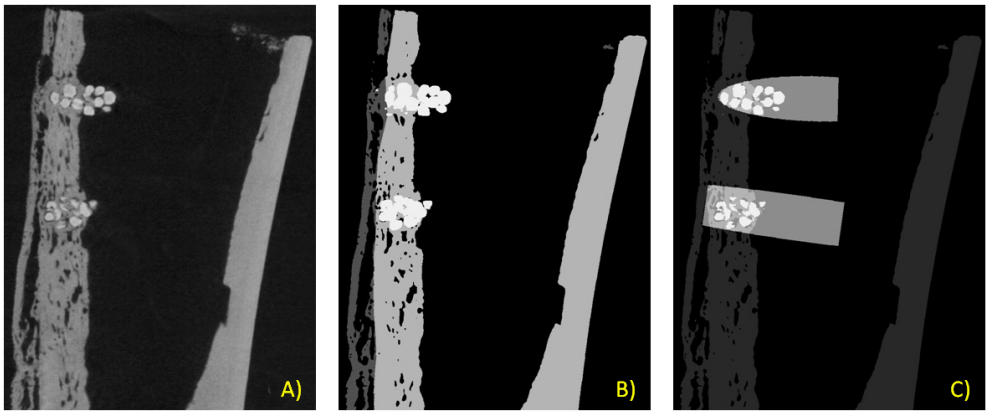

Fig. 3.10 Example of a A) grey-level and B) corresponding segmented image. The images were segmented in the three phases new bone, old bone (shaft), and biomaterial. C) Cylindrical masks were fitted to the estimated location of the defects. The sample shown is βTCP.

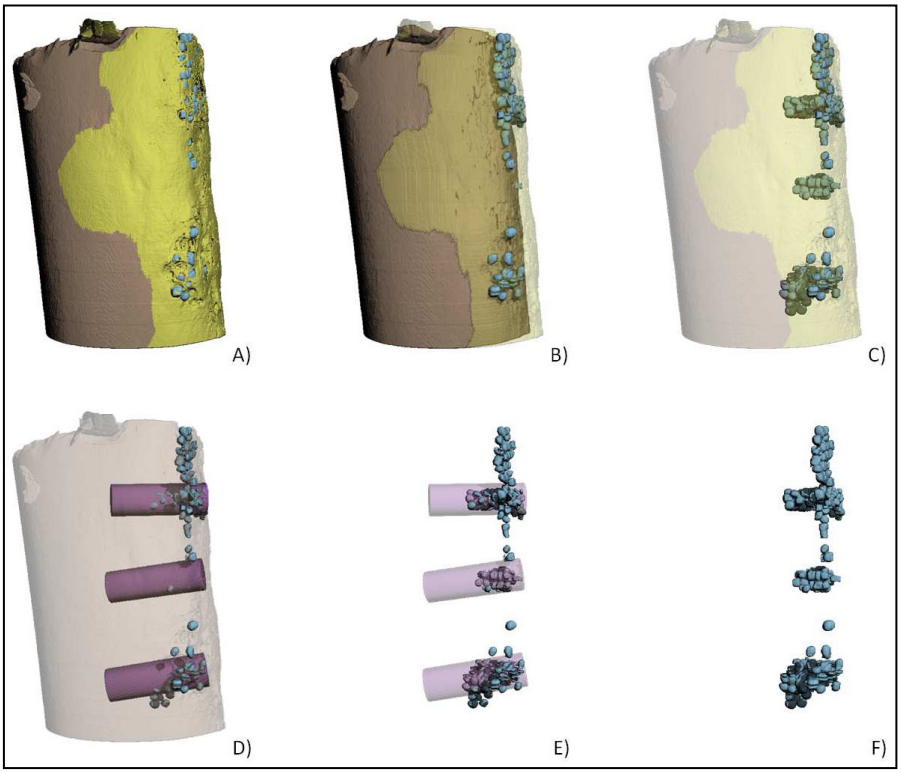

Fig. 3.11 Three-dimensional representation of the different phases and volumes analyzed. A) – C) Old shaft bone is shown in brown, callus bone in yellow and biomaterial in blue, where the bone phases are shown in different transparencies. D) – F) Bone is shown in brown, biomaterial in blue and the masks in purple, where bone and the masks are shown in different transparencies. The sample shown is βTCP.

Morphometric analyses were also performed on the samples. In the cylinder masks, bone volume (BV) and biomaterial volume (BMV) as well as the corresponding densities bone volume density (BV/TV) and biomaterial volume density (BMV/TV) were computed, where the total volume (TV) is the volume of the cylinder mask. Furthermore, the total residual biomaterial volume (Res. BMV), the average granule diameter (BM.Th) and the total callus

bone volume (Callus BV) were computed. To get an overview on the dataset, two-dimensional (2D) overview images of each sample were created. The overview images show consecutive slices through the sample along the three principal directions XY, XZ and YZ, but results will not presented. To identify statistical differences between the groups several samples per group are required, for this reason, only a qualitative evaluation of the performances of the granules and their degradation behavior could be performed.

3.9.2 Sinus lift test

Sinus floor elevation is one of the most used applications in dental field for bone substitutes, in particular for the granular shape. Different synthetic materials in alternative to allograft and xenograft are used for sinus lift, but calcium phosphates are the most applied. Example CaP granules used in clinical studies are: βTCP (Synthograft)[94], βTCP (Cerasorb) [92], HA (Engipore) [93], HA/βTCP (Boneceramic) [145], Mg-HA (Sintlife) [96].

In this work, the sinus lift test was performed as a pilot study in animal model more similar to human considering this specific clinical application. This preliminary *in vivo* study was approved by the Italian Ministry of health, with ministerial decrees 31/2008-B and 32/2008-C of 14/03/2008. The test was performed in ENEA (Italian National agency for new technologies, Energy and sustainable economic development) Casaccia (Rome).

The biomaterial used in this test was only the biphasic one, HA/TTCP, in composition 60% HA and 40% TTCP, because it has never been applied in granular form in *vivo* test. Moreover, the material was evaluated not being

cytotoxic from in vitro experiments and implantation test performed on rabbit showed that mature neo formed bone has growth around granules without any inflammation reactions and in a reasonable time, 6 weeks. The granules size range was 400-600 μm, with respect to normal used size 500-1000 or 1000-2000 μm because the implantation site has the same morphology, but smaller size than human sinus.

For in vivo experiment the animal model choice depends on three different aspects: species, implantation site and recovery time. The animal model has to simulate as much as possible the human conditions of the specific clinical application. Also the implantation site has to be chosen on the basis on the similarity with bone structure, biomechanics conditions and remodeling behavior of the different human bone structures. In this specific study the maxillary bone has peculiar characteristics that make it very difficult to find a proper animal model. Considering recovery time the only one animal model avalaible is the primate. For this reasons this study was performed on Macaca Fascicularis.

Two different explantation times were chosen: 14 weeks to observe the remodelling/new bone formation processes and study the degradation rate of the biomaterials and 17 weeks to simulate the recovery time applied during the normal clinical practice.

The procedure included the use of a piezoelectric bone surgery device for the opening of the window (Mectron Piezosurgery 3, Carasco, Italy).

About 2 g of material were added to saline and antibiotic powder, and then grafted to the upside. A collagen membrane has also been positioned to the closing of the window and to a protection of the slightly perforated

membrane. The procedure lasted upwards of a total of 45 minutes without complications.

A histological study was performed on all available samples. All bone biopsies were immediately rinsed in saline, fixed in 10% neutral buffered formalin, and processed to obtain thin ground sections. The specimen were dehydrated in an ascending series of alcohol rinses and then embedded in resin. After polymerization of the resin, the specimens were sectioned to obtain about 40 to 50 μm thick slices. The histological slices were than stained with toluidine blue. Histomorphometric analyses were performed with IAS 2000 image-analysis software.

The following parameters were calculated for each retrieved samples:

- bone volume (BV): the density of the total bone volume over the total volume after the exclusion of the bone marrow and the soft tissues. It was calculated as vital bone volume over total volume (BV/TV).
- vital bone (VB): the density of newly formed bone around granules and inside the 3D macroporous structure formed by granules close to each other. It was calculated as vital bone volume over total volume (VB/TV).
- graft volume (GV): the amount of the residual volume of granules and it was calculated as the volume of graft over the total volume (GV/TV).

Taking into account ethical aspects only two animals were included in this preliminary *in vivo* studies; for such reason statistical analysis could not be performed and only a qualitative and semi-quantitative evaluation of the in vivo performances of the granules was possible.

4 RESULTS AND DISCUSSION

This chapter is dedicated to the development of the production process with the aim to point out different factors that can influence the properties of the final product. Results of the influence of distinct parameters linked to the material or to the droplet extrusion process are presented and discussed. Specific chemical and mineralogical compositions for pure and doped granules were obtained with particular properties.

In vitro results are also presented, showing the solubility, the degradation and the bioactivity behavior in specific solutions and the cytotoxicity performance in contact with cells. At the end of the chapter in vivo outcomes are exposed to demonstrate the biocompatibility with host tissue and the performance in bone repairing and remodelling.

4.1 Characterization of bioceramics powders

Bioceramics powders are the most important materials because they determine the final composition and purity, the surface roughness and internal microporosity. A small amount of foreign crystalline phase not declared by the commercial supplier could drastically modify the composition of the final granules.

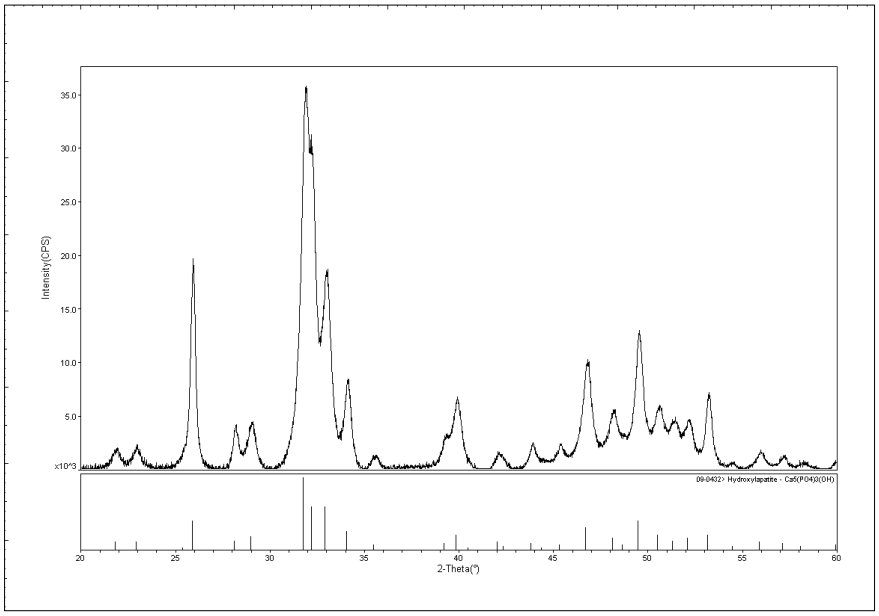

Fig. 4.1 XRD pattern of HA powder.

Hydroxyapatite used for production of the HA and HA/TTCP granules was characterized by a less ordered structure as shown from XRD pattern (Fig. 4.1), which exhibits the broadening of peaks.

CDHA powder is the only one that is treated before the process. No chemical transformations took place except the evolution of adsorbed water upon calcination (Eq.12) [146].

$$Ca_{10-x}(HPO_4)_x(PO4)_{6-x}(OH)_{2-x} \rightarrow Ca_{10}(PO_4)_6(OH)_2+\beta Ca_3(PO_4)_2 +xH_20 \quad (12)$$

where $0<x<1$. If $x=0.5$ (Eq.13).

$$Ca_{9.5}(HPO_4)_{0.5}(PO4)_{5.5}(OH)_{1.5} \rightarrow Ca_{10}(PO_4)_6(OH)_2+3\beta Ca_3(PO_4)_2+H_20 \quad (13)$$

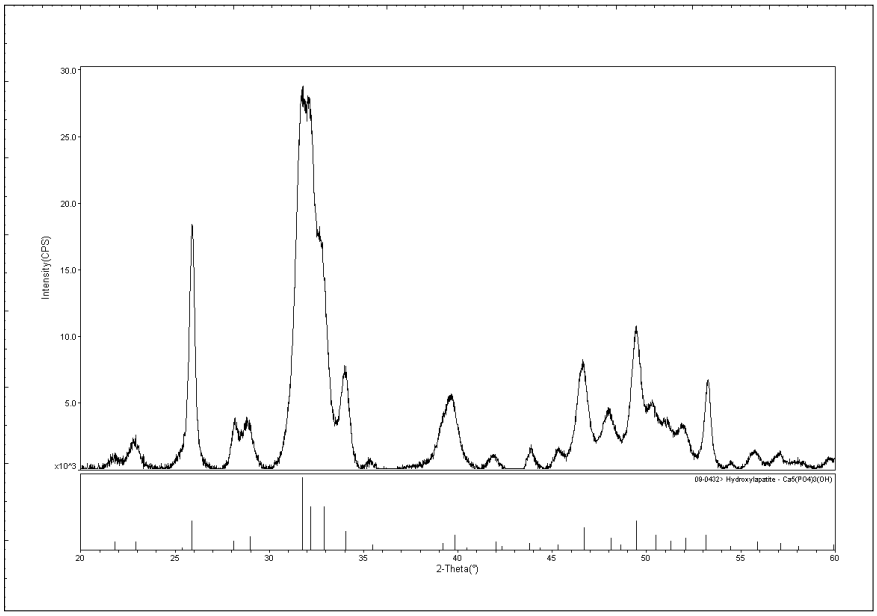

Fig. 4.2 XRD pattern of CDHA before calcination at 1000°C.

βTCP is formed during the CDHA transformation, but a small part of HA remains in the calcined powder. CDHA contains HPO_4^{2-} ions, visible in FT-IR spectra (Fig. 4.4) with specific bands at 870 cm^{-1}; moreover HPO_4^{2-} ions, not detected in FT_IR, do not completly condense in PO_4^{3-} ions and a small amount of CDHA is still present in the calcined powder. In fact, the XRD pattern (Fig. 4.3) confirms the presence of βTCP and small amount of CDHA (09-432) that has not completely transformed.

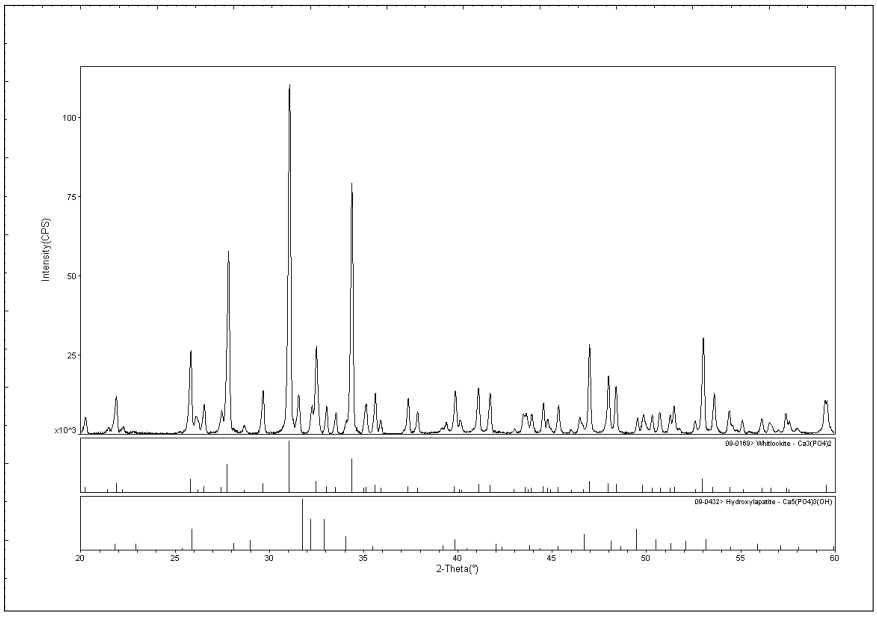

Fig. 4.3 XRD pattern of CDHA after calcination at 1000°C.

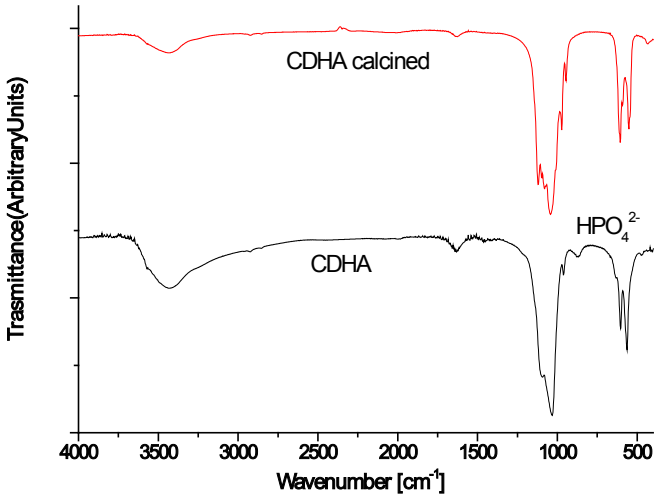

Fig. 4.4 FT-IR pattern of CDHA and calcined CDHA powders.

From the XRD results it is possible to confirm that the βTCP_1 commercial powder used here consists of a pure crystalline phase as seen in Fig. 4.5.

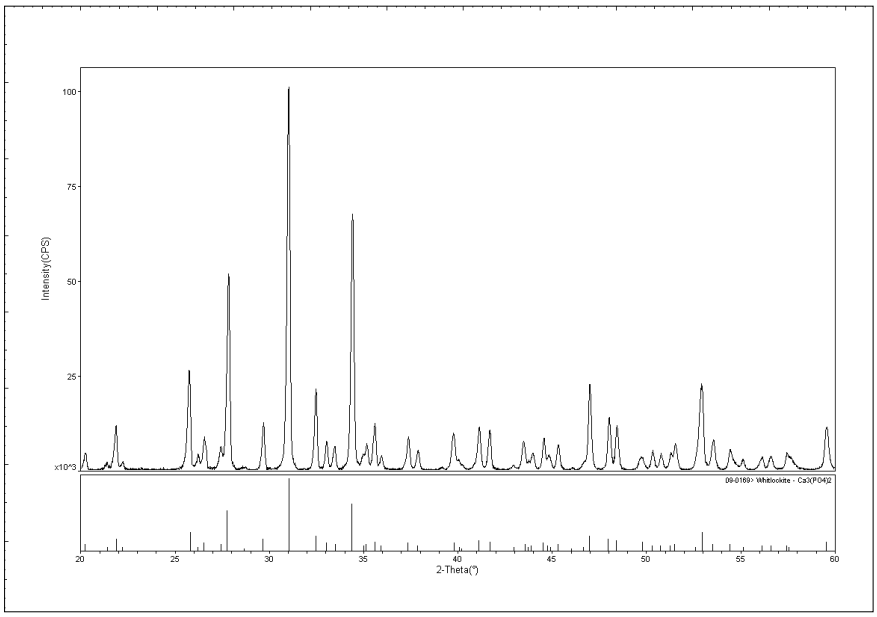

Fig. 4.5 XRD pattern of pure βTCP_1 powder.

The βTCP_2 powder is not pure but contains a foreign phase of calcium pyrophosphate ($Ca_2P_2O_7$) in small amount that has to be taken in account during the quantitative analysis of the final doped βTCP granules. Fig. 4.6 shows the XRD pattern of βTCP_2 powder.

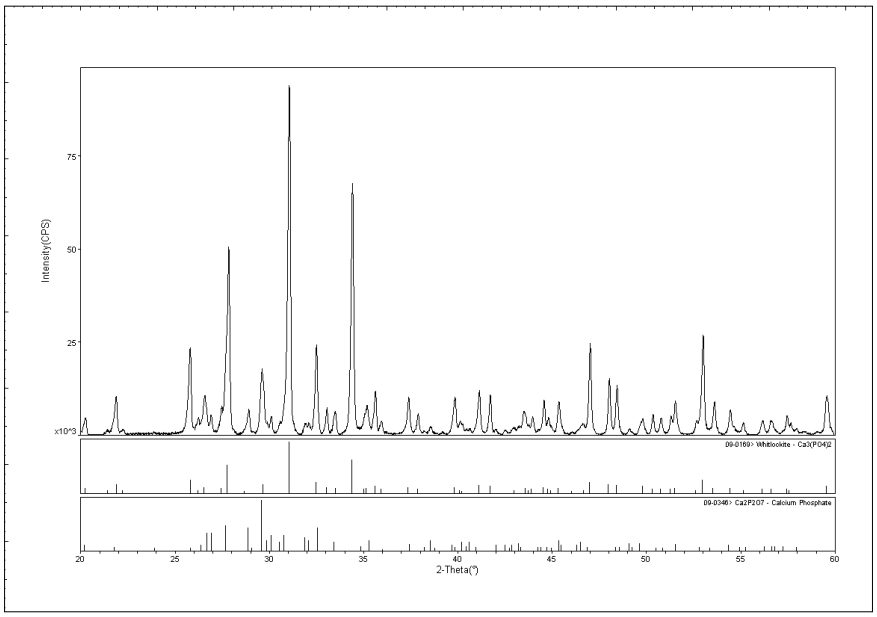

Fig. 4.6 XRD pattern of pure βTCP_2 powder.

SEM observations point out that HA powder did not have a regular shape and the grain size is in the range of 1-10 μm (Fig. 4.7).

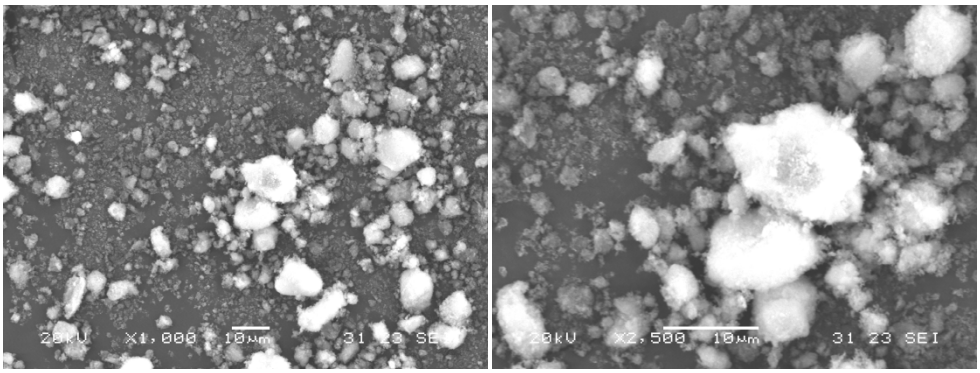

Fig. 4.7 SEM images of hydroxyapatite powder.

CDHA powder was supplied in two distinct batches with 2.5 μm and 5 μm average size (Fig. 4.8).

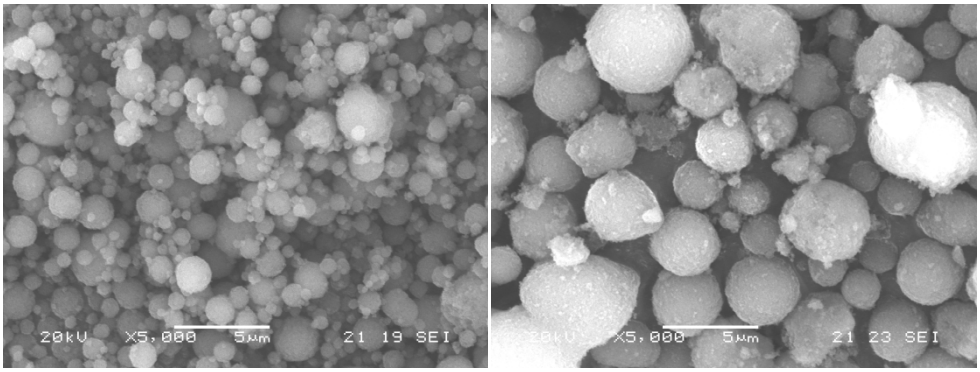

Fig. 4.8 SEM images of CDHA powder supplied with two different average grain size: 2.5 μm and 5 μm.

CDHA powder is produced by spray-drying and has the typical spherical morphology. After calcination this morphology is totally lost and a more irregular shape is observed (Fig. 4.9).

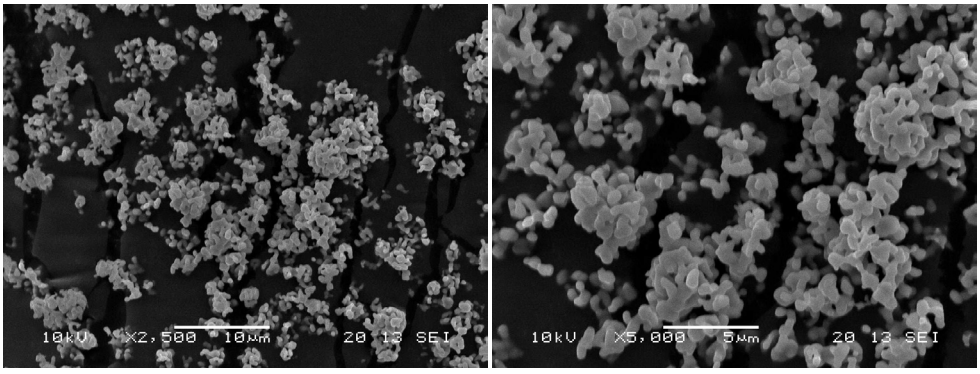

Fig. 4.9 SEM images of CDHA powder calcined at 1000°C.

βTCP_1 powder (Fig. 4.10) is more irregular and acicular and the average size is 5-10 μm.

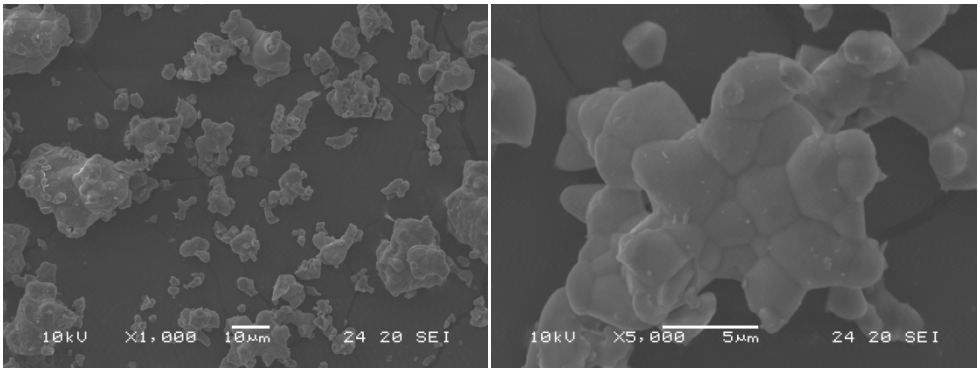

Fig. 4.10 SEM images of βTCP_1 powder.

βTCP_2 powder (Fig. 4.11) is similar in morphology to βTCP_1, but the average size is 5-20 μm.

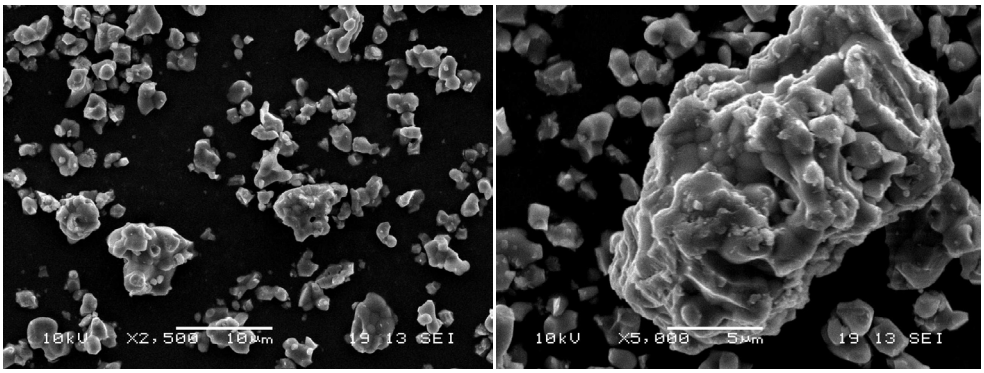

Fig. 4.11 SEM images of of βTCP_2 powder.

4.1 The general process

The process layout includes various steps that have to be analyzed in a sequential way. The first stage is the preparation of the ceramic suspension composed by a polysaccharide aqueous solution and bioceramic powders. This suspension is pumped in an automatic encapsulator that allows the production of drops which gelify instantaneously in a crosslinker/hardening solution maintaining the spherical shape by using different gelification mechanism. Granules can be produced in pure form, but they can also be doped by using crosslinker solution containing divalent ions, in particular zinc and strontium, that can be chelated by the alginate biopolymer. After a hardening time and deep washing to eliminate the excess of crosslinker solution, wet granules are subsequently dried in a microwave oven to eliminate water (Fig. 4.12).

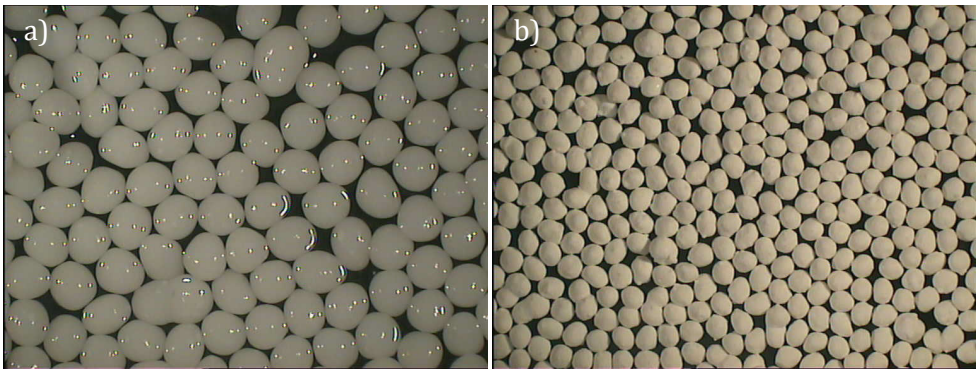

Fig. 4.12 Optical images of a) wet granules and b) dried granules.

Dried granules are successively sintered at high temperature, to burn-off the polymer and obtain spheres with an interconnected porosity and a uniform round shape (Fig. 4.13).

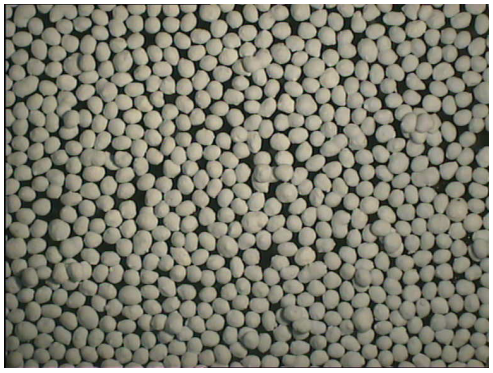

Fig. 4.13 Sintered granules.

After the thermal treatment spherical microspheres have to be sieved to obtain the desired granulometry, but rejection is very low due to very narrow size distribution.

4.1.1 Composition: influence of materials

Initial **bioceramic powder** plays a fundamental role in the control of mineralogical composition. The inorganic part is the only component that remains throughout the entire process. From experiments done, it is not assumed that, the final granules possess the same initial composition as the starting powder. In fact the interaction of CaP powder with external organic matrix is important to change the stoichiometry and can favour one or more phase transformation depending on the stability and on the purity of starting material.

Crosslinker solution plays a fundamental effect on the chemical composition of final granules. By varying the molarity or the ion concentration in the crosslinker solutions, the main crystalline phases and extraneous phases can be controlled. During the development of the definitive composition, different situations were found.

Calcium, zinc and strontium ions, due to their chemical properties, can favour or limit the formation of one specific phase. Table 4.1 summarizes the main stabilization mechanisms starting from CDHA powder.

Divalent Ion	Powder	Stabilized and substituted phase
Calcium	CDHA	HA
Zinc	CDHA	βTCP
Strontium	CDHA	HA

Table 4.1 Stabilization mechanism of zinc and strontium.

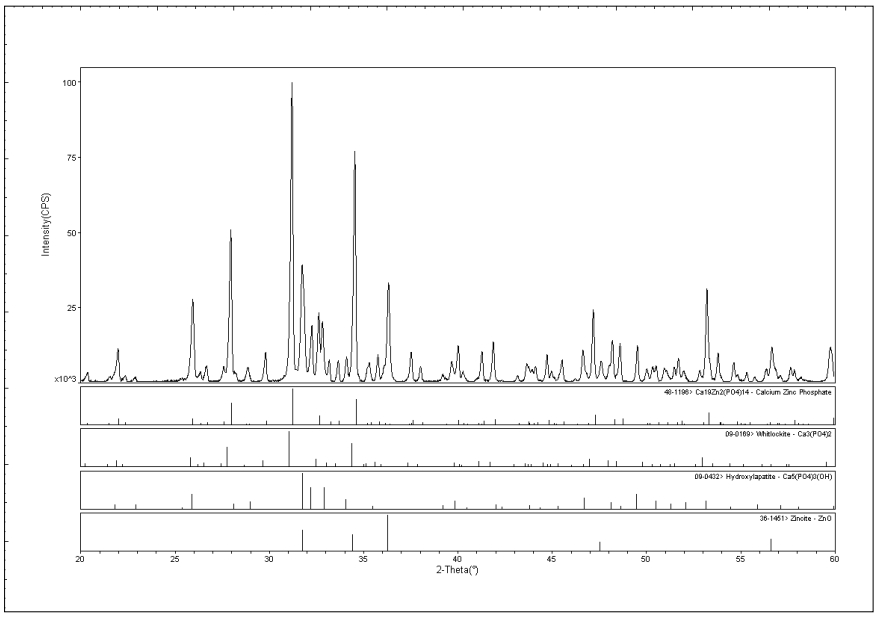

Fig. 4.14 XRD pattern of granules obtained from CDHA powder, alginate and 0.02 M of Zn(CH3COO)2.

Fig. 4.14 and Fig. 4.15 show the XRD pattern of granules obtained from CDHA powder and $Zn(CH_3COO)_2$ and $SrCl_2$ solution of same molarity, 0.02 M. In one case, (Fig. 4.14) biphasic material HA/βTCP with a high content of ZnO is achieved; in the case of Sr stabilization only crystalline HA was obtained (Fig. 4.15).

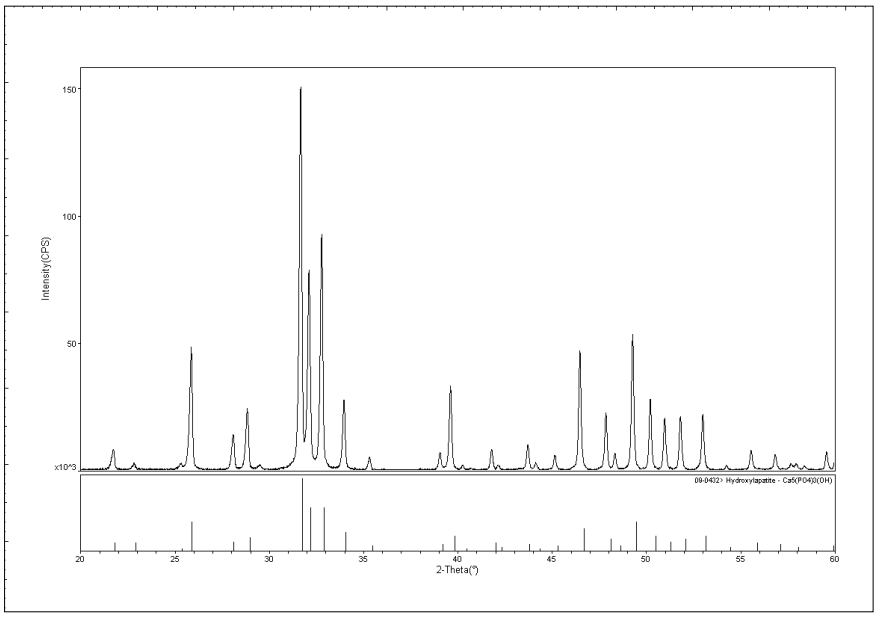

Fig. 4.15 XRD pattern of granules obtained from CDHA powder, alginate and 0.02 M of $SrCl_2$.

4.1.2 Shape: influence of materials

The **alginate concentration** has an influence on the shape of wet microspheres. In fact if the concentration of the same alginate is low, less than 1% (10g/l), using the same molarity of crosslinker, the effect is totally different.

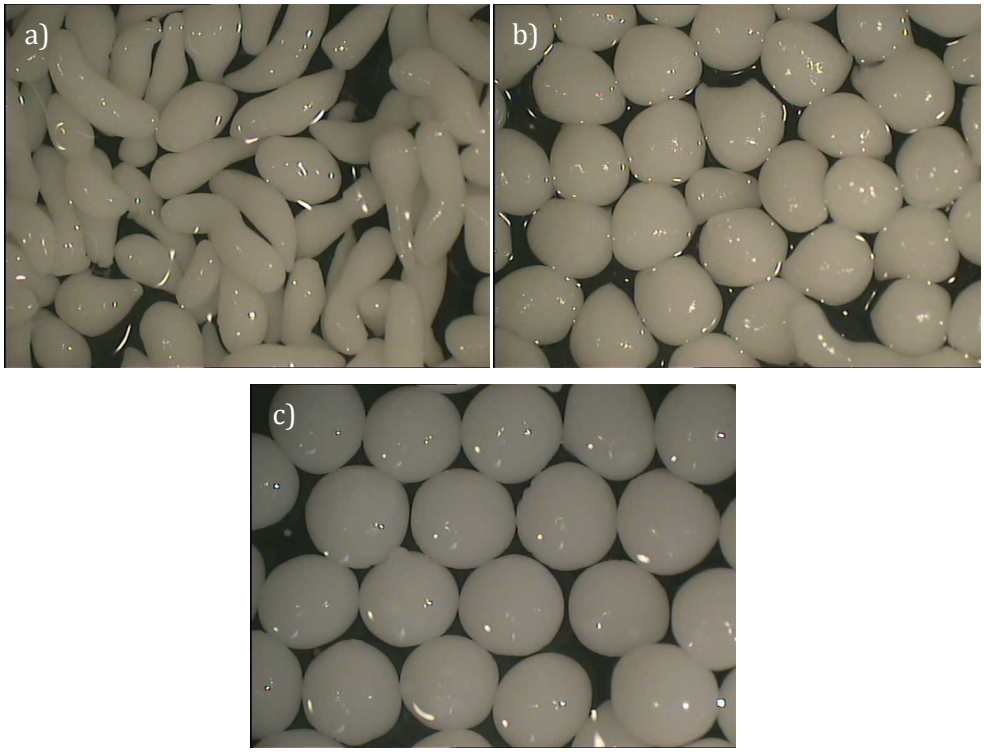

Fig. 4.16 Wet granules at different alginate concentration: a) 0.5%, b) 1% and c) 2 %.

Fig. 4.16 shows that for alginate concentration of 0.5 %, the obtained gels drops are lumps; at 1% the shape is spherical, but not like in the case of 2% where the size distribution of granules is narrow and the shape is very regular.

The **vibration frequency** is an important parameter for size and shape control of wet microspheres. From numerous experiments, keeping the nozzle, pump flux and the gelification ingredients constant, it is possible to

find that a slight increase of frequency, 0.1 KHz, causes shape distortion and spheres tend to bond together as seen in Fig. 4.17. The vibrational cutting rate of the laminar flow is too high and suspension drops are too close for gelifying alone. Table 4.2 shows the process parameters in one specific experiment chosen as an example.

Sample	Cross-linking solution	Nozzle [µm]	Pump Flux [ml/min]	Vibration Frequency [KHz]
A	0.1M $CaCl_2$	400	14	**0.13**
B	0.1M $CaCl_2$	400	14	**0.14**

Table 4.2 Experimental parameters for checking the vibration frequency influence.

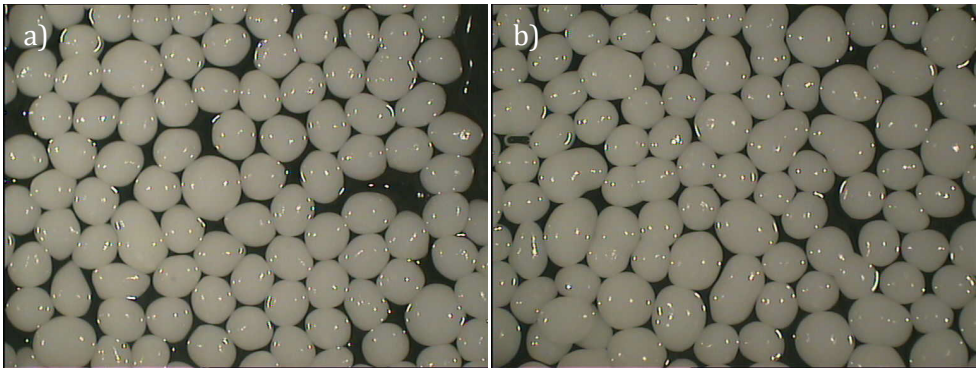

Fig. 4.17 Wet granules obtained a two different vibration frequency: a) 0.13 KHz and b) 0.14 KHz.

4.1.3 Size: influence of processing parameters

The final granules size is controlled by the choice of the correct **nozzle**. For understanding how the nozzle diameter can influence the granulometry

different experiments were carried out. Fixed encapsulator parameters are shown in Table 4.3. The nozzles and pump flux chosen are listed in Table 4.4.

Encapsulator parameter	Fixed value
Vibration Frequency	0.14 KHz
Amplitude	100%
Drop Height	25 cm

Table 4.3 Fixed encapsulator parameters.

Sample	Powder	Alginate	Cross-linking solution	Nozzle [μm]	Pump Flux [ml/min]	Thermal Treatment
A	HA	B	0.1M $Zn(CH_3COO)_2$	**400**	16	1250°C_2h
B	HA	B	0.1M $Zn(CH_3COO)_2$	**500**	21	1250°C_2h
C	HA	B	0.1M $Zn(CH_3COO)_2$	**600**	28	1250°C_2h
D	HA	B	0.1M $Zn(CH_3COO)_2$	**800**	38	1250°C_2h
E	HA	B	0.1M $Zn(CH_3COO)_2$	**1000**	45	1250°C_2h

Table 4.4 Experimental parameters used for checking the nozzle size influence.

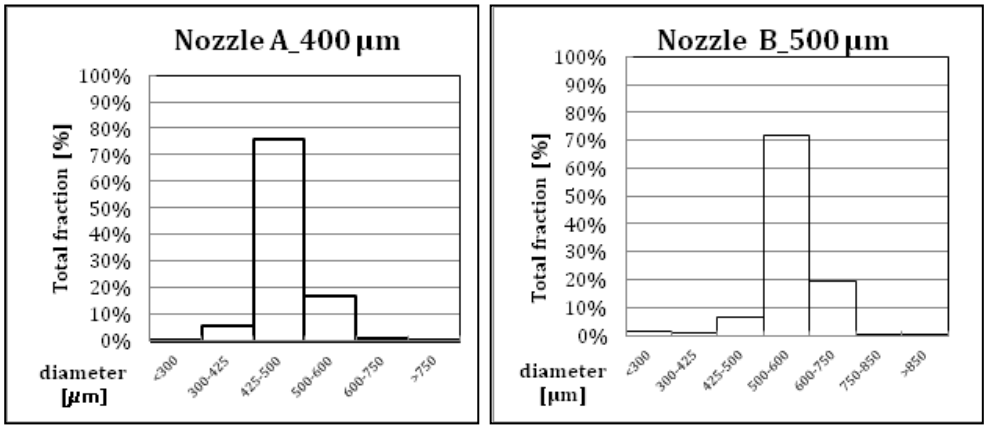

Fig. 4.18 Granules size distribution obtained with: A=400 nozzle and B=500 nozzle.

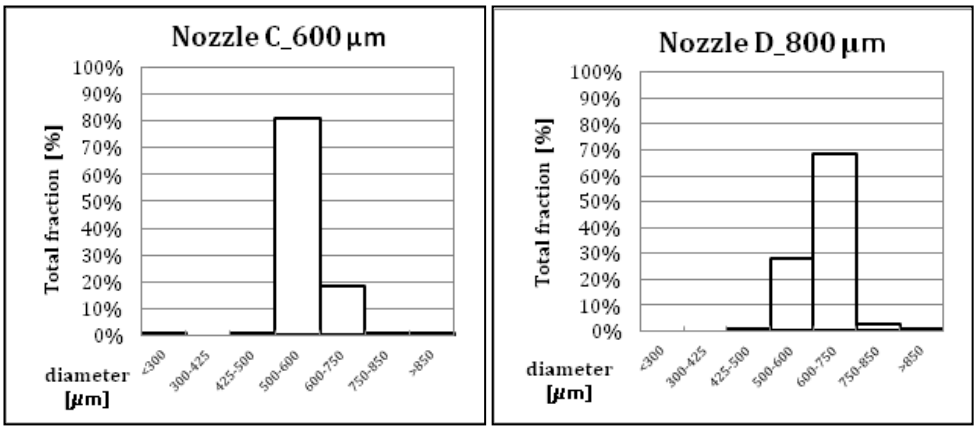

Fig. 4.19 Granules size distribution obtained with: C=600 nozzle and D=800 nozzle.

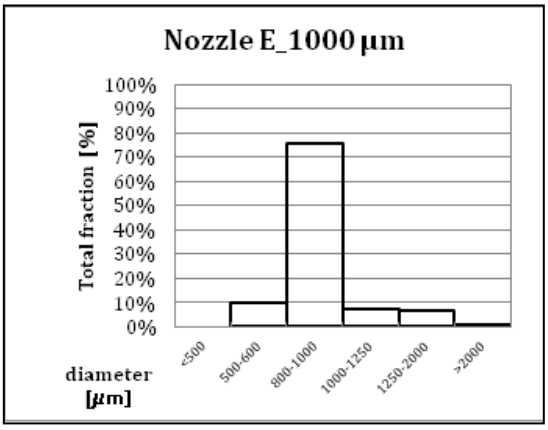

Fig. 4.20 Granules size distribution obtained with: E=1000 nozzle.

Data corresponding to granules size (Fig. 4.18- Fig. 4.20) demonstrated that with different nozzles it is possible to obtain various range of granulometry and very narrow size distribution. The more representative size range is more or less the 70% of all sintered granules and the calculated size is equivalent to nozzle diameter. By using a small nozzle. such as 400 µm or 500 µm. the size distribution curve is very sharp because the control of the dimension of the falling drop is easier with less material involved. Perturbation and gravity forces have more influence when the suspension volume is increased. The theory developed on alginate drop confirmed the data and the trend follow a proposed Tate's law (Eq.14) [147].

$$Dp = K\,(0.006 d_T \gamma/\rho g)^{1/3} \qquad (14)$$

where dp is the diameter of drop (mm). d_T is the outer diameter of nozzle (mm). ρ is the density of alginate solution (kg/m^3). g is the gravitational force

(9.81 m/s²). γ is the surface tension of alginate solution (mN/m). The K factor is the product of liquid lost factor (kLF) and shrinkage factor (kSF).

If the density of alginate solution is constant because the concentration is kept at 2% (20 g/L). the final wet diameter depends on nozzle diameter and on gravity force associated to the droplet mass. The calculation of the granules size was performed on sintered product and. for this reason the thermal treatment also has a high influence on the total shrinkage. 70-80 % of the sintered granules are in the range that represents the nozzle size. as shown in Table 4.5.

Sample	Nozzle [µm]	Main size range [µm]	% Main size range
A	400	425-500	**76.80**
B	500	500-600	**71.74**
C	600	500-600	**81.19**
D	800	600-750	**68.20**
E	1000	800-1000	**75.45**

Table 4.5 Percentage of main size using different nozzles.

The **pump flux** has an influence on the shape and on diameter of sintered granules. Only ±2ml/min can change in a large way the size distribution curve and the main size range can vary of many percentage points. For example Table 4.6 shows the parameters of experiments performed with the same nozzle and vibration frequency, by varying only the pump flux between 14 and 18 ml/min.

Sample	Cross-linking solution	Nozzle [μm]	Pump Flux [ml/min]	Vibration Frequency [KHz]	Thermal Treatment
A	0.1M $Zn(CH_3COO)_2$	400	**14**	0.14	1250°C_2h
B	0.1M $Zn(CH_3COO)_2$	400	**16**	0.14	1250°C_2h
C	0.1M $Zn(CH_3COO)_2$	400	**18**	0.14	1250°C_2h

Table 4.6 Experimental parameters for pump flux test.

The main size range, in this case 425-500 μm. can vary up to 20% as shown in Table 4.7 and in Fig. 4.21.

Size range	A-14	B-16	C-18
<300	0.10%	0.15%	1.68%
300-425	12.28%	5.63%	7.51%
425-500	**70.57%**	**75.68%**	**55.15%**
500-600	12.89%	17.10%	34.33%
600-750	4.15%	1.15%	0.99%
>750	0.00%	0.29%	0.35%

Table 4.7 Percentage of different size range for each production batch.

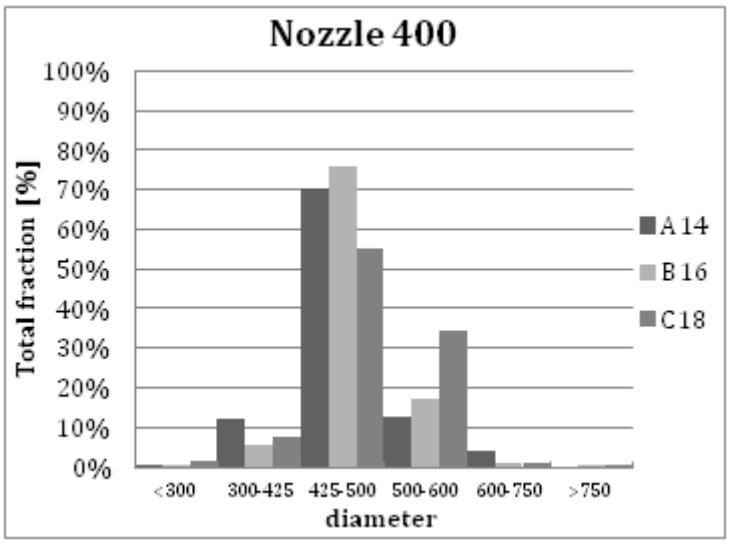

Fig. 4.21 Influence of pump flux on granules size.

4.1.4 Microporosity: materials

Different **sodium alginates** were used to analyze their influence on gelification mechanism and consequently on the granule morphology. During the experiments three sodium alginates, dissolved in demineralized water. were mixed with calcium phosphate powders in the ceramic suspensions. The gelification process depends mainly on the percentage of guluronic acid. The data in Table 4.8 represent the main characteristic of sodium alginate chosen as M/G and % GG blocks which determine the interconnectivity grade of the alginate gel.

Sodium Alginate	M/G	%GG blocks
A	1.56	16
B	1.56	16
C	0.8	57

Table 4.8 Sodium alginate typologies used.

The first experiments involved granules produced with HA powder and 0.05 M $CaCl_2$ crosslinker and the 800 nozzle. After a thermal treatment at high temperature, 1000°C for 2 h. the section microstructure was analyzed to see the effect of the alginate on microporosity. Experimental parameters are listed in Table 4.9.

Powder	Alginate	Cross-linking solution	Nozzle	Thermal Treatment
HA	**A**	0.05M $CaCl_2$	800	1000°C_2h
HA	**B**	0.05M $CaCl_2$	800	1000°C_2h
HA	**C**	0.05M $CaCl_2$	800	1000°C_2h

Table 4.9 Experimental parameters for checking the alginate type influence.

SEM observations (Fig. 4.22) show the granules section and the internal microstructure appears more open for samples produced with an alginate containing less GG blocks (a. b) respect to those with a higher content of GG (c).

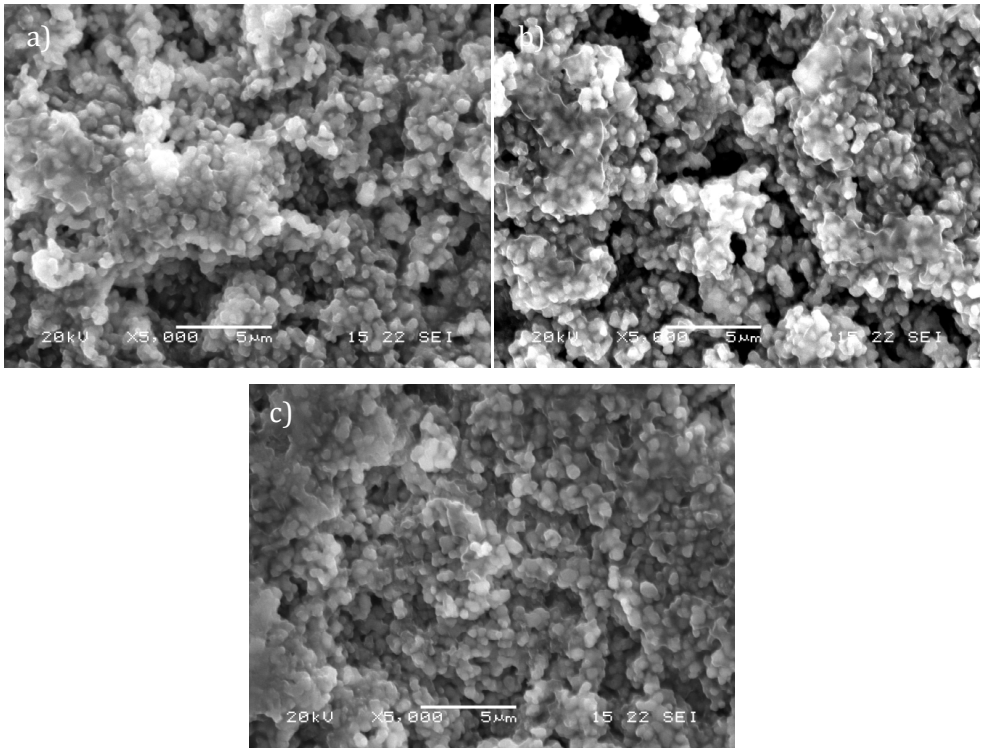

Fig. 4.22 SEM images of granules section produced by different alginate.

The result is different in the case of polyelectrolyte complexation performed with CDHA powder and the crosslinker solution of Chitosan 0.01 % in 1% of acetic acid combined with two types of alginate: A and C. Experimental parameters are listed in Table 3.10. Fig. 4.23 shows the difference between the A-alginate microstructure (a) and the C-alginate microstructure (b). The microstructure produced by the rich GG C-alginate is more open and porous due to the gel structure than the A-alginate granules.

Powder	Alginate	Cross-linking solution	Nozzle	Thermal Treatment
2.5 µm CDHA calcined	**A**	Chitosan 0.01% in 1% v/v acetic acid	800	1000°C_2h
2.5 µm CDHA calcined	**C**	Chitosan 0.01% in 1% v/v acetic acid	800	1000°C_2h

Table 4.10 Experimental parameters for checking alginate type influence.

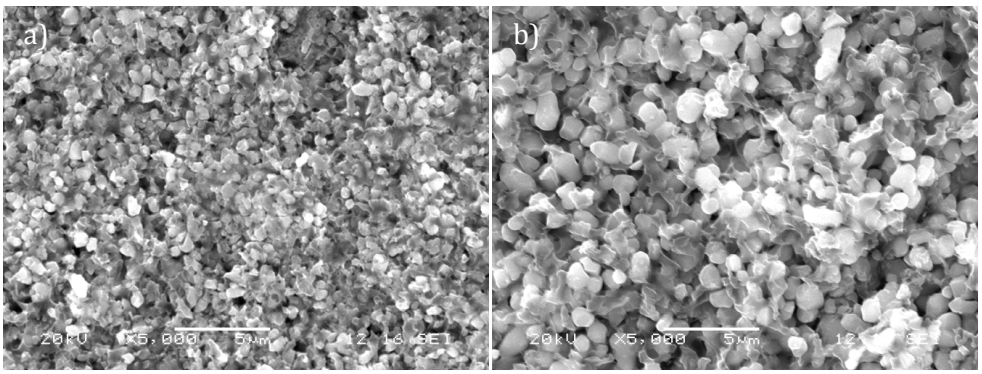

Fig. 4.23 Microstructure of granules section with poor a) GG alginate and c) rich GG alginate.

The **crosslinker solution** has an important effect on the gelification mechanisms, which depend on the molarity and on availability of free ions with opposite charge. In this section the effects on microporosity of several crosslinker solutions ($CaCl_2$. $Zn(CH_3COO)_2$. $SrCl_2$) and mixed reagents are explained. Each dopant ion has an effect on microstructure due to different dimension and various interactions with Na-Alginate. Crosslinking solutions are listed in Table 4.11. The Zn ion can interact with GG. MM and GM linkages of B Alginate and in fact it is possible to observe in Fig. 4.25 that the (a)

granule's microstructure is more porous than (b) and (c) without Zn. Moreover. Ca molarity has an influence on microporosity. The b) microstructure seems less dense than c) microstructure because if more Ca^{2+} ions are chelated by carboxyl group of GG blocks (only the 18% in *alga Macrocystis pyrifera*) the gel matrix is more opened and the subsequent micropores are smaller (Fig. 4.24).

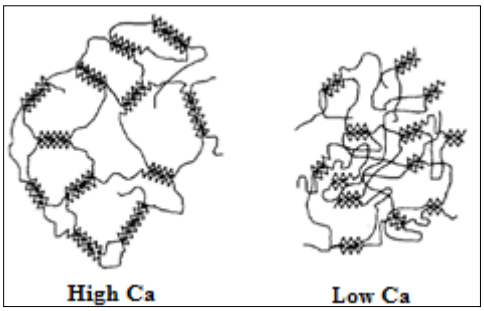

Fig. 4.24 Gel matrix structure with high and low Ca concentration.

Powder	Alginate	Cross-linking solution	Nozzle	Thermal Treatment
HA	B	**0.01M $CaCl_2$ + $Zn(CH_3COO)_2$ 0.01M**	800	1400°C_2h
HA	B	**0.05M $CaCl_2$**	800	1400°C_2h
HA	B	**0.1M $CaCl_2$**	800	1400°C_2h

Table 4.11 Experimental parameters for checking crosslinker type influence.

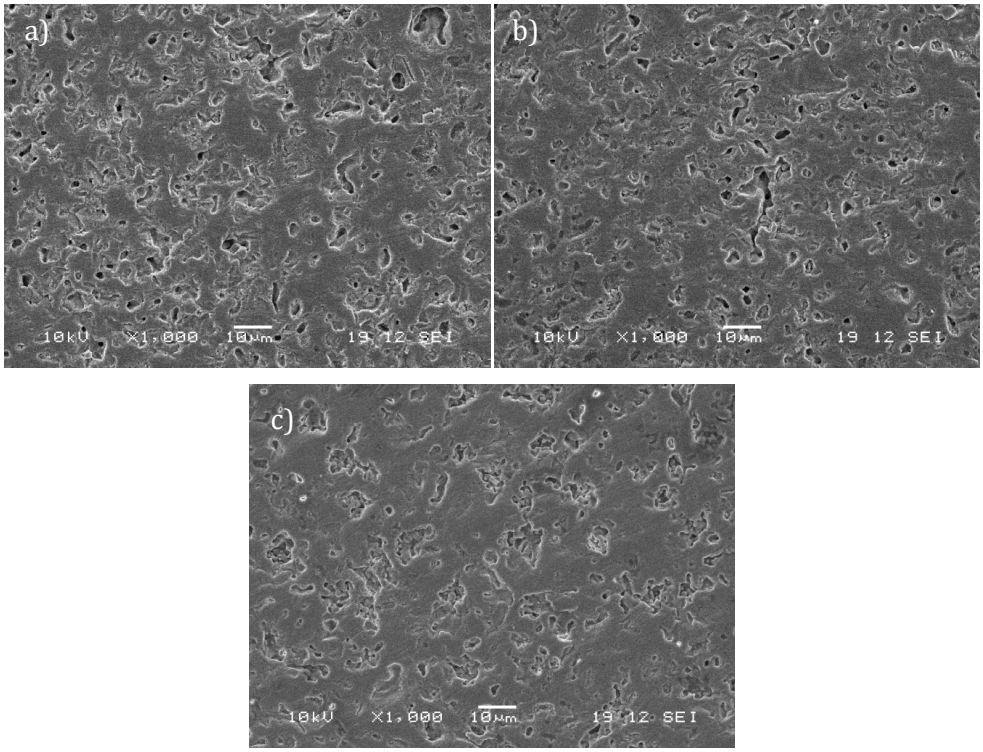

Fig. 4.25 SEM observation of granules section with different microporosity obtained due to distinct crosslinker type and concentration: a) 0.01M $CaCl_2$ + $Zn(CH_3COO)_2$ 0.01M. b) 0.05M $CaCl_2$ and c) 0.1M $CaCl_2$.

One further study was performed by using the process parameters listed in Table 4.12. The average pore size does not change and it is between 0.1 µm and 10 µm. There is a difference between Zn and Ca interactions with the same B alginate in granules sintered at the same temperature, 1250°C. The Ca microstructure (a) is less porous and less interconnected than Zn microstructure (b) (Fig. 4.26).

Powder	Alginate	Cross-linking solution	Nozzle	Thermal Treatment
HA	B	**0.1M $CaCl_2$**	1000	1250°C_2h
HA	B	**0.1M $Zn(CH_3COO)_2$**	1000	1250°C_2h

Table 4.12 Experimental parameters for checking crosslinker type influence.

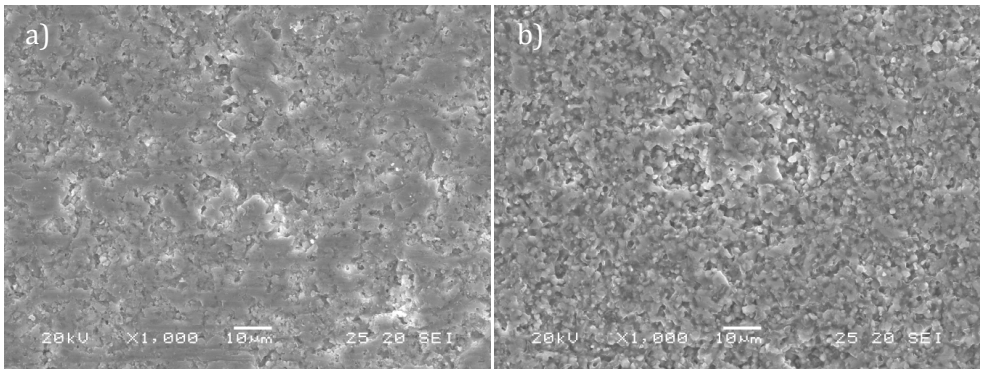

Fig. 4.26 Granules microstructure using Ca^{2+} and Zn^{2+} ions.

4.2 Development of optimized CaP granules compositions

By using the results collected from different experiments, the production process was optimized to reach the specific final composition for round shape granules with an interconnected microporosity.

4.2.1 HA granules

At the beginning HA granules were produced from a bioceramic suspension of commercial HA with Na-alginate (G/M=0.8) in water manually poured in form of small droplets in a crosslinking solution of $CaCl_2$ at 0.1 M to obtain round microspheres.

HA granules were analyzed by XRD (Fig. 4.27) and a foreign phase, 5 wt% CaO, was detected. For this reason the molarity of crosslinking solution of $CaCl_2$ was decreased and Na-Alginate with a higher G/M = 1.6 was chosen for achieving the same gelation effect with less Ca^{2+} available. The molarity was reduced to 0.01 M and CaO was still present in final composition. but it was not always less than 5%wt.

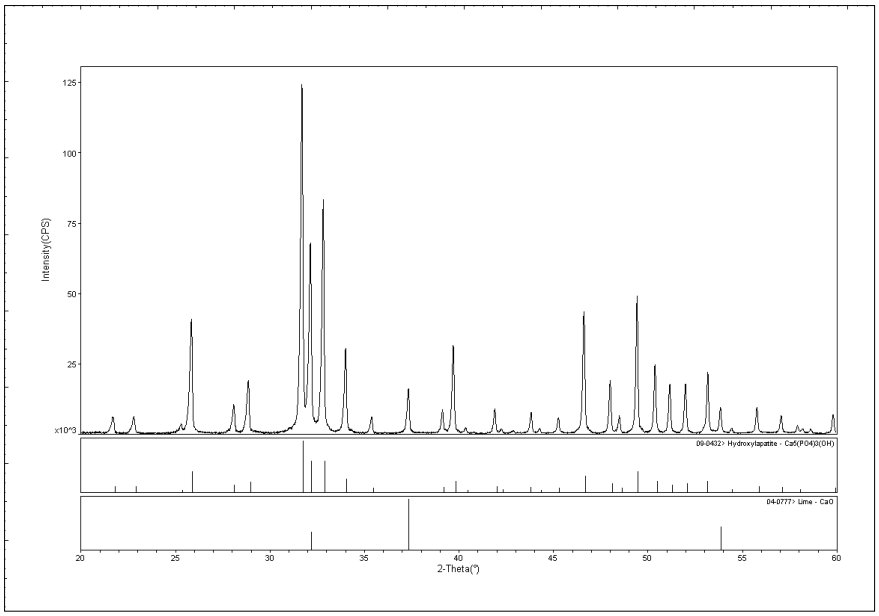

Fig. 4.27 XRD pattern of HA granules obtained with 0.05 $CaCl_2$.

For this reason another method was used to avoid the crosslinking solution of $CaCl_2$ and the polyelectrolyte complexation between the Na-alginate and chitosan. The CaO amount was reduced to values less than 3%wt as shown by the XRD pattern (Fig. 4.28 and Table 4.13) and HA granules were more denser with a sensible reduction of the internal microporosity due to the different gelification mechanism. In addition, preliminary cytotoxicity tests revealed. the percentage of cell viability was reduced to 43.17% beyond the safe 30% due to the presence of CaO. For this reason another step was introduced: after sieving HA granules, they were washed with Na_3PO_4 aqueous solution (0.9%) to accelerate the CaO solubilization and reduce it at values lower than 1%wt.

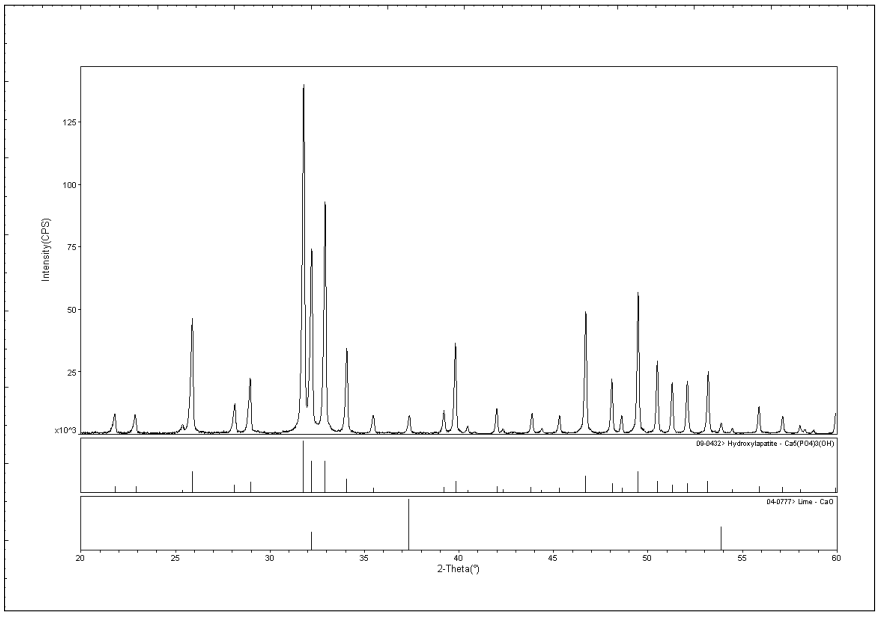

Fig. 4.28 XRD pattern of HA granules obtained with 0.3 Chitosan in 1% of Acetic Acid.

Polysac	Cross-linking solution	Sintering	HA %	βTCP %	**CaO %**	TTCP %	αTCP %
Alg	0.5 M $CaCl_2$	1000 /2h	93.7	0.0	**4.2**	1.2	0.0
Alg	Chi 0.3% in 1% A.A.	1000 /2h	97.2	0.0	**1.9**	0.9	0.0

Table 4.13 XRD pattern of no optimized HA granules.

The sintering temperature was chosen at 1000°C to allow material consolidations and densification without closing all interconnected porosity while still having enough mechanical properties for handling the HA granules in surgical procedures. The weight loss upon sintering is 25%. due to the water loss at 100°C and 200°C and the organic matrix burning off in the range 250-600°C reported in Fig. 4.29.

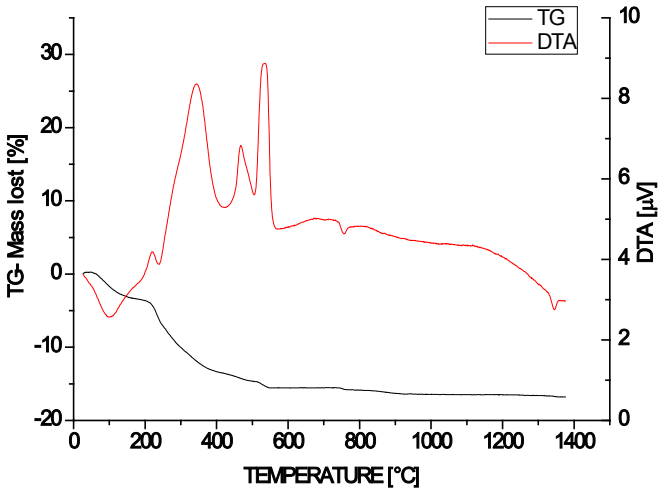

Fig. 4.29 TG/DTA measurements on dried HA granules.

4.2.2 HA/TTCP granules

HA/TTCP granules were developed from HA granules. From literature it is known that tetra-calcium phosphate ($Ca_4(PO_4)_2O$) can be formed by a phase transformation of HA between 1350°C and 1400°C [148]. From dehydratation process, the oxyhydroxyapatite (OCP) is formed and then it is transformed in TTCP and αTCP (Eq. 15).

$$Ca_{10}(PO_4)_6(OH)_2 \rightarrow Ca_4(PO_4)_2O + 2Ca_3(PO_4)_2 + H_2O \quad (15)$$

In the HA/TTCP production process an excess of Ca^{2+} is present due to the use of $CaCl_2$ as a hardening solution. This excess leads to the formation of CaO that reacts with αTCP and forms only TTCP (Eq.16).

$$Ca_3(PO_4)_2 + CaO \rightarrow Ca_4(PO_4)_2O \quad (16)$$

Therefore, upon sintering at 1390°C, HA granules made by Na-alginate and HA commercial powder crosslinked in a 0.05 M $CaCl_2$ solution, it is possible to get HA/TTCP granules. XRD quantitative analysis confirmed the final composition consisting of 60%wt HA and 40% TTCP (Table 4.14).

Polysac.	Cross-linking solution	Sintering	HA %	βTCP %	CaO %	TTCP %	αTCP %	$CaCO_3$ %
Alg	0.5 M $CaCl_2$	1390°C /2h	59.6	0.0	0.8	39.7	0.0	0.0

Table 4.14 Quantitative XRD analysis of HA/TTCP granules.

TG/DTA curves (Fig. 4.30). referred to dried HA granules. show the endothermic peak of the OCP→TTCP transformation at 1340°C. below the sintering temperature defined at 1390°C chosen to reach the amount of 40% of TTCP. TG data show clearly the sintering weight loss of 40%. During the thermal treatment a loss of residual water is observed until 150°C. the chemical water at 240°C and the burn-off of the Ca-alginate organic matrix at 700°C. No particular endothermic or exothermic peaks relative to chemical reaction of the organic matrix are present in DTA data.

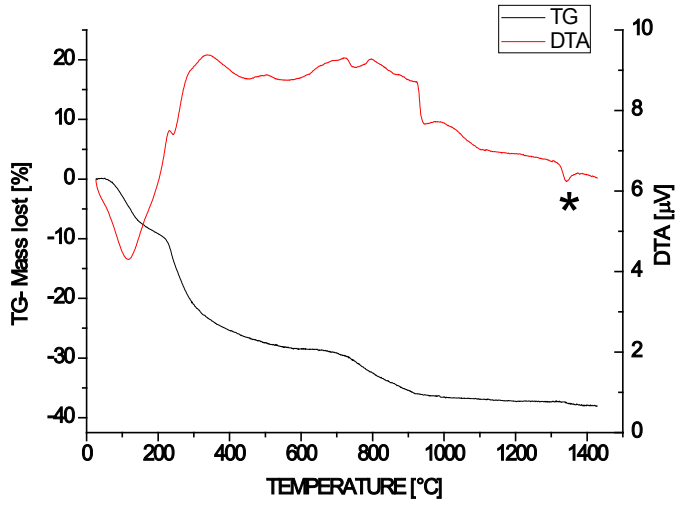

Fig. 4.30 TG/DTA measurements on dried HA/TTCP granules. The asterisk indicates the endothermic peak of OPC→TTCP transformation.

4.2.3 HA/βTCP granules

HA/βTCP granules could not be produced from HA granules because HA powder does not transform into βTCP in any range of temperature from 700 to 1400°C.A combination of Na-alginate and chitosan was chosen as in HA granules and it was initially applied to CDHA (Fig. 4.31 and Table 4.16). After microwave drying and sintering at 1000°C the composition was 70%wt of HA and 30%wt of βTCP according to reaction (Eq.17).

$$Ca_{10-x}(HPO_4)_x(PO4)_{6-x}(OH)_{2-x} \rightarrow Ca_{10}(PO_4)_6(OH)_2+\beta Ca_3(PO_4)_2 +xH_20 \quad (17)$$

The biphasic granules were obtained because the organic gel matrix has an influence on the total transformation of HA into βTCP, because of the presence of the hydroxyl ion group in the lattice during the sintering.

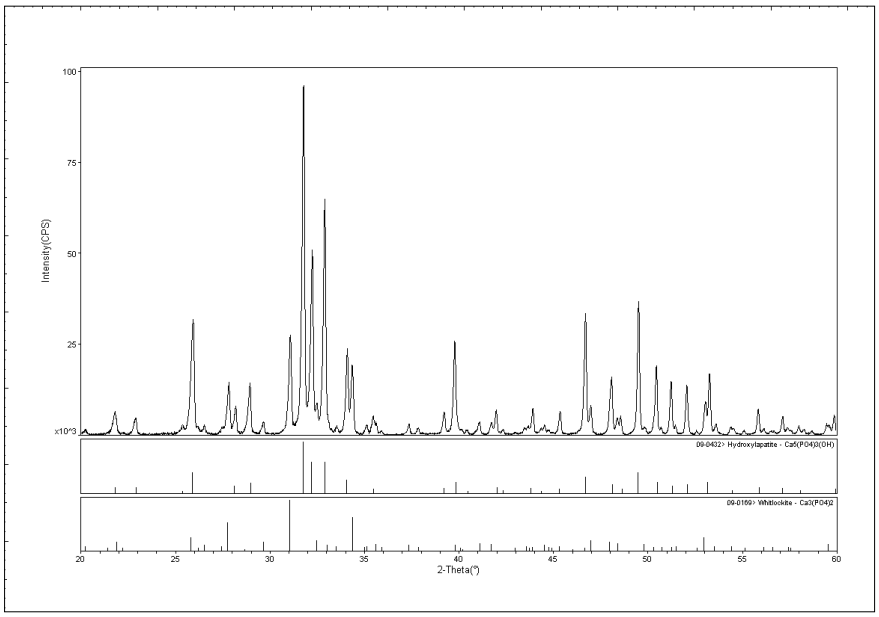

Fig. 4.31 XRD pattern of HA/βTCP granules obtained with only CDHA powder.

Polysac	Powder	Cross-linking	Sintering	HA %	βTCP %	TTCP %	αTCP %
Alg	CDHA	Chi 0.3% in 1% A.A	1000°C 2h	74.4	24.7	1.0	0.0

Table 4.15 Quantitative analysis of HA/βTCP granules.

The target composition was 60%wt HA and 40%wt βTCP and the inverse transformation from βTCP to HA were applied starting from βTCP powder derived from CDHA calcination. This powder was mixed with Na-alginate and droplets gelled in chitosan solution. Drops were washed. dried and sintered at 1000°C for 2 h and the final composition 60% HA and 40% βTCP was obtained. Some Ca ions captured from the alginate gel combined with

hydroxyl groups form $Ca(OH)_2$ and the partial transformation from βTCP to HA occured (Eq.18).

$$3\beta Ca_3(PO_4)_2 + Ca(OH)_2 \rightarrow Ca_{10}(PO_4)_6(OH)_2 \qquad (18)$$

The final biphasic composition is obtained and from TG/DTA performed on dried granules it is possible to observe that at 540°C there is an exothermic peak related to the combustion of organic matrix of alginate-chitosan. The weight loss upon sintering until 1000°C is only 13% due to the adsorbed water until 200°C and the burning off of the gel (Fig. 4.32).

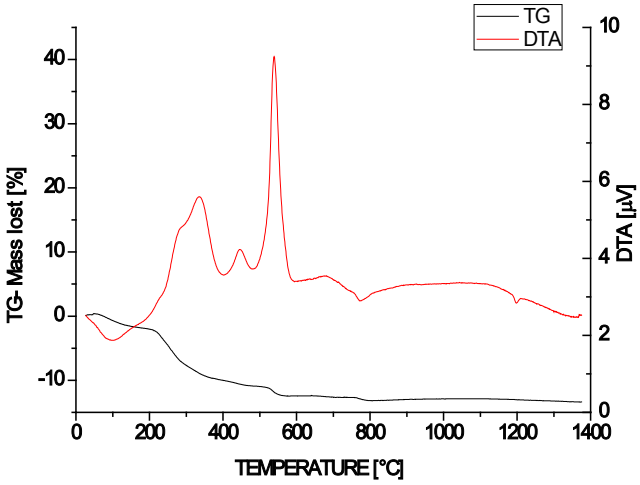

Fig. 4.32 TG/DTA measurements of HA/βTCP granules.

4.2.4 βTCP granules

At the beginning βTCP granules were produced from a suspension of CDHA powder mixed with Na-alginate crosslinked in a solution of zinc acetate. The final composition after drying and sintering was mainly βTCP. but a foreign phase of ZnO was present in excess to an allowable value (≥ 1.5%wt) [72]. Another solution combination of Na-alginate and chitosan was chosen to solve the problem of foreign phases. but the final granules were always biphasic HA/βTCP. In fact, by using the CDHA powder or calcined CDHA powder the results were almost the same. In the first case the CDHA was not totally transformed into βTCP at 1000°C; in the second case βTCP phase was not maintained and was partially transformed in HA.

The following steps were to use a commercially stabilized βTCP powder in combination with the matrix gel of alginate and chitosan, but again biphasic granules with more βTCP were produced.

The commercial βTCP_1 was also mixed with Na-Alginate and dropped in a crosslinking solution of zinc acetate because Zn stabilizes βTCP phase. In fact, βTCP was produced, but some residual ZnO was found and to respect the ASTM F1088-04a standard this solution was discarded.

The last solution applied for βTCP production was the combination of chitosan with sodium tripolyphosphate (TPP) solution. In fact the amino groups of chitosan can interact with the terminal OH- group of the TPP and form a gel. The ionotropic gelification is less efficient than in the Na-alginate-salt case and more time is required for the hardening of the spheres. TPP did not react directly with the βTCP_1 powder during sintering at 1150°C and βTCP

granules were obtained. The only foreign phase detected by XRD was calcium pyrophosphate ($Ca_2P_2O_7$) in amount less than 5%wt. The presence of $Ca_2P_2O_7$ phase is due to the transformation of polyphosphate into pyrophosphate and the incomplete transformation of pyrophosphate into orthophosphate that can be re-transformed in βTCP. This process can be controlled by regulating the humidity of the granules with slow drying after the incomplete microwave treatment and washing wet granules more times in water to eliminate any excess TPP. Granules are sintered at 1150°C for 6 h to burn out the organic matrix which leaves an interconnected microporosity. The sintering temperature and time were chosen to reach sufficient mechanical consistency and to preserve the monophasic composition. thus avoiding any foreign phase. No exothermic or endothermic peaks are visible from DTA curves and the sintering weight loss is 30% (Fig. 4.33).

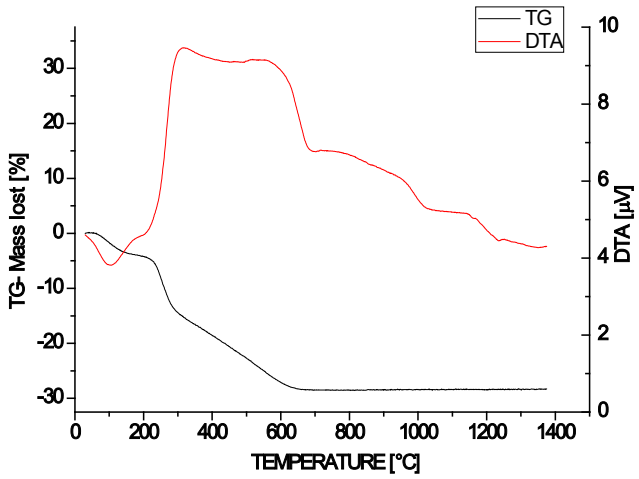

Fig. 4.33 TG/DTA measurements on dried βTCP granules.

4.3 Optimized processes for pure granules

An optimized process was defined for each composition for achieving the target properties. A desired composition combined with spherical shape and microporosity could be reached.

The optmized bioceramic suspension for each family of pure granules is summarized in Table 4.16. and the specific crosslinker solution and the relative gelification mechanism to produce always spherical granules are also reported.

Family	CaP powder	Poly saccharide	Crosslinking solution	Gelification mechanism
HA	60g/l of HA ; 5µm	1% Alg	0.3% Chi in 1% A.A.	PC
HA/βTCP	60g/l of CDHA calc →βTCP; 5 µm	1% Alg	0.3% Chi in 1% A.A.	PC
HA/TTCP	60g/l of HA; 5 µm	1% Alg	0.05 M $CaCl_2$	IG
βTCP	60 g/l of βTCP_1; 10 µm	2% Chi in 1% A.A.	5% TPP	IG

Table 4.16 Optimized ingredients for bioceramic suspension and crosslinking solution for each granules family.

Table 4.17 shows an example of the optimized processing parameters established for one specific composition and one specific range of granulometry. Processing parameters are fixed for each family and depend on the viscosity of the ceramic suspension.

Product	Granulomtery [µm]	Nozzle [µm]	Pump flux [ml/min]	Vibration frequency [KHz]	Hardening time [min]
Granules	300-600	500	21	0.13	30
	500-1000	1000	42	0.10	35
	1000-1200	1400	76	0.10	40
Aggregates	1200-5000	800	36	0.10	35

Table 4.17 Example of processing parameters for specific range of granulometry.

Hardening time was kept constant for 3 typologies (HA. HA/βTCP and HA/TTCP) and was varied for only βTCP granules that are left in a crosslinking solution for 16 h for the gelification hardening and then washed with demineralized water to eliminate the crosslinker excess as well as other products. A washing step after hardening was carried out in demineralized water from 2 to 5 times depending on the specific product. Subsequently, all families of granules are dried in a microwave drier for 1 hour for eliminating the water. All granules are then sintered at different temperature to burn-off the organic matrix, consolidate sufficiently the product but maintain interconnected microporosity. Table 4.18 shows all process parameters.

Family	Washing steps [n]	Air drying time [h]	Microwave drying time [h]	Sintering
HA	2 (+1)	-	1	1000°C 2h
HA/βTCP	2	-	1	1000°C 2h
HA/TTCP	2	-	1	1390°C 2h
βTCP	5	12	1	1150°C 6h

Table 4.18 Number of washing steps. drying times and sintering parameters for each family.

Specific and more controlled granulometry is obtained by an automatic sieve that allows eliminating the finer and larger parts. HA granules are then washed with Na_3PO_4 to eliminate the CaO in excess, washed again in deionised water and dried again with the industrial microwave.

4.4 Development of doped granules

Doped granules have been developed based on the experience of pure granules production and by using the ionotropic gelation mechanism between divalent ions, strontium and zinc, and the carboxyl group of sodium alginate. The target was to produce spherical granules with good distribution of doped ions in throughout whole volume. The problem was to combine the droplet extrusion process with the doping, because there is a toxicity limit for Zinc and Strontium that limits the choice of the best molarity.

The first solution was to use of powder of calcium deficient HA that. once doped with zinc ions. can be transformed at high temperature in βTCP. The ionic radius of zinc ion is smaller than Ca ion and it can substitute Ca and stabilized the βTCP phase which has a crystal cell shorter than HA. The bioceramic suspension of HA Cad and Na-alginate was dropped in a solution of zinc acetate for crosslinking. The wet granules were dried and sintered at 1000°C to burn out the organic part and allow consolidation. In this solution ZnO is present in the granules composition and the main crystalline phase is βTCP.

For obtaining biphasic granules the Sr-substitution was used as well with $SrCl_2$ crosslinking solution because Sr stabilizes HA phase and can induce the

partial transformation of βTCP phase into HA. In this case only Sr-HA phase was obtained and all βTCP was transformed in HA because Sr has the similar ion ratio of calcium.

4.5 Optimized process for doped granules

Four different types of optimized doped granules were developed finding the best solution between composition, shape and mechanical consistency. In Table 4.19 the optimized compositions are reported. The gelification mechanism used for all compositions is the ionotropic gelation between the alginate and divalent ions such as zinc and strontium. The production system of spherical wet granules is the same than pure granules passing from the automatic encapsulator. Successive steps are the washing in deminarilzed water to eliminate the crosslinker excess after hardening time of 35-45 min depending on the size and the drying in the microwave. The sintering temperature was kept fixed for all compositions at 1150°C for 2 h.

Monophasic Zn-βTCP is produced from 60g/l βTCP_2 powder and 1% alginate suspension dropped in a 0.03 M solution of zinc acetate.

Biphasic Zn-βTCP granules are produced from 90g/l calcined CDHA powder. The involved gelification mechanism is the ionotropic gelation between the guluronic chains of the 1% Na-alginate with divalent zinc ions of the 0.03 M solution of zinc acetate.

Sr-HA/βTCP granules are produced with similar process of Zn-HA/βTCP granules by changing only the crosslinking solution containing divalent strontium ions, a 0.02 M strontium chloride solution. The molarity is a little bit

less than 0.03 of zinc acetate, because the strontium ion can be chelated more strongly because its ionic radius (1.13 Å) is large than zinc's ionic radius (0.74 Å). The crosslinker time, driying procedure and thermal treatment are the same of Zn-HA/βTCP granules. At the end of the process strontium-doped microporous biphasic granules are obtained.

ZnSr-HA/βTCP granules represent one example of combination of different ions in a biphasic structure. Starting from a calcined CDHA powder (90 g/l) mixed with of Na-alginate solution (1%). the ceramic suspension is dropped in a particular crosslinker solution made by fifty percent 0.015 M $SrCl_2$ and fifty percent 0.005 M zinc acetate to reach a combined molarity of 0.02 M that is equivalent to Sr-HA/βTCP granules.

Zinc and strontium doped granules have been made with interconnected microporosity and biphasic chemical composition. HA and βTCP. All optimized parameters for doped granules are shown in Table 3.19.

Sample	Powder	Poly saccharide	Crosslinking solution	Gelification mechanism	Sintering
Zn-βTCP	60g/l βTCP_2; 10 µm	1% Alg	0.03 M $Zn(CH_3COO)_2$	IG	1150°C 2h
Zn-HA/βTCP	90g/l CDHA calc →βTCP; 2.5 µm	1% Alg	0.03 M $Zn(CH_3COO)_2$	IG	1150°C 2h
Sr-HA/βTCP	90g/l CDHA calc →βTCP; 2.5 µm	1% Alg	0.02 M $SrCl_2$	IG	1150°C 2h
ZnSr-HA/βTCP	90g/l CDHA calc →βTCP; 2.5 µm	1% Alg	0.015 M $SrCl_2$ 0.005 M $Zn(CH_3COO)_2$	IG	1150°C 2h

Table 4.19 Optimized composition for doped CaP granules.

4.6 Chemical-physical characterization: optimized pure granules

4.6.1 Mineralogical characterization

Mineralogical characterization is necessary to analyze the purity of the product and to check if any unwanted substances have been introduced during the production process. Ca and P percentage in solid are comparable in all granules, while in βTCP it is a little bit lower. In HA powder the amount of Ca and P is the lowest, because some Ca and P ions are introduced during the production process as $CaCl_2$ for HA/TTCP and as impurities for other compositions (Table 4.20).

Element [%]	HA granules	HA/βTCP granules	HA/TTCP granules	βTCP granules	HA powder
Ca	10.6	10.7	10.2	9.1	3.4
P	4.7	5.4	4.2	4.9	1.4

Table 4.20 Ca and P concentration of pure granules and Ca/P.

Expected nominal of Ca/P ratio are not strictly confirmed by ICP analysis results listed in (Table 4.21). Considering the possible error and the presence of small amount of other foreign crystalline phases, however, values are comparable and the composition is confirmed. ICP is an adequate technique to identify and quantify the ions present in the granules samples. The Ca/P ratio measurements were performed in triplicate and data are shown in Table 4.21.

Material	Nominal Ca/P ratio	Granules Ca/P ratio
HA	1.67	1.74±0.01
60HA/40βTCP	1.60	1.55±0.01
60HA/40TTCP	1.80	1.86±0.02
βTCP	1.50	1.42±0.03

Table 4.21 Comparison of stoichiometric and granules Ca/P ratio.

Impurities concentrations (see in Table 4.22) are acceptable and other elements have not been found. This result confirmed that the production process is safe and none of the steps introduce risky substances for human health.

Element [ppm]	HA granules	HA/βTCP granules	HA/TTCP granules	βTCP granules	HA powder
Mg	19.0	38.0	24.9	27.1	28.2
Na	18.0	41.0	21.5	18.0	40.8
Sr	1.5	1.2	1.7	1.7	0.8
Zn	0.1	0.8	7.3	8.1	0.5
Fe	2.4	3.1	2.3	2.1	3.8

Table 4.22 Concentration of impurities in pure materials

Other specific ICP-OES analysis demonstrated that CaP granules contain no heavy metals, fulfilling the requirement of the ASTM 1088 standard for βTCP and ISO 13779-3 and ASTM 1185-03 for HA and biphasic material containing HA. This result confirms that the production process is safe for biomedical devices and no dangerous metals are present in the final product (Table 4.23).

Element	HA [mg/Kg]	HA/βTCP [mg/Kg]	HA/TTCP [mg/Kg]	βTCP [mg/Kg]
As	<0.1	<0.1	<0.1	<0.1
Cd	<0.1	<0.1	<0.1	<0.1
Hg	<0.1	<0.1	<0.1	<0.1
Pb	<0.1	<0.1	<0.1	<0.1
Heavy metals	<50	<50	<50	<50

Table 4.23 Heavy metals analyses for pure granules.

As for the infrared spectroscopy spectrum of **HA** granules shown in Fig. 4.34 occluded water gives rise to a band at 2362-2816–2923 cm^{-1}. Other bands appear at 473 (v2), 570 (v4), 601 and 962 (v1) cm^{-1} that correspond to PO_4^{3-} group. The O-H stretching peak is observed in the band at 3571 cm^{-1}, and the O-H stretch H_2O is shown in the band 3442 cm^{-1}. The most intense feature in the IR spectra is the 1045 cm^{-1} band, this suggests the presence of HA phase. The band at 1089 cm^{-1} corresponds to P-O stretching vibrations. The broad bands at 3405 and 1988 cm^{-1} are due to the presence of both water and structural hydroxyl groups. The bands at 3571 and 634 cm^{-1} can be assigned to stretching and bending vibrations of the structural hydroxyl group.
The broad band at 1450 cm^{-1} and the narrow bands at 957 cm^{-1} are typical for CO_2^{3-} group showing that there is a formation calcium carbonate during the process.

As for infrared spectroscopy spectrum of **HA/TTCP** granules shown in Fig. 4.34 occluded water gives rise to a band at 2362-2816–2923 cm^{-1}. Additional bands appears at 473 (v2), 523.570 (v4), 601 and 962 (v1) cm^{-1} that

correspond to the PO_4^{3-} group. The O-H stretching peak is observed not too clearly in the band at 3567 cm^{-1}, and the O-H stretch H_2O is shown in the band 3432 cm^{-1}. The most intense feature in the IR spectrum is the 1045 cm^{-1} band with some shoulders at 1118 and 962^{-1} that suggest the presence of HA phase. The band at 1089 cm^{-1} corresponds to P-O stretching vibrations. Broad bands at 3405 and 1988 cm^{-1} are due to the presence of both water and structural hydroxyl groups. The bands at 3567 and 633 cm^{-1} can be assigned to stretching and bending vibrations of the structural hydroxyl group.

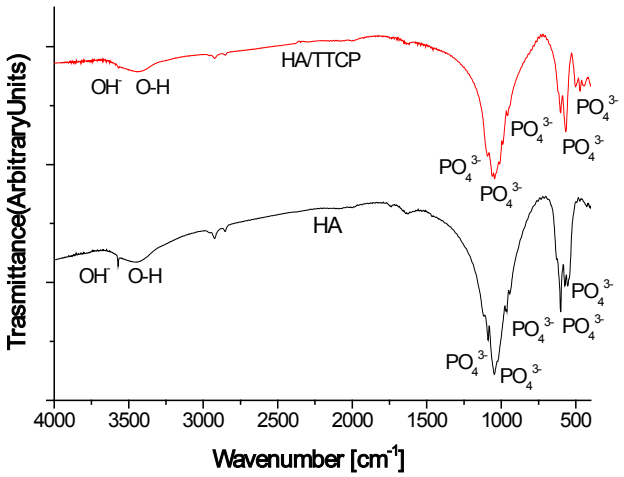

Fig. 4.34 FT-IR trasmittance spectrum of HA granules and HA/TTCP granules.

As for infrared spectroscopy spectrum of **HA/βTCP** granules shown in Fig. 4.35 presents relative intensities. Strong bands attributed to PO_4^{3-} groups. the strongest ones result from the stretching vibrations. The bands at 1088 cm^{-1} and about 1045 cm^{-1} are assigned to the components of the triply degenerated ν3 antisymmetric P-O stretching mode. The 962 cm^{-1} band is assigned to ν1.

the non-degenerate P-O symmetric stretching mode. The bands at 603 cm^{-1} and 570 cm^{-1} are assigned to components of the triply degenerate ν4 Q-P-O bending mode. Absence of any distinct band in the range of 1400-1550 cm^{-1} indicates that the samples do not contain large quantities of carbonate ions. The broad band of low intensity in the range 3000-3400 cm^{-1} can be attributed to the traces of water incorporated into the structure. The band coming from the hydroxyapatite OH stretching vibrations at 3571 cm^{-1} is visible on the FTIR spectra corresponding to the hydroxyapatite containing.

The FTIR spectrum of **β-TCP** granules sample is shown in Fig. 4.35. The range of 800 – 1200 cm-1 exhibits a wide absorption band typical of tetrahedral anions $XO4^{n}$, in particular, PO_4^{3-}, FTIR analysis demonstrated PO_4^{3-} adsorption peaks around 1045-1115; 603. and 543 cm^{-1} attributable to ß-TCP. FTIR spectrum of sintered beta-tricalcium phosphate showed typical spectrum for TCP material. The 961 cm^{-1} band is assigned to ν1, the non-degenerate P-O symmetric stretching mode. The characteristic phosphate peaks for β-TCP at wave numbers of 1115- 1045; 603 and 543 cm^{-1} were present.

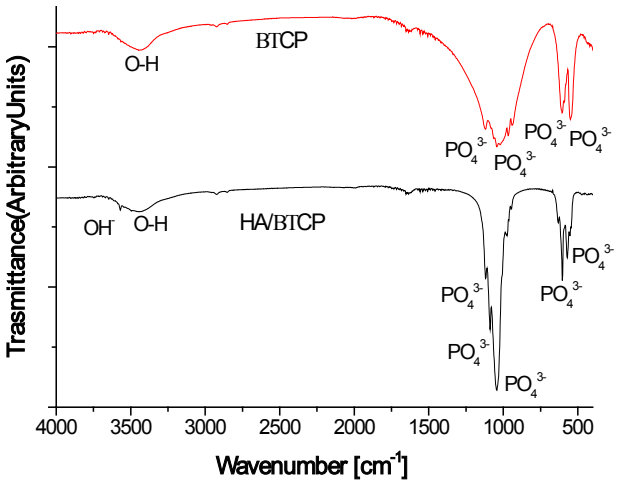

Fig. 4.35 FT-IR trasmittance spectrum of HA/βTCP granules and βTCP granules.

Fig. 4.36 shows the diffraction patterns of the **HA** granules produced from HA powders. The XRD pattern of HA shows good correlation with stoichiometric hydroxyapatite (JCPDS 09-0432 card). Other phases were identified, like CaO (JCPDS 037-1497) and β-TCP (JCPDS 09-0169), although they are less than 1% thus fulfilling the requirement of the ISO 13779-3 standard.

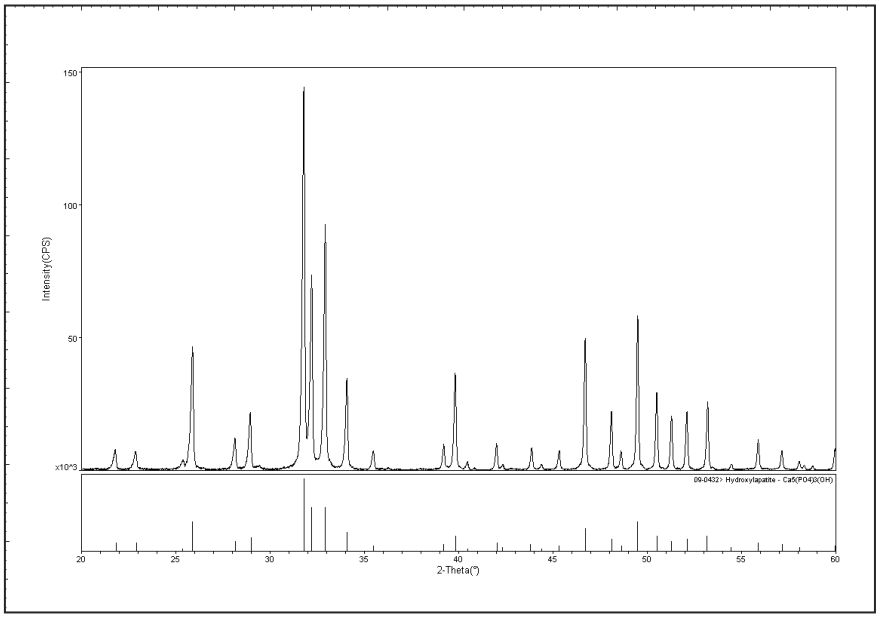

Fig. 4.36 XRD pattern of HA granules.

The quantitative mineralogical analysis was performed by Maud (Fig. 4.37 and Table 4.24). Granules can be considered monophasic consisting of 98% HA ±2%. Detectable foreign phases are TTCP, CaO (residual of washing process) and $CaCO_3$.

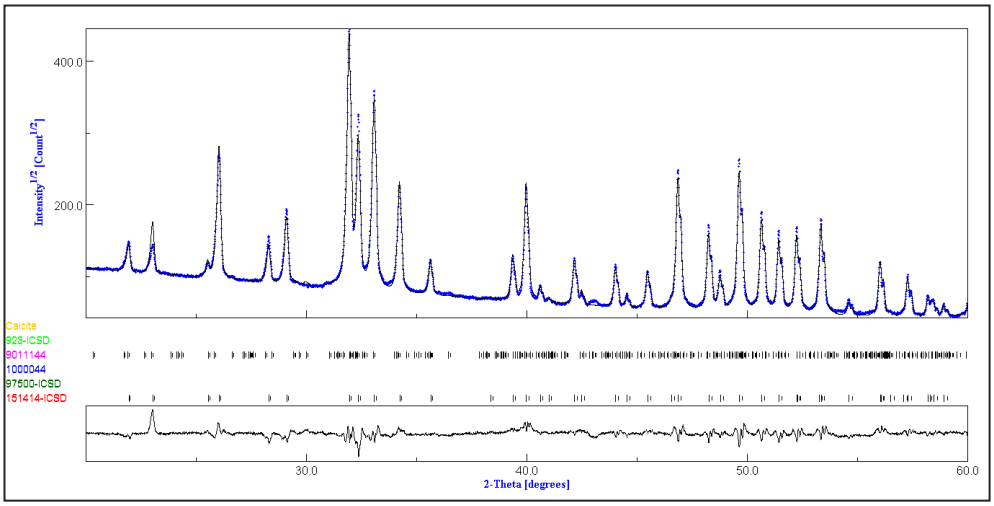

Fig. 4.37 Plot of XRD quantitative Maud Analysis of HA granules.

Sample	HA [%]	βTCP [%]	CaO [%]	TTCP [%]	αTCP [%]	$CaCO_3$ [%]
HA	98.2	0.0	0.00	1.7	0.0	0.2

Table 4.24 XRD quantitative Maud Analysis.

Fig. 4.38 shows the diffraction patterns of the **HA/TTCP** granules produced from HA powders. The XRD pattern of HA/TTCP granules shows a good correlation with stoichiometric hydroxyapatite (JCPDS 09-0432 card) and tetracalcium phosphate (JCPDS 25-1137). CaO phase (JCPDS 037-1497) was also identified.

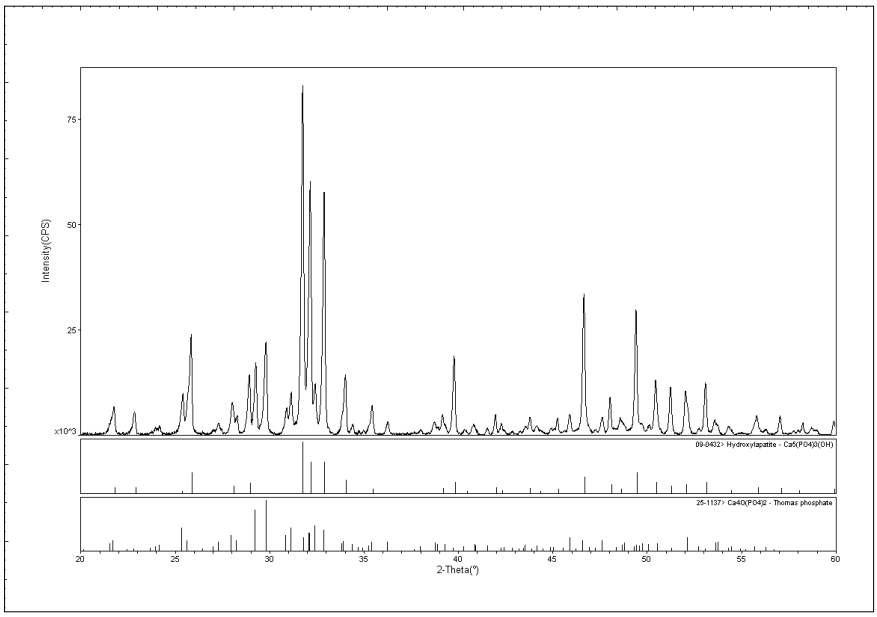

Fig. 4.38 XRD pattern of HA/TTCP granules.

Granules can be considered biphasic consisting of ≃60% HA and ≃40% TTCP. Detectable foreign phase can be only CaO because it is formed by free Ca^{2+} that does not react during the gelification process and does not participate to chemical transformation at 1340°C of HA into TTCP (Fig. 4.39 and Table 4.25).

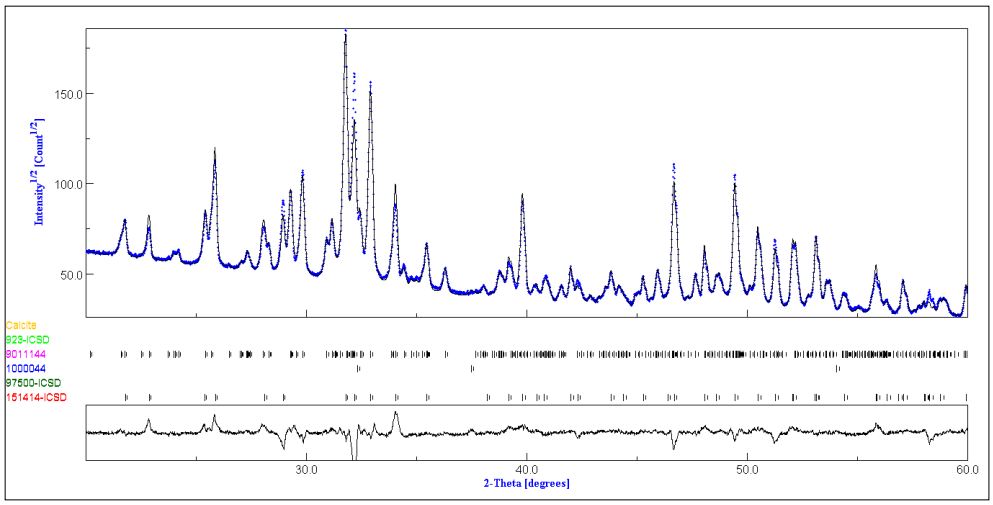

Fig. 4.39 Plot of XRD quantitative Maud Analysis of HA/TTCP granules.

Sample	HA [%]	βTCP [%]	CaO [%]	TTCP [%]	αTCP [%]
HA/TTCP	60.3	0.0	0.2	39.5	0.0

Table 4.25 XRD quantitative Maud Analysis of HA/TTCP granules.

Fig. 4.40 shows the diffraction patterns of the **HA/βTCP** granules produced from CDHA calcined powders. The XRD pattern of HA shows good correlation with stoichiometric hydroxyapatite (JCPDS 09-0432 card) and and β-TCP phase (JCPDS 09-0169).

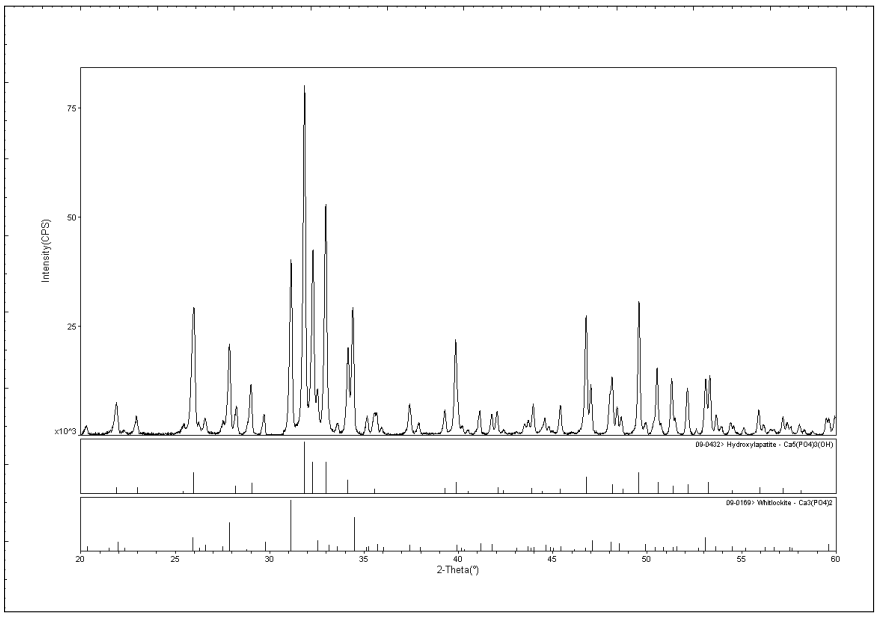

Fig. 4.40 XRD pattern of HA/βTCP granules.

Granules can be considered biphasic containing ≃60% HA and ≃40% βTCP. During the experiments some foreign phases ware found such as TTCP < 2% and αTCP from possible transformation of βTCP at high temperature. Other identified phases like TTCP (JCPDS 25-1137) and α-TCP (JCPDS 09-0348) are however less than 5% thus fulfilling the requirement of the ISO 13779-3 standard (Fig. 4.41 and Table 4.26).

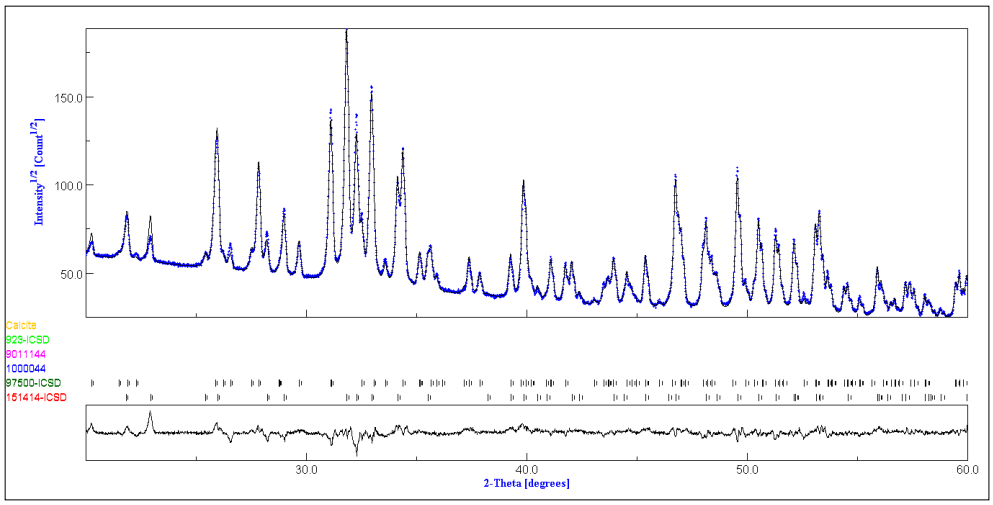

Fig. 4.41 Plot of XRD quantitative Maud Analysis of HA/βTCP granules.

Sample	HA [%]	βTCP [%]	CaO [%]	TTCP [%]	αTCP [%]
HA/βTCP	61.7	38.3	0.00	0.00	0.00

Table 4.26 XRD quantitative Maud analysis of HA/βTCP granules.

Fig. 4.42 shows the diffraction patterns of the βTCP granules produced from βTCP powders. The XRD pattern of βTCP shows good correlation with stoichiometric β-TCP phase (JCPDS 09-0169).

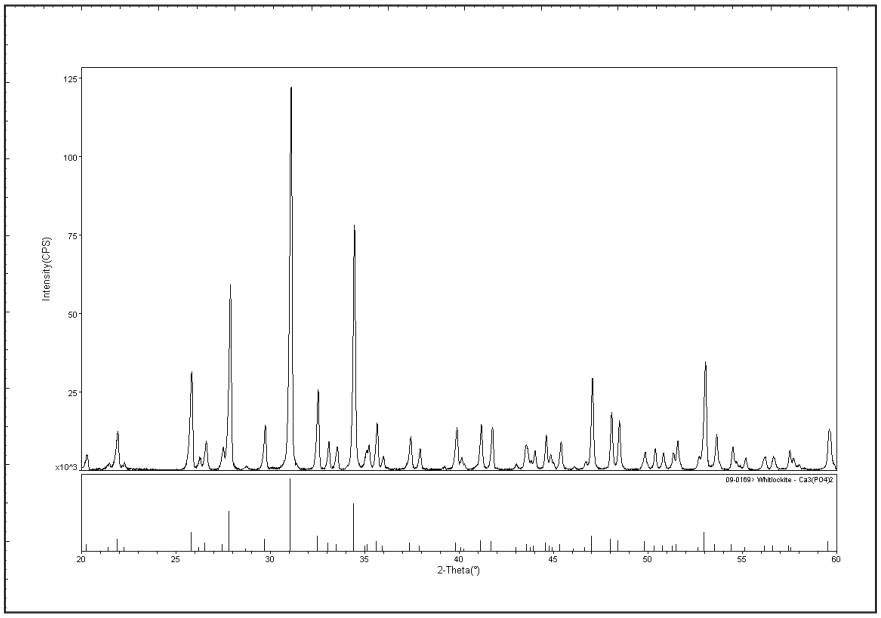

Fig. 4.42 XRD pattern of βTCP granules

Granules can be considered monophasic 97% βTCP ±3%. Typical foreign phases could be TTCP. HA and αTCP, but they were found always less than 5% in conform with the standard ISO 13779-3. From Maud quantitative analysis (Fig. 4.43 and Table 4.27) a foreign phases was detected, calcium pyrophosphate ($Ca_2P_2O_7$). The presence of this crystalline phase can be favourite by pH changing or when the Ca/P ratio is lower than 1.5. the typical ratio of βTCP [149].

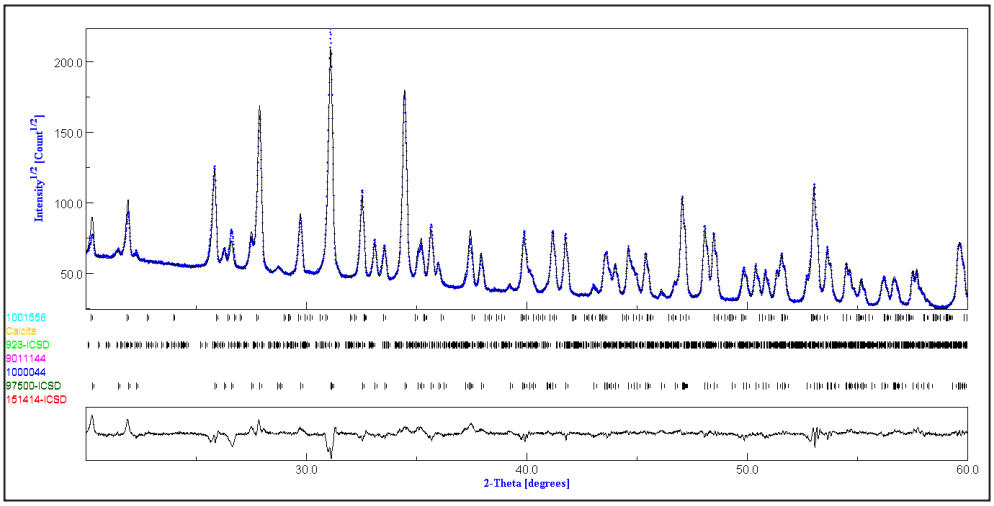

Fig. 4.43 Plot of XRD quantitative Maud Analysis of βTCP granules.

Sample	HA [%]	βTCP [%]	CaO [%]	TTCP [%]	αTCP [%]	$Ca_2P_2O_7$ [%]
βTCP	0.00	98.0	0.00	0.00	0.7	1.3

Table 4.27 XRD quantitative Maud Analysis of βTCP granules.

4.6.2 Morphology

OM images of **pure granules** show the round morphology and the regular dimension and shape. The HA granules color is light blue; HA/βTCP and βTCP granules are white; HA/TTCP granules are blue. The different coloration of HA and HA/TTCP is due to the raw HA powder that at high temperature when it reaches high crystallinity reflects the blue light due to the colour changes with the presence of manganese ions or other transition elements located in the crystal lattice structure [150]. In fact, when HA/TTCP granules are smashed

in powder for XRD or FT_IR analyses, they return to white color. For HA/βTCP and βTCP granules the colour is the same of the initial powders.

Fig. 4.44 and Fig. 4.45 show some example of granules in different composition and size.

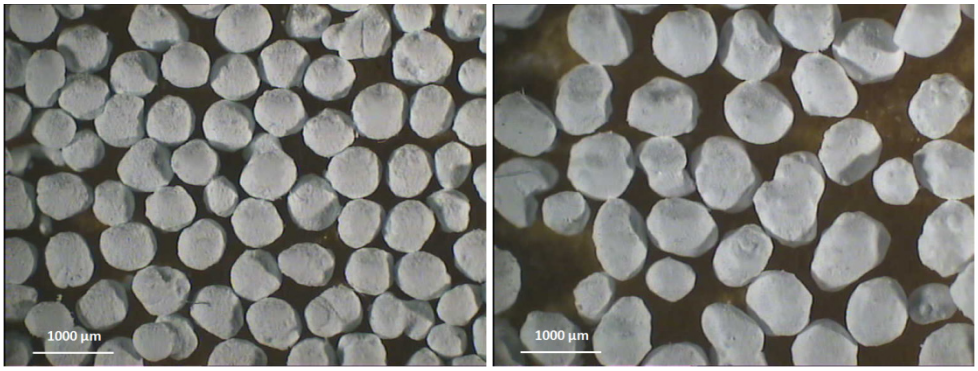

Fig. 4.44 Example of 600-700 µm HA granules and 800-1000 µm HA/βTCP granules.

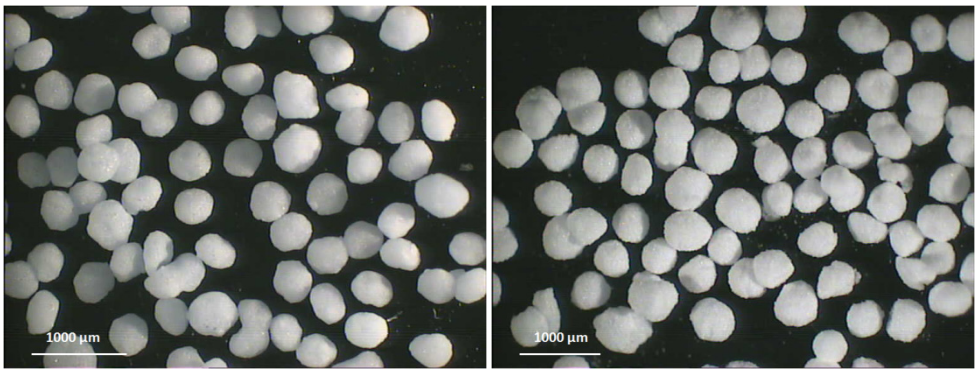

Fig. 4.45 Example of 300-500 µm HA/TTCP granules and 400-600 µm βTCP granules.

Fig. 4.46 and Fig. 4.47 show **pure aggregates** morphology. The range size is between 1200-5000 µm. Aggregates shape is less regular than in granules because the agglomeration process is poorly controlled during the drying

process. Moreover, the round shape of the granules forming the aggregates allows forming geometric structures without sharp edges; this may be important to obtain better respect of delicate anatomic structures such as nerves or sinus membrane.

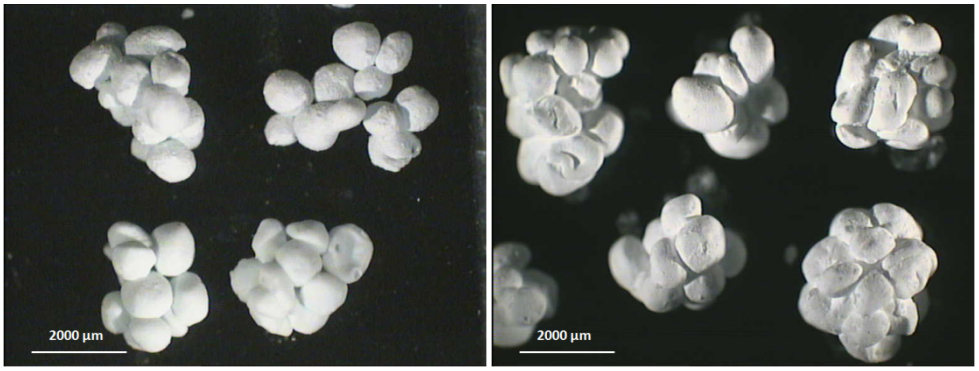

Fig. 4.46 HA and HA/βTCP aggregates.

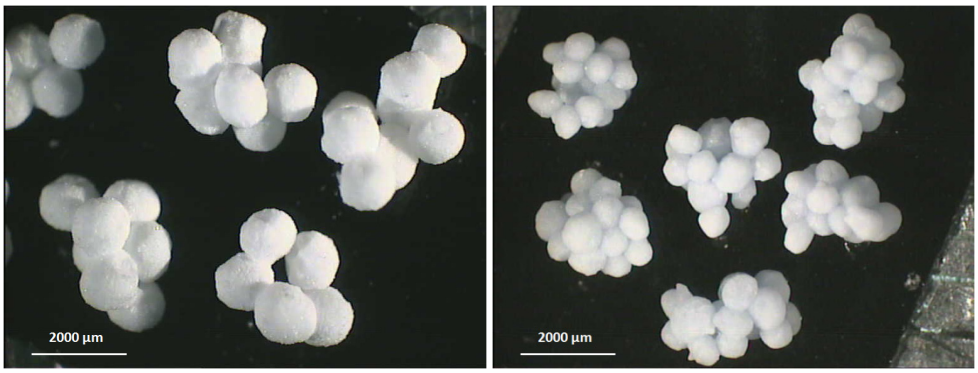

Fig. 4.47 HA/TTCP and βTCP aggregates

SEM images at low magnification confirm that with a control of gelification processes and hardening step associated with drying and sintering. a spherical shape is obtained. In fact, all granules present a round shape that is

maintained after the whole process, even if the size decreases due to organic gel burn-off. Granules analyzed are the range 300-600 μm after a sieving procedure. The external morphology of HA and HA/βTCP are very similar due to same production process (Fig. 4.48). HA/TTCP and βTCP are spherical as well (Fig. 4.49).

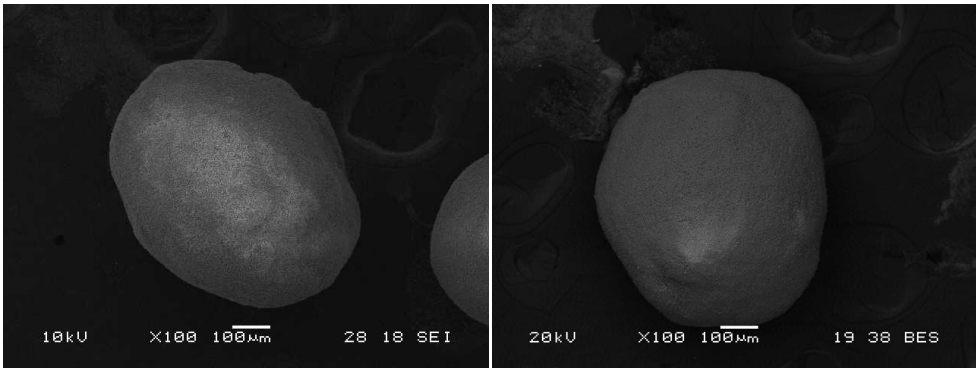

Fig. 4.48 HA and HA/βTCP granules.

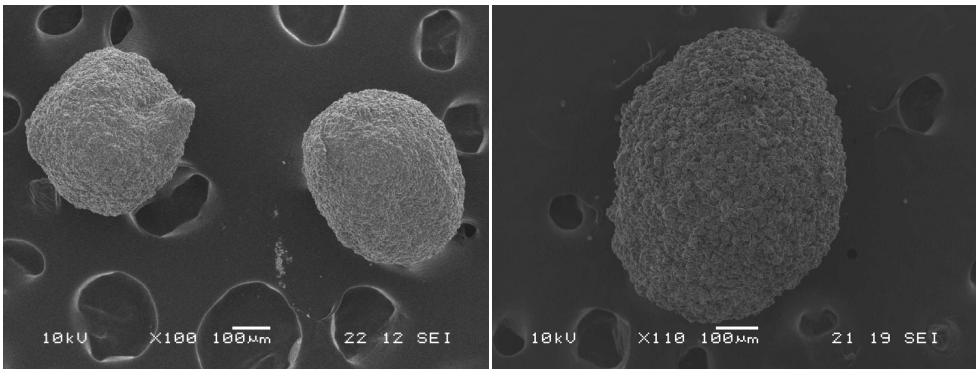

Fig. 4.49 HA/TTCP and βTCP granules

Aggregates of granules are produced for all compositions. The external morphology appears very similar even if they are produced with different

method and gelification mechanism. For HA and HA/ βTCP the granules bond appears more defined, but the sphere shape is a little bit lost (Fig. 4.50). HA/TTCP and βTCP aggregates seem to be less resistant. due to the limited connection area between granules (Fig. 4.51). Random global morphology is useful to reach an incompletely dense structure when they are applied in implant sites. An additional benefit for the aggregate is the increased volume/surface ratio, the ability to fill large bone defects and the ability to obtain a better stabilization of the bone graft when large amount of material are needed. Another advantage of aggregates morphology is the possibility to be stabilized into protected defect without mechanical tools (e.g screws. pins. etc) that are commonly needed to avoid micro-movement of bone blocks graft.

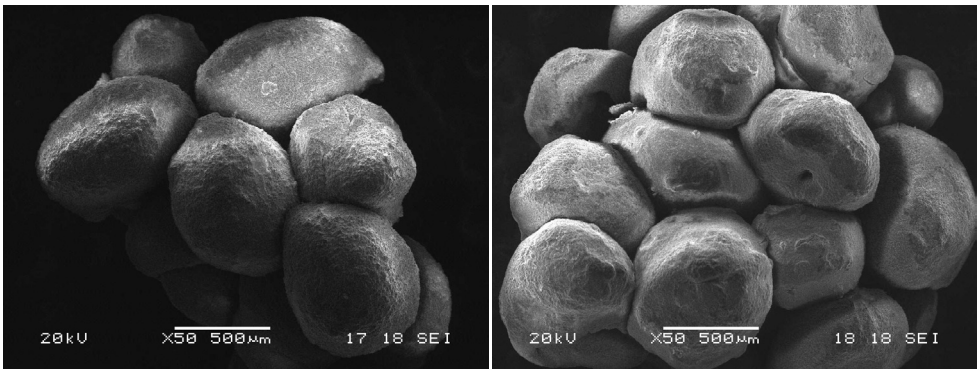

Fig. 4.50 SEM images of HA and HA/βTCP aggregates.

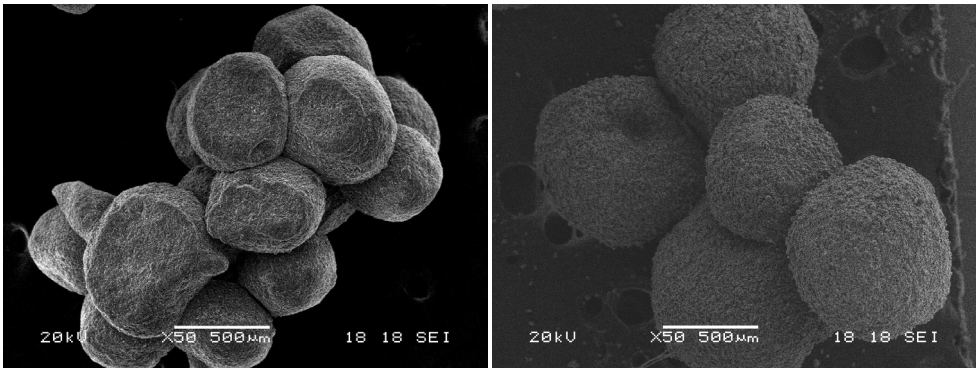

Fig. 4.51 SEM images of HA/TTCP and βTCP aggregates.

4.6.3 Microstructure

Surface roughness is important property to favour cell attachment and ion exchange with host tissue and physiological environment. HA and HA/βTCP granules have similar surface roughness. in a range of 0.1-3 µm (Fig. 4.52).

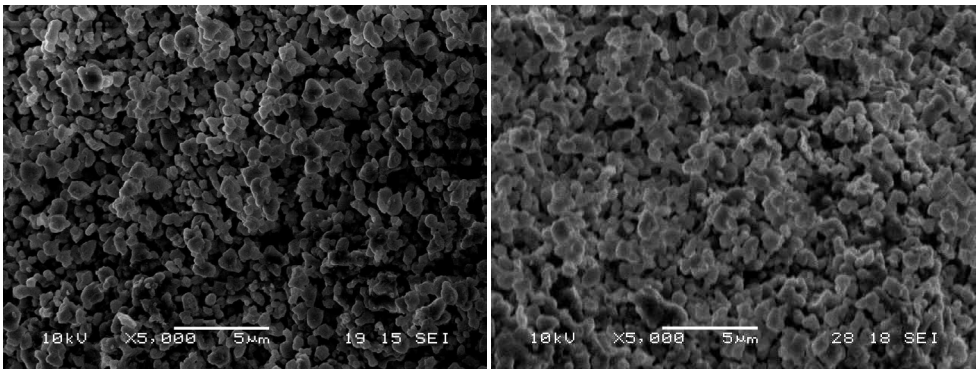

Fig. 4.52 SEM images of HA and HA/βTCP granules surface.

HA/TTCP and βTCP granules are denser on the surface and the roughness is estimated in the range 1-10 μm (Fig. 4.53). Differences are affected mainly by initial powder size and the sintering temperature.

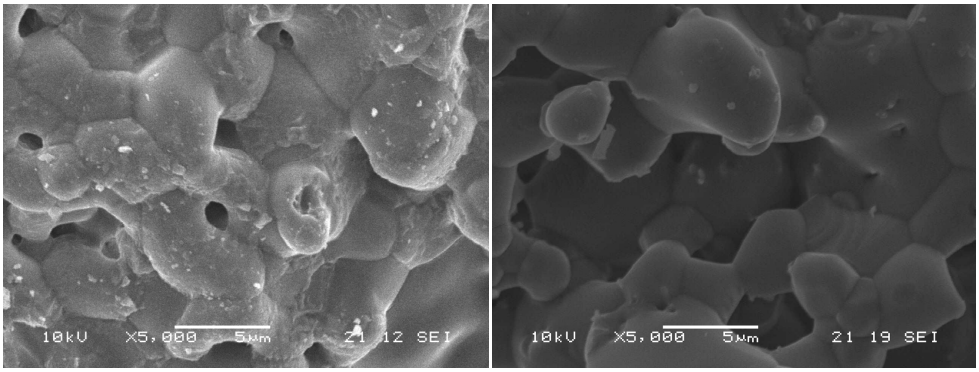

Fig. 4.53 SEM images of HA/TTCP and βTCP granules surface.

Internal microporosity is obtained upon sintering the polymer phase that is substituted by a porous network after burnout. The microstructure of HA granules seems to be more microporous than HA/βTCP, but the range is almost the same 0.1-3 μm (Fig. 4.54). Pore size is strictly dependent on the different powder size because the gelation mechanism, polysaccharide ingredients and the thermal treatment (1000°C) are equivalent.

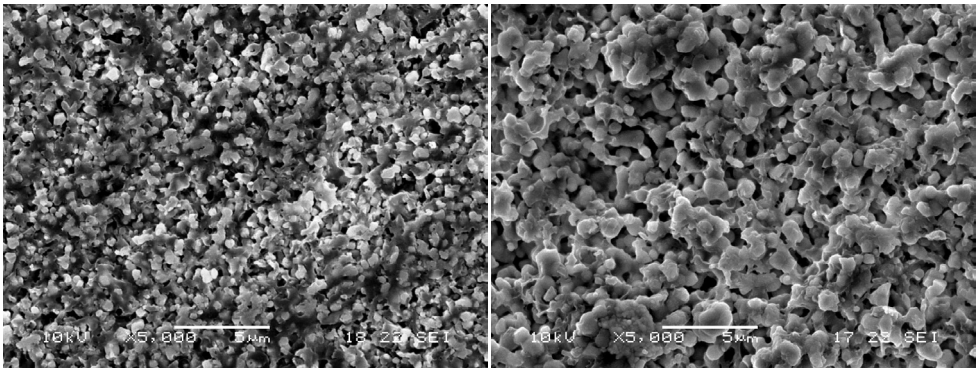

Fig. 4.54 SEM images of HA and HA/βTCP granules section.

HA/TTCP and βTCP granules have comparable microporosity even if they were produced with different procedures. The size range of micropores is between 0.1-10 μm (Fig. 4.55).

Differences in microporosity can be attributed to the different sizes of the two compounds, which result in different packing of the ceramic particles during drying and sintering. The microporosity can accelerate the ions exchange between the host tissue and the biomaterial, accelerating the bone remodeling process and the consequent resorption of CaP granules. Moreover, the pore interconnectivity allows the perfusion of blood and nutrients necessary for bone repair at the core of granules.

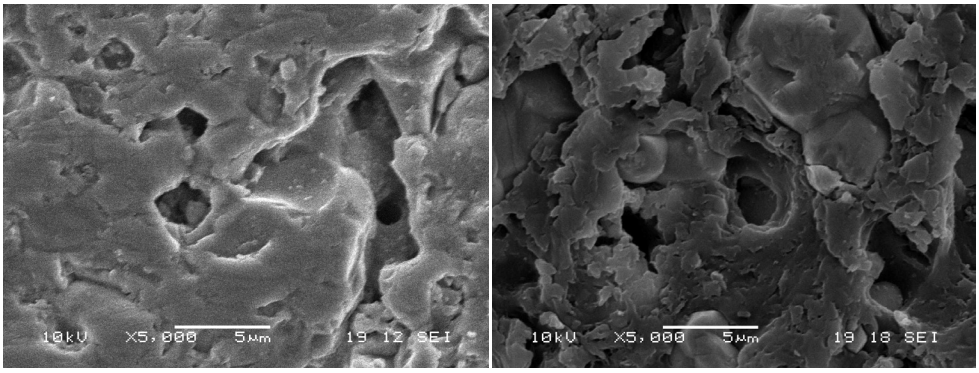

Fig. 4.55 SEM images of HA/TTCP granules and βTCP granules.

Inter-granules macroporosities are observed in all cases. but its value is different between pure aggregates. The manufacturing process of HA and HA/βTCP allows to reduce the surface of the wet granules before agglomeration due to the action of acetic acid, which degrades the round surface (Fig. 4.56).For this reason the HA granules bond is stronger than in HA/TTCP and βTCP (Fig. 4.57).

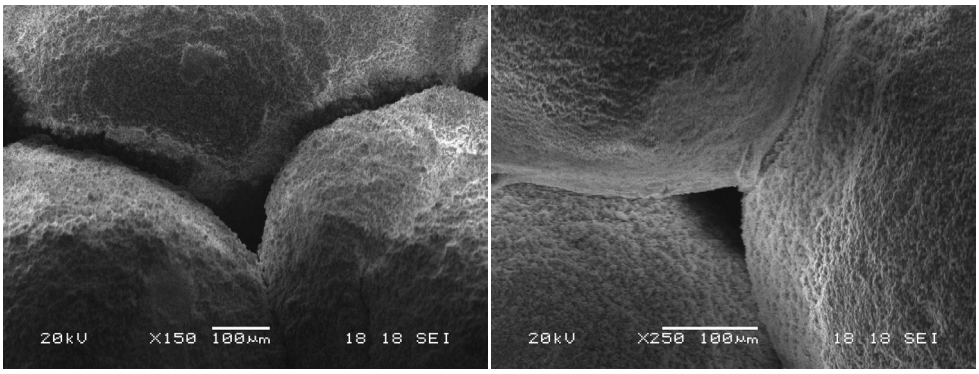

Fig. 4.56 SEM images of macroporosity of HA aggregates and HA/βTCP aggregates.

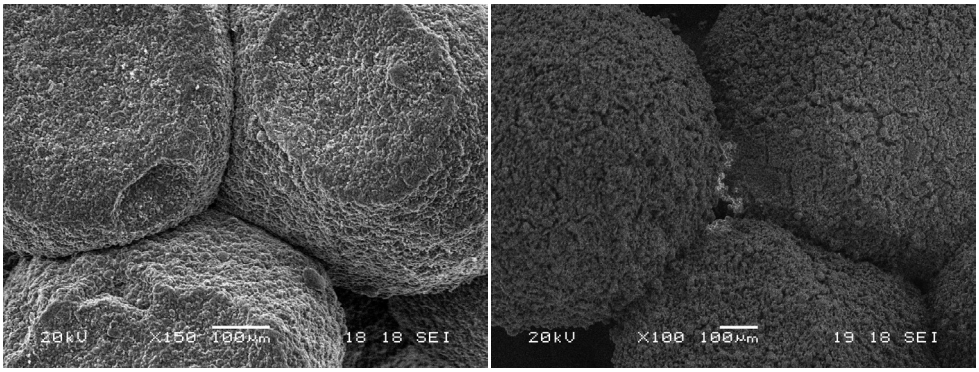

Fig. 4.57 SEM images of macroporosity of HA/TTCP aggregates and βTCP aggregates.

The macroporosity can be evaluated always in the range of 50-100 µm. The macroporosity depends strictly by the granules size that can not be too high because the resistance section can be reduced deceasing the mechanical consistency useful to hand these product in surgical procedure.

4.6.4 Porosity and specific surface area

Analyses of the data obtained from mercury intrusion porosimetry are presented in Table 4.28. HA granules show many pores in the range of 100-1000 nm and the lowest average pore size. HA/βTCP granules have similar microstructure of HA granules and in fact relative apparent porosities are comparable, around 50%. HA/TTCP granules show a lower amount of pores, though bigger (100-10000 nm). and a total porosity of only 11%. This low porosity is due to the high sintering temperature which causes the densification of the material. βTCP granules show higher average pore size due to the higher powder size (10 µm) compared to other powders used (5 µm).

Product	Average pore size [nm]	Pore size distribution [nm]	Apparent Porosity [%]
HA granules	190	100-1000	48
HA/βTCP granules	290	100-1000	50
HA/TTCP granules	250	100-10000	11
βTCP granules	3400	1000-10000	56

Table 4.28 Data of mercury intrusion porosimetry method.

The BET method is helpful for calculating the SSA and effective pore size because N_2 is adsorbed on the whole available surface area. Table 4.29 shows the results that confirm the same trend of Hg-porosimetry. In fact HA granules result to be the most porous material with the highest SSA. 4.7m^2/g. and HA/TTCP are the most dense granules, with only 0.5 m^2/g. Average pore size is in order of 3-16 nm, the highest value for HA granules and the lowest for HA/TTCP granules, sintered at 1390°C.

Product	SSA [m^2/g]	Average Pore size [nm]
HA granules	4.7	16.2
HA/βTCP granules	2.5	8.6
HA/TTCP granules	0.5	3.8
βTCP granules	0.7	10.6

Table 4.29 BET data of pure granules.

4.7 Chemical-physical characterization: optimized doped granules

4.7.1 Mineralogical characterization

ICP-OES analyses results in terms of Ca and P concentration for doped granules are shown in Table 4.30.

Element [wt.%]	Zn-βTCP	Zn-HA/βTCP	Sr-HA/βTCP	SrZn-HA/βTCP
Ca	10.3	10.8	10.7	10.2
P	5.5	5.7	5.4	5.2

Table 4.30 ICP analysis of doped CaP granules.

The granules, depending on the crosslinker solution used, contain different concentration of doping ions. In all cases the concentration can be considered high with respect to normal Zn and Sr content in natural bone (Table 1.7) and these values need to be considered in the cytotoxicity test to understand their influence on the cell viability. Zn and Sr concentration is 0.4-0.5% is 0.4-0.5%, respectively. This result demonstrates that wet granules during the gelification adsorbed the same amount of each type of ion. In the case of combined crosslinking solution the sum of two ions (5043 ppm) is similar of the case with one crosslinker ion. 4150-5700 ppm (Table 4.31).

Element	Zn-βTCP	Zn-HA/βTCP	Sr-HA/βTCP	SrZn-HA/βTCP
Mg [ppm]	775	13	13	13
Na [ppm]	750	975	925	875
Doped ions				
Zn [ppm]	4150	5300	13	618
Sr [ppm]	35	33	5700	4425

Table 4.31 ICP analysis of doped CaP granules.

The nominal ratio Ca/P =1.5 in the case of Zn-βTCP is respected and the Zn substitution in βTCP is complete, without the presence of foreign phases. In other compositions the nominal Ca/P decreases due to the ions substitution. In the case of Zn-HA/βTCP there is not complete correspondence and the refined Ca+Zn/P ratio is a little bit lower. In other types of biphasic granules the nominal ratio and the refined ratio are very similar and this result confirm the complete substitution of Ca by Zn and Sr. Table 3.31 shows results about the Ca/P ratio, nominal and refined from ICP data.

Material	Nominal Ca/P ratio	Granules Ca/P ratio	X	Granules X/P
Zn-βTCP	1.50	1.46±0.01	(Ca+Zn)	1.50±0.01
Zn-25HA/75βTCP	1.54	1.46±0.01	(Ca+Zn)	1.51±0.01
Sr-30HA/70βTCP	1.55	1.52±0.02	(Ca+Sr)	1.56±0.02
SrZn-30HA/70βTCP	1.55	1.51±0.01	(Ca+Sr+Zn)	1.54±0.01

Table 4.32 Ca/P ratio and modified (Ca+X)/P ratio for doped granules.

Infrared spectroscopy was performed to check if other organic or inorganic phases are still present in final granules after the sintering process at high temperature. Moreover, FT-IR test is useful to check if other calcium phosphate phases, not detectable with XRD, were formed.

FTIR spectrum for **Zn-β-TCP** granules is shown in Fig. 4.58. The range of 800 –1200 cm^{-1} corresponds to a wide absorption band typical for tetrahedral anions $XO4^{n}$, in particular PO_4^{3-}. FTIR analysis shows PO_4^{3-} adsorption peaks around 1045-1115, 601 and 551 cm^{-1} corressponding to ß-TCP. FTIR spectrum for sintered beta-tricalcium phosphate shows typical signals for TCP material. The 968 cm^{-1} band is assigned to ν1, the non-degenerate P-O symmetric stretching mode.

As for infrared spectroscopy the spectrum of **Zn-HA/βTCP** granules is shown in Fig. 4.58. Strong bands are attributed to PO_4^{3-} groups, the strongest ones resulting from the stretching vibrations. The bands at 1085 cm^{-1} and about 1041 cm^{-1} are assigned to the components of the triply degenerated ν3 antisymmetric P-O stretching mode. The 968 cm^{-1} band is assigned to ν1. the non-degenerate P-O symmetric stretching mode. The bands at 599 cm^{-1} and 568 cm^{-1} are assigned to components of the triply degenerate ν4 Q-P-O bending mode. The absence of any distinct band in the range of 1400-1550 cm^{-1} indicates that the samples do not contain large quantities of carbonate ions. The broad band of low intensity in the range 3000-3400 cm^{-1} can be attributed to the traces of water incorporated into the structure. The band coming from the hydroxyapatite OH stretching vibrations at 3571 cm^{-1} is visible on the FTIR spectra corresponding to the hydroxyapatite containing.

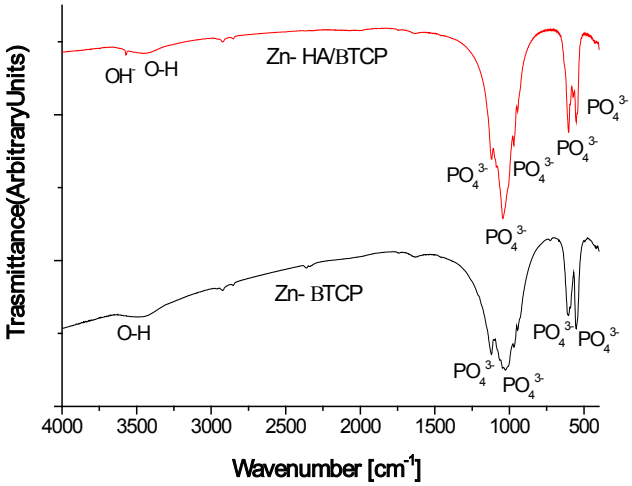

Fig. 4.58 FT-IR spectrum of Zn-βTCP and Zn-HA/βTCP.

As for infrared spectroscopy the spectrum of **Sr-HA/βTCP** granules is shown in Fig. 4.59.Strong bands attributed to PO_4^{3-} groups, the strongest ones result from the stretching vibrations. The bands at 1085 cm^{-1} and about 1041 cm^{-1} are assigned to the components of the triply degenerated ν 3 antisymmetric P-O stretching mode. The 968 cm^{-1} band is assigned to ν 1, the non-degenerate P-O symmetric stretching mode. The bands at 601 cm^{-1} and 568 cm^{-1} are assigned to components of the triply degenerate ν 4 Q-P-O bending mode. Absence of any distinct band in the range of 1400-1550 cm^{-1} indicates that the samples do not contain large quantities of carbonate ions. The band coming from the hydroxyapatite OH stretching vibrations at 3571 cm^{-1} is visible on the FTIR spectra corresponding to the hydroxyapatite containing. but is attenuated respect to pure material. FT-IR spectrum for **SrZn-HA/βTCP**

granules (Fig. 4.59) is very similar to Sr-HA/βTCP granules spectrum. Strong bands attributed to PO_4^{3-} groups, the strongest ones result from the stretching vibrations. The bands at 1085 cm^{-1} and about 1041 cm^{-1} are assigned to the components of the triply degenerated ν3 antisymmetric P-O stretching mode. The 968 cm^{-1} band is assigned to ν1, the non-degenerate P-O symmetric stretching mode. The bands at 601 cm^{-1} and 568 cm^{-1} are assigned to components of the triply degenerate ν4 Q-P-O bending mode. Absence of any distinct band in the range of 1400-1550 cm^{-1} indicates that the samples do not contain large quantities of carbonate ions. The broad band of low intensity in the range 3000-3450 cm^{-1} can be attributed to the traces of water incorporated into the structure. The band coming from the hydroxyapatite OH stretching vibrations at 3571 cm^{-1} is visible on the FTIR spectra corresponding to the hydroxyapatite containing, but is attenuated respect to pure material. A broad band at 1625 cm^{-1} corresponds to H_20 adsorbed (ν2).

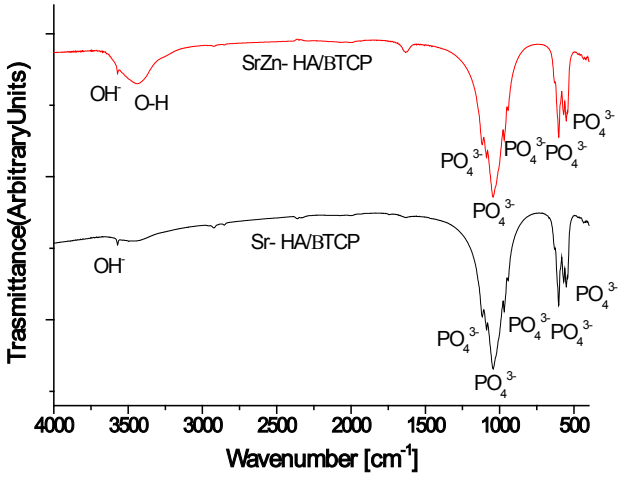

Fig. 4.59 FT-IR spectrum of Sr-HA/βTCP and SrZn-HA/βTCP.

XRD pattern (Fig. 4.60) recorded on **Zn-βTCP** granules shows that there are no significant differences in the phase behavior. The formation of zinc substituted βTCP was pointed out according to shift of peaks and the variation of lattice parameters. No ZnO (36-1451) was identified in XRD pattern.

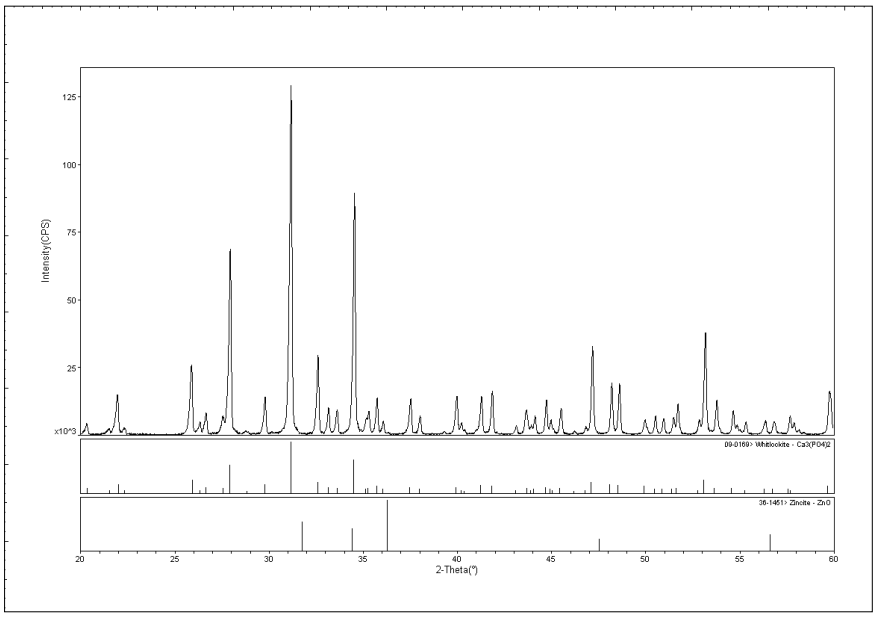

Fig. 4.60 XRD pattern of Zn-βTCP granules.

Maud quantitative analysis (Fig. 4.61 and Table 4.33) was performed by using standard βTCP as starting values to refine zinc containing βTCP. The refined XRD pattern confirms the presence of Zn-βTCP with additional phases as TTCP and αTCP.

Sample	HA [%]	βTCP [%]	TTCP [%]	αTCP [%]	ZnO [%]
Zn-βTCP	0.0	98.0	0.70	1.3	0.0

Table 4.33 XRD quantitative Maud Analysis of Zn-βTCP granules.

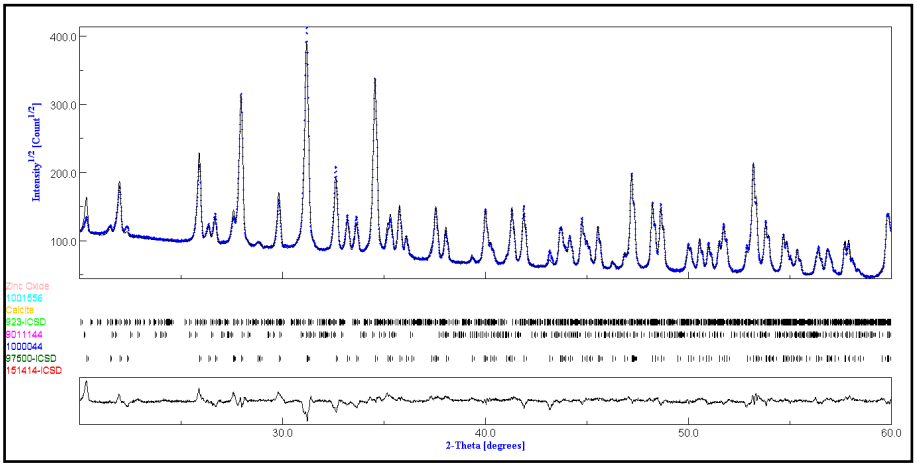

Fig. 4.61 Plot of XRD quantitative Maud Analysis of Zn-βTCP granules.

The structural data for Zn-βTCP after refinement showed βTCP structure with unit cell parameters a=b=10.3915 Å. c=37.289 Å in the hexagonal setting (space group R_3c). All the Zn-substituted βTCP investigated in the present study were also confirmed to retain the rhombohedral structure.

It can be easily noticed from the refined parameters obtained by Maud software of zinc substituted βTCP that both a and c unit cell parameters have indicated a decreasing trend thereby leading to the observed contraction in the unit cell volume when compared with the standard 09-169 and pure βTCP. This decreasing trend in the lattice data can be ascribed to the incorporation of lower ionic radii of Zn^{2+} (0.745 Å for sixfold coordination with O) at Ca^{2+} (1.00 Å for sixfold coordination with O) sites in the βTCP structure. The crystallite size is reduced as well from 2740 Å to 2573 Å. Table 4.34 shows all lattice parameters for β-TCP structures.

Sample	a=b	c	Crystallite size [Å]
βTCP standard	10.4	37.4	-
βTCP pure	10.4	37.4	2740
βTCP Zn	10.4	37.3	2573

Table 4.34 Lattice parameters for βTCP structure.

The decrease of lattice parameters in Zn-βTCP structure is represented also in the graph of Fig. 4.62, which can be easily compared with the graph of Fig. 4.63 rearranged from Kannan et al. work [151]. By using the literature data calculated for βTCP powder, the possible content of zinc in the granules can be calculated theoretically. The corresponding theoretical molarity of zinc in Zn-βTCP granules results to be 4.5 %.

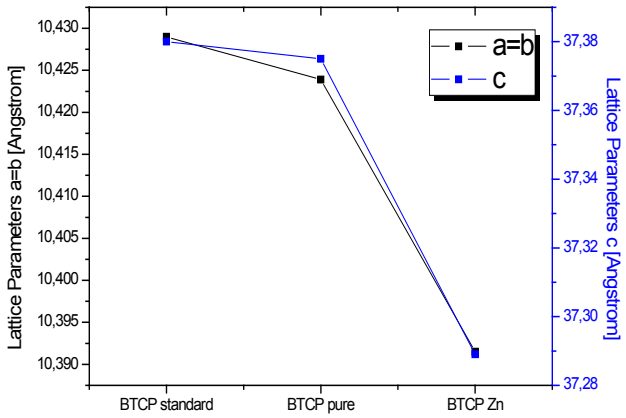

Fig. 4.62 Lattice a- and c-axis parameters in βTCP structures.

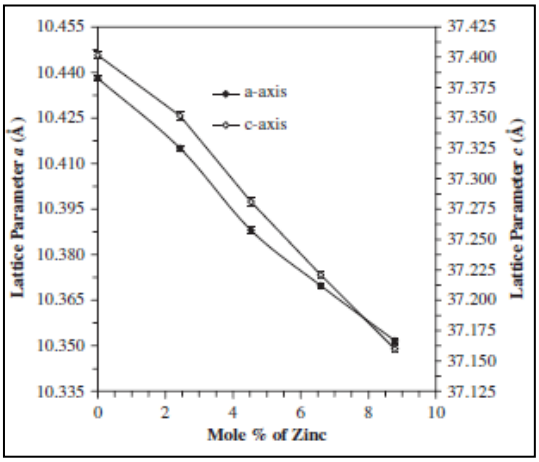

Fig. 4.63 Influence of lattice a- and c-axis parameters with respect to different cont of zinc in βTCP structure [151].

For biphasic materials is not possible only by using Maud refinement to calculate how the lattice parameters are influenced by the ionic substitution of Zinc and Strontium and how they can stabilize preferably one crystalline phase or both at the same time. Refined HA and βTCP patternwere calculated and lattice parameters were modified, but the substitution is not univocal.

The XRD pattern for **Zn-HA/βTCP** granules (Fig. 4.64) shows the correspondence with standard βTCP (09-169) and HA (09-432). The presence of small amount of Zincite (ZnO. 36-1451) was observed and this indicates that total zinc is not completely substituted within CaP structure. The molarity of crosslinking solution is the same used in Zn-HA/βTCP granules (0.03 M zinc acetate) but the final structure being biphasic. zinc substitutes calcium only in βTCP cell. Rietvield quantitative analyses for Zn-HA/βTCP confirmed the presence of ZnO and the amount of βTCP and HA, equal to 76.3% and 21.4,

respectively. Small contents of TTCP and αTCP were also identified (Fig. 4.65 and Table 3.35).

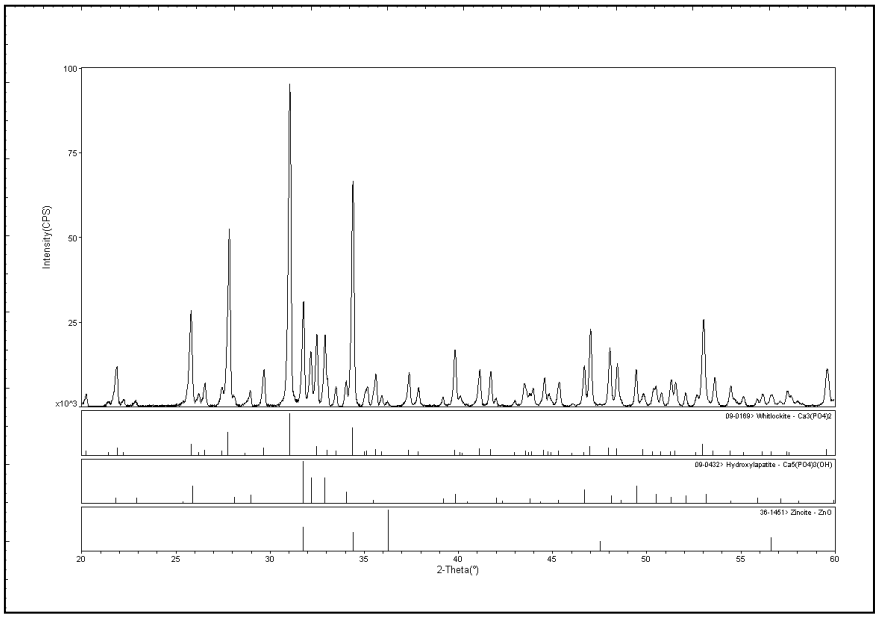

Fig. 4.64 XRD pattern of Zn-HA/βTCP granules.

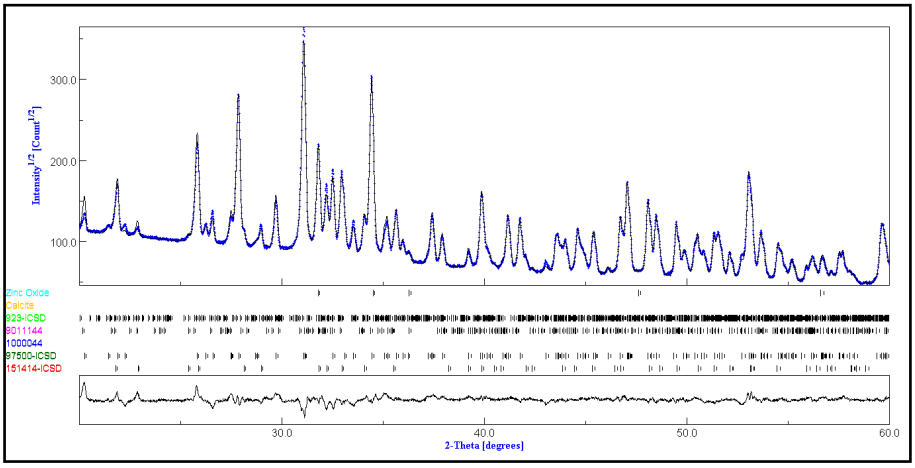

Fig. 4.65 Plot of XRD quantitative Maud analysis of Zn-HA/βTCP granules.

Sample	HA [%]	βTCP [%]	TTCP [%]	αTCP [%]	ZnO [%]
Zn-HA/βTCP	21.4	76.3	1.3	0.7	0.3

Table 4.35 XRD quantitative Maud analysis of Zn-HA/βTCP granules.

The XRD pattern for **Sr-HA/βTCP** granules (Fig. 4.66) shows the correspondence with standard βTCP (09-169) and HA (09-432). Only TTCP was detected by the Rietvield refinement. The phase content of βTCP is 69.3 and it decreases in the Sr-HA/βTCP granules due to the absence of stabilizing Zn ion. Moreover, strontium substitutes calcium ion in hydroxyapatite structure, that increases its amount, but in a sufficient amount to transform all βTCP (Fig. 4.67 and Fig. 4.37).

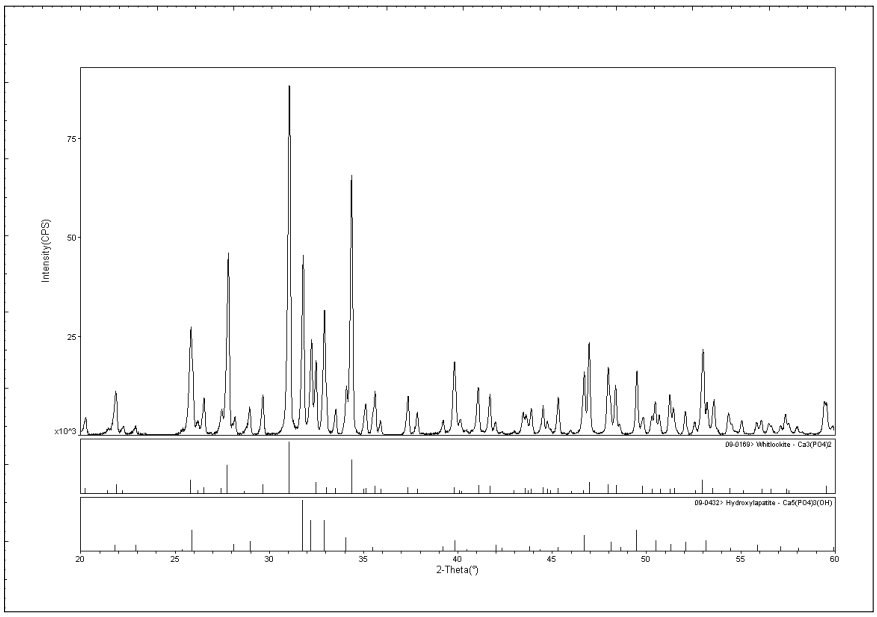

Fig. 4.66 XRD pattern of Sr-HA/βTCP granules.

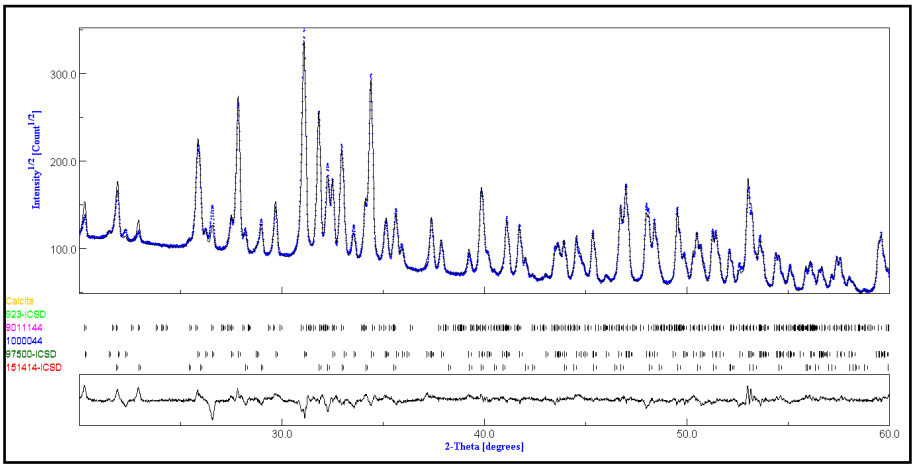

Fig. 4.67 Plot of XRD quantitative Maud analysis of Sr-HA/βTCP granules.

Sample	HA [%]	βTCP [%]	TTCP [%]	αTCP [%]
Sr-HA/βTCP	30.0	69.3	0.7	0.0

Table 4.36 XRD quantitative Maud Analysis of Sr-HA/βTCP granules

XRD pattern for **SrZn-HA/βTCP** granules (Fig. 4.38) shows the correspondence with standard βTCP (09-169) and HA (09-432). Small content of zinc, starting from 0.05 M Zn combined with 0.015 M strontium, necessary for gelification process. is sufficient for the stabilization of high amount of βTCP (70.8%). Moreover, Sr can easily substitute calcium in HA structure, but it is not enough to limit the zinc substitution that has lower ionic radius and can penetrate more easily. In this type of granules no other phases were detected by quantitative analysis performed by Maud (Fig. 4.39 and Table 4.37).

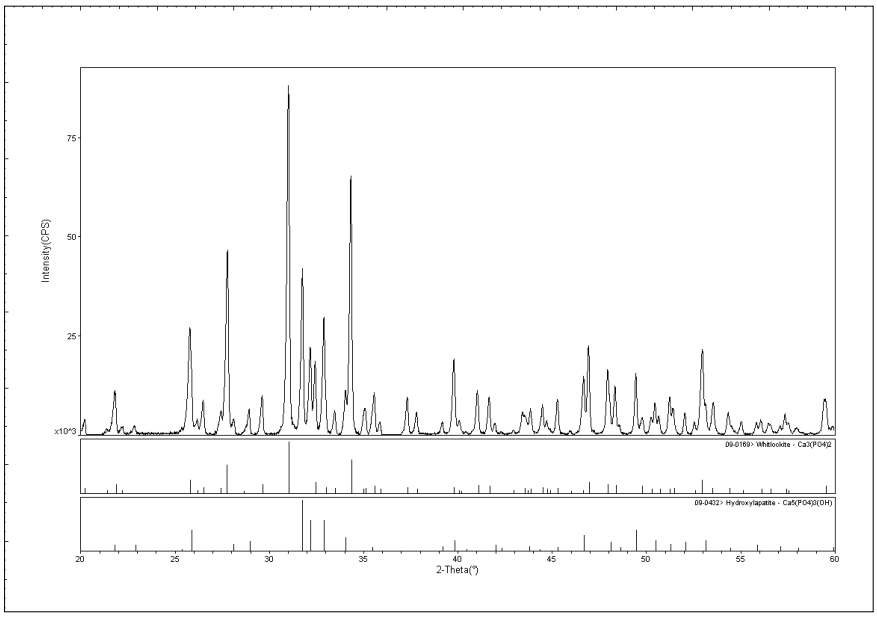

Fig. 4.68 XRD pattern of SrZn-HA/βTCP granules.

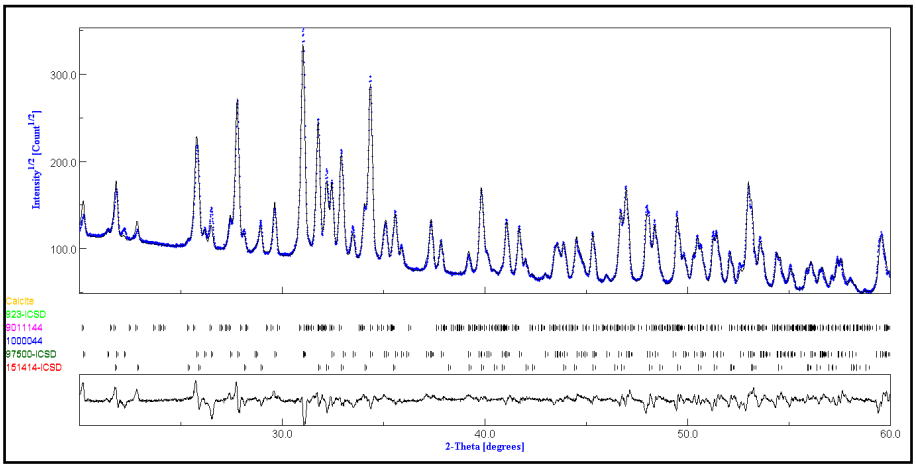

Fig. 4.69 Plot of XRD quantitative Maud Analysis of SrZn-HA/βTCP granules.

Sample	HA [%]	βTCP [%]	TTCP [%]	αTCP [%]	ZnO [%]
SrZn-HA/βTCP	29.2	70.8	0.0	0.0	0.0

Table 4.37 XRD quantitative Maud Analysis of SrZn-HA/βTCP granules.

4.7.2 Morphology

All doped granules show round morphology that is slightly lost during drying and sintering. The color is white for all chemical composition and zinc and strontium addition has no effect. (Fig. 4.70 and Fig. 4.71)

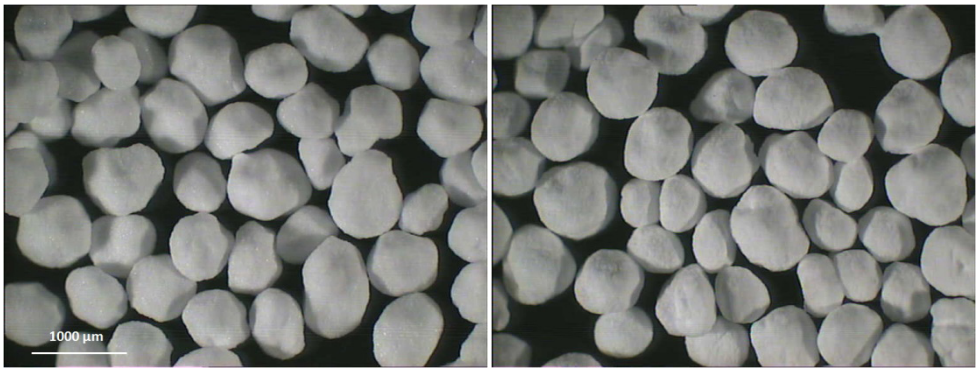

Fig. 4.70 Zn-βTCP granules and Zn-HA/βTCP granules

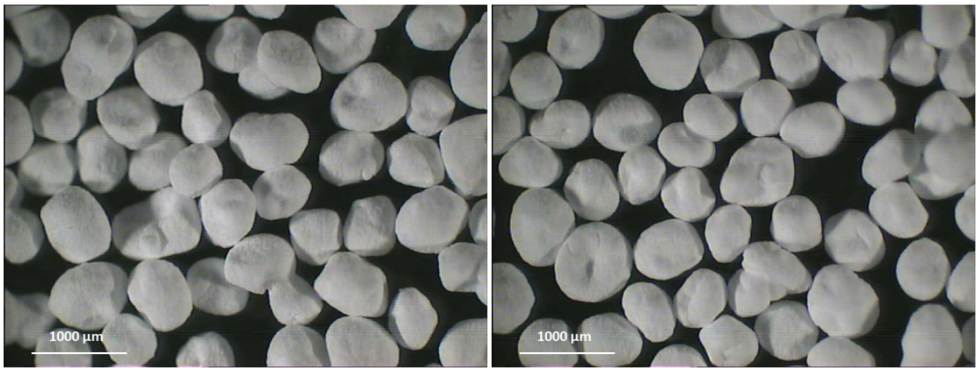

Fig. 4.71 Sr-HA/βTCP granules and SrZn-HA/βTCP granules

All doped CaP granules (Fig. 4.72 and Fig. 4.73) show regular and round morphology. Samples observed are in the range of 500-600 µm. but the size can be varied by changing the diameter of the nozzle. The round shape is maintained after a thermal treatment at 1150°C.

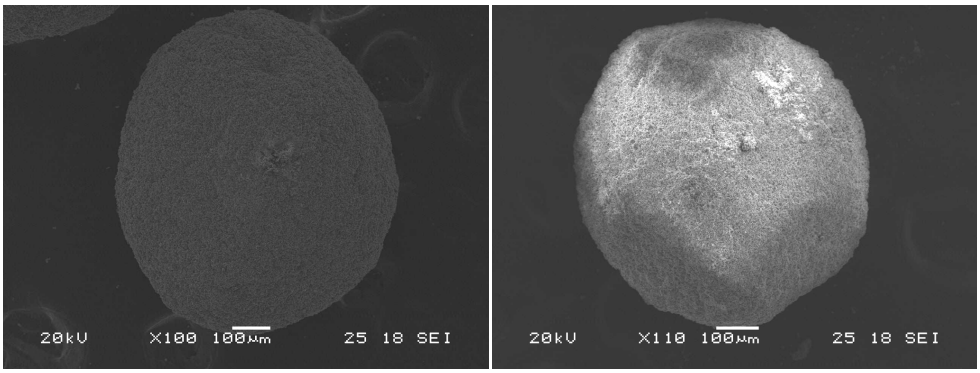

Fig. 4.72 SEM images of Zn-βTCP granules and Zn-HA/βTCP granules.

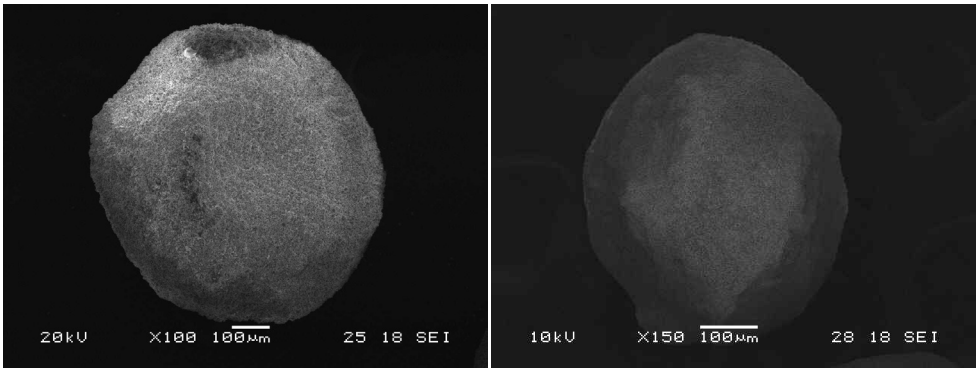

Fig. 4.73 SEM images of Sr HA/βTCP and SrZn-HA/βTCP granules.

4.7.3 Microstructure

Surface roughness is larger than in pure granules due to different gelification mechanism (ionotropic gelation) which determines a more interconnectivity gel matrix that leaves a more porous microstructure. The difference between Zn-βTCP and other doped granules is due to the distinct initial powder size. Zn-βTCP surface appears more tortous and powder grains are more connected to each other thus increasing the mechanical consistency of the material. The surface open microporosity for all granules is in the range of 1-5 μm and can be sufficient to accelerate the ion exchange with physiological liquid and the perfusion of blood and other liquids (Fig. 4.74 and Fig. 4.75).

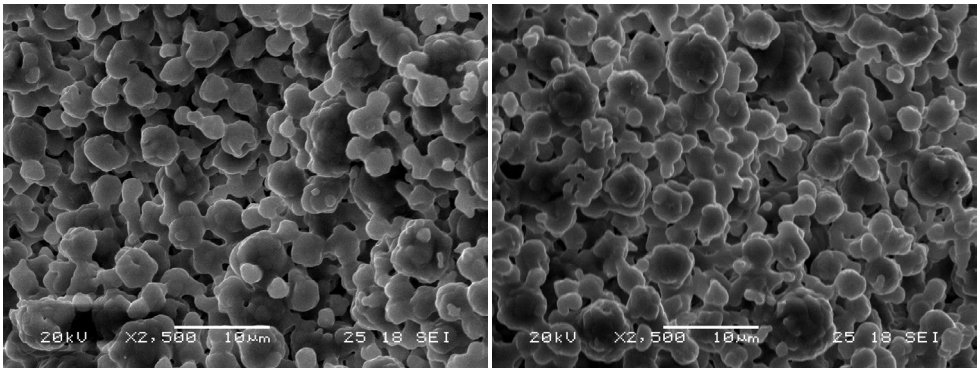

Fig. 4.74 SEM images of Zn βTCP and Zn-HA/βTCP granules

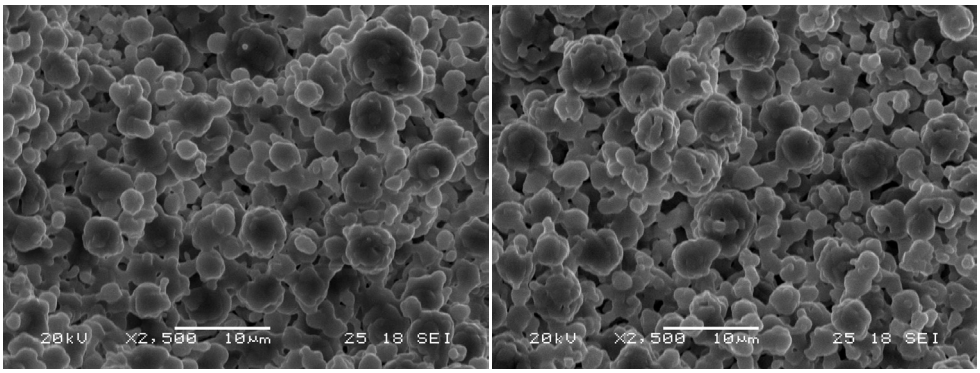

Fig. 4.75 SEM images of Sr HA/βTCP and SrZn-HA/βTCP granules.

Internal microporosity caused by burning-off of gel-matrix seems to be different between Zn-βTCP granules and other composition. Micropores are in the range of 5-30 µm. The interconnectivity in HA/βTCP doped granules is less regular due to grain powder shape, although in the range of 5-30 µm (Fig. 4.76 and 3.76).

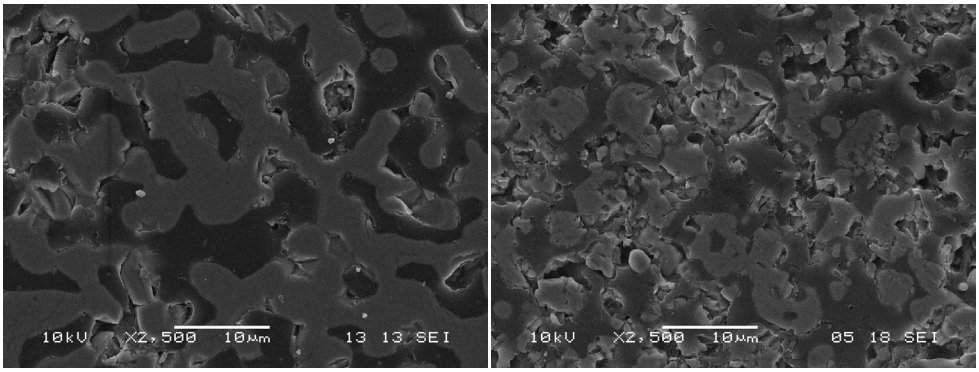

Fig. 4.76 SEM images of Zn βTCP and Zn-HA/βTCP granules.

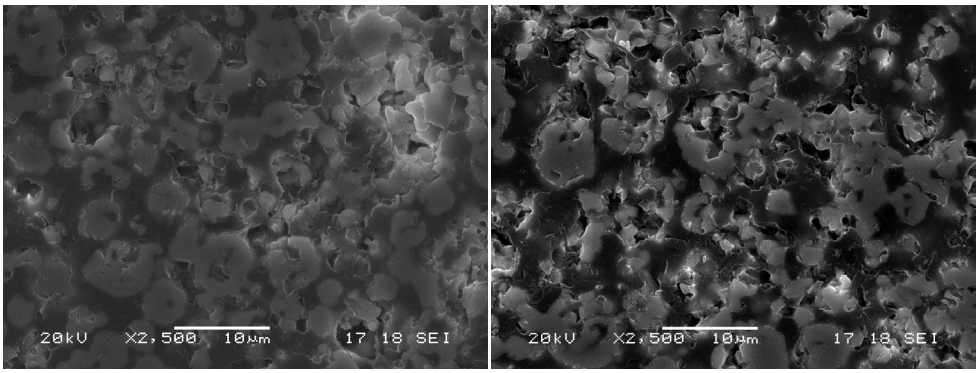

Fig. 4.77 SEM images of Sr-HA/βTCP granules and SrZn-HA/βTCP granules.

4.7.4 Porosity

Table 4.38 shows Hg-porosimetry results for doped granules. Zn-βTCP presents the highest average micropore size. This result can be related to closer porosity with respect to other types of granules as confirmed by apparent porosity values. Average pore size and porosity for biphasic doped granules are very similar. The microstructure is not influenced by the use of

different crosslinker solutions. The wide pore size distribution, 100-10000 nm, can be considered similar among all chemical compositions, always higher than in pure granules.

	Average pore size [nm]	Pore size distribution [nm]	Apparent Porosity [%]
Zn-βTCP	1551	100-10000	35
Zn-HA/βTCP	1059	100-10000	40
Sr-HA/βTCP	1083	100-10000	38
SrZn-HA/βTCP	1081	100-10000	43

Table 4.38 Hg-porosimetry data for doped granules.

4.8 *In vitro* experiments

4.8.1 Dissolution rate

The dissolution rate analyses were carried out in two different buffer solution, MES pH 5.5 and TRIS pH 7.3. In both analyses the obtained dissolution trends are the same.

As it is well known from literature, changes in solution pH does not modify the mechanism of dissolution process and the use of a low pH solution only increases the dissolution rate [142].

The granules which show the highest solubility trend are the HA/βTCP, followed by HA/TTCP and βTCP ones. The granules with lower solubility

trend are the HA ones. Calcium and phosphate concentrations are plotted versus time for TRIS (Fig. 4.78 and Fig. 4.79) and MES (Fig. 4.80 and Fig. 4.81) case. The data correspond to the average values calculated from 3 repeated experiments.

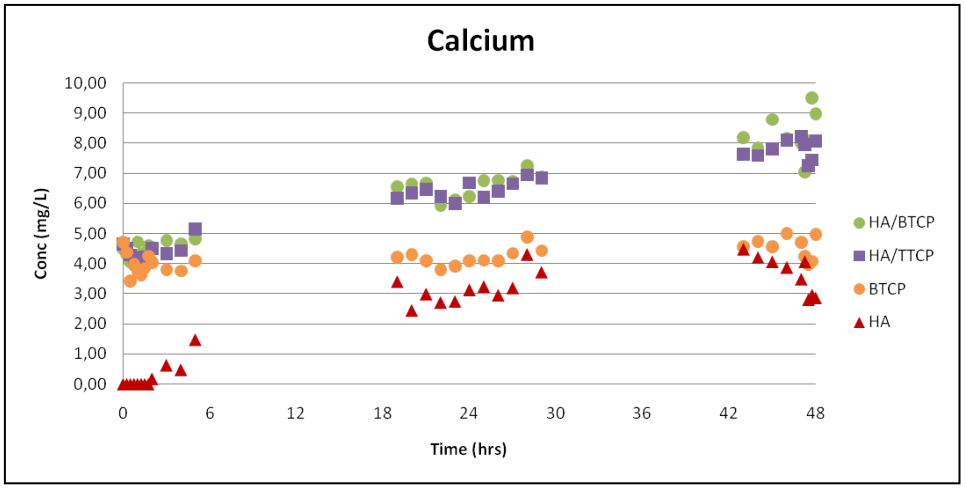

Fig. 4.78 TRIS buffer solution pH 7.3: plot of calcium concentration versus time.

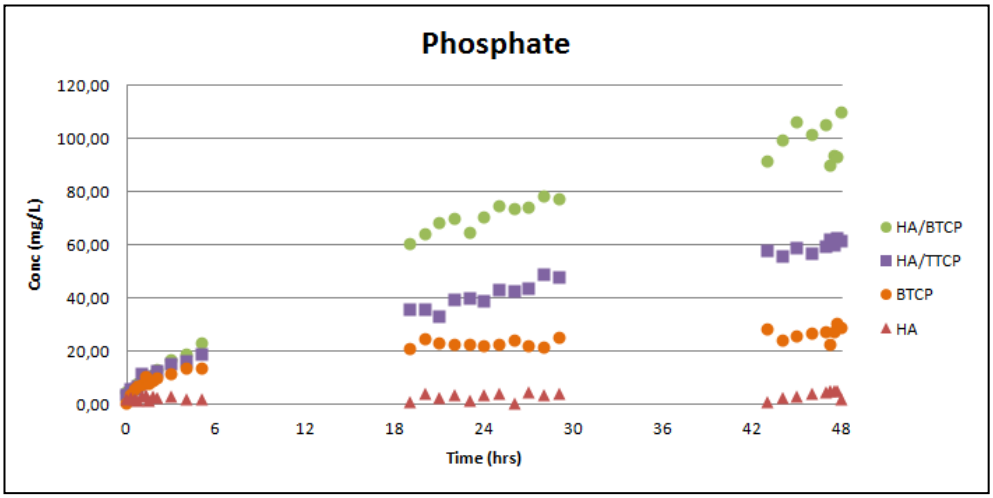

Fig. 4.79 TRIS buffer solution pH 7.3: plot of phosphate concentration versus time.

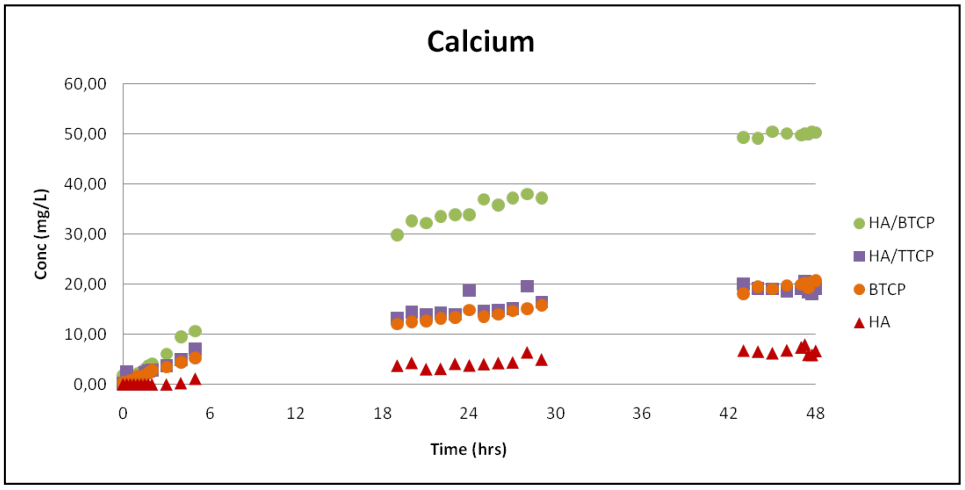

Fig. 4.80 MES buffer solution pH 5.5: plot of calcium concentration versus time.

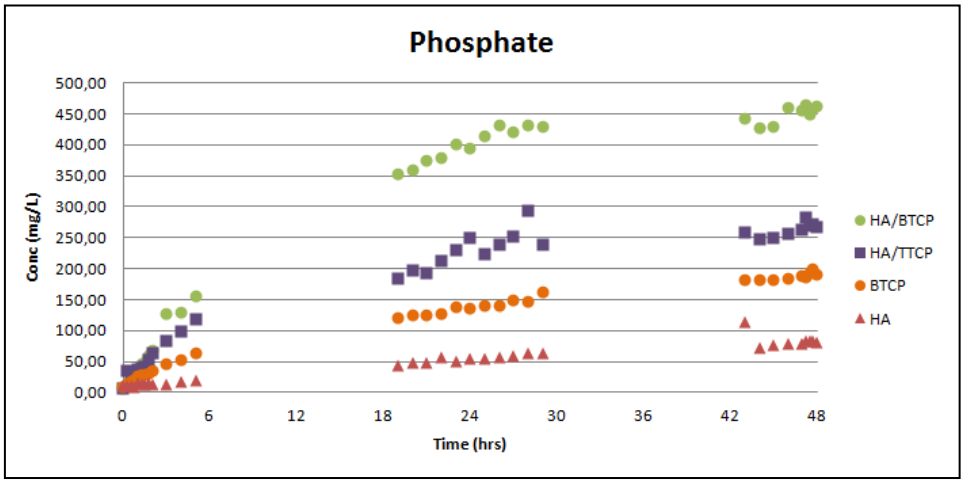

Fig. 4.81 MES buffer solution pH 5.5: plot of phosphate concentration versus time.

In order to explain the observed dissolution trend it is necessary to consider both chemical composition and surface morphology of the granules. In terms of dissolution of calcium, the order of solubility of the most common calcium phosphate materials is: TTCP>>αTCP>>βTCP>>CDHA>>HA [152].

In this study, the most soluble granules result to be the HA/βTCP. These granules, if the morphological characteristics are considered, are the most porous, that means they possess higher exposed surface area with respect to the other types of granules. The above considerations explain why HA/βTCP granules are more soluble than βTCP pure granules. Moreover, in other studies where it was clear that the TCP and HA react together, this resulting in the conversion of TCP into Ca-deficient apatite, the higher solubility of BCP with respect to HA was verified [16].This Ca-deficient apatite is considered to have a higher dissolution rate than the stoichiometric HA, because it contains high level of defect concentration within the crystal structure. The relatively

high solubilities observed in the BCP samples might therefore be related to this phenomenon [17].

The second most soluble granules are the HA/TTCP granules, followed by the βTCP granules; this result confirms the trends of reported dissolution rates where TTCP is more soluble than βTCP [152].

The least soluble of all composition is HA, even if its porosity and sintering temperature (1000°C) is comparable to the HA/βTCP granules. In this case, even if the total exposed surface area is increased, the solubility behavior of the granules strongly depends on their chemical composition, these results being consistent with the solubility trends described in literature [152].

4.8.2 Solubility parameter (Ksp) and behavior of pure granules in determined solutions

The solubility analyses carried out to calculate Ksp values in TRIS (pH 7.3). where the equilibrium for each solid form was reached after 70 days, were used also for calculating the dissolution behavior in determined solutions. Ksp were calculated only for HA and for βTCP with Eq. 19 and Eq.20.

$$Ksp_{(HA)} = [Ca^{2+}]^{10}[PO_4^{3-}]^6 \quad (19)$$

$$Ksp_{(\beta TCP)} = [Ca^{2+}]^{3}[PO_4^{3-}]^2 \quad (20)$$

by using the average values calculated from the data set of the 3 repeated experiments for each composition. The comparison between all four families and the reference standard HA NIST is performed using the concentration

product of HA. The results and Ksp for both HA and for βTCP are reported in Table 4.39.

Chemical composition	Concentration product $[Ca^{2+}]^{10}[PO_4^{3-}]^6$ (37°C)	Ksp $_{(HA)}$ $[Ca^{2+}]^{10}[PO_4^{3-}]^6$ (37°C)	Ksp $_{(\beta TCP)}$ $[Ca^{2+}]^{3}[PO_4^{3-}]^2$ (37°C)
60HA/40β-TCP granules	$8.5 \cdot 10^{29}$	-	-
60HA/40TTCP granules	$6.3 \cdot 10^{27}$	-	-
β-TCP granules	$1.1 \cdot 10^{21}$	-	$4.87 \cdot 10^{6}$
HA granules	$2.4 \cdot 10^{20}$	$2.4 \cdot 10^{20}$	-
HA NIST (Control)	$7.4 \cdot 10^{24}$	$7.4 \cdot 10^{24}$	-

Table 4.39 Concentration products and Ksp(HA) and Ksp(βTCP) values in TRIS solution.

The decision to use the same concentration product in order to compare all the compound is due to the fact that it is not possible to calculate Ksp for biphasic compound. Ksp depends on the particular formula of specific monophasic compound. The obtained concentration products for granules confirm the initial dissolution rate trends: HA/βTCP<<HA/TTCP<<βTCP<<HA. HA granules have lower Kps value of HA NIST powder due to the different morphology and consequently distinct specific surface area. Fig. 4.82 and Fig. 4.83 show that dissolution curves corresponding to calcium and phosphate reach a relatively stable level for all different composition. Thus, equilibrium of solid form in TRIS is reached at the end of the 70 days in all the analyses.

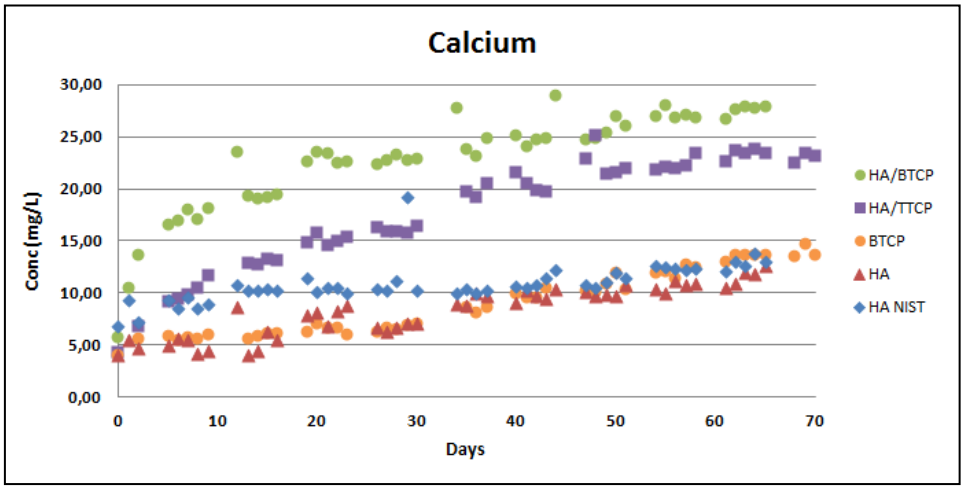

Fig. 4.82 TRIS pH 7.3: Plot of calcium concentration versus time

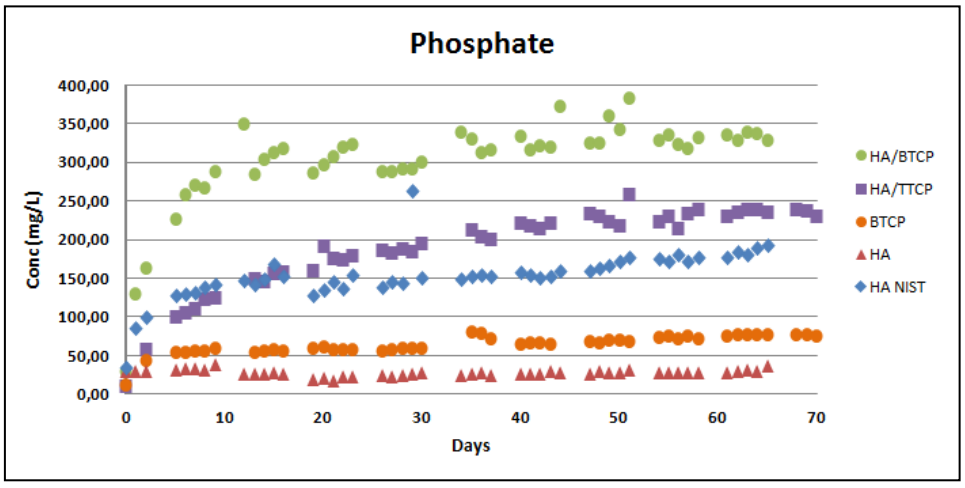

Fig. 4.83 TRIS pH 7.3: Plot of phosphate concentration versus time.

4.8.3 Degradation behavior in acid solution

In order to quantify the amount of dissolved materials, granules were accurately weighted before and after the analysis. The results are reported in Table 4.40.

Sample	Starting weight (g)	Final weight (g)	Final weight after additional washing step (g)	Tricalcium citrate (g)	Weight loss [%]
HA granules	1.0003	0.9503	-	-	5.0%
HA Calcitite 4060	1.0092	0.9692	-	-	4.0%
β-TCP granules	1.0005	1.0983	0.7631	0.3352	23.7%
β-TCP Cerasorb	1.0015	0.8245	0.8245	-	17.7%
HA/ β-TCP granules	1.0018	1.0437	0.7151	0.3286	28.6%
HA/TTCP granules	1.0019	1.1077	0.8754	0.2323	12.6%

Table 4.40 Sample weight before and after degradation test.

After 5 days in the acidic solution, β-TCP granules and β-TCP Cerasorb turn into powders. Granules of the others compositions remain in the granular form. The weight differences after the additional washing step demonstrated that HA/βTCP are the most soluble granules with a weight loss of 28.6%. HA/βTCP dissolves rapidly due to the microporous structure (0.1-3 μm) and more than pure βTCP which is denser and with larger micropores (0.1-10 μm). The extreme solution in which the experiments are carried out is prepared mainly with citric acid. It is well know from literature that citric acid in calcium containing solution acts as an entrapment agent for calcium ions. especially under acidic condition [153]. This behavior leads to the formation

of a new. low solubility white precipitate identified as tricalcium dicitrate tetrahydrate (calcium citrate) [154].

As the calcium phosphate granules dissolves in the extreme solution. both the concentration of free calcium ions and the pH value. The free calcium ions are chelated by the citrate anions leading to the formation of calcium citrate that starts to precipitate when its solubility limit is exceeded [155]. This results in the precipitation of calcium citrate at the granules boundaries [156].

In our study, traces of calcium citrate were found attached to the surface of the biphasic granules. HA/TTCP and HA/β-TCP, and to the powder of β-TCP dissolved from granules as they are the most soluble and the amount of free calcium ion released exceeded the solubility limit of calcium citrate. No signs of calcium citrate were found on HA granules and HA calcitite, because the concentration of free calcium ions does not reach the solubility limit of calcium citrate. In the case of the biphasic granules, the calcium citrate was easily separable from the granules by high porous paper filter because it was not bound chemically to the surface and it could be separated just by washing the granules with hot water. It was not easy to separate the calcium citrate powder from the β-TCP dissolved granules because they possess the same size.

To quantify the amount of the calcium citrate the granules were accurately weighted after the hot water washing step. The results are summarized in Table 4.40.

The calcium citrate was separated from the granules to obtain better XRD diffraction patterns in order to quantify through Rietveld quantification analysis the exact composition of each product.

After the 5 days of degradation test the pH of the extreme solution was checked (Table 4.41).

Sample	Starting pH	Final pH
HA granules	3	4
HA Calcitite 4060	3	4
β-TCP granules	3	4
β-TCP Cerasorb	3	5.5
HA/ β-TCP granules	3	5
HA/TTCP granules	3	5

Table 4.41 The pH measurement of acid solution at the beginning and at the end of the degradation test.

An increase in the pH value was measured for all the compositions which is justifiable with the presence of the alkali calcium ions; it is also well known from literature that the precipitation of the calcium citrate is accompanied by an increase in pH [155]. The increase of pH from 3 to 5 in βTCP Cerasorb and in biphasic granules is due to the higher dissolution of the products that free Ca ions in solution.

Granules surface was analyzed by SEM after the degradation test. Changes in surface morphology of the granules, such as formation of new pores, can be easily detected for all the compositions. This phenomenon is related to the dissolution of the calcium phosphate materials and it is an intrinsic property of bioresorbable materials which does not compromise the performance and safety of the materials. After the immersion in acid solution HA granules do not degrade in any drastic way. The round morphology is maintained and the

surface is a little bit modified. Open micropores are bigger and the specific area decrease (Fig. 4.84 and Fig. 4.85).

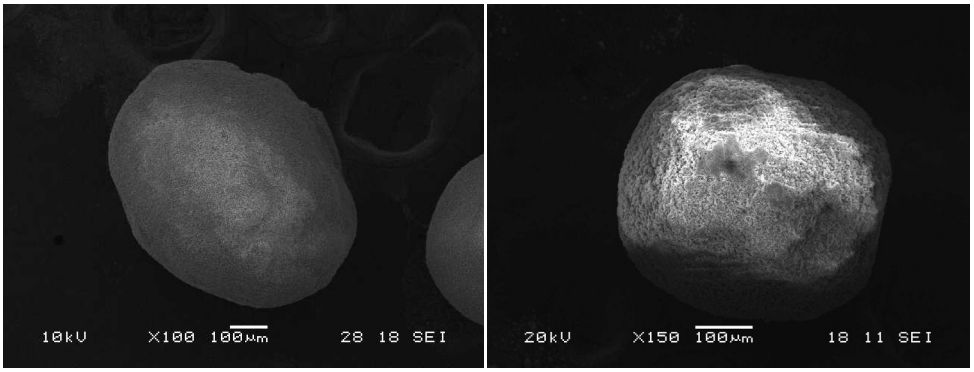

Fig. 4.84 SEM images of HA granules morphology before and after the degradation test.

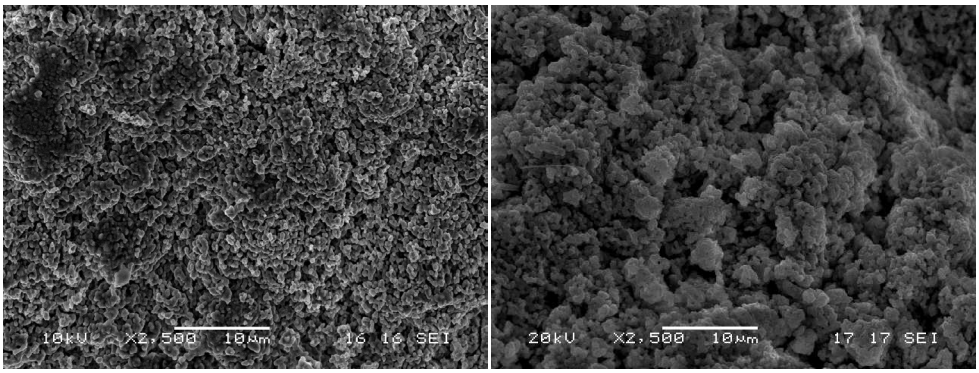

Fig. 4.85 SEM images of HA granules surface before and after the degradation test.

Calcitite HA granules do not show signs of degradation after the test. The microstructure remains compact; this is also due to higher sintering temperature (Fig. 4.86 and Fig. 4.87).

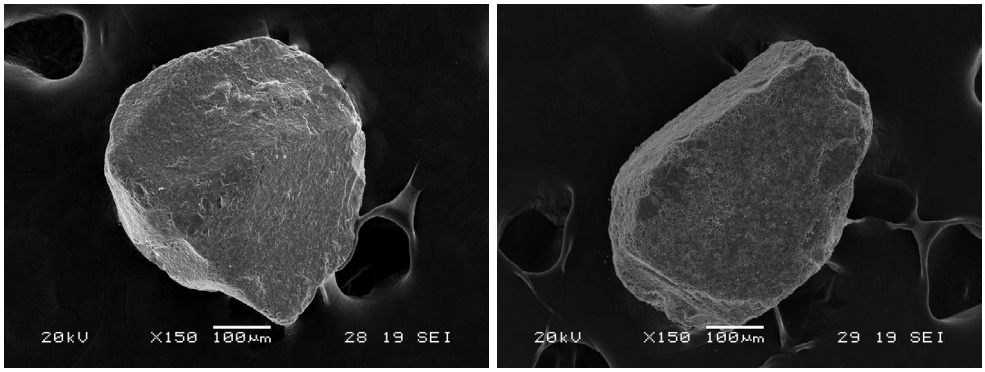

Fig. 4.86 SEM images of HA Calcitite granules morphology before and after the degradation test.

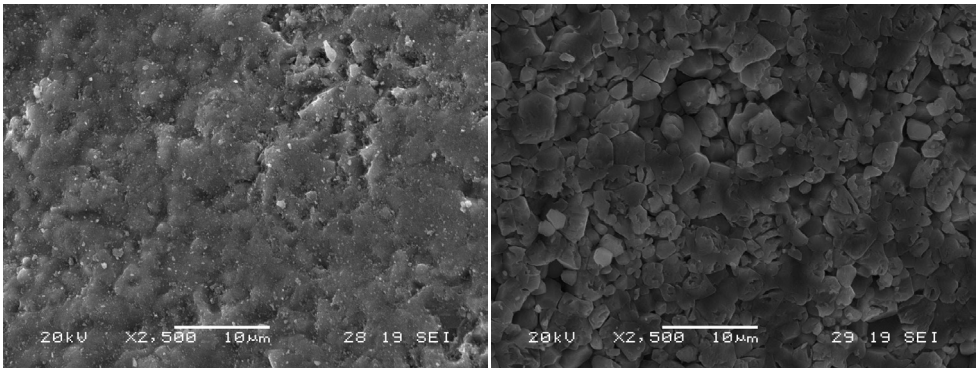

Fig. 4.87 SEM images of HA Calcitite granules surface before and after the degradation test.

After 5 days in acid solution βTCP granules lose the round morphology and degrade into powders. The Microporous structure does not exist anymore. but this situation represents the worse case because in the implantation site the bone substitute are not completely immersed in solution as in degradation test so the exposition of the material to the solution is limited (Fig. 4.88 and Fig. 4.89).

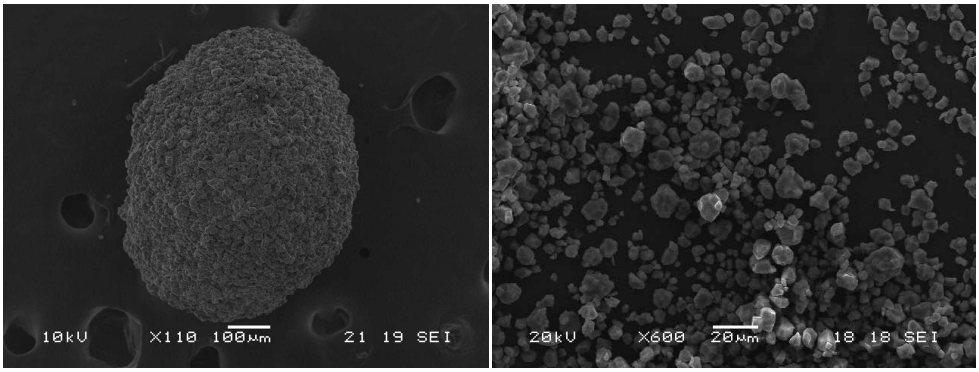

Fig. 4.88 SEM images of βTCP granules morphology before and after the degradation test.

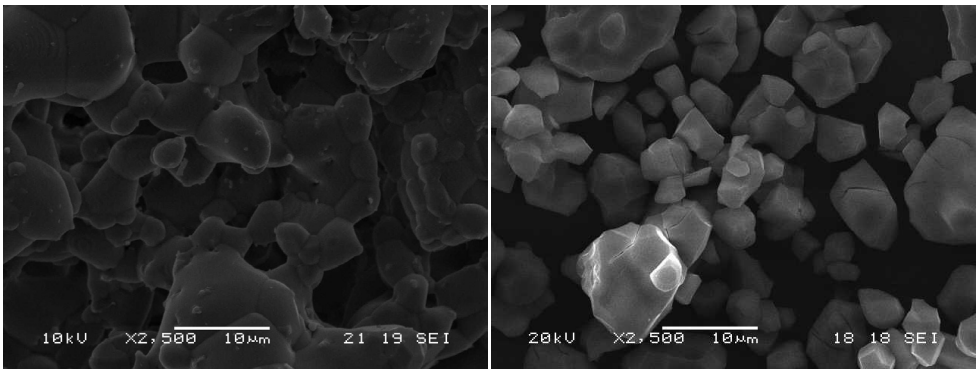

Fig. 4.89 SEM images of βTCP granules surface before and after the degradation test.

Commercial β-TCP Cerasorb granules dissolve quickly in acid solution and after 5 days granules lose the round morphology and degrade into powders (Fig. 4.90 and Fig. 4.91)

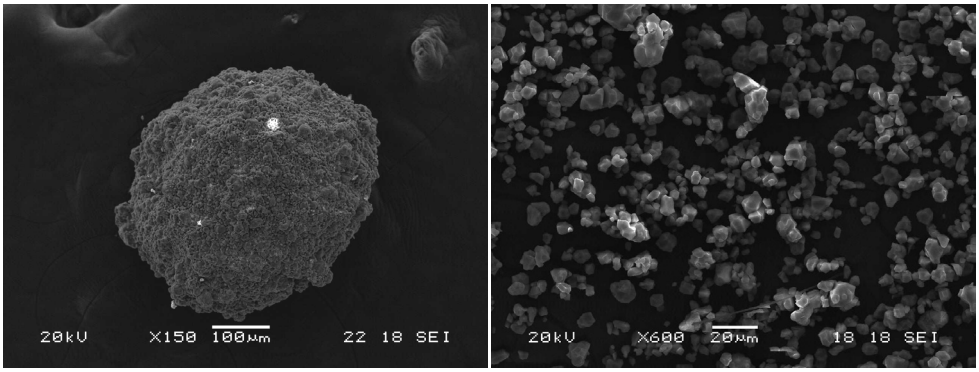

Fig. 4.90 SEM images of βTCP Cerasorb granules morphology before and after the degradation test.

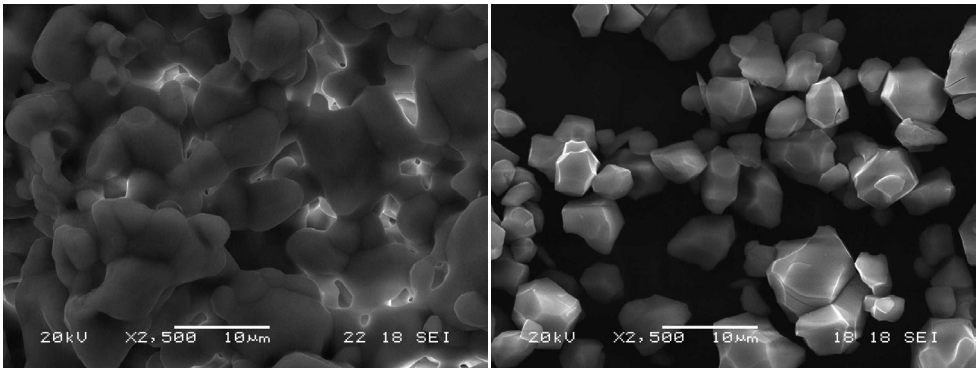

Fig. 4.91 SEM images of βTCP Cerasorb granules surface before and after the degradation test.

After the immersion in acid solution the surface of HA/BTCP granules show evident signs of erosion. The round morphology is maintained and the surface is a little bit modified. Some small citrate crystals are visible despite the washing step (Fig. 4.92 and Fig. 4.93)

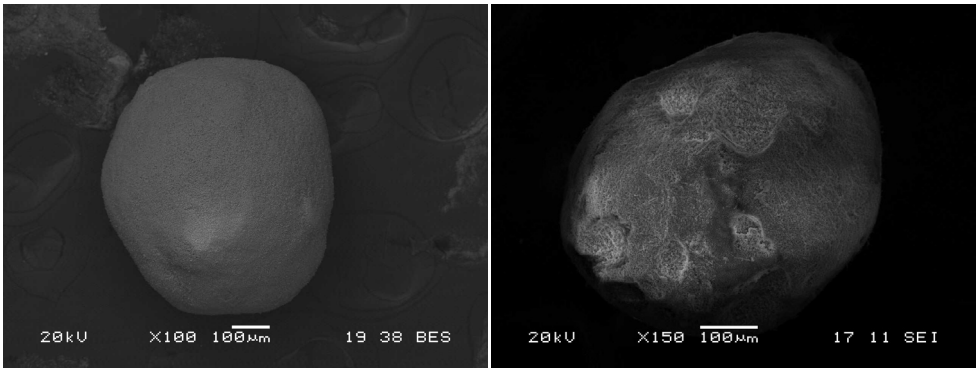

Fig. 4.92 SEM images of HA/βTCP granules morphology before and after the degradation test.

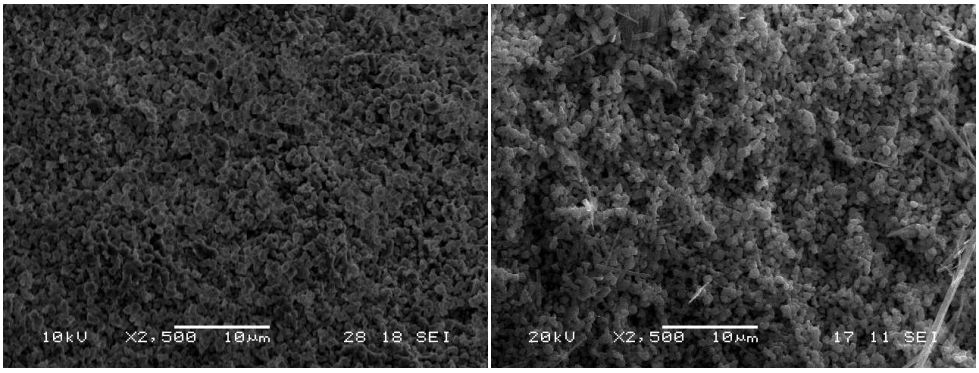

Fig. 4.93 SEM images of HA/βTCP granules surface before and after the degradation test.

After the immersion in acid solution the surface of HA/TTCP granules show evident signs of erosion. The round morphology is maintained and the surface is a little bit modified. Some small citrate crystals are visible despite the washing step (Fig. 4.94 and Fig. 4.95).

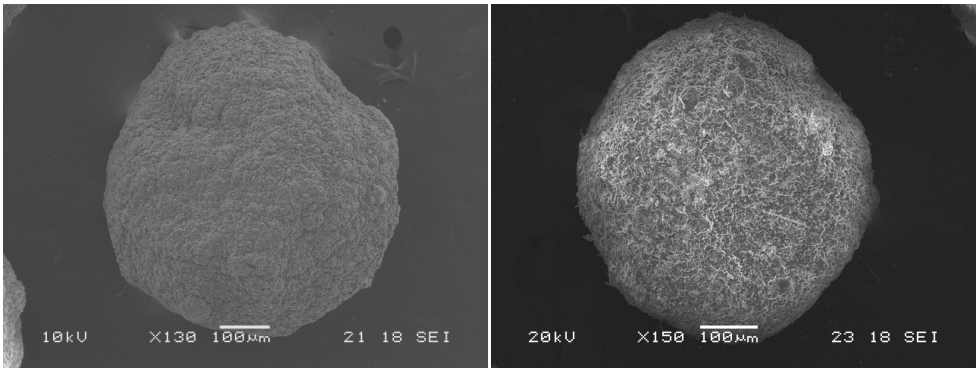

Fig. 4.94 SEM images of HA/TTCP granules morphology before and after the degradation test.

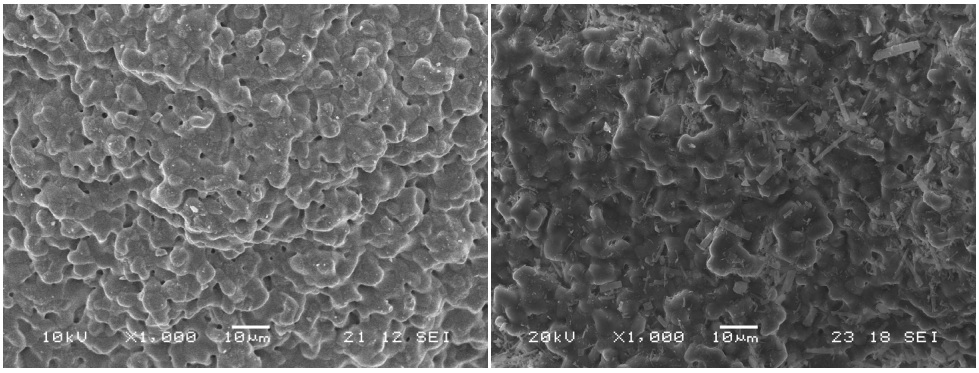

Fig. 4.95 SEM images of HA/TTCP granules surface before and after the degradation test.

XRD analysis was performed on all granules and powder before and after the degradation test in order to identify all the modifications in the chemical composition of the granules. In this study, traces of calcium citrate, precipitated from the acidic solution, were found attached to the surface of the biphasic granules. HA/TTCP and HA/β-TCP, and in the powder of β-TCP dissolved granules. No signs of calcium citrate were found on HA granules

because the amount of available free calcium ions does not exceed the solubility limit of calcium citrate. In the case of the biphasic granules the calcium citrate was easily separable from biomaterial because it was not bound chemically to the surface. The calcium citrate was separated from the granules to obtain a better XRD diffraction patterns in order to quantify the exact composition of each product.

The XRD diffraction patterns for HA granules before (Fig. 4.96) and after (Fig. 4.97) the dissolution test did not present significant differences. No differences were seen in the XRD patterns for HA Calcitite granules, before (Fig. 4.98) and after (Fig. 4.99) the test. The quantitative analysis conducted with MAUD (Table 4.42) indicates that all the impurities initially detected in the HA granules are dissolved and no other calcium phosphate re-precipitates during the test; in HA Calcitite granules foreign phases. TTCP and CaO, do not degrade during the test and no other calcium phosphates re-precipitate during the analysis.

Sample	HA [%]	βTCP [%]	CaO [%]	TTCP [%]	αTCP [%]	$CaCO_3$ [%]
HA before	98.0	0.0	0.0	1.8	0.2	0.00
HA after	100.0	0.0	0.0	0.0	0.0	0.0
HA Calcitite before	98.0	0.0	0.2	1.8	0.0	0.0
HA Calcitite after	98.1	0.0	0.2	1.8	0.0	0.0

Table 4.42 Quantitative analysis of HA granules by Maud Program

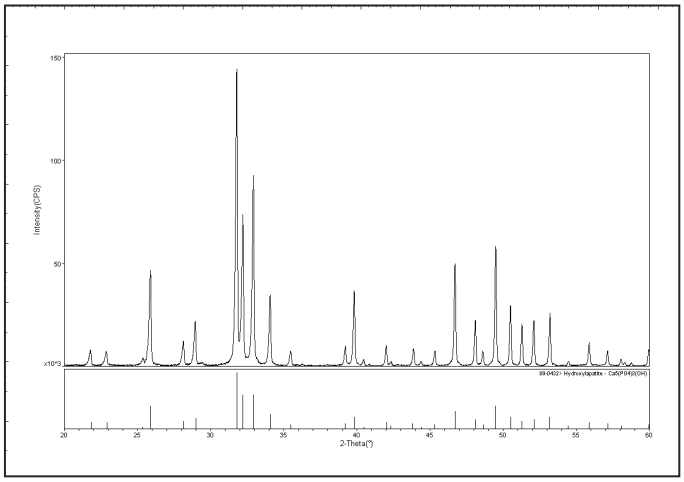

Fig. 4.96 XRD pattern of HA granules before the degradation test.

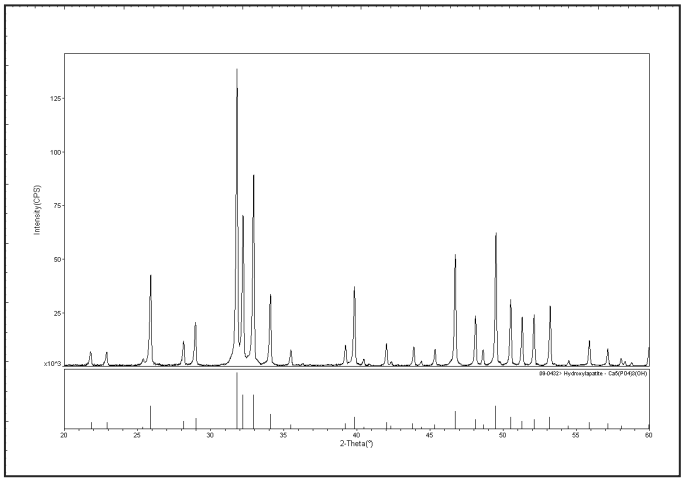

Fig. 4.97 XRD pattern of HA granules after the degradation test.

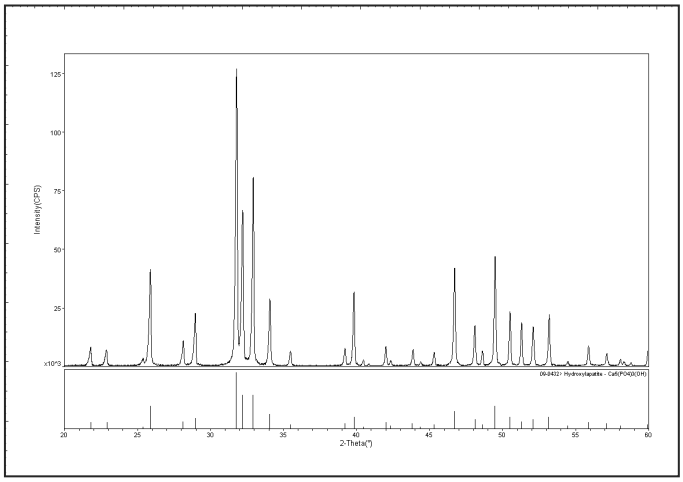

Fig. 4.98 XRD pattern of HA Calcitite granules before the degradation test.

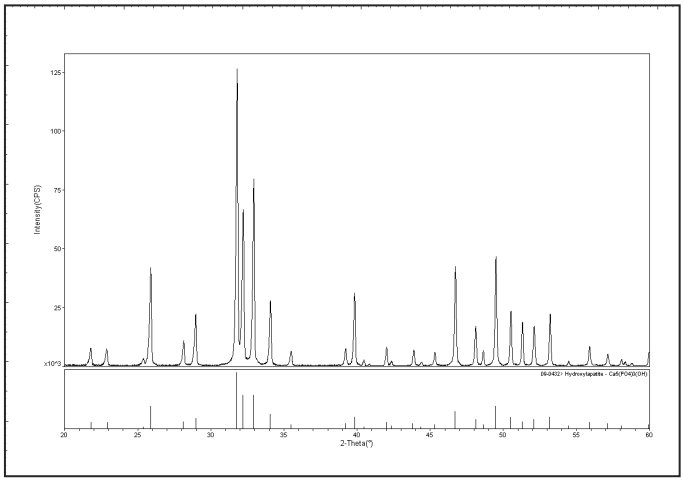

Fig. 4.99 XRD pattern of HA Calcitite granules after the degradation test.

The XRD diffraction patterns for βTCP granules before (Fig. 4.100) and after (Fig. 4.101) the dissolution test do not present any significant differences; the peaks intensity is lower and this could indicate the initial degradation of the

product. Also the XRD diffraction patterns of βTCP Cerasorb granules before (Fig. 4.102) and after (Fig. 4.103) the dissolution test do not present significant differences.

The quantitative analyses conducted with MAUD are presented in Table 4.43. Data point out that all the impurities initially detected in the βTCP granules are dissolved and a small amount of TTCP is reprecipitated during the analysis. Also. a little amount of pyrophosphate is visible from XRD pattern but it is below 1% and is not quantifiable. Due to the large amount of free calcium ions released in the solution. some calcium citrate precipitates. Because after 5 days in the acidic solution β-TCP granules turned into fine powders it was not possible to eliminate all the calcium citrate from the granules powder and peaks at 22.6° and 28.9° indicate the presence of calcium citrate. In βTCP Cerasorb granules turned into fine powders and no signs of calcium citrate can be detected, this is probably because the β-TCP Cerasorb granules are a little less soluble than β-TCP granules and the solubility limit. that allows the precipitation of calcium citrate. is not reached. The fact that β-TCP Cerasorb granules are less soluble than β-TCP granules is probably due to a higher sintering temperature during the production cycles for the β-TCP Cerasorb granules that result to be a more ordered structure.

Sample	HA [%]	βTCP [%]	CaO [%]	TTCP [%]	αTCP [%]	$CaCO_3$ [%]
βTCP before	0.0	97.9	0.0	0.0	0.8	1.3
βTCP after	0.0	97.0	0.0	1.1	0.0	0.0
βTCP Cerasorb before	0.5	98.3	0.0	0.6	0.6	0.0
βTCP Cerasorb after	0.7	97.2	0.0	1.0	1.1	0.0

Table 4.43 Quantitative analysis of βTCP granules by Maud Program.

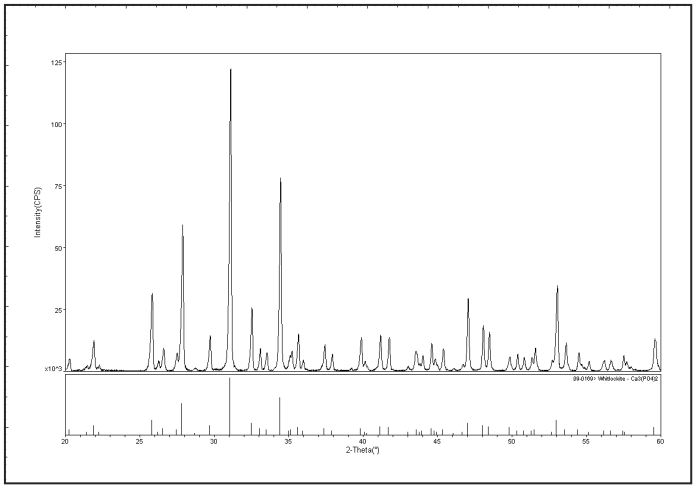

Fig. 4.100 XRD pattern of βTCP granules before the degradation test.

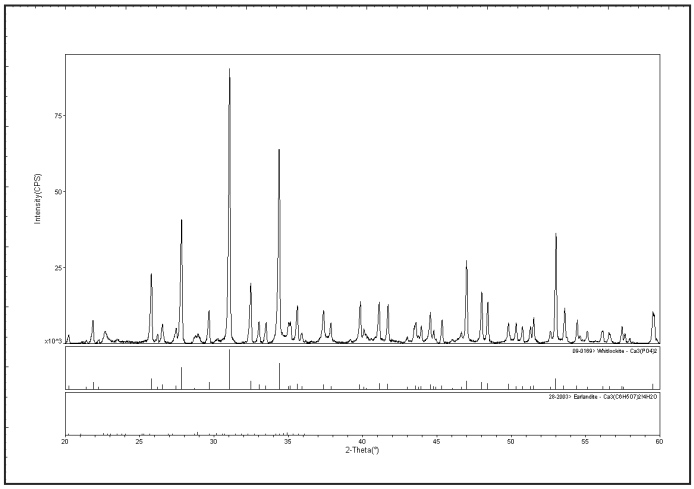

Fig. 4.101 XRD pattern of βTCP granules after the degradation test.

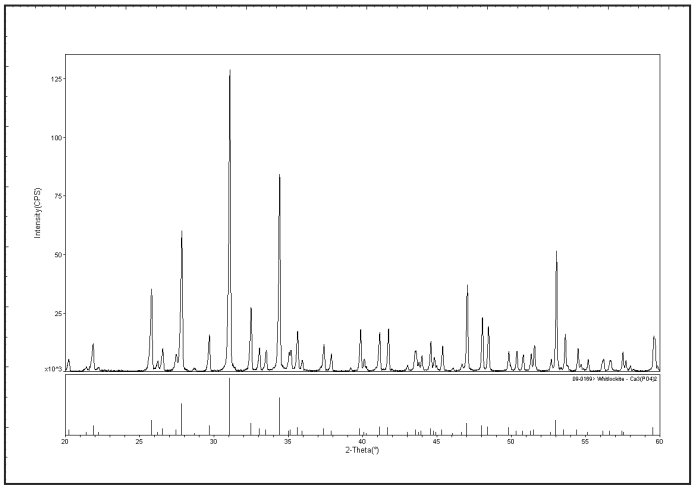

Fig. 4.102 XRD pattern of βTCP Cerasorb granules before the degradation test.

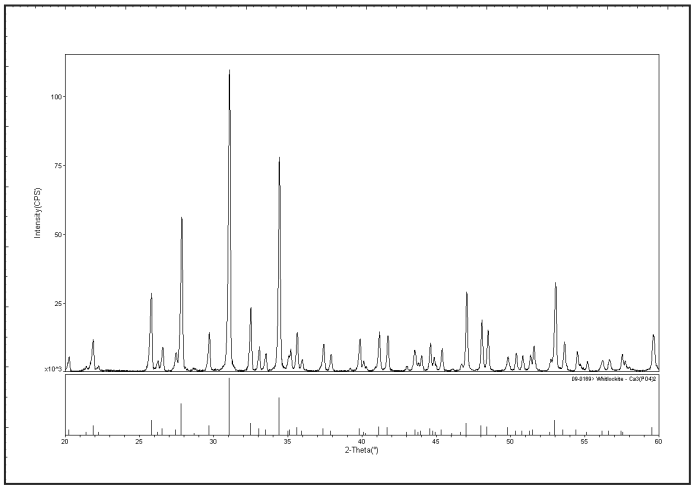

Fig. 4.103 XRD pattern of βTCP Cerasorb granules after the degradation test.

The XRD diffraction patterns for HA/βTCP granules, before (Fig. 4.104) and after (Fig. 4.105) the dissolution test do not present significant differences.

The quantitative analysis carried out with MAUD (Table 4.44) indicates a small amount of TTCP that is reprecipitated during the analysis. Due to the large amount of free calcium ions released in the solution. some calcium citrate precipitates were formed for HA/βTCP and HA/TTCP granules; calcium citrate was easily separable from the granules because it was not attached chemically to the surface and could be removed just by washing the granules with hot water to obtain better XRD diffraction patterns that allowed the quantification of the exact composition of each product.

Sample	HA [%]	βTCP [%]	CaO [%]	TTCP [%]	αTCP [%]	$CaCO_3$ [%]
HA/βTCP before	67.4	32.6	0.0	0.0	0.0	0.0
HA/βTCP after	67.2	31.0	0.0	1.8	0.0	0.0

Table 4.44 Quantitative analyses of HA/βTCP granules by Maud Program.

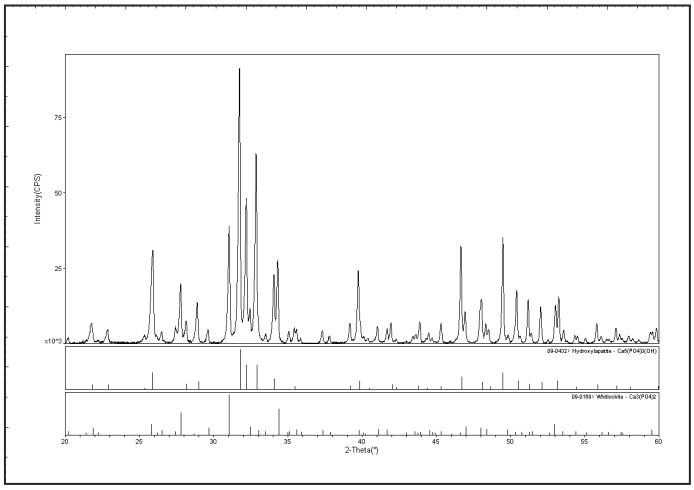

Fig. 4.104 XRD pattern of HA/βTCP granules before the degradation test.

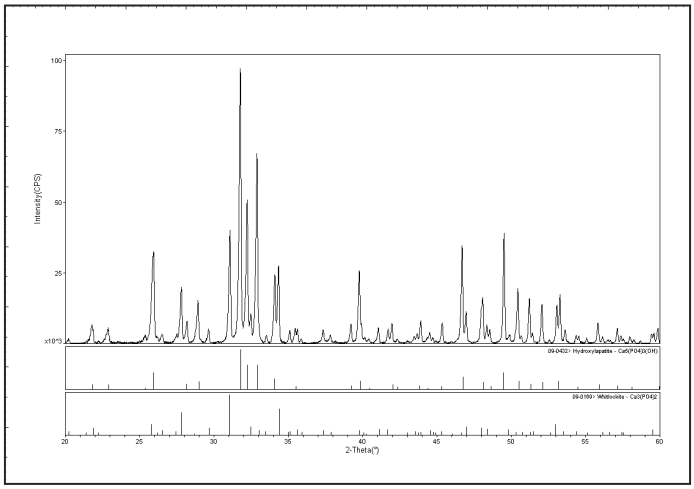

Fig. 4.105 XRD pattern of HA/βTCP granules after the degradation test.

XRD diffraction patterns of HA/TTCP granules, before (Fig. 4.106) and after (Fig. 4.107) the dissolution test present significant differences in correspondence of main peaks of TTCP (each at 29.2° and 29.8°). The peak intensities decrease and the quantitative analysis (Table 4.45) indicates that 19.1% of TTCP dissolved during the test. Also αTCP initially detected in the granules is dissolved in acid solution.

Sample	HA [%]	βTCP [%]	CaO [%]	TTCP [%]	αTCP [%]	$CaCO_3$ [%]
HA/TTCP before	55.4	0.0	0.0	41.3	3.3	0.0
HA/TTCP after	77.8	0.0	0.0	22.2	0.0	0.0

Table 4.45 Quantitative analysis of HA/TTCP granules by Maud Program.

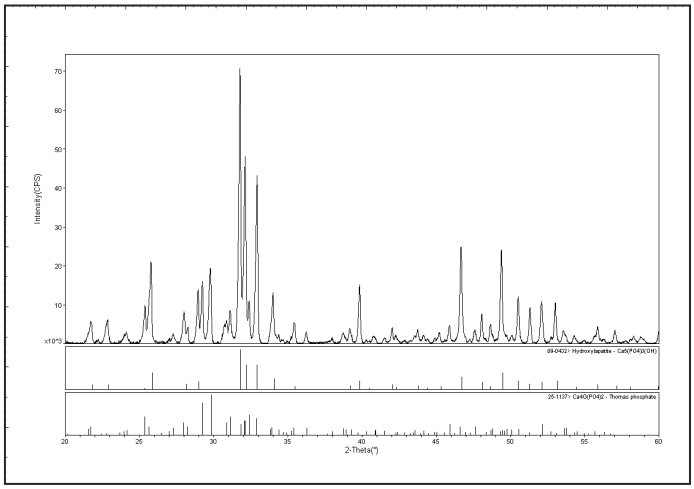

Fig. 4.106 XRD pattern of HA/TTCP granules before the degradation test.

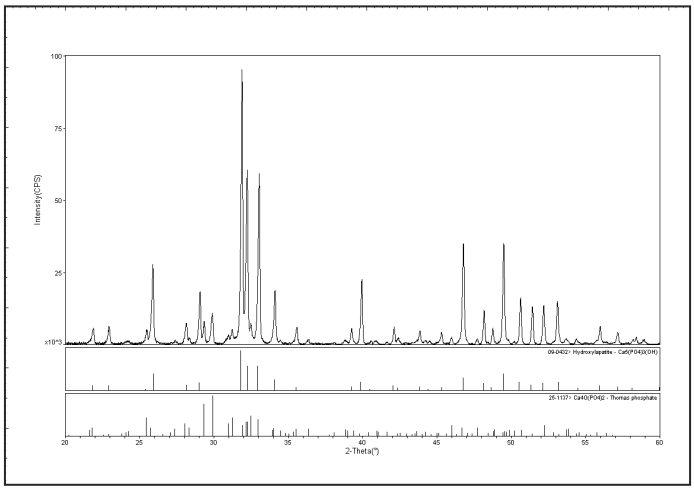

Fig. 4.107 XRD pattern of HA/TTCP Eurocoating granules after the degradation test.

All filtrated acid solutions, obtained from the degradation tests, were characterized by using ICP-OES analyses in order to evaluate the calcium and

phosphorus contents and the presence of impurities. No anomalous degradation product or particular impurities were found after the degradation test (Table 4.46 and Table 4.47).

Element [ppm]	HA	HA Calcitite	βTCP	βTCP Cerasorb	HA/βTCP	HA/TTCP
Ca	106.67	85.87	121.67	147.73	79.73	35.93
P	55.80	39.67	148.00	99.60	16.33	101.67

Table 4.46 Solid concentrations of Ca and P in ppm.

Element [ppm]	HA	HA Calcitite	βTCP	βTCP Cerasorb	HA/βTCP	HA/TTCP
Mg	8.30	0.06	2.09	3.09	0.19	1.10
K	0.86	0.26	1.47	1.07	7.93	1.11
Mn	31.00	0.004	0.010	0.027	0.014	0.021
Ba	9.97	0.017	0.049	0.033	1.068	0.038

Table 4.47 Solid concentrations of impurities in ppm.

By resuming the degradation test results, one can point out that all calcium phosphate granules degrade into calcium and phosphorus ions. β-TCP granules correspond to the most soluble material. HA/β-TCP granules are more soluble than β-TCP granules because they are more porous and they were sintered at lower temperature (1000°C instead of 1150°C). HA granules are the least soluble, followed by HA/TTCP granules. Some calcium phosphates re-precipitate during the dissolution test and were individuated as degradation product through XRD analysis. The reference selected for HA

granules. Calcitite, follows the same degradation pattern of HA granules. Calcitite granules are less soluble than HA granules, this due to the morphological difference in microporosity. As a matter of fact, HA granules are characterized by higher specific surface area. The reference selected for β-TCP granules. Cerasorb, is less soluble probably because of higher sintering production temperature and it results in a more ordered structure; nevertheless, they both follow the same degradation pattern. The ICP results corresponding to phosphorus concentration, confirm the granules weight loss trend after the degradation test. The solubility behavior order in acid solution can be predicted and the trend is: HA<HA/TTCP<β-TCP<HA/β-TCP. as summarized in Fig. 4.108.

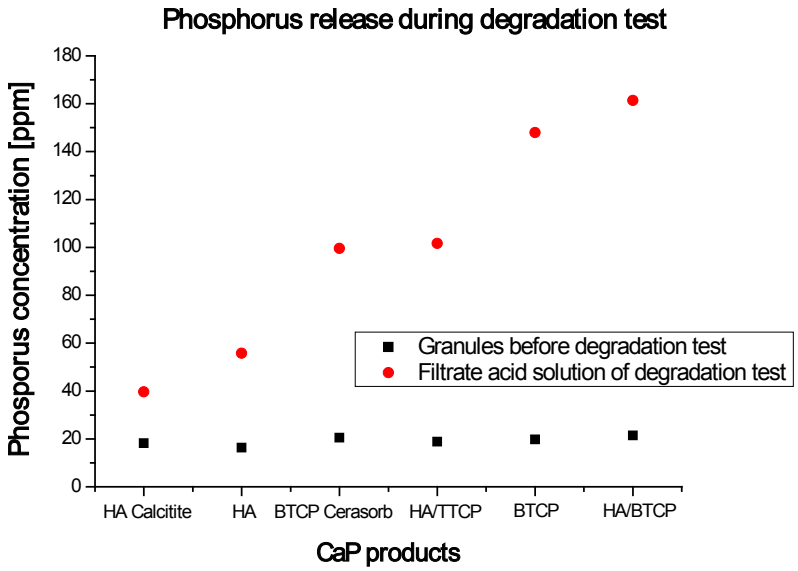

Fig. 4.108 Concentration of phosphorus in the filtered solution after degradation test.

4.8.4 Bioactivity behavior

SEM observations (Fig. 4.109. Fig. 4.110. Fig. 4.111) show that after 7 and 28 days on **HA**. **HA/βTCP** and **βTCP** granules surface there is no clear Ca-P precipitation. After 28 days the HA surface appears more opaque and microporosity is less regular at high magnifications, although this could be due to the immersion in SBF for a long period.

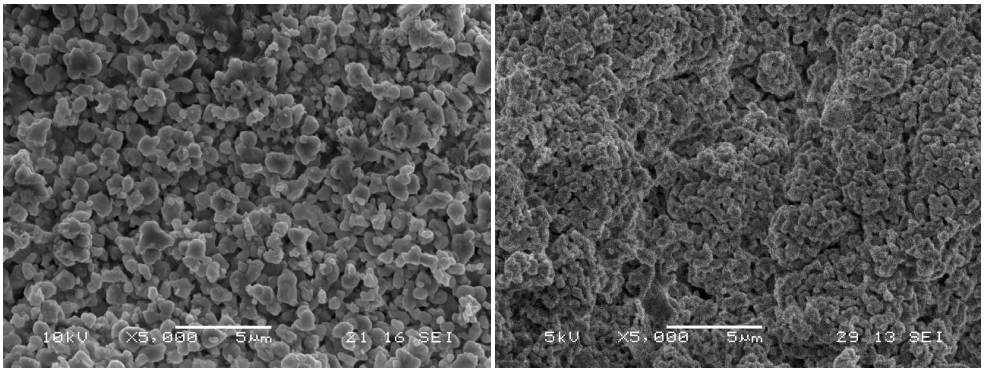

Fig. 4.109 SEM images of HA granules surface after 7 and 28 days in SBF.

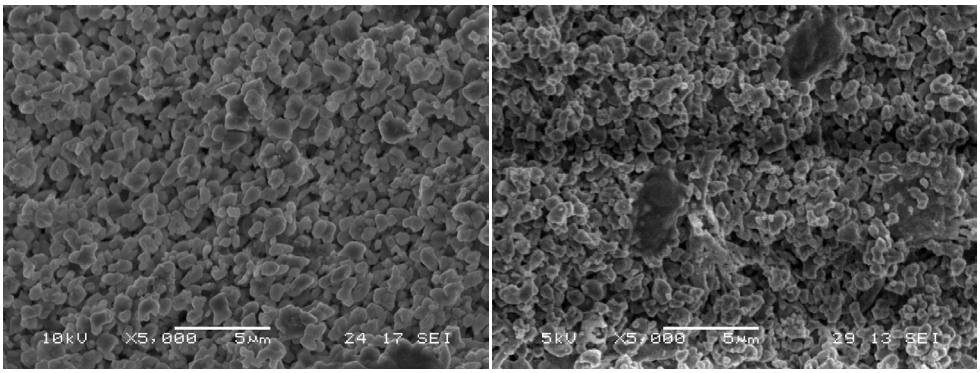

Fig. 4.110 SEM images of HA/βTCP granules surface after 7 and 28 days in SBF.

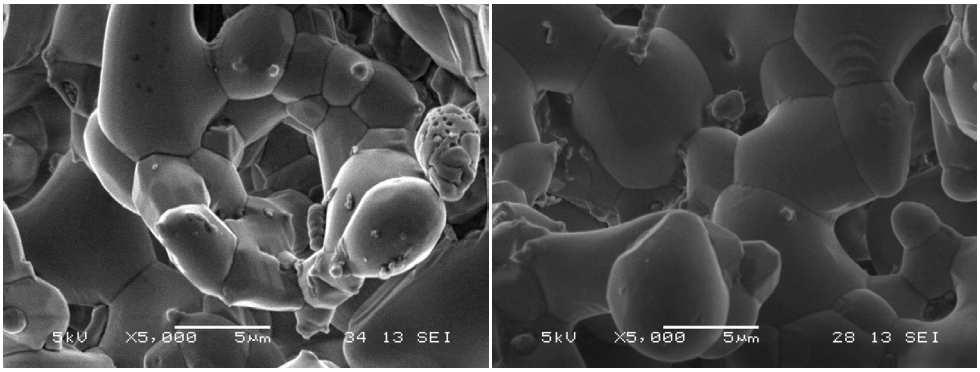

Fig. 4.111 SEM images of βTCP granules surface after 7 and 28 days in SBF.

The **HA/TTCP** granules surface after 7 days in SBF were covered by thin film of apatite in the form of crystals (Fig. 4.112). Calcium precipitation is not uniform on the surface. Apatite layers have a particular and not regular shape and the Ca-P precipitation starts from sites with a sharp curvature.

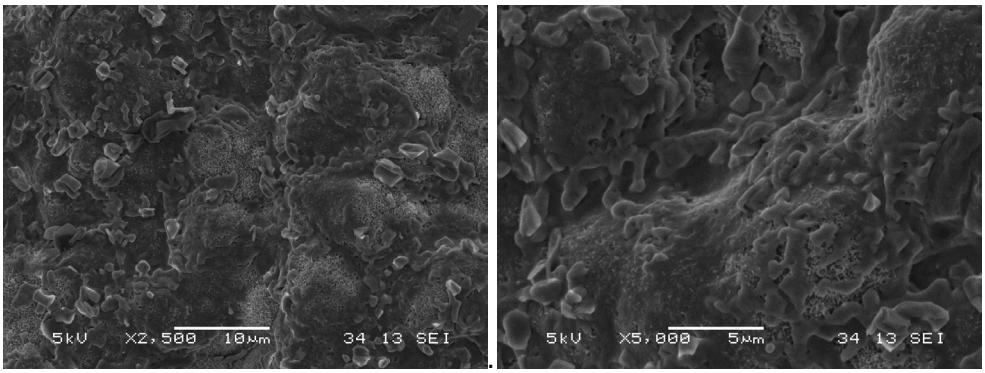

Fig. 4.112 SEM images of HA/TTCP granules surface after 7 days in SBF, particular of CaP layer.

After 28 days of SBF immersion the HA/TTCP surface appears more opaque and the Ca-P layer covers completely all available sites. SEM observations

revealed two different types of layers. One is more regular and has a particular structure developed in crystal strips (Fig. 4.113).

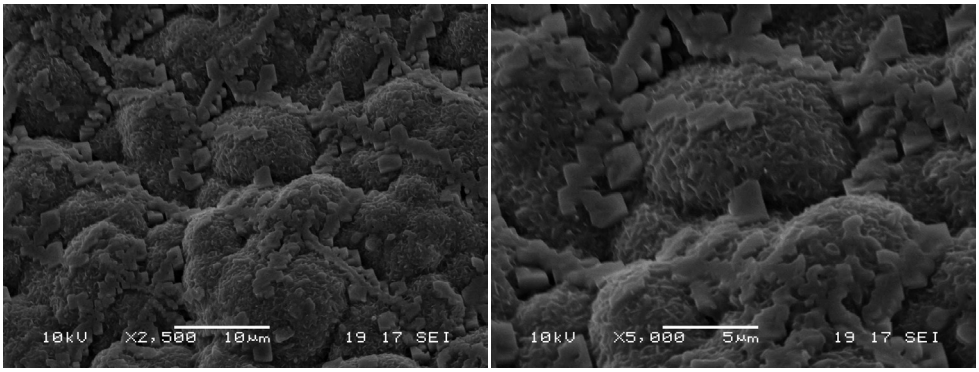

Fig. 4.113 SEM images of HA/TTCP granules surface after 28 days in SBF. particular of CaP precipitate.

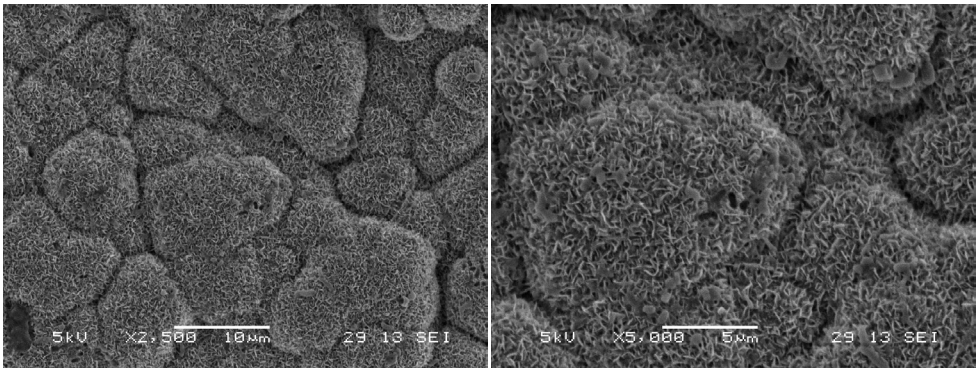

Fig. 4.114 SEM images of HA/TTCP granules surface after 28 days in SBF. particular of needle shape apatite layer.

One precipitate has a needle shape and it seems to be a carbonated apatite layer as reported in previous study performed on HA/TCP material [60] (Fig. 4.114).

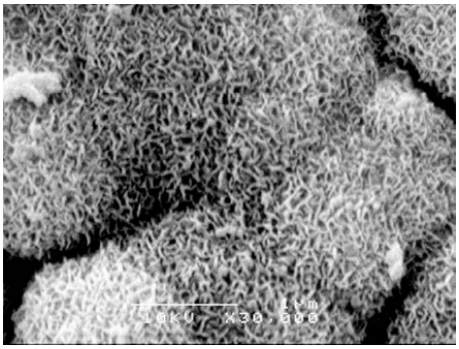

Fig. 4.115 SEM images of Ca-P granules formed after 1 day in SBF [60].

TTCP was found to transform extensively to poorly crystallized carbonated apatite as weel after 2 days of immersion in SBF [157] (Fig. 4.115).

The commercial reference **βTCP (Cerasorb)** cannot be considered a material that stimulates the Ca-P precipitation on its surface in SBF (Fig. 4.116).

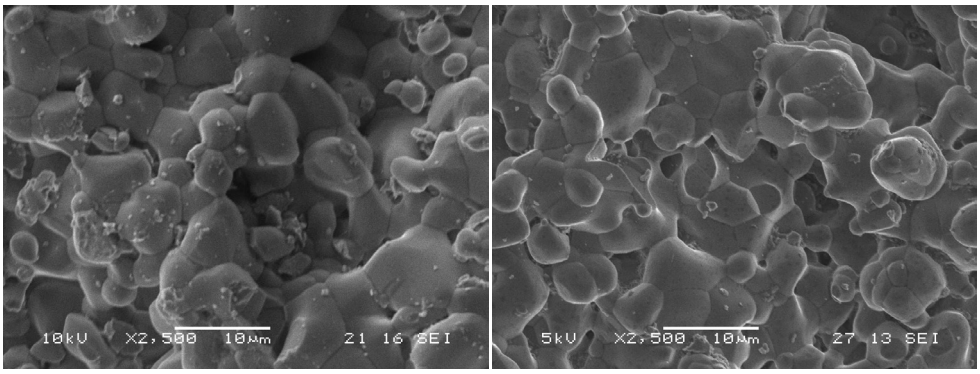

Fig. 4.116 SEM images of βTCP Cerasorb granules after 7 days and 28 days in SBF.

All **doped granules**, on the basis of the experience made with pure granules, were extracted at 7 and 28 days, but were observed by SEM (Fig. 4.117 and

Fig. 4.118) at only 28 days. Some small precipitates are visible on the grain boundaries of Zn-βTCP where Ca and P concentration is higher.

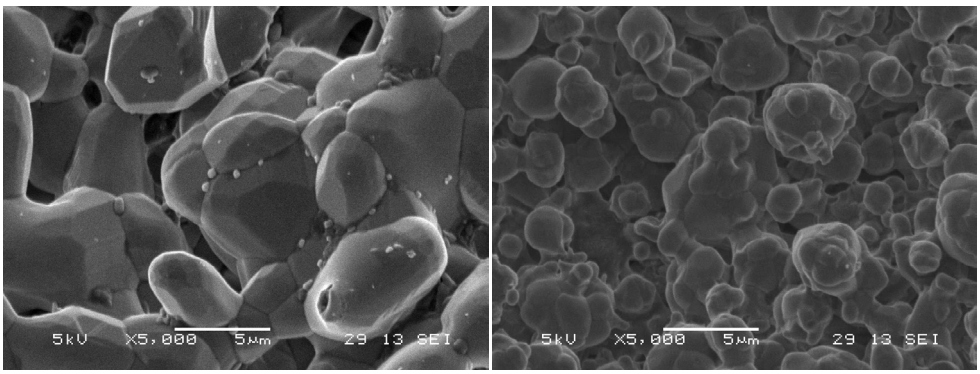

Fig. 4.117 SEM images of Zn βTCP granules and Zn HA-βTCP granules after 28 days in SBF immersion.

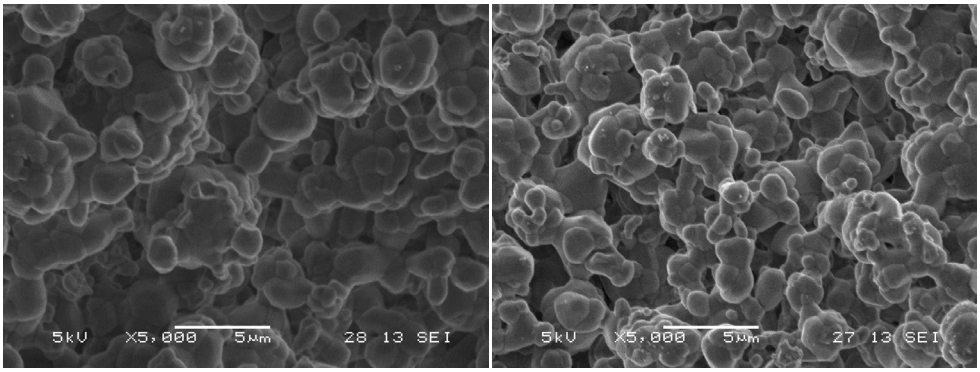

Fig. 4.118 SEM images of Sr HA-βTCP granules and SrZn HA-βTCP granules after 28 days in SBF immersion.

Bioactivity test results point out that on HA and HA/βTCP granules surfaces come CaP layer or precipitate is formed. The Kokubo's SBF solution used was very dilute with respect to other solutions in other similar test and this difference could be the reason for CaP surface not being bioactive. In fact,

another factor that can influence the text is the variability of SBF solution. which increases the risk of obtaining non reproducible results [158]. Both βTCP and control βTCP Cerasorb surface were confirmed to be not bioactive *in vitro*. showing that the presence of particular impurities or different morphologies does not induce any change in the vitro behavior of this material [60].

The only surface that seems bioactive *in vitro* is the HA/TTCP one. The material is able to form two types of precipitate in the SBF solution thus favouring the formation of biological apatite in real bone environment.

4.8.5 Cytotoxicity behavior

Pure granules were shown to be non-cytotoxic from the performed qualitative evaluation (Table 4.48). HA has some deformed cells under specimen probably due to residual CaO on the sample.

Material	Grade of test sample	Y/N
HA	2	No
HA/ βTCP	1	No
HA/TTCP	1	No
βTCP	1	No

Table 4.48 Qualitative evaluation of pure granules.

Doped granules results are only in part cytotoxic (Table 4.49). In fact the material Zn-HA/βTCP shows a reactive zone extending farther than 1 cm beyond the specimen.

Material	Grade of test sample	Cytotoxicity Y/N
Zn- βTCP	1	No
Zn-HA/βTCP	4	Yes
Sr-HA/βTCP	1	No
SrZn-HA/βTCP	1	No

Table 4.49 Qualitative evaluation of doped granules.

Pure materials are confirmed to be no-cytotoxic from quantitative evaluation as well (Table 4.50). The reduction of cell viability is from 14% for HA/βTCP to 28 % for HA.

Material	% of cell viability reduction	Cytotoxicity Y/N
HA	28%	No
HA/βTCP	14 %	No
HA/TTCP	15 %	No
βTCP	17 %	No

Table 4.50 Quantitative evaluation of pure granules.

Quantitative evaluation (Table 4.51) demonstrates that Zn-HA/βTCP is very cytotoxic; in fact cell viability reduction is near 100%. The results can be explained by the fact that some ZnO (0.3%) is present in the material and Zn is less stable in biphasic granules containing HA with respect to pure βTCP; in fact. monophasic Zn-βTCP was shown to be non-cytotoxic although it contains a comparable value of Zn. Moreover. other studies have to be planned to understand better this behavior.

Material	% of cell viability reduction	CytotoxicityY/N
Zn- βTCP	19 %	No
Zn-HA/βTCP	99%	Yes
Sr-HA/βTCP	8 %	No
SrZn-HA/βTCP	25 %	No

Table 4.51 Quantitative evaluation of doped granules.

4.9 *In vivo* experiments

4.9.1 Behavior in bone implantation

After six week from implantation, the bone tissue of all implanted sites were removed and observed macroscopically to exclude presence of local infection. toxicity reaction or other adverse events due to the interaction between CaP implanted materials and the host bone.

For each implanted materials, including the control. no local or systemic effect due to the samples were observed and no abnormalities were observed in all implantation sites.

As shown by Table 4.52, the semi-quantitative analysis performed on the histological blocks points out the absence of any inflammatory or foreign body reaction. or any bone necrosis. In some histological slides, a narrow bands of fibrotic tissue associated with the periosteum of neoformed cortical bone were observed; this phenomenon can be related to the healing process of the injury connected to the surgical procedure.

Therefore, all four types of granules were osteocompatible and safe for orthopaedic and maxillofacial applications. Moreover, as demonstrated also by the histological images and by the μCt analyses, they are also osteoconductive and able to reach fast and high osteointegration with the surrounding bone tissue. Nevertheless, in this kind of implantation design they were put only partially in contact with cortical bone and the main amount of materials were in contact with bone marrow. They were able to induce new bone formation comparable to the commercial control (Table 4.53).

Inflammation	**HA**	**βTCP**	**HA/ βTCP**	**HA/TTCP**	**Control**
Polymorphonuclear	0	0	0	0	0
Lymphocytes	0	0	0	0	0
Plasma Cells	0	0	0	0	0
Macrophages	1	2	1	1	2
Giant cell	1	1	1	1	1
Necrosis	0	0	0	0	0
Sub total	4	6	4	4	6
Neovascularisation	0	0	0	0	0
Fibrosis	1	0	1	1	1
Fatty Infiltrate	0	0	0	0	0
Sub total	1	0	1	1	1
Total	**5**	**6**	**5**	**5**	7

Table 4.52 Histological evaluation: cell/response and general response of CaP granules and control.

Bone tissue changes	**HA**	**βTCP**	**HA/ βTCP**	**HA/TTCP**	**Control**
New bone formation	3	3	4	3	3
Bone resorption	0	0	0	0	0

Table 4.53 Histological evaluation: bone changes of CaP granules and control.

Also, histological images confirm that all the implanted CaP granules are osteoconductive, bioresorbable materials. Each type of granules appears partially resorbed, surrounded by neo-formed cortical bone and in some cases it is possible to also appreciate the presence of the cells families that are normally involved in the remodelling/repairing process of the bone, such as osteoclasts, osteoblasts, giant cells and macrophage.

Fig. 4.119 shows the presence of large rounded deposits of pale granular material (asterisks) associated with neoformed cortical bone (black arrows) in **HA granules**. In the high power field image (Fig. 4.120) infiltration of macrophages (red arrows) adjacent to the granular material is detectable.

Fig. 4.119 Histological images of HA granules.

Fig. 4.120 Particular of histological images of HA granules.

Fig. 4.121 shows the presence of large amounts of reticular/floccular material (asterisks) associated with neoformed cortical bone (arrows) in **βTCP granules**. In the high power field (Fig. 4.122) the particular of the bond between βTCP granule and the trabecular bone.

Fig. 4.121 Histological images of βTCP granules.

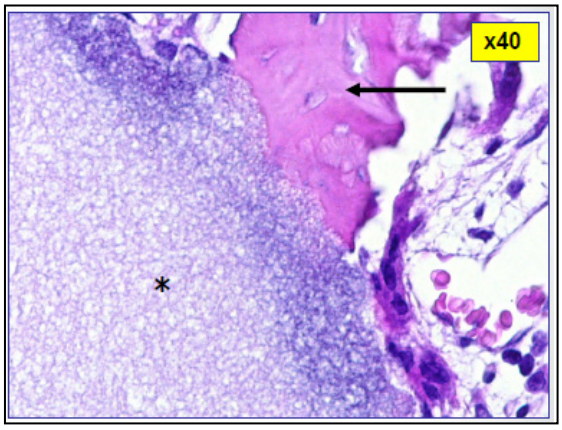

Fig. 4.122 Particular of histological images of βTCP granules.

Fig. 4.123 and Fig. 4.124 illustrate the presence of moderate amount of coarse pale granular material (arrowheads) and floccular reticular material (asterisks) associated with neoformed cortical bone (arrows) in **HA/βTCP granules**.

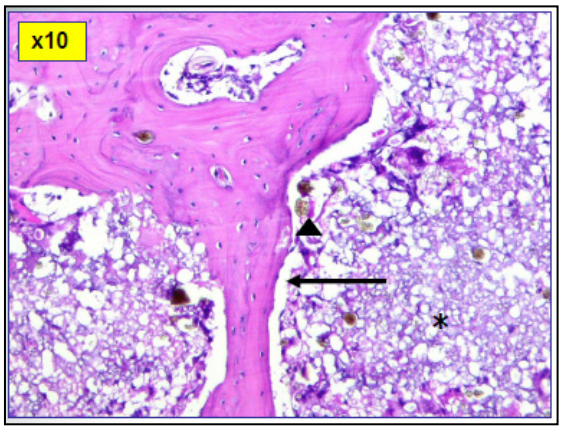

Fig. 4.123 Histological images of HA/βTCP granules.

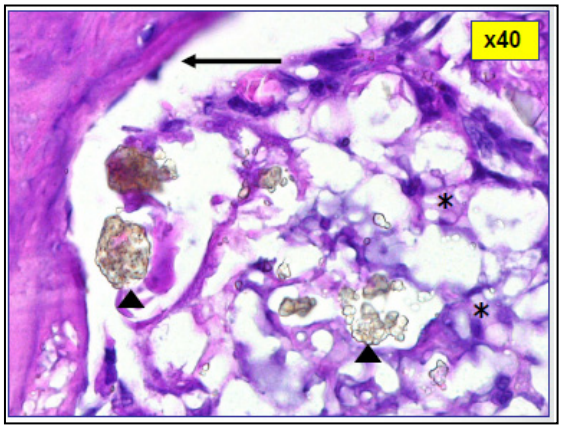

Fig. 4.124 Particular of histological images of HA/βTCP granules.

Fig. 4.125 and (Fig. 4.126) show the presence of a minimal amount (arrow) of pale granular material associated with neoformed cortical bone (asterisks) in **HA/TTCP granules**.

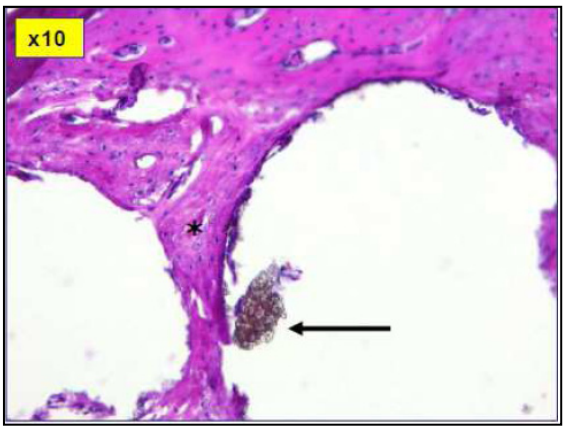

Fig. 4.125 Histological images of HA/TTCP granules.

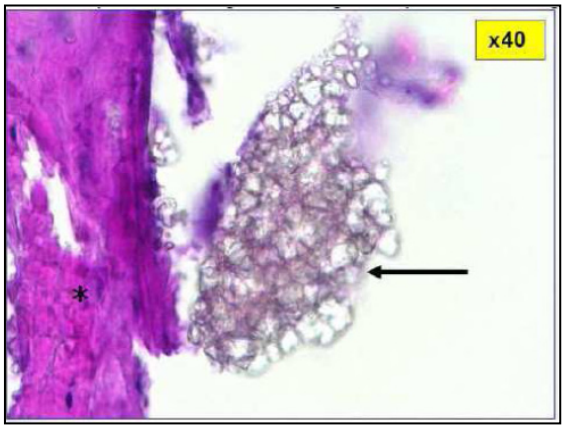

Fig. 4.126 Particular of histological images of HA/TTCP granules.

Fig. 4.127 and Fig. 4.128 show the presence of large amounts of basophilic/amphofilic reticular/floccular material (asterisks) associated with neoformed cortical bone (arrows) in **βTCP control granules**.

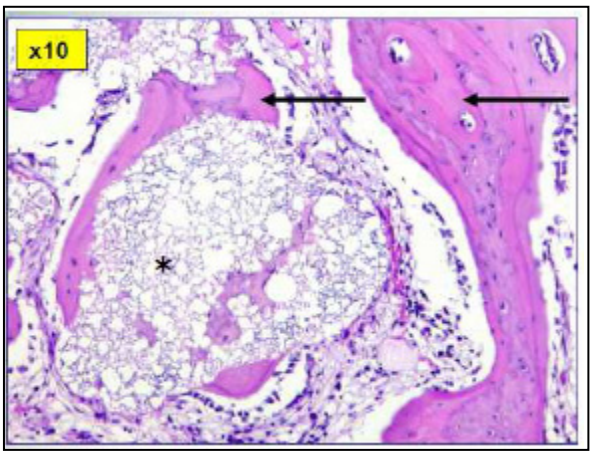

Fig. 4.127 Histological images of control of βTCP control granules.

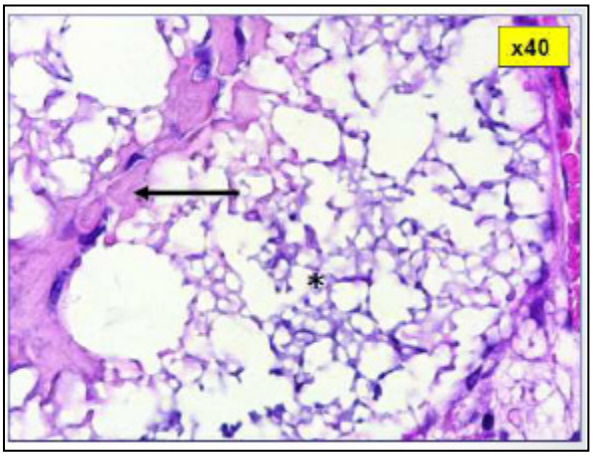

Fig. 4.128 Particular of histological images of control of βTCP control granules.

On the basis of histological findings after the implantation test, it can be concluded that CaP granules are safe and biocompatible and they perform similarly to the commercial reference.

Table 4.54 shows the results calculated in the cylindrical masks. In general, the density (BV/TV) values are all smaller than 26%. Thus, bone and biomaterial volume taken together do not fill half of the mask volume. The reason for this is that the masks were relatively long as compared to the actual filled volume. To identify statistical differences between the groups several samples per group are required. Some qualitative consideration could be done: no high differences between the four families tested were found in BV. but considering the bone volume density (BV/TV). HA/TTCP granules have the lowest value (13%); more new bone seems to form compared to other chemical composition around HA/βTCP granules that appear also partially resorbed after 6 weeks.

Sample	TV [mm^3]	BV [mm^3]	BV/TV [%]	BMV [mm^3]	BMV/TV [%]
HA	18.477	3.882	21.008	3.553	19.229
BTCP	18.476	4.721	25.553	2.332	12.624
HA/BTCP	18.477	3.944	21.344	2.534	13.717
HA/TTCP	18.477	2.489	13.468	4.009	21.699

Table 4.54 Semi-quantitative evaluation of BV/TV and BMV/TV.

The goal of this study was to analyze the amount of total residual biomaterial and the amount of callus bone as with micro-computed tomography (μCT). Table 4.55 shows the results from the residual biomaterial analysis as well as the amount of callus bone in the samples. As the residual mean granule diameter values shows. all the granules types underwent partial resorption and were substituted by a large amount of newly formed bone. The most osteconductive and resorbable material in vivo is HA/βTCP due to dissolution of βTCP phase favored by its high SSA. The most stable is HA/TTCP due to its dense structure. but moreover. it forms more callus (BV) than porous HA.

Sample	Callus BV [mm^3]	Residual BMV [mm^3]	Nominal granules size [μm]	Residual BM. Th [μm]	Material resorption [%]
HA	27.70	7.61	305.00	169.27	45%
BTCP	96.22	10.54	550.56	303.35	45%
HA/BTCP	125.94	5.59	569.49	240.12	58%
HA/TTCP	37.14	7.57	540.97	384.83	29%

Table 4.55 Residual biomaterial and new bone.

Fig. 4.129-Fig. 4.132 show the µCT-3D reconstructions of the retrieved samples: in each of the four analyzed defect, residual granules (in blue) are surrounded and well integrated in a visible and large region of callus bone (in light green). The samples were not delivered as intact samples but were proximally cut. Unfortunately, the portion of the sample delivered did not include all three defects for all samples and thus, the amount of total residual biomaterial and the amount of callus bone has to be considered with care. Furthermore, the results of the defects close to the cut may be affected by the cutting (i.e. debris).

Fig. 4.129 3D reconstruction image of HA granules in analyzed defect.

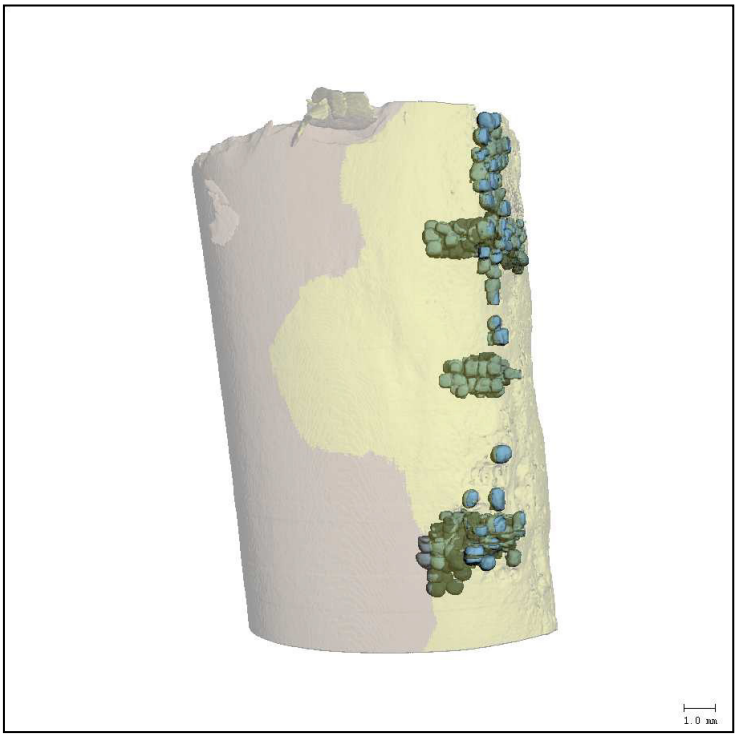

Fig. 4.130 3D reconstruction image of βTCP granules in analyzed defect.

Fig. 4.131 3D reconstruction image of HA/βTCP granules in analyzed defect.

Fig. 4.132 3D reconstruction image of HA/TTCP granules in analyzed defect.

4.9.2 Behavior in sinus lift application

During the sinus lift tests there were no surgical or post-operative complications, indications of infection or abnormal tissue response at the time of retrieval. In both animals grafts healed without any adverse reactions and reconstruction of the post-extraction sites and gingival recessions treated were obtained.

Macroscopic evaluation of the retrieved bone samples revealed bone integration of the grafts both at 14 weeks and at 17 weeks after surgery.

On sections at low magnification, the entire jaw section can be observed. The macroscopic image (Fig. 4.133) shows a homogenous distribution of HA/TTCP granules at **14 weeks.**

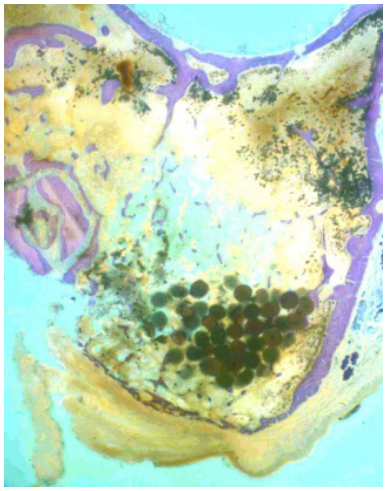

Fig. 4.133 Macroscopic image of HA/TTCP implantation site at 14 weeks

At 14 weeks the surgical access is still present, but is it completely surrounded by neo formed bone. All around the graft it is possible to identify newly formed trabeculae and the granules are in contact only with new bone tissue.

A small amount of HA/TTCP granules is broken into some parts or subjected to re-absorption phenomena (Fig. 4.134). Granule size appears mostly homogenous and the characteristic surface microporosity seems intact, especially in areas in contact with the bone trabeculae. The internal ceramic structure is still dense and compacted and it is not subjected at rapid degradation. Bone bridges join granules together and the percentage of neo-

formed and mineralized bone is greater in the areas where granules are present, comparing with surrounding sites where the vital bone appears to be less dense.

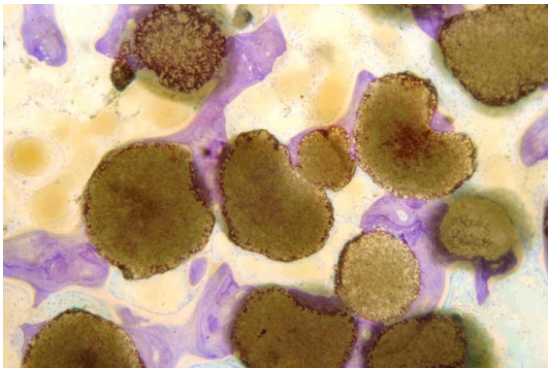

Fig. 4.134 Hystological appearance of trabecular bone ingrowth within HA/TTCP granule, still present and dense after 14 weeks.

The grafted particles showed histologically a large amount of osteoid this means that after 14 weeks bone is still forming (arrows in Fig. 4.135)

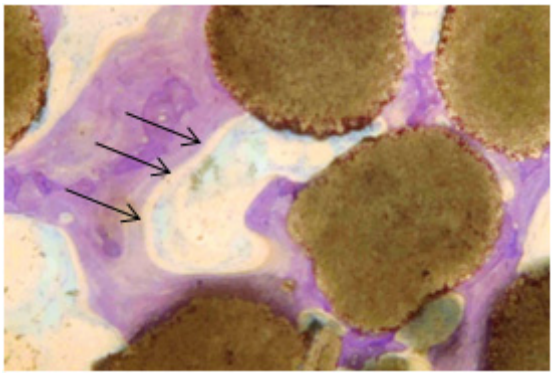

Fig. 4.135 Hystological appearance of trabecular bone ingrowth within HA/TTCP granule, still present and dense with particular (arrows) of osteoide.

Also at **17 weeks** after implantation the granules are well distributed in the lower part of the maxillary bone, in the same position where they were implanted (Fig. 4.136). In this case, the surgery access can no longer be identified because it was completely remodeled and substituted by neo formed bone. Also in this case, new trabeculae are present all around and among the granules.

The density and structures of new bone tissue in both case is comparable to the native bone. All this findings demonstrate that the granules are able to promote and enhance the physiological remodelling/healing process of the bone.

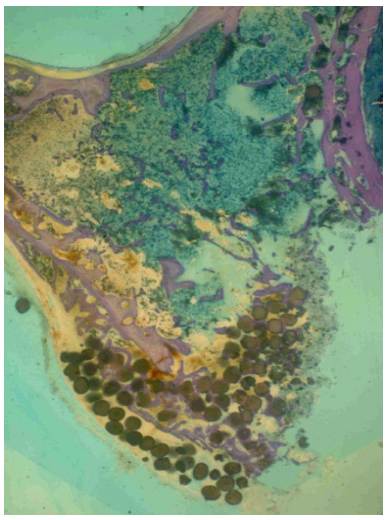

Fig. 4.136 Macroscopic image of HA/TTCP implantation site at 17 weeks.

After 17 weeks HA/TTCP are still present and are dense and homogenous in internal structure (Fig. 4.137). No resorption is detectable by a microscopic evaluation in comparison with previous explantation time. Neo-formed bone

trabeculae are present around CaP granules and seem thicker when compared to the result at 14 weeks.

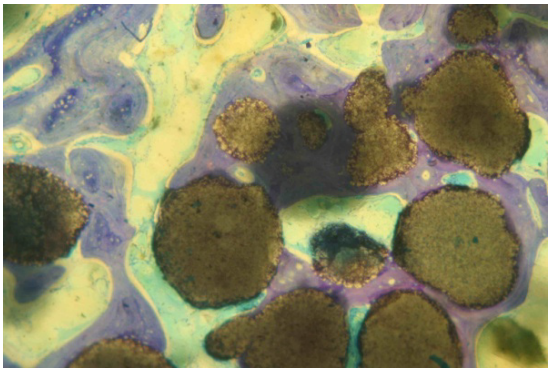

Fig. 4.137 Hystological appearance of trabecular bone ingrowth within HA/TTCP granules after 17 weeks.

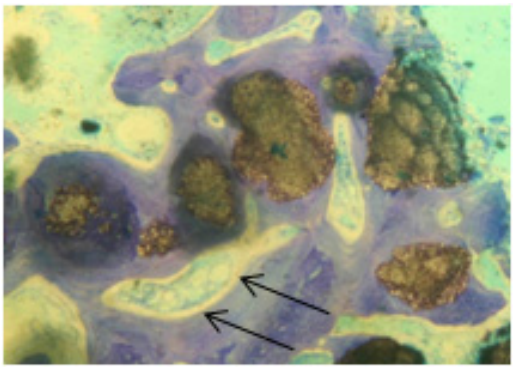

Fig. 4.138 Hystological appearance of trabecular bone ingrowth within HA/TTCP granule, still present and dense with particular (arrows) of osteoide.

The new neo-formed bone trabeculae are more predominantly covered with continuous layers of osteide (arrows in Fig. 4.138), suggesting an intense activity of bone formation. In fact, the thickening of trabeculae and close gaps between neighboring trabeculae are increased respect to previous time.

After 17 weeks the mineralized bone was higher than at 14 weeks but also bone formation rate was still very high.

The surface of the granules showed microscopically a characteristic porosity and shape. Some particles from the implant surface seemed to be exposed to resorption activity and slow disintegration into microscopic particles of about 1-10 μms.

The usual timing for implants placement after sinus graft is generally 24-36 weeks. The obtained bone after 14 and 17 weeks was enough for a stable implant placement so this HA/TTCP material seems to perform well as osteoconductive material and could speed and enhance healing phase.

It is common knowledge that commercially available bone substitutes. if compared to vital bone, have different mechanical properties, lack of cells, different structures and different biological behaviors. A completely resorbable bone substitute should be in theory preferable due to these reasons [159]. The present study showed that at 4 months after surgery, a large amount of the granules were still unresorbed, but the mechanical properties of the grafted bone particles should give the regenerated bone a strong structure.

Explantation time	BV Bone Volume [%]	VB Vital bone [%]	GV Graft Volume [%]	BGV Bone Graft Contact [%]
14 weeks	54,74	17,39	37,35	39
17 weeks	56,93	27,58	29,36	64

Table 4.56 Histomorphometrics values after 14 and 17 weeks.

Table 4.56 illustrates histomorphometric values at 14 and 17 weeks around HA/TTCP granules calculated as average percentage of measured values referred to all implantation zone where the new bone is more formed. The percentage difference of BV between two explantation times is not high and it is 54.74% and 56.93%, at 14 weeks and at 17 weeks. The percentage of VB evolves from 17.39% to 27.58%. The BV is maintained constant, while the graft is slightly resorbed, the percentage changes from 37.35% to 29.36%. BGC passed from 42% at 14 weeks to 64% at 17 weeks.

Biomaterial is partially resorbed and the GV (Graft Volume) decrease between 14 and 17 weeks. The biphasic material HA/TTCP, may be classified as a slowly resorbable synthetic biomaterial as evaluated by the previous bone implantation study on rabbit.

The BGC (bone-graft contact) passed from 39% to 64% after four months; this is a very good result in the primates model. Bone graft contact is the contact area between bone and graft that generally strongly connects the graft to the newly formed bone trabeculae. If the grafted bone has strong mechanical properties, bone-graft connections, associated with slow resorption may help the regenerated tissue to be better at sustaining the implant. On the contrary, if the material has weak structure, the material should disappear during bone formation, because weak granules that connect bone trabeculae, may form a weaker regenerated bone tissue.

In conclusion, even though the number of samples is not enough for good statistics, the preliminary in vivo results showed that HA/TTCP synthetic bone grafts could improve new bone formation, and reduce the time needed for graft healing, achieving high quantity of newly formed bone. Since bone

substitutes are often used for sinus grafts, the need of more studies is evident, especially for some of the characteristics such as the ability to conduct bone, the ability to be resorbed after healing, and the functional behavior when bone is subjected to different load conditions and the behavior of the graft in the case of infection.

5 CONCLUSIONS

The object of this work was the production and the characterization of porous calcium phosphate granules for the repairing of bone. In this study the droplet extrusion method was used for the production of the granules and the production of different types of calcium phosphates was possible. Spherical granules, formed by controlled gelification mechanisms at room temperature, with sizes ranging from 300 to 1200 μm were obtained after sintering. Granules were always characterized by a particular surface roughness and interconnected microporosity. Distinct compositions consisting of pure HA and βTCP or mixtures like HA/βTCP and HA/TTCP, and in some cases doped with Zn and Sr. were obtained. Characterization tests pointed out promising results in term of cytotoxicity thus demonstrating the safety of the production process. *In vitro* solubility tests showed that the dissolution behavior is mainly influenced by morphological and microstructural properties and only to a limited extent by the composition. In addition, preliminary *in vivo* studies showed the biocompatibility of granules when implanted in bones and very good performance of the granules consisting of HA/TTCP.

6 REFERENCES

[1] A. Bandyopadhyay, S. Bernard, W. Xue, and S. Bose, "Calcium Phosphate-Based Resorbable Ceramics: Influence of MgO, ZnO, and SiO2 Dopants," *Journal of the American Ceramic Society*, vol. 89, no. 9, pp. 2675-2688, Aug. 2006.

[2] A. M. C. Barradas, H. Yuan, C. A. V. Blitterswijk, P. Habibovic, and T. Medicine, "Osteoconductive biomaterials: current knowledge of properties," *European Cells and Materials*, vol. 21, pp. 407-429, 2011.

[3] W. I. R. M. Oore, S. T. E. G. Raves, and G. R. I. B. Ain, "Rewiev article: Synthetic bone graft substitutes," *Journal of Surgery*, pp. 354-361, 2001.

[4] P. C. Salgado, "Bone Remodeling, Biomaterials And Technological Applications: Revisiting Basic Concepts," *Journal of Biomaterials and Nanobiotechnology*, vol. 2, no. 3, pp. 318-328, 2011.

[5] M. Perez-Sanchez, E. Ramirez-Glindon, M. Lledo-Gil, J. Calvo-Guirado, and C. Perez-Sanchez, "Biomaterials for bone regeneration," *Medicina Oral Patología Oral y Cirugia Bucal*, vol. 15, no. 3, p. e517-e522, 2010.

[6] P. V. Giannoudis, H. Dinopoulos, and E. Tsiridis, "Bone substitutes: an update," *Injury*, vol. 36 Suppl 3, pp. S20-7, Nov. 2005.

[7] K. A. Hing, "Bioceramic Bone Graft Substitutes: Influence of Porosity and Chemistry," *International Journal*, vol. 199, pp. 184-199, 2005.

[8] R. Z. Legeros, "Calcium Phosphate-Based Osteoinductive Materials," *Chemical rewiev*, pp. 4742-4753, 2008.

REFERENCES

[9] D. . Metseger, R. Rieger, M, and D. W. Foreman, "Mechanical properties of sintered hydroxyapatite and tricalcium phosphate ceramic," *Journal of materials science. Materials in medicine*, vol. 10, pp. 9-17, 1999.

[10] S. V. Dorozhkin, "Medical Application of Calcium Orthophosphate Bioceramics," *Bio*, pp. 1-51, 2011.

[11] S. Kannan, F. Goetz-Neunhoeffer, J. Neubauer, and J. M. F. Ferreira, "Ionic Substitutions in Biphasic Hydroxyapatite and β-Tricalcium Phosphate Mixtures: Structural Analysis by Rietveld Refinement," *Journal of the American Ceramic Society*, vol. 91, no. 1, pp. 1-12, Dec. 2007.

[12] Y. Pan, "Preparation of β-TCP with high thermal stability by solid reaction route," *Journal of Materials Science:*, vol. 38, pp. 1049-1056, 2003.

[13] C. Moseke and U. Gbureck, "Tetracalcium phosphate: Synthesis, properties and biomedical applications.," *Acta biomaterialia*, vol. 6, no. 10, pp. 3815-23, Oct. 2010.

[14] U. Posset, E. Löcklin, R. Thull, and W. Kiefer, "Vibrational spectroscopic study of tetracalcium phosphate in pure polycrystalline form and as a constituent of a self-setting bone cement.," *Journal of biomedical materials research*, vol. 40, no. 4, pp. 640-5, Jun. 1998.

[15] J. M. Ruan, J. P. Zou, J. N. Zhou, and J. Z. Hu, "Porous hydroxyapatite–tricalcium phosphate bioceramics," *Powder Metallurgy*, vol. 49, no. 1, pp. 66-69, Mar. 2006.

[16] G. Daculsi, O. Laboux, O. Malard, and P. Weiss, "Current state of the art of biphasic calcium phosphate bioceramics," *Journal of materials science. Materials in medicine*, vol. 14, no. 3, pp. 195-200, Mar. 2003.

[17] Y.-min Kong, H.-ee Kim, and H.-won Kim, "Phase Conversion of Tricalcium Phosphate Into Ca-Deficient Apatite During Sintering of

Hydroxyapatite – Tricalcium Phosphate Biphasic Ceramics," *Journal of Biomedical Materials Research*, pp. 334-339, 2007.

[18] O. Gauthier, J. M. Bouler, E. Aguado, R. Z. Legeros, P. Pilet, and G. Daculsi, "Elaboration conditions influence physicochemical properties and in vivo bioactivity of macroporous biphasic calcium phosphate ceramics," *Journal of materials science. Materials in medicine*, vol. 10, no. 4, pp. 199-204, Apr. 1999.

[19] Z. Z. Zyman, M. V. Tkachenko, and D. V. Polevodin, "Preparation and characterization of biphasic calcium phosphate ceramics of desired composition.," *Journal of materials science. Materials in medicine*, vol. 19, no. 8, pp. 2819-25, Aug. 2008.

[20] E. Goyenvalle, E. Aguado, P. Pilet, and G. Daculsi, "Biofunctionality of MBCP ceramic granules (TricOs) plus fibrin sealant (Tisseel) versus MBCP ceramic granules as a filler of large periprosthetic bone defects: an investigative ovine study," *Journal of materials science. Materials in medicine*, vol. 21, no. 6, pp. 1949-58, Jun. 2010.

[21] S. V. Dorozhkin, "Biphasic, triphasic and multiphasic calcium orthophosphates," *Acta biomaterialia*, vol. 8, no. 3, pp. 963-77, Mar. 2012.

[22] S. V. Dorozhkin, "Functional Biomaterials Calcium Orthophosphates as Bioceramics : State of the Art," *Review Literature And Arts Of The Americas*, pp. 22-107, 2010.

[23] C. C. Barrias, C. C. Ribeiro, and M. a. Barbosa, "Adhesion and Proliferation of Human Osteoblastic Cells Seeded on Injectable Hydroxyapatite Microspheres," *Key Engineering Materials*, vol. 254-256, pp. 877-880, 2004.

[24] A. Yovana et al., "Comparative study of nanohydroxyapatite microspheres for medical applications," *Journal of Biomedical Materials Research Part A*, 2007.

REFERENCES

[25] S. Qu, H. Fan, J. Chen, and J. Feng, "Effect of the crystallinity of calcium phosphate ceramics on osteoblast proliferation in vitro," pp. 331-332, 2001.

[26] S. Teixeira, M. P. Ferraz, and F. J. Monteiro, "Biocompatibility of highly macroporous ceramic scaffolds: cell adhesion and morphology studies," *Journal of Materials Science: Materials in Medicine*, vol. 19, no. 2, pp. 855-859, Aug. 2007.

[27] L. Chou, B. Marek, and W. R. Wagner, "Effects of hydroxylapatite coating crystallinity on biosolubility , cell attachment efficiency and proliferation in vitro," *Cell*, vol. 20, pp. 977-985, 1999.

[28] H. Yoshikawa, N. Tamai, T. Murase, and A. Myoui, "Interconnected porous hydroxyapatite ceramics for bone tissue engineering," *In Vivo*, no. 2008, 2009.

[29] Y.-jae Jo et al., "Various bone graft substitutes," *Journal of Periodontal & Implant Science*, pp. 67-72, 2011.

[30] O. L. Kubarev et al., "Bioceramic Granules with Controlled Resorbability for Bone Tissue Therapy," *Text*, vol. 409, no. 1, pp. 124-127, 2006.

[31] E. Kauschke, E. Rumpel, T. Bayerlein, T. Gedrange, and P. Proff, "The in vitro viability and growth of fibroblasts cultured in the presence of different bone grafting materials (NanoBone ® and Straumann Bone Ceramic ®)," *differences*, vol. 65, no. 1, pp. 37-42, 2006.

[32] V. I. Chissov et al., "In Vitro Study of Matrix Surface Properties of Porous Granulated Calcium Phosphate Ceramic Materials Made in Russia," *Experimental Biology*, vol. 145, no. 4, pp. 499-503, 2008.

[33] E. Landi, G. Logroscino, L. Proietti, A. Tampieri, M. Sandri, and S. Sprio, "Biomimetic Mg-substituted hydroxyapatite: from synthesis to in vivo behaviour.," *Journal of materials science. Materials in medicine*, vol. 19, no. 1, pp. 239-47, Jan. 2008.

REFERENCES

[34] N. Patel et al., "A comparative study on the in vivo behavior of hydroxyapatite and silicon substituted hydroxyapatite granules.," *Journal of materials science. Materials in medicine*, vol. 13, no. 12, pp. 1199-206, Dec. 2002.

[35] G. Daculsi, P. Corre, O. Malard, R. Legeros, and E. Goyenvalle, "Performance for bone ingrowth of Biphasic calcium phosphate ceramic versus Bovine bone substitute," *New York*, pp. 3-6.

[36] N. Ikeda, K. Kawanabe, and T. Nakamura, "Quantitative comparison of osteoconduction of porous , dense A-W glass-ceramic and hydroxyapatite granules (effects of granule and pore sizes)," *Biomaterials*, vol. 20, pp. 1087-1095, 1999.

[37] L. Galois and D. Mainard, "Bone ingrowth into two porous ceramics with different pore sizes: an experimental study," *Acta orthopaedica Belgica*, vol. 70, no. 6, pp. 598-603, Dec. 2004.

[38] H. Oonishi et al., "Comparative bone growth behavior in granules of bioceramic materials of various sizes," *Journal of biomedical materials research*, vol. 44, no. 1, pp. 31-43, Jan. 1999.

[39] O. Malard, J. M. Bouler, D. Heymann, and P. Pilet, "Influence of biphasic calcium phosphate granulometry on bone ingrowth , ceramic resorption , and inflammatory reactions Preliminary in vitro and in vivo study," 1998.

[40] O. Gauthier, J. M. Bouler, E. Aguado, P. Pilet, and G. Daculsi, "Macroporous biphasic calcium phosphate ceramics: influence of macropore diameter and macroporosity percentage on bone ingrowth.," *Biomaterials*, vol. 19, no. 1-3. pp. 133-9.

[41] N. Matsushita et al., "Accelerated repair of a bone defect with a synthetic biodegradable bone-inducing implant.," *Journal of orthopaedic science : official journal of the Japanese Orthopaedic Association*, vol. 11, no. 5, pp. 505-11, Oct. 2006.

REFERENCES

[42] J. J. C. Arts, L. H. B. Walschot, N. Verdonschot, B. W. Schreurs, and P. Buma, "Biological Activity of Tri-Calciumphosphate / Hydroxyl-Apatite Granules Mixed With Impacted Morsellized Bone Graft . A Study in Rabbits," *Direct*, pp. 24-27, 2006.

[43] Z. Zyman, V. Glushko, N. Dedukh, S. Malyshkina, and N. Ashukina, "Porous calcium phosphate ceramic granules and their behaviour in differently loaded areas of skeleton.," *Journal of materials science. Materials in medicine*, vol. 19, no. 5, pp. 2197-205, May 2008.

[44] F. Schwarz et al., "Guided bone regeneration at dehiscence-type defects using biphasic hydroxyapatite + beta tricalcium phosphate (Bone Ceramic) or a collagen-coated natural bone mineral (BioOss Collagen): an immunohistochemical study in dogs.," *International journal of oral and maxillofacial surgery*, vol. 36, no. 12, pp. 1198-206, Dec. 2007.

[45] H. a Merten, J. Wiltfang, U. Grohmann, and J. F. Hoenig, "Intraindividual comparative animal study of alpha- and beta-tricalcium phosphate degradation in conjunction with simultaneous insertion of dental implants.," *The Journal of craniofacial surgery*, vol. 12, no. 1, pp. 59-68, Jan. 2001.

[46] B. Flautre, M. Descamps, C. Delecourt, M. C. Blary, and P. Hardouin, "Porous HA ceramic for bone replacement: role of the pores and interconnections - experimental study in the rabbit.," *Journal of materials science. Materials in medicine*, vol. 12, no. 8, pp. 679-82, Aug. 2001.

[47] O. F. Materials, "Granules of osteoapatite and glass-reinforced hydroxyapatite implanted in rabbit tibiae," vol. 7, pp. 10-13, 1996.

[48] H. Yuan, H. Fernandes, P. Habibovic, J. D. Boer, A. M. C. Barradas, and A. D. Ruiter, "Osteoinductive ceramics as a synthetic alternative to autologous bone grafting," *Image (Rochester, N.Y.)*, vol. 107, no. 31, pp. 10-15, 2010.

REFERENCES

[49] I. R. D. Lima et al., "Understanding the impact of divalent cation substitution on hydroxyapatite: An in vitro multiparametric study on biocompatibility," *Methods*, pp. 351-358, 2011.

[50] V. S. Komlev and S. M. Barinov, "Porous hydroxyapatite ceramics of bi-modal pore size distribution," *Jouranl of Meterials Science: Materials in Medicine*, vol. 3, pp. 295-299, 2002.

[51] M. T. Fulmer, I. C. Ison, C. R. Hankermayer, B. R. Constantz, and J. Ross, "Measurements of the solubilities and dissolution rates of several hydroxyapatites," *Biomaterials*, vol. 23, pp. 751-755, 2002.

[52] R. Drevet, F. Velard, J. Faure, S. Potiron, and H. Benhayoune, "In vitro dissolution behaviour of calcium phosphate coatings on Ti6Al4V substrate elaborated by pulsed electrodeposition current," vol. 50, no. 2003, p. 4748, 2005.

[53] H. Search, C. Journals, A. Contact, M. Iopscience, and I. P. Address, "Porous spherical hydroxyapatite and fluorhydroxyapatite granules processing and characterization," *Science and Technology of Advanced Materials*, vol. 503, 2003.

[54] T. Kokubo and H. Takadama, "How useful is SBF in predicting in vivo bone bioactivity?," *Biomaterials*, vol. 27, no. 15, pp. 2907-15, May 2006.

[55] C. Wu, "Bone and Tissue Regeneration Insights evaluation of the In Vitro Bioactivity of Bioceramics," *In Vitro*, pp. 25-29.

[56] M. M. Monteiro, N. C. Campos da Rocha, A. M. Rossi, and G. de Almeida Soares, "Dissolution properties of calcium phosphate granules with different compositions in simulated body fluid.," *Journal of biomedical materials research. Part A*, vol. 65, no. 2, pp. 299-305, May 2003.

[57] Y. Duan, Z. . Zhnag, and C. . Wang, "Apatite formation on HA-TCP ceramics in dynamic simulated body fluid," *Key Engineering Materials*, vol. 254-256, pp. 131-254, 2004.

REFERENCES

[58] J. S. Cho, C.-P. Chung, and S.-H. Rhee, "Bioactivity and Osteoconductivity of Biphasic Calcium Phosphates," *Bioceramics Development and Applications*, vol. 1, pp. 1-3, 2010.

[59] R. Rohanizadeh, M. Padrines, J. M. Bouler, D. Couchourel, Y. Fortun, and G. Daculsi, "Apatite precipitation after incubation of biphasic calcium-phosphate ceramic in various solutions: influence of seed species and proteins.," *Journal of biomedical materials research*, vol. 42, no. 4, pp. 530-9, Dec. 1998.

[60] R. Xin, Y. Leng, J. Chen, and Q. Zhang, "A comparative study of calcium phosphate formation on bioceramics in vitro and in vivo," *Biomaterials*, vol. 26, no. 33, pp. 6477-86, Nov. 2005.

[61] L. Wang and G. H. Nancollas, "Calcium orthophosphates: crystallization and dissolution.," *Chemical reviews*, vol. 108, no. 11, pp. 4628-69, Nov. 2008.

[62] E. Boanini, M. Gazzano, and a Bigi, "Ionic substitutions in calcium phosphates synthesized at low temperature.," *Acta biomaterialia*, vol. 6, no. 6, pp. 1882-94, Jun. 2010.

[63] W. I. Abdel-fattah, M. S. Talaat, and A. Adawy, "Comparative Study of Sr + 2 and Zn + 2 Incorporation in the Biomimetic Coating of a Prosthetic Alloy," *Biomaterials*, pp. 4-13, 2011.

[64] L. Yang, S. Perez-Amodio, F. Y. F. Barrère-de Groot, V. Everts, C. a van Blitterswijk, and P. Habibovic, "The effects of inorganic additives to calcium phosphate on in vitro behavior of osteoblasts and osteoclasts.," *Biomaterials*, vol. 31, no. 11, pp. 2976-89, Apr. 2010.

[65] D. Norhidayu, I. Sopyan, S. Ramesh, and U. T. Nasional, "Development of Zinc Doped Hydroxyapatite for Bone Implant Applications," *In Vitro*, no. 24, pp. 257-270.

REFERENCES

[66] A. Bigi, E. Foresti, M. Gandolfi, and M. Gazzano, "Inhibiting effect of zinc on hydroxylapatite crystallization," *Journal of inorganic*, 1995.

[67] F. Ren, R. Xin, X. Ge, and Y. Leng, "Characterization and structural analysis of zinc-substituted hydroxyapatites.," *Acta biomaterialia*, vol. 5, no. 8, pp. 3141-9, Oct. 2009.

[68] F. Miyaji, Y. Kono, and Y. Suyama, "Formation and structure of zinc-substituted calcium hydroxyapatite," *Materials Research Bulletin*, vol. 40, no. 2, pp. 209-220, Feb. 2005.

[69] E. Jallot et al., "STEM and EDXS characterisation of physico-chemical reactions at the periphery of sol-gel derived Zn-substituted hydroxyapatites during interactions with biological fluids.," *Colloids and surfaces. B, Biointerfaces*, vol. 42, no. 3-4, pp. 205-10, May 2005.

[70] X. Li et al., "The optimum zinc content in set calcium phosphate cement for promoting bone formation in vivo.," *Materials science & engineering. C, Materials for biological applications*, vol. 29, no. 3, pp. 969-975, Apr. 2009.

[71] Y. Sogo, a. Ito, K. Fukasawa, T. Sakurai, and N. Ichinose, "Zinc containing hydroxyapatite ceramics to promote osteoblastic cell activity," *Materials Science and Technology*, vol. 20, no. 9, pp. 1079-1083, Sep. 2004.

[72] A. Bandyopadhyay, E. a. Withey, J. Moore, and S. Bose, "Influence of ZnO doping in calcium phosphate ceramics," *Materials Science and Engineering: C*, vol. 27, no. 1, pp. 14-17, Jan. 2007.

[73] a. Cuneyt Tas, S. B. Bhaduri, and S. Jalota, "Preparation of Zn-doped β-tricalcium phosphate (β-Ca3(PO4)2) bioceramics," *Materials Science and Engineering: C*, vol. 27, no. 3, pp. 394-401, Apr. 2007.

[74] A. Ito et al., "Zinc-releasing calcium phosphate for stimulating bone formation," *Materials Science and Engineering: C*, vol. 22, no. 1, pp. 21-25, Oct. 2002.

[75] Z. Li, L. Yubao, Z. Yi, W. Lan, and J. a Jansen, "In vitro and in vivo evaluation on the bioactivity of ZnO containing nano-hydroxyapatite/chitosan cement.," *Journal of biomedical materials research. Part A*, vol. 93, no. 1, pp. 269-79, Apr. 2010.

[76] V. Stanić et al., "Synthesis, characterization and antimicrobial activity of copper and zinc-doped hydroxyapatite nanopowders," *Applied Surface Science*, vol. 256, no. 20, pp. 6083-6089, Aug. 2010.

[77] S. G. Dahl et al., "Incorporation and distribution of strontium in bone.," *Bone*, vol. 28, no. 4, pp. 446-53, Apr. 2001.

[78] P. J. Marie, "Strontium ranelate: a novel mode of action optimizing bone formation and resorption.," *Osteoporosis international a journal established as result of cooperation between the European Foundation for Osteoporosis and the National Osteoporosis Foundation of the USA*, vol. 16 Suppl 1, pp. S7-10, Jan. 2005.

[79] A. Bigi, E. Boanini, C. Capuccini, and M. Gazzano, "Strontium-substituted hydroxyapatite nanocrystals," *Inorganica Chimica Acta*, vol. 360, no. 3, pp. 1009-1016, Feb. 2007.

[80] H. B. Pan et al., "Solubility of strontium-substituted apatite by solid titration.," *Acta biomaterialia*, vol. 5, no. 5, pp. 1678-85, Jun. 2009.

[81] E. Landi, A. Tampieri, G. Celotti, S. Sprio, M. Sandri, and G. Logroscino, "Sr-substituted hydroxyapatites for osteoporotic bone replacement.," *Acta biomaterialia*, vol. 3, no. 6, pp. 961-9, Nov. 2007.

[82] B. Bracci, P. Torricelli, S. Panzavolta, E. Boanini, R. Giardino, and a Bigi, "Effect of Mg(2+), Sr(2+), and Mn(2+) on the chemico-physical and in vitro biological properties of calcium phosphate biomimetic coatings.,"

Journal of inorganic biochemistry, vol. 103, no. 12, pp. 1666-74, Dec. 2009.

[83] W. Xue, J. Moore, and H. Hosick, "Osteoprecursor cell response to strontium-containing hydroxyapatite ceramics," *Research Part A*, 2006.

[84] C. Capuccini, P. Torricelli, E. Boanini, M. Gazzano, R. Giardino, and a Bigi, "Interaction of Sr-doped hydroxyapatite nanocrystals with osteoclast and osteoblast-like cells.," *Journal of biomedical materials research. Part A*, vol. 89, no. 3, pp. 594-600, Jun. 2009.

[85] S. C. Verberckmoes, M. E. De Broe, and P. C. D'Haese, "Dose-dependent effects of strontium on osteoblast function and mineralization.," *Kidney international*, vol. 64, no. 2, pp. 534-43, Aug. 2003.

[86] J. Christoffersen, M. R. Christoffersen, N. Kolthoff, and O. Bärenholdt, "Effects of strontium ions on growth and dissolution of hydroxyapatite and on bone mineral detection.," *Bone*, vol. 20, no. 1, pp. 47-54, Jan. 1997.

[87] H. H. K. Xu, M. D. Weir, E. F. Burguera, and A. M. Fraser, "Injectable and macroporous calcium phosphate cement scaffold," *Biomaterials*, vol. 27, no. 24, pp. 4279-87, Aug. 2006.

[88] M. Fabbri, G. C. Celotti, and A. Ravaglioli, "Granulates based on calcium phosphate with controlled morphology and porosity for medical applications: physico-chemical parameters and production technique," *Biomaterials*, vol. 15, no. 6, pp. 474-7, May 1994.

[89] W. Paul and C. P. Sharma, "Development of porous spherical hydroxyapatite granules: application towards protein delivery," *Journal of materials science. Materials in medicine*, vol. 10, no. 7, pp. 383-8, Jul. 1999.

[90] S. P. Victor and T. S. S. Kumar, "BCP ceramic microspheres as drug delivery carriers: synthesis, characterisation and doxycycline release,"

Journal of materials science. Materials in medicine, vol. 19, no. 1, pp. 283-90, Jan. 2008.

[91] D. Bilk and M. Germany, "Cerasorb M in dental surgery," *Bone*, pp. 40-46, 2002.

[92] H. P. Jr, L. Chyplyk, and J. Lederer, "Unique Bone Substitution of TCP-Granulates (Cerasorb ®) during Degradation in Human Sinus Floor Elevations," *European Cells and Materials*, vol. 14, no. 24, p. 2262, 2007.

[93] C. Mangano, A. Scarano, V. Perrotti, G. Iezzi, and A. Piattelli, "Maxillary sinus augmentation with a porous synthetic hydroxyapatite and bovine-derived hydroxyapatite: a comparative clinical and histological study," *The International Journal of Oral and Maxillofacial Implants*, pp. 980-986, 2007.

[94] U. Schulze-späte et al., "Sinus Augmentation Procedure Using Beta-Tricalcium-Phosphate : Histological Analysis of Grafted Bone at Time of Implant Placement."

[95] A. Scarano et al., "Maxillary sinus augmentation with different biomaterials: a comparative histologic and histomorphometric study in man," *Implant dentistry*, vol. 15, no. 2, pp. 197-207, Jun. 2006.

[96] A. Rebaudi, A. A. Maltono, M. Pretto, and S. Benedicenti, "Sinus grafting with magnesium-enriched bioceramic granules and autogenous bone: a microcomputed tomographic evaluation of 11 patients.," *The International journal of periodontics & restorative dentistry*, vol. 30, no. 1, pp. 53-61, Feb. 2010.

[97] Z. Zyman, V. Glushko, V. Filippenko, V. Radchenko, and V. Mezentsev, "Nonstoichiometric hydroxyapatite granules for orthopaedic applications," *Journal of materials science. Materials in medicine*, vol. 15, no. 5, pp. 551-8, May 2004.

REFERENCES

[98] H.-H. Horch, R. Sader, C. Pautke, a Neff, H. Deppe, and a Kolk, "Synthetic, pure-phase beta-tricalcium phosphate ceramic granules (Cerasorb) for bone regeneration in the reconstructive surgery of the jaws.," *International journal of oral and maxillofacial surgery*, vol. 35, no. 8, pp. 708-13, Aug. 2006.

[99] P. Trisi, W. Rao, A. Rebaudi, and P. Fiore, "Histologic effect of pure-phase beta-tricalcium phosphate on bone regeneration in human artificial jawbone defects," *The International journal of periodontics & restorative dentistry*, vol. 23, no. 1. pp. 69-77, Feb-2003.

[100] H. Oonishi, Y. Kadoya, H. Iwaki, and N. Kin, "Hydroxyapatite granules interposed at bone-cement interface in total hip replacements: histological study of retrieved specimens," *Journal of biomedical materials research*, vol. 53, no. 2, pp. 174-80, Jan. 2000.

[101] K. V. Menon and H. K. Varma, "Radiological outcome of tibial plateau fractures treated with percutaneously introduced synthetic porous Hydroxyapatite granules," *European Journal of Orthopaedic Surgery & Traumatology*, vol. 15, no. 3, pp. 205-213, May 2005.

[102] P. Hinz, E. Wolf, G. Schwesinger, E. Hartelt, and A. Ekkernkamp, "A new resorbable bone void filler in trauma: Early clinical experience and h ...," *Health (San Francisco)*, no. May, 2002.

[103] A. O. Ransford et al., "Synthetic porous ceramic compared with autograft in scoliosis surgery," *The Journal of Bone and Joint Surgery*, pp. 13-18.

[104] M. Bohner, "Physical and chemical aspects of calcium phosphates used in spinal surgery.," *European spine journal: official publication of the European Spine Society, the European Spinal Deformity Society, and the European Section of the Cervical Spine Research Society*, vol. 10 Suppl 2, pp. S114-21, Oct. 2001.

REFERENCES

[105] M. Maruyama and M. Ito, "In vitro properties of a chitosan-bonded self-hardening paste with hydroxyapatite granules," *Journal of biomedical materials research*, vol. 32, no. 4, pp. 527-32, Dec. 1996.

[106] A. C. C. da Cruz, M. T. Pochapski, J. B. Daher, J. C. Z. da Silva, G. L. Pilatti, and F. A. Santos, "Physico-chemical characterization and biocompatibility evaluation of hydroxyapatites.," *Journal of oral science*, vol. 48, no. 4, pp. 219-26, Dec. 2006.

[107] M. C. Sunny, P. Ramesh, and H. K. Varma, "Microstructured microspheres of hydroxyapatite bioceramic," *Journal of materials science. Materials in medicine*, vol. 13, no. 7, pp. 623-32, Jul. 2002.

[108] F. Y. Hsu, S. C. Chueh, and Y. J. Wang, "Microspheres of hydroxyapatite/reconstituted collagen as supports for osteoblast cell growth," *Biomaterials*, vol. 20, no. 20, pp. 1931-6, Oct. 1999.

[109] B. S. Chang et al., "Osteoconduction at porous hydroxyapatite with various pore configurations," *Biomaterials*, vol. 21, no. 12, pp. 1291-8, Jun. 2000.

[110] V. S. Komlev, S. M. Barinov, V. P. Orlovskii, and S. G. Kurdyumov, "Porous ceramic granules of hydroxyapatite," *Refractories and Industrial Ceramics*, vol. 42, pp. 242-244, 2001.

[111] K. Itatani, A. Ooe, I. J. Davies, T. Umeda, Y. Musha, and S. Koda, "Effect of colloidal silica addition on the formation of porous spherical α -calcium orthophosphate agglomerates by spray pyrolysis technique," *Journal Of The Ceramic Society Of Japan*, vol. 3, no. 3, pp. 363-368, 2009.

[112] K. Itatani, T. Umeda, Y. Musha, and I. J. Davies, "Microstructures of spherical calcium phosphate agglomerates prepraed by spray pyrolysis and freeze drying techniques," *Phosphorous Res. Bull*, vol. 20, pp. 47-60, 2006.

[113] H. Yuan, K. Kurashina, J. D. de Bruijn, Y. Li, K. de Groot, and X. Zhang, "A preliminary study on osteoinduction of two kinds of calcium phosphate ceramics," *Biomaterials*, vol. 20, no. 19, pp. 1799-806, Oct. 1999.

[114] D. Liu, "Fabrication and characterization of porous hydroxyapatite granules," *Biomaterials*, vol. 17, no. 20, pp. 1955-1957, 1996.

[115] V. S. Komlev, S. M. Barinov, and E. V. Koplik, "A method to fabricate porous spherical hydroxyapatite granules intended for time-controlled drug release," *Biomaterials*, vol. 23, no. 16, pp. 3449-54, Aug. 2002.

[116] K. Ioku, G. Kawachi, S. Sasaki, H. Fujimori, and S. Goto, "Hydrothermal preparation of tailored hydroxyapatite," *Journal of Materials Science*, vol. 41, no. 5, pp. 1341-1344, Mar. 2006.

[117] Y. H. Hsu, I. G. Turner, and a W. Miles, "Fabrication and mechanical testing of porous calcium phosphate bioceramic granules," *Journal of materials science. Materials in medicine*, vol. 18, no. 10, pp. 1931-7, Oct. 2007.

[118] N. Kawai, S. Niwa, M. Sato, Y. Sato, Y. Suwa, and I. Ichihara, "Bone formation by cells from femurs cultured among three-dimensionally arranged hydroxyapatite granules," *Journal of biomedical materials research*, vol. 37, no. 1, pp. 1-8, Oct. 1997.

[119] a C. Tas, "Preparation of porous apatite granules from calcium phosphate cement.," *Journal of materials science. Materials in medicine*, vol. 19, no. 5, pp. 2231-9, May 2008.

[120] J. S. Patil, M. V. Kamalapur, S. C. Marapur, and D. V. Kadam, "Ionotrpic gelation and polyelectrolyte complexation: the novel techniques to design hydrogel particulate sustained, modulated drug delivery system : a review," *Drug Delivery*, vol. 5, no. 1, pp. 241-248, 2010.

[121] B. Thu, B. Bruheim, and T. Espevik, "Alginate polycation microcapsules," *Biomaterials*, vol. 10, pp. 1031-1040, 1996.

[122] E. Guibal, "Heterogeneous catalysis on chitosan-based materials: a review," *Progress in Polymer Science*, vol. 30, no. 1, pp. 71-109, Jan. 2005.

[123] F.-long Mi, S.-shing Shyu, T.-bi Wong, S.-fang Jang, S.-tao Lee, and K.-tai Lu, "Chitosan – Polyelectrolyte Complexation for the Preparation of Gel Beads and Controlled Release of Anticancer Drug . II . Effect of pH-Dependent Ionic Crosslinking or Interpolymer Complex Using Tripolyphosphate or Polyphosphate as Reagent," *Polymer*, vol. 74, pp. 1093-1107, 1999.

[124] D. R. Bhumkar and V. B. Pokharkar, "Studies on Effect of pH on Cross-linking of Chitosan With Sodium Tripolyphosphate: A Technical Note," *Aaps Pharmscitech*, vol. 7, no. 2, pp. 2-7, 2006.

[125] A. Nasti, M. G. Rimoli, and N. Tirelli, "Chitosan-based nanoparticles and microparticles."

[126] M. N. . Ravi Kumar, "A review of chitin and chitosan applications," *Reactive and Functional Polymers*, vol. 46, no. 1, pp. 1-27, Nov. 2000.

[127] U. Prüsse et al., "Comparison of different technologies for alginate beads production," *Chemical Papers*, vol. 62, no. 4, pp. 364-374, Jul. 2008.

[128] C. C. Ribeiro, C. C. Barrias, and M. a Barbosa, "Calcium phosphate-alginate microspheres as enzyme delivery matrices," *Biomaterials*, vol. 25, no. 18, pp. 4363-73, Aug. 2004.

[129] P. L. Granja, a. I. N. Silva, J. P. Borges, C. C. Barrias, and I. F. Amaral, "Preparation and Characterization of Injectable Chitosan-Hydroxyapatite Microspheres," *Key Engineering Materials*, vol. 254-256, pp. 573-576, 2004.

[130] C. C. Barrias, M. Lamghari, P. L. Granja, M. C. Sá Miranda, and M. a Barbosa, "Biological evaluation of calcium alginate microspheres as a

vehicle for the localized delivery of a therapeutic enzyme," *Journal of biomedical materials research. Part A*, vol. 74, no. 4, pp. 545-52, Sep. 2005.

[131] E. Krylova, A. Ivanov, V. Orlovski, and S. Barinov, "Hydroxypatite-polysaccharide granules for drug delivery," *Synthesis*, vol. 3, pp. 87-90, 2002.

[132] C. C. Ribeiro, C. C. Barrias, and M. a Barbosa, "Preparation and characterisation of calcium-phosphate porous microspheres with a uniform size for biomedical applications.," *Journal of materials science. Materials in medicine*, vol. 17, no. 5, pp. 455-63, May 2006.

[133] Y. C. Fu, M. L. Ho, S. C. Wu, H. S. Hsieh, and C. K. Wang, "Porous bioceramic bead prepared by calcium phosphate with sodium alginate gel and PE powder," *Materials Science and Engineering: C*, vol. 28, no. 7, pp. 1149-1158, Aug. 2008.

[134] A. Y. P. Mateus, C. C. Barrias, C. Ribeiro, M. P. Ferraz, and F. J. Monteiro, "Comparative study of nanohydroxyapatite microspheres for medical applications," *Journal of biomedical materials research. Part A*, vol. 86, no. 2, pp. 483-93, Aug. 2008.

[135] C. C. Barrias, C. C. Ribeiro, D. Rodrigues, M. C. Sá Miranda, and M. a. Barbosa, "Effect of Calcium Phosphate Addition to Alginate Microspheres: Modulation of Enzyme Release Kinetics and Improvement of Cell Adhesion," *Key Engineering Materials*, vol. 284-286, pp. 689-692, 2005.

[136] M. Rinaudo, G. Pavlov, and J. Desbrie, "Influence of acetic acid concentration on the solubilization of chitosan," *Polymer*, vol. 40, pp. 7029-7032, 1999.

[137] M. Piccinini, V. Sglavo, and P. Robotti, "Elementi porosi e granuli in idrossiapatite per applicazioni biomediche," University of Trento, Master Thesis, 2008.

REFERENCES

[138] D. Vasconcelos, I. Amaral, C. Barrias, M. Barbosa, and C. Ribeiro, "Preparation and Characterization of Porous Microspheres based on a Naturally Occurring Polymer for Minimally- Invasive Bone Regenerative Therapies," *Abstract ESB*, p. 2010, 2011.

[139] O. Ga and G. Skja, "Microcapsules of alginate-chitosan — I A quantitative study of the interaction between alginate and chitosan Olav Ga," *Distribution*, vol. 19, pp. 1815-1825, 1998.

[140] P. S. Mrdel, M. B. Ogataj, and A. M. Rhar, "The Influence of Selected Parameters on the Size and Shape of Alginate Beads Prepared by Ionotropic Gelation," *Reproduction*, pp. 77-89, 2008.

[141] M. Kucharska, K. Walenko, B. Butruk, T. Brynk, M. Heljak, and T. Ciach, "Fabrication and characterization of chitosan microspheres agglomerated scaffolds for bone tissue engineering," *Materials Letters*, vol. 64, no. 9, pp. 1059-1062, May 2010.

[142] H. M. da Silva, I. R. de Lima, P. G. P. Bezerra, G. Peregrino, and G. D. de Almeida Soares, "In Vitro Dynamic Degradation of Strontium-Hydroxyapatite Granules," *Key Engineering Materials*, vol. 493-494, pp. 205-208, Oct. 2011.

[143] S. Ghanaati et al., "Acta Biomaterialia Influence of b-tricalcium phosphate granule size and morphology on tissue reaction in vivo," *Acta Biomaterialia*, vol. 6, no. 12, pp. 4476-4487, 2010.

[144] B. H. Fellah, N. Josselin, D. Chappard, P. Weiss, and P. Layrolle, "Inflammatory reaction in rats muscle after implantation of biphasic calcium phosphate micro particles.," *Journal of materials science. Materials in medicine*, vol. 18, no. 2, pp. 287-94, Feb. 2007.

[145] L. Cordaro, D. D. Bosshardt, P. Palattella, W. Rao, G. Serino, and M. Chiapasco, "Maxillary sinus grafting with Bio-Oss or Straumann Bone Ceramic: histomorphometric results from a randomized controlled

multicenter clinical trial.," *Clinical oral implants research*, vol. 19, no. 8, pp. 796-803, Aug. 2008.

[146] E. I. Dorozhkina and S. V. Dorozhkin, "Mechanism of the Solid-State Transformation of a Calcium-Deficient Hydroxyapatite (CDHA) into Biphasic Calcium Phosphate (BCP) at Elevated Temperatures," *Transformation*, vol. 138, no. 12, pp. 4267-4272, 2002.

[147] E.-S. Chan, B.-B. Lee, P. Ravindra, and D. Poncelet, "Prediction models for shape and size of ca-alginate macrobeads produced through extrusion-dripping method.," *Journal of colloid and interface science*, vol. 338, no. 1, pp. 63-72, Oct. 2009.

[148] C. J. Liao, F. H. Lin, K. S. Chen, and J. S. Sun, "Thermal decomposition and reconstitution of hydroxyapatite in air atmosphere.," *Biomaterials*, vol. 20, no. 19, pp. 1807-13, Oct. 1999.

[149] a. Destainville, E. Champion, D. Bernache-Assollant, and E. Laborde, "Synthesis, characterization and thermal behavior of apatitic tricalcium phosphate," *Materials Chemistry and Physics*, vol. 80, no. 1, pp. 269-277, Apr. 2003.

[150] S. W. . Kweh, K. . Khor, and P. Cheang, "The production and characterization of hydroxyapatite (HA) powders," *Journal of Materials Processing Technology*, vol. 89-90, pp. 373-377, May 1999.

[151] S. Kannan, F. Goetz-Neunhoeffer, J. Neubauer, and J. M. F. Ferreira, "Synthesis and Structure Refinement of Zinc-Doped β-Tricalcium Phosphate Powders," *Journal of the American Ceramic Society*, vol. 92, no. 7, pp. 1592-1595, Jul. 2009.

[152] G. Berger, R. Gildenhaar, U. Ploska, F. C. M. Driessens, and J. A. Planell, "Short-term dissolution behaviour of some calcium phosphate cements and ceramics," *Mat. Science Letters*, vol. 6, pp. 7-9, 1997.

REFERENCES

[153] A. I. Mitsionis, T. C. Vaimakis, and C. C. Trapalis, "The effect of citric acid on the sintering of calcium phosphate bioceramics," *Ceramics International*, vol. 36, no. 2, pp. 623-634, Mar. 2010.

[154] E. Herdtweck, T. Kornprobst, R. Sieber, L. Straver, and J. Plank, "Crystal Structure, Synthesis, and Properties of tri-Calcium di-Citrate tetra-Hydrate [Ca3(C6H5O7)2(H2O)2]·2H2O," *Zeitschrift für anorganische und allgemeine Chemie*, vol. 637, no. 6, pp. 655-659, May 2011.

[155] D. N. Misra, "Interaction of Citric Acid with Hydroxyapatite: Surface Exchange of Ions and Precipitation of Calcium Citrate," *Journal of Dental Research*, vol. 75, no. 6, pp. 1418-1425, Jun. 1996.

[156] M. H. Al-Khaldi, H. a. Nasr-El-Din, S. Mehta, and a. D. Al-Aamri, "Reaction of citric acid with calcite," *Chemical Engineering Science*, vol. 62, no. 21, pp. 5880-5896, Nov. 2007.

[157] S. R. Radin and P. Ducheyne, "The effect of calcium phosphate ceramic composition and structure on in vitro behavior. II. Precipitation," *Journal of biomedical materials research*, vol. 27, no. 1, pp. 35-45, Jan. 1993.

[158] M. Bohner and J. Lemaitre, "Can bioactivity be tested in vitro with SBF solution?," *Biomaterials*, vol. 30, no. 12, pp. 2175-9, Apr. 2009.

[159] P. Trisi, W. Rao, A. Rebaudi, and P. Fiore, "Histologic effect of pure-phase beta-tricalcium phosphate on bone regeneration in human artificial jawbone defects," *Int. J. of oral implantology implantologist* , vol. 23, no. 1, pp. 69-77, Feb. 2003.

ACKNOWLEDGEMENTS

- ✓ *Thanks to my wonderful family: my parents, Lilia and Nello, my brother Manlio and sister Maila and my nephews Jada, Gabriele, Alex and Asia for the continue support during these years;*
- ✓ *Thanks to those persons no longer with me, but they protect me from the sky;*
- ✓ *Thanks to my tutor Vincenzo for this thesis proposal and scientific help;*
- ✓ *Thanks to my company advisor Francesco and Eurocoating S.p.A. for the technical. financial and scientific support;*
- ✓ *Thanks to all Ph.D. students and laboratory colleagues, in particular Annarita, Michele, Vincenzo, Aylin, Andrè, Tatiana, Ricardo, Amaia, Francesca, Andrea, John, Madi, Livio;*
- ✓ *Thanks to my R&D colleagues in Eurocoating: Susanna, Gianluca, Eleonora, Giacomo, Luca, Pierfrancesco and Emanuele and to other collaborators as Alberto, Domenico and Stefano;*
- ✓ *Thanks to my flat mates: Ale, Giulia, Jessica and Valentina;*
- ✓ *Thanks to all my friends, near or far, but always with me.*